



HAL
open science

Processing of natural rubber composites and blends : relation between structure and properties

Subhan Salaeh

► **To cite this version:**

Subhan Salaeh. Processing of natural rubber composites and blends : relation between structure and properties. Other. Université Claude Bernard - Lyon I; Prince of Songkla University, 2014. English. NNT : 2014LYO10141 . tel-01127232

HAL Id: tel-01127232

<https://theses.hal.science/tel-01127232v1>

Submitted on 7 Mar 2015

HAL is a multi-disciplinary open access archive for the deposit and dissemination of scientific research documents, whether they are published or not. The documents may come from teaching and research institutions in France or abroad, or from public or private research centers.

L'archive ouverte pluridisciplinaire **HAL**, est destinée au dépôt et à la diffusion de documents scientifiques de niveau recherche, publiés ou non, émanant des établissements d'enseignement et de recherche français ou étrangers, des laboratoires publics ou privés.



THESIS



Presented in

PRINCE OF SONGKLA UNIVERSITY (PSU) – PATTANI (THAILAND)

and

UNIVERSITY CLAUDE BERNARD LYON 1 (UCBL) – VILLEURBANNE (FRANCE)

for obtaining

DOCTOR OF PHILOSOPHY

Speciality « POLYMERS TECHNOLOGY »

and

DOCTORAL DEGREE

Speciality « INNOVATIVE MATERIALS »

(Arrêté du 7 Août 2006)

Defense of the thesis is proposed on 4 July 2014

By

Mr. Subhan SALAEH

Processing of Natural Rubber Composites and Blends: Relation between Structure and Properties

Thesis supervisors: Charoen Nakason / Philippe Cassagnau

Co-advisor: Gisèle Boiteux

JURY:

Prof. Dr. Suda KIATKAMJORNWONG	Chulalongkorn University	Reviewer
Prof. Dr. René MULLER	Université de Strasbourg	Reviewer
Assoc. Prof. Dr. Charoen NAKASON	Prince of Songkla University	Supervisor
Prof. Dr. Philippe CASSAGNAU	Université Lyon1	Supervisor
Dr. Gisèle BOITEUX	Université Lyon1	Co-advisor
Assoc. Prof. Azizon KAESAMAN	Prince of Songkla University	Examiner



THESE



Présentée devant

L'UNIVERSITE PRINCE DE SONGKLA (PSU) – PATTANI (THAILAND)

et

L'UNIVERSITE CLAUDE BERNARD LYON 1 (UCBL) – VILLEURBANNE (FRANCE)

pour l'obtention du DIPLOME de

DOCTEUR EN PHILOSOPHIE

Spécialité « TECHNOLOGIE DE POLYMERE »

et du

DIPLOME DE DOCTORAT

Spécialité « MATERIAUX INNOVANTS »

(Arrêté du 7 Août 2006)

Soutenance proposée le 4 Juillet 2014

Par

Mr. Subhan SALAEH

**Elaboration des Composites et Mélanges à base de
Caoutchouc Naturel: Relations Structure – Propriétés**

Directeurs de thèse: Charoen Nakason / Philippe Cassagnau

Co-directeur: Gisèle Boiteux

JURY:

Prof. Dr. Suda KIATKAMJORNWONG	Chulalongkorn University	Rapporteur
Prof. Dr. René MULLER	Université de Strasbourg	Rapporteur
Assoc. Prof. Dr. Charoen NAKASON	Prince of Songkla University	Directeur
Prof. Dr. Philippe CASSAGNAU	Université Lyon1	Directeur
Dr. Gisèle BOITEUX	Université Lyon1	Co-directeur
Assoc. Prof. Azizon KAESAMAN	Prince of Songkla University	Examineur

UNIVERSITE CLAUDE BERNARD - LYON 1

Président de l'Université

Vice-président du Conseil d'Administration

Vice-président du Conseil des Etudes et de la Vie Universitaire

Vice-président du Conseil Scientifique

Directeur Général des Services

M. François-Noël GILLY

M. le Professeur Hamda BEN HADID

M. le Professeur Philippe LALLE

M. le Professeur Germain GILLET

M. Alain HELLEU

COMPOSANTES SANTE

Faculté de Médecine Lyon Est – Claude Bernard

Faculté de Médecine et de Maïeutique Lyon Sud – Charles Mérieux

Faculté d'Odontologie

Institut des Sciences Pharmaceutiques et Biologiques

Institut des Sciences et Techniques de la Réadaptation

Département de formation et Centre de Recherche en Biologie Humaine

Directeur : M. le Professeur J. ETIENNE

Directeur : Mme la Professeure C. BURILLON

Directeur : M. le Professeur D. BOURGEOIS

Directeur : Mme la Professeure C. VINCIGUERRA

Directeur : M. le Professeur Y. MATILLON

Directeur : Mme. la Professeure A-M. SCHOTT

COMPOSANTES ET DEPARTEMENTS DE SCIENCES ET TECHNOLOGIE

Faculté des Sciences et Technologies

Département Biologie

Département Chimie Biochimie

Département GEP

Département Informatique

Département Mathématiques

Département Mécanique

Département Physique

UFR Sciences et Techniques des Activités Physiques et Sportives

Observatoire des Sciences de l'Univers de Lyon

Polytech Lyon

Ecole Supérieure de Chimie Physique Electronique

Institut Universitaire de Technologie de Lyon 1

Institut Universitaire de Formation des Maîtres

Institut de Science Financière et d'Assurances

Directeur : M. F. DE MARCHI

Directeur : M. le Professeur F. FLEURY

Directeur : Mme Caroline FELIX

Directeur : M. Hassan HAMMOURI

Directeur : M. le Professeur S. AKKOUCHE

Directeur : M. Georges TOMANOV

Directeur : M. le Professeur H. BEN HADID

Directeur : M. Jean-Claude PLENET

Directeur : M. Y. VANPOULLE

Directeur : M. B. GUIDERDONI

Directeur : M. P. FOURNIER

Directeur : M. G. PIGNAULT

Directeur : M. C. VITON

Directeur : M. A. MOUGNIOTTE

Directeur : M. N. LEBOISNE

Thesis Title Processing of Natural Rubber Composites and Blends: Relation
between Structure and Properties
Author Mr. Subhan Salaeh
Major Program Polymer Technology

Major Advisors:

.....
(Assoc. Prof. Dr. Charoen Nakason)

.....
(Prof. Dr. Philippe Cassagnau)

Co-advisor:

.....
(Dr. Gisèle Boiteux)

Examining Committee:

.....Chairperson
(Prof. Dr. Suda Kiatkamjornwong)

.....
(Assoc. Prof. Dr. Charoen Nakason)

.....
(Prof. Dr. Philippe Cassagnau)

.....
(Dr. Gisèle Boiteux)

.....
(Prof. Dr. René Muller)

.....
(Assoc. Prof. Azizon Kaesaman)

The Graduate School, Prince of Songkla University has approved this thesis as fulfillment of the requirements for the Degree of Doctor of Philosophy in Polymer Technology.

.....
(Assoc. Prof. Dr. Teerapol Srichana)
Dean of Graduate School

This is to certify that the work here submitted is the result of the candidate's own investigation. Due acknowledgement has been made of any assistance received.

.....Signature

(Assoc. Prof. Dr. Charoen Nakason)

Major Advisor

.....Signature

(Mr. Subhan Salaeh)

Candidate

I hereby certify that work has not already been accepted in substance for any degree,
and is not being concurrently submitted in candidature for any degree.

.....Signature

(Mr. Subhan Salaeh)

Candidate

ชื่อวิทยานิพนธ์	การแปรรูปยางธรรมชาติคอมพอสิตและเบลนด์: ความสัมพันธ์ระหว่างโครงสร้างกับสมบัติ
ผู้เขียน	นายสุภฮาน สาและ
สาขาวิชา	เทคโนโลยีพอลิเมอร์
ปีการศึกษา	2556

บทคัดย่อ

ศึกษาอิทธิพลของโครงสร้างโมกุลยางธรรมชาติ (NR) และยางธรรมชาติอีพอกไซด (ENR) ต่อสมบัติ พบว่าการมีหมู่อีพอกไซดอยู่ในยาง ENR ทำให้มีการปรับปรุงสมบัติเชิงกล เช่น โมดูลัสและความต้านทานต่อแรงดึง นอกจากนี้สมบัติไดอิเล็กทริกได้แสดงให้เห็นถึงการนำไฟฟ้าที่ความถี่ต่ำและอุณหภูมิสูง ยางที่มีหมู่อีพอกไซด 50 โมล% (ENR-50) มีค่าการนำไฟฟ้าและค่า permittivity สูงที่สุด ดังนั้นจึงนำยาง ENR-50 ไปใช้ในการเตรียมคอมพอสิตที่ใช้แบเรียมไททาเนตและเซมาต้าเป็นตัวเติม ซึ่งพบว่าค่า permittivity และค่าการนำไฟฟ้าสูงขึ้นตามปริมาณตัวเติมที่ใส่ลงไป ที่ปริมาณ 50% โดยปริมาตรของแบเรียมไททาเนตในยางให้ค่า permittivity สูงถึง 48.7 ในขณะที่เดียวกันก็พบว่าการเตรียม ENR-50 คอมพอสิตที่ใช้เซมาต้ามี percolation threshold ที่ 6.3 vol% ของเซมาต้า สำหรับการศึกษากการเปลี่ยนแปลงของสัญญาณวิทยาและความเข้ากันได้ของพอลิเมอร์เบลนด์ระหว่างพอลิไวนิลลิดีนฟลูออไรด์ (PVDF) กับยาง ENR พบว่า สัญญาณวิทยาของพอลิเมอร์ที่เตรียมได้ขึ้นอยู่กับปริมาณหมู่อีพอกไซดในยาง ENR และอัตราส่วนการเบลนด์ อัตราส่วนการเบลนด์ในช่วง 40 ถึง 60% โดยน้ำหนักของยาง ENR-50 ให้ลักษณะสัญญาณวิทยาแบบวัฏภาคร่วม (co-continuous) นอกจากนี้ผลการทดสอบจากสมบัติพลวัตเชิงกลและสมบัติไดอิเล็กทริกแสดงให้เห็นถึงความเข้ากันได้บางส่วน (partial miscibility) ทำยที่สุดนี้ได้เตรียมคอมพอสิตจากพอลิเมอร์เบลนด์ที่เติมแบเรียมไททาเนต สัญญาณวิทยาของคอมโพสิตที่เตรียมได้นั้น พบว่าแบเรียมไททาเนตกระจายตัวในเฟสยางเป็นหลัก อย่างไรก็ตามการเติมแบเรียมไททาเนตหลังจากการวัลคาไนซ์แบบไดนามิกส์ทำให้แบเรียมไททาเนตกระจายตัวในเฟสพอลิไวนิลลิดีนฟลูออไรด์ (PVDF) และที่ผิวประจัญ (interface) นอกจากนี้คอมพอสิตที่เตรียมจากเทอร์โมพลาสติกวัลคาไนซ์ของ PVDF/ENR-50 ที่อัตราส่วนการเบลนด์ที่ 80/20 ให้ค่า permittivity ที่สูง

คำสำคัญ: ยางธรรมชาติ ยางธรรมชาติอีพอกไซด แบเรียมไททาเนต พอลิไวนิลลิดีนฟลูออไรด์ พอลิเมอร์เบลนด์ การเบลนด์ด้วยเทคนิควัลคาไนซ์แบบไดนามิก

Thesis Title	Processing of Natural Rubber Composites and Blends: Relation between Structure and Properties
Author	Mr. Subhan Salaeh
Major Program	Polymer Technology
Academic Year	2013

ABSTRACT

Natural rubber (NR) and epoxidized natural rubber (ENR) were chosen to study the composites and blends of polymers. The presence of epoxide group caused to improve the mechanical properties in terms of modulus and tensile strength. Furthermore, dielectric spectroscopy revealed that ENR showed conductivity process at low frequency and high temperature. Epoxidized natural rubber containing 50 mol% of epoxide group or ENR-50 exhibited the highest dielectric permittivity and electrical conductivity. Therefore, ENR-50 was then selected to prepare polymer composite filled with barium titanate (BT) and carbon black (CB) particles. The permittivity and conductivity of the composites increased with the volume content of the fillers. The BT/ENR-50 composites reached a high permittivity of 48.7 for addition of 50 vol% BT. Meanwhile, CB/ENR-50 composite reached percolation threshold at 6.3 vol% of CB. The phase development and miscibility of poly(vinylidene fluoride) (PVDF)/epoxidized natural rubber (ENR) blends were then investigated. It was also found that phase structure depended on epoxidation level and blend compositions. The blend exhibited a co-continuous phase morphology in the region of 40 to 60 wt% of ENR-50. Furthermore, the results from dynamic mechanical and dielectric analysis revealed that these blends present a partial miscibility. Finally, the composites based on binary blends of PVDF/ENR-50 containing BT were prepared. The study of the morphologies revealed that BT was dispersed in ENR-50 phase in the case of simple blend. However, the addition of BT after dynamic vulcanization induced localization of BT in PVDF phase and at interface. The highest increment of permittivity can be observed for the composite based on dynamically cured PVDF/ENR-50 (80/20) blend.

Key words: natural rubber, epoxidized natural rubber, barium titanate, poly(vinylidene fluoride), polymer blends, dynamically cured blends

Titre	Elaboration de Composites et Mélanges à base de Caoutchouc Naturel: Relations Structure-Propriétés
Auteur	Mr. Subhan Salaeh
Programme	Technologie de polymère
Année	2013

RÉSUMÉ

Le caoutchouc naturel (NR) et le caoutchouc époxydé (ENR) ont constitué la base de cette étude consacrée à l'étude des composites et mélanges de polymères. La présence du groupe époxyde a conduit à une amélioration des propriétés mécaniques de ces formulations en termes de module et de la résistance à la traction. De plus, l'utilisation de la spectroscopie diélectrique a révélé que les ENRs présentent une conductivité plus élevée que le NR à basse fréquence et à haute température. En particulier, le caoutchouc naturel époxydé contenant 50 mol% de groupes époxyde ENR-50 présente des conductivités et permittivités les plus élevées. Par conséquent, ce dernier a été choisi pour préparer des composites polymères en incorporant des particules de titanate de barium (BT) et de noir de carbone (CB). Les résultats montrent que la permittivité et conductivité des composites élaborés augmentent avec le taux d'incorporation de ces charges. Par exemple, les composites BT/ENR-50 atteignent une permittivité élevée 48.7 pour 50 vol% de BT. De plus, les composites CB/ENR-50 présentent un seuil de percolation de 6.3 vol% de CB. Enfin les mélanges à base de poly(fluorure de vinylidène) (PVDF) et d'ENR ont été étudiés. Il a été observé que la morphologie de ces mélanges dépend du degré d'époxydation du caoutchouc naturel et bien entendu de la composition du mélange. Une morphologie co-continue peut être observée dans l'intervalle 40 et 60% en masse d'ENR-50. En outre, les résultats issus d'analyses dynamiques mécanique et diélectrique montrent que ces mélanges présentent une miscibilité partielle. Enfin, des composites à base de ces mélanges binaires PVDF/ENR-50 contenant BT ont été préparés. L'étude des morphologies a révélé que les particules de BT étaient dispersées dans la phase d'ENR-50 pour le mélange classique. Cependant, les particules de BT sont localisées à l'interface et dans la phase PVDF pour le mélange réticulé dynamiquement. En termes de propriétés, la permittivité plus élevée est obtenue pour le mélange PVDF/ENR-50 (80/20) ayant été réticulé dynamiquement.

Mots clés: caoutchouc naturel, caoutchouc naturel époxydé, titanate de barium, poly (fluorure de vinylidène), mélange de polymères, réticulation dynamique.

ACKNOWLEDGEMENTS

I would like to thank many people who have helped me directly or indirectly in this thesis over a few past years.

First of all, I would first like to express my deep gratitude to my supervisor, Assoc. Prof. Dr. Charoen Nakason and Prof. Dr. Philippe Cassagnau, my co-advisor, Dr. Gisèle Boiteux for their helpful support, and the opportunity to study under their supervisions. They have coached me in completion of this thesis and gave all means necessary for the realization of this thesis. Their skills and experience in leadership have been a great help for the completion of this thesis. Working with them was very pleasant and I have learned a lot over the years, both scientific and human levels. Also, they have helped me for life experience in Lyon. First meeting at Lyon-Saint Exupéry Airport remain a great memory for me. Thank you again to them for their encouragement and all proofreading of articles, presentations and thesis chapters.

My thanks are then directed to Prof. Dr. Suda Kiatkamjornwong and Prof. Dr. René Muller for giving me the honor to report this thesis. I also thank Assoc. Prof. Azizon Kaesaman who has been examiner of this study.

This work was financial supported by the Thailand Research Fund (TRF) through the Royal Golden Jubilee Ph.D. Program (Grant No. PHD/0245/2549), French Embassy in Thailand and graduate school of Prince of Songkla University. They have been made this research possible.

I also thank all the lecturers and staffs in Department of Rubber Technology and Polymer Science, Pattani, Thailand for teaching me the basic of rubber and polymer science which is useful knowledge for this thesis. I would like to thank to Dr. Sitisaiyidah Saiwari and Dr. Methakarn Jarnthong for their proofreading. Sincere thanks are also extended to all technician in the lab namely Absorn Jongrakwattana, Inyars Kama, Somkid Srisuwan, Siradanai Sulung and Haseumah Deoraot for their invaluable service and advice. Thanks to all my best colleagues in rubber and polymer technology program who I have met since the beginning of my studies. Their good humor and kindness have made life in the lab more enjoyable. All the best moments with them are always in my memory.

ACKNOWLEDGEMENTS

I also would like to express my thanks to permanent staffs in IMP@Lyon1 especially Olivier Gain, Pierre Alcouffe, Thiery Tamet, Flovien Melis, Sylvie Novat, Ali Haddane and others for their invaluable service and assistance. Also, I will not forget to thank friends who I have met there. I would like to thank to Volodymyr Levchenko, Muhammad Jouni, Anna Lakowska and Anna Marzec for being best friends and also helping me to do research experiment in the lab. Their discussions related to electrical properties of polymer composite is very helpful. Thank you all friends in IMP@Lyon1, Romina, Samir, Sofiane, Mikaël, Marine, Elodie, Imen, Afef, Fatima, Antony, Nicolas and Brice for their friendship and humor. All people in IMP@Lyon actively participated to make my exciting life in France very happy. They always teach French language during my stay in Lyon.

These acknowledgments would not be complete without a thought my family. I want to especially express my deep gratitude to my dearest parents, Makorsee Salaeh and Sujanya Salaeh for their endless support. They have always been there for me during all these years of study and encouraged me to finish PhD study. A big thank to my wife, Maisaro for her support and love in me. It was because of strong support of my family and wife that I am able to complete my PhD work.

MERCI à TOUTES et à TOUS

Subhan SALAEH



CONTENTS

ABSTRACT (THAI)	6
ABSTRACT (ENGLISH)	7
ABSTRACT (FRENCH)	8
ACKNOWLEDGEMENTS	9
CONTENTS	11
LIST OF TABLES.....	16
LIST OF FIGURES.....	19
LIST OF ABBREVIATIONS.....	28
LIST OF SYMBOLS.....	31
CHAPTER 1: Introduction	33
1.1 Introduction.....	33
1.2 Scope of thesis.....	35
1.3 The aim of thesis.....	36
1.4 Novelty of the work.....	36
1.5 The thesis outline.....	37
CHAPTER 2: Literature Review	39
2.1 Polymer composites.....	39
2.1.1 Ceramic-polymer composites.....	40
2.1.2 Conductive polymer composites.....	44
2.2 Thermoplastic elastomer blends.....	50
2.2.1 The miscibility of polymer blend.....	50
2.2.2 Simple blend.....	53
2.2.3 Thermoplastic vulcanizate.....	54
2.3 Binary polymer composites.....	56
2.3.1 Filler localization.....	56

CONTENTS

2.3.2	Compatibilization effect of particles.....	59
2.4	Natural rubber.....	60
2.4.1	Epoxidized natural rubber.....	61
2.4.2	Composites and polymer blends based on ENR.....	62
2.5	Poly(vinylidene fluoride).....	63
2.5.1	Composites and polymer blends based on PVDF.....	64
2.6	Conclusions.....	65
2.7	References.....	66
CHAPTER 3: Materials and Experiment Methodology.....		77
3.1	Materials.....	77
3.2	Experimental procedure.....	80
3.2.1	Preparation of natural rubber vulcanizate.....	80
3.2.2	Preparation of barium titanate.....	80
3.2.3	Preparation of BT/ENR-50 and CB/ENR-50 composites.....	81
3.2.4	Preparation of PVDF/ENR simple blends.....	82
3.2.5	Preparation of BT/PVDF/ENR-50 composites.....	83
3.3	Testing and characterization.....	85
3.3.1	Cure characteristic.....	85
3.3.2	Morphological properties.....	86
3.3.3	Mechanical properties.....	88
3.3.4	Differential scanning calorimetry analysis.....	91
3.3.5	Dynamic mechanical analysis.....	92
3.3.6	Dielectric analysis.....	93
3.4	References.....	97
CHAPTER 4: Characterization of Natural Rubber and Epoxidized Natural Rubber.....		99
4.1	Introduction.....	99
4.2	Effect of natural rubber types on properties of vulcanizate.....	100
4.2.1	Cure characteristic.....	100
4.2.2	Mechanical properties.....	101

4.2.3	Dynamic mechanical analysis.....	102
4.2.4	Dielectric analysis.....	104
4.3	Conclusions.....	115
4.4	References.....	116
CHAPTER 5: Flexible Ceramic-Polymer Composites based on BT/ENR-50 Composites.....		121
5.1	Introduction.....	121
5.2	Barium titanate characterization.....	122
5.2.1	XRD pattern.....	122
5.2.2	Microstructure of barium titanate.....	123
5.2.3	Dielectric properties.....	124
5.3	Effect of BT loading level on properties of BT/ENR-50 composites.....	125
5.3.1	Cure characteristic.....	125
5.3.2	Morphological properties.....	126
5.3.3	Mechanical properties.....	128
5.3.4	Dynamic mechanical analysis.....	130
5.3.5	Dielectric analysis.....	132
5.4	Conclusions.....	143
5.5	References.....	144
CHAPTER 6: Conductive Elastomer Composites based on CB/ENR-50 Composites.....		149
6.1	Introduction.....	149
6.2	Effect of different carbon black structure and content on properties of carbon black filled ENR-50 composites.....	150
6.2.1	Cure characteristic.....	150
6.2.2	Mechanical properties.....	152
6.2.3	Dynamic mechanical analysis.....	157
6.2.4	Electrical properties.....	160
6.3	Conclusions.....	167
6.4	References.....	168

CONTENTS

CHAPTER 7: Phase Development and Miscibility of PVDF/ENR-50 Simple	
	Blends..... 173
7.1	Introduction..... 173
7.2	Effect of difference epoxidation level in ENR on the properties of PVDF/ENR simple blend..... 175
7.2.1	Morphological properties..... 175
7.2.2	Mechanical properties..... 177
7.2.3	Differential scanning calorimetry..... 178
7.2.4	Dynamic mechanical analysis..... 180
7.2.5	Consideration of physical properties improvement..... 183
7.2.6	Dielectric analysis..... 185
7.3	The effect of blend composition on the properties of PVDF/ENR-50 simple blend..... 191
7.3.1	Morphological properties..... 191
7.3.2	Mechanical properties..... 192
7.3.3	Differential scanning calorimetry..... 196
7.3.4	Dynamic mechanical analysis..... 198
7.3.5	Dielectric analysis..... 202
7.4	Conclusions..... 207
7.5	References..... 209
CHAPTER 8: Selective Localization of Barium Titanate in PVDF/ENR-50	
	Blends..... 215
8.1	Introduction..... 215
8.2	Effect of barium titanate in the simple and dynamically vulcanized PVDF/ENR-50 blends..... 216
8.2.1	Morphological properties..... 216
8.2.2	Mechanical properties..... 224
8.2.3	Dynamic mechanical analysis..... 227
8.2.4	Dielectric properties..... 230

CONTENTS

8.3	Effect of barium titanate loading in dynamically vulcanized PVDF/ENR-50 blend.....	234
8.3.1	Morphological properties.....	234
8.3.2	Mechanical properties.....	236
8.3.3	Dynamic mechanical analysis.....	238
8.3.4	Dielectric properties.....	241
8.4	Conclusions.....	245
8.5	References.....	246
CHAPTER 9: General Conclusion.....		249
APPENDIX.....		253
CURRICULUM VITAE.....		275

LIST OF TABLES

Tables	Page
CHAPTER 2: Literature Review.....	39
2.1 Dielectric constant (ϵ') and loss tangent ($\tan \delta$) of some polymers.....	40
2.2 The dielectric permittivity of 0-3 ceramic polymer composites. The value with “~” is obtained from graphical representations.....	44
2.3 Properties of selected CBs for electric conductivity.....	48
CHAPTER 3: Materials and Experiment Methodology.....	77
3.1 Characteristics of used carbon black.....	79
3.2 Compounding formulation used to prepare rubber vulcanizate.....	80
3.3 Composition of simple and dynamically cured PVDF/ENR-50 blends with addition of BT.....	84
3.4 Composition of dynamically cured PVDF/ENR-50 blend with various BT loadings.....	85
3.5 Dimensions of dumbbell test specimens.....	90
CHAPTER 4: Characterization of natural rubber and epoxidized natural rubber.....	99
4.1 Cure characteristic of NR, ENR-25 and ENR-50 compounds.....	100
4.2 Mechanical properties of NR, ENR-25 and ENR-50 gum vulcanizates.....	102
4.3 Storage modulus and $\tan \delta$ of NR, ENR-25 and ENR-50 gum vulcanizates.....	103
4.4 Fitting parameters of VFT equation to the experimental data.....	107
4.5 Dielectric properties at frequency 1 kHz of NR, ENR-25 and ENR-50 vulcanizates.....	110

Tables	Page
CHAPTER 5: Flexible Ceramic-Polymer Composites based on BT/ENR-50	
Composites.....	121
5.1 Cure characteristic of BT/ENR-50 composites with various BT loadings.....	126
5.2 Mechanical properties of BT/ENR-50 composites with various BT loadings.....	129
5.3 Storage modulus (E') and loss tangent ($\tan \delta$) of BT/ENR-50 with various BT loadings.....	132
5.4 Permittivity (ϵ'), loss factor (ϵ'') and loss tangent ($\tan \delta$) at fixed frequency 1 kHz of BT/ENR-50 composites with various BT loadings.....	136
5.5 Fitting parameters of VFT and Arrhenius equations to the experimental data.....	143
CHAPTER 6: Conductive Elastomer Composites based on CB/ENR-50	
Composites.....	149
6.1 Cure characteristic of HAF and ECF filled ENR-50 composites.....	151
6.2 Young's modulus (E), tensile strength (σ_B), elongation at break (ϵ_B) and hardness of HAF/ENR-50 and ECF/ENR-50 composites.....	152
6.3 Storage modulus (E') and loss tangent ($\tan \delta$) of HAF/ENR-50 and ECF/ENR-50 composites with various CB loadings.....	158
6.4 DC conductivity values obtained from the power law fitting curves of the conductivity plots.....	164
CHAPTER 7: Phase Development and Miscibility of PVDF/ENR-50 Simple Blends.....	
Blends.....	173
7.1 Solubility parameter of PVDF, ENR-25 and ENR-50.....	176
7.2 Mechanical properties of PVDF, PVDF/ENR-25 and PVDF/ENR-50 blends.....	178
7.3 Thermal characteristic of PVDF and its blend during cooling and heating sweeps.....	179

LIST OF TABLES

Tables	Page
7.4	Dynamic mechanical properties of PVDF and its blends..... 182
7.5	Fitting parameters for PVDF, ENR-25, ENR-50 and their blends..... 188
7.6	Fitting parameters of conductivity process for PVDF, ENR-25, ENR-50 and their blends..... 190
7.7	Mechanical properties of PVDF/ENR-50 blend with different blend proportions..... 194
7.8	Thermal characteristic of PVDF/ENR-50 blends with different compositions..... 197
7.9	Storage modulus (E') and loss tangent ($\tan \delta$) of PVDF/ENR-50 blends with various blend compositions..... 200
7.10	Fitting parameter for glass-rubber transition and conductivity peaks of PVDF/ENR-50 blends with various blend ratios..... 207
CHAPTER 8: Selective Localization of Barium Titanate in PVDF/ENR-50	
	Blends..... 215
8.1	Mechanical properties of simple and dynamically cured PVDF/ENR-50 blends without and with 5 vol% BT..... 226
8.2	Dynamic mechanical properties of simple and dynamically cured PVDF/ENR-50 blends without and with 5 vol% BT..... 230
8.3	Permittivity (ϵ'), loss factor (ϵ'') and loss tangent ($\tan \delta$) at frequency 1 kHz of simple and dynamically cured PVDF/ENR-50 blends with and without BT..... 232
8.4	Mechanical properties of dynamically cured PVDF/ENR-50 blend with various amounts of BT..... 238
8.5	Dynamic mechanical properties of dynamically cured PVDF/ENR-50 blend with various amounts of BT..... 240
8.6	Permittivity (ϵ'), loss factor (ϵ'') and loss tangent ($\tan \delta$) at frequency 1 kHz of dynamically cured PVDF/ENR-50 blend with various BT loadings 243

LIST OF FIGURES

Figures	Page
CHAPTER 2: Literature Review	39
2.1 (a) Cubic perovskite-type structure ABO_3 (b) another view of the ABO_3 structure.....	41
2.2 Connectivity of constituent phases in piezoelectric ceramic–polymer composites.....	42
2.3 Dependence of electrical conductivity (σ) on the volume fraction (φ) of conductive fillers.....	45
2.4 Structure of carbon black.....	47
2.5 Schematic of the concept of CB structure and surface area.....	47
2.6 (a) Interface between the carbon black filler and the polymer. (b) A schematic diagram of the physical network in a carbon black filled elastomer.....	49
2.7 Formation mechanism of the morphology in the polymer blends.....	52
2.8 The evolution of the morphology of simple blend with different blend compositions.....	53
2.9 Schematic diagram of morphology transformation during the dynamic vulcanization of polymer blends.....	55
2.10 Selective localization of particles in polymer blends.....	56
2.11 The mechanism for epoxidation of natural rubber.....	61
2.12 Chemical structure of PVDF.....	63
CHAPTER 3: Materials and Experiment Methodology	77
3.1 Molecular structure of HRJ-10518.....	79
3.2 Mixing torque-time graph for PVDF/ENR simple blend.....	83
3.3 Mixing torque-time graph for dynamically cured PVDF/ENR-50 blends with different methods to introduce BT particles in the blends	84
3.4 Torque as function of time during the vulcanization.....	86

LIST OF FIGURES

Figures	Page
3.5 Schematic diagram of the various signals generated by the interaction of the electron beam with the sample.....	87
3.6 Typical stress–strain curve for polymeric materials.....	88
3.7 Standard die shape for cutting dumbbell specimens.....	90
3.8 Schematic presentation of the (a) frequency and (b) temperature dependences of ϵ' and ϵ'' for typical dielectric relaxation in polymers.....	95
 CHAPTER 4: Characterization of Natural Rubber and Epoxidized Natural Rubber.....	
	99
4.1 Rheograph of gum vulcanizates of NR, ENR-25 and ENR-50 at 160°C.....	101
4.2 Stress-strain curves of NR, ENR-25 and ENR-50 gum vulcanizates.....	102
4.3 Temperature dependence of E' and $\tan \delta$ of NR, ENR-25 and ENR-50 gum vulcanizates.....	103
4.4 Temperature dependence of (a) ϵ' and (b) ϵ'' of vulcanized NR at several frequencies (\square) 1, (\circ) 10, (\triangle) 100, (∇) 1k and (\diamond) 10k Hz.....	105
4.5 Temperature dependence of (a) ϵ' and (b) ϵ'' of vulcanized ENR-25 at several frequencies (\square) 1, (\circ) 10, (\triangle) 100, (∇) 1k and (\diamond) 10k Hz.....	105
4.6 Temperature dependence of (a) ϵ' and (b) ϵ'' of vulcanized ENR-50 at several frequencies (\square) 1, (\circ) 10, (\triangle) 100, (∇) 1k and (\diamond) 10k Hz.....	106
4.7 Chemical structure and dipole moment of poly(<i>cis</i> -1,4-isoprene).....	106
4.8 Relaxation time at maximum of ϵ'' for α -relaxation of NR, ENR-25 and ENR-50 as a function of reciprocal temperature. Solid line represent the overall best fits according to Equation 3.20.....	107
4.9 Temperature dependence of $\tan \delta$ of NR, ENR-25 and ENR-50 vulcanizates obtained from DMA and DEA techniques at frequency 1 Hz.....	109
4.10 Frequency dependence of (a) ϵ' and (b) ϵ'' of NR, ENR-25 and ENR-50 vulcanizates at room temperature.....	110
4.11 Temperature dependence of M'' of (a) NR, (b) ENR-25 and (c) ENR-50 vulcanizates at several frequencies (\square) 1, (\circ) 10, (\triangle) 100, (∇) 1k and (\diamond) 10k Hz	112

LIST OF FIGURES

Figures	Page
4.12	Frequency dependence of M'' of NR, ENR-25 and ENR-50 vulcanizates... 113
4.13	Frequency dependence of AC conductivity of NR, ENR-25 and ENR-50 vulcanizates..... 114
4.14	Relaxation time at maximum of M'' for conduction process of NR, ENR-25 and ENR-50 as a function of reciprocal temperature. Solid line represent the overall best fits according to Equation 3.19..... 115
CHAPTER 5: Flexible Ceramic-Polymer Composites based on BT/ENR-50 Composites..... 121	
5.1	XRD patterns of mixed $BaCO_3+TiO_2$ and $BaTiO_3$ 123
5.2	(a) SEM micrograph and (b) particle size distribution of BT powders..... 123
5.3	Permittivity (ϵ'), loss factor (ϵ'') and loss tangent ($\tan \delta$) as function of frequency of synthesized barium titanate..... 124
5.4	Rheographs of BT/ENR-50 composites with various BT loadings..... 126
5.5	SEM micrographs of BT/ENR-50 composites with various BT loadings (a) 0, (b) 5, (c) 10, (d) 15, (e) 20, (f) 30, (g) 40 and (h) 50 vol%..... 127
5.6	Enlarged SEM micrographs of BT/ENR-50 composites with (a) 10 and (b) 50 vol% of BT..... 128
5.7	Stress-strain curves of BT/ENR-50 composites with various BT loadings..... 129
5.8	Tensile strength and elongation at break as a function of BT loading in BT/ENR-50 composites..... 130
5.9	Temperature dependence of E' and $\tan \delta$ of BT/ENR-50 composites with various BT loadings..... 131
5.10	Temperature dependence of (a) ϵ' and (b) ϵ'' of BT/ENR-50 composite with 10 vol% BT at several frequencies (\square) 1, (\circ) 10, (\triangle) 100, (∇) 1k and (\diamond) 10k Hz..... 133
5.11	Temperature dependence of (a) ϵ' and (b) ϵ'' of BT/ENR-50 composite with 20 vol% BT at several frequencies (\square) 1, (\circ) 10, (\triangle) 100, (∇) 1k and (\diamond) 10k Hz..... 133

LIST OF FIGURES

Figures	Page
5.12 Temperature dependence of (a) ϵ' and (b) ϵ'' of BT/ENR-50 composite with 30 vol% BT at several frequencies (\square) 1, (\circ) 10, (\triangle) 100, (∇) 1k and (\diamond) 10k Hz.....	134
5.13 Temperature dependence of (a) ϵ' and (b) ϵ'' of BT/ENR-50 composite with 50 vol% BT at several frequencies (\square) 1, (\circ) 10, (\triangle) 100, (∇) 1k and (\diamond) 10k Hz.....	134
5.14 Frequency dependence of (a) ϵ' and (b) ϵ'' of BT/ENR-50 composites with various BT loadings	135
5.15 Schematic representations the structure of ceramic-polymer composite....	136
5.16 Experimental and theoretical values from different models of permittivity (at 1 kHz) of composite as a function of BT content in BT/ENR-50 composites.....	138
5.17 Unit cell representations for composites (a) 0-3 connectivity (b) 3-3 connectivity and (c) containing both 0-3 and 3-3 connectivity.....	139
5.18 Temperature dependence of M'' of ENR-50 composites with (a) 10, (b) 20, (c) 30 and (d) 50 vol% BT at (\square) 1, (\circ) 10, (\triangle) 100, (∇) 1k and (\diamond) 10k Hz	140
5.19 Frequency dependence of M'' of BT/ENR-50 composites with various BT loadings.....	141
5.20 Relaxation time of α -process and conduction process as a function of reciprocal temperature for BT/ENR-50 composites with various amounts of BT. Dash and solid lines represent the overall best fits according to Equation 3.19 and 3.20, respectively.....	142

Figures	Page
CHAPTER 6: Conductive Elastomer Composites based on CB/ENR-50	
Composites.....	149
6.1 Rheographs of (a) HAF and (b) ECF filled ENR-50 at various CB loading levels.....	151
6.2 Stress-strain curves of (a) HAF and (b) ECF filled ENR-50 with various HAF and ECF loadings.....	152
6.3 (a) Tensile strength and (b) elongation at break as a function of CB loading in ENR-50 vulcanizates.....	154
6.4 Vulcanizate properties as a function of the extent of vulcanization.....	154
6.5 Kraus plot of HAF and ECF filled ENR-50.....	155
6.6 The physical network of (a) HAF and (b) ECF in rubber.....	156
6.7 (a) Young's modulus and (b) hardness versus CB loading in ENR-50.....	157
6.8 Temperature dependence of E' and $\tan \delta$ of (a) HAF and (b) ECF filled ENR-50 at various HAF and ECF loadings.....	159
6.9 (a) E' at -60 and 25°C and (b) glass transition temperature as a function of CB content in HAF/ENR-50 and ECF/ENR-50 composites.....	159
6.10 Dielectric permittivity (ϵ') at room temperature as a function of frequency for (a) HAF/ENR-50 (b) ECF/ENR-50 composites.....	161
6.11 Dielectric loss factor (ϵ'') at room temperature as a function of frequency for (a) HAF/ENR-50 (b) ECF/ENR-50 composites	162
6.12 AC conductivity at room temperature as a function of frequency for (a) HAF and (b) ECF filled ENR-50 vulcanizate with various CB loading levels. The solid line is a fit of Equation 6.3.....	163
6.13 DC conductivity (σ_{DC}) versus CB loading levels of HAF and ECF composites.....	165
6.14 The formation of conductive network of two different CB structures.....	166
6.15 The conductivity for ENR-50 filled with HAF and ECF as function of $(p-p_c)$	167

LIST OF FIGURES

Figures	Page
CHAPTER 7: Phase Development and Miscibility of PVDF/ENR-50 Simple Blends.....	173
7.1 SEM micrographs of (a) PVDF/ENR-25 and (b) PVDF/ENR-50 blends.....	176
7.2 Stress-strain curves of PVDF, PVDF/ENR-25 and PVDF/ENR-50 blends...	178
7.3 DSC (a) cooling and (b) heating sweeps for PVDF, PVDF/ENR-25 and PVDF/ENR-50 blends.....	179
7.4 Temperature dependence of E' and $\tan \delta$ of PVDF at 1 Hz.....	180
7.5 Temperature dependence of E' and $\tan \delta$ of PVDF, PVDF/ENR-25 and PVDF/ENR-50.....	182
7.6 Schematic diagram of morphology of compatibilized PVDF/ENR blends....	183
7.7 Proposed mechanism for interfacial reaction between PVDF and ENR.....	184
7.8 Infrared spectra of neat ENR-25, ENR-50, PVDF, extracted ENR-25 and extracted ENR-50.....	185
7.9 Temperature dependence of (a) ϵ' and (b) ϵ'' of PVDF at several frequencies (\square) 1, (\circ) 10, (\triangle) 100, (∇) 1k and (\diamond) 10k Hz.....	186
7.10 Temperature dependence of (a) ϵ' and (b) ϵ'' of PVDF/ENR-25 blend at several frequencies (\square) 1, (\circ) 10, (\triangle) 100, (∇) 1k and (\diamond) 10k Hz.....	187
7.11 Temperature dependence of (a) ϵ' and (b) ϵ'' of PVDF/ENR-50 blend at several frequencies (\square) 1, (\circ) 10, (\triangle) 100, (∇) 1k and (\diamond) 10k Hz.....	187
7.12 Activation plot for segmental motion (square symbols) of PVDF, ENR-25 and ENR-50 and α -relaxation (circle symbols) of PVDF.....	188
7.13 Temperature dependence of M'' of (a) PVDF (b) PVDF/ENR-25 and (c) PVDF/ENR-50 at several frequencies (\square) 1 Hz, (\circ) 10 Hz, (\triangle) 100 Hz, (∇) 1 kHz and (\diamond) 10 kHz.....	189
7.14 Activation plot for conductivity process for ENR-25, ENR-50 and their blends.....	190
7.15 SEM micrographs of PVDF/ENR-50 simple blend with different blend ratios (a) 80/20, (b) 70/30, (c) 60/40, (d) 50/50, (e) 40/60, (f) 30/70 and (g) 20/80.....	192

LIST OF FIGURES

Figures	Page
7.16 Stress-strain curves of PVDF/ENR-50 blend with different blend ratios.....	194
7.17 Mechanical properties as a function of ENR-50 content in PVDF/ENR-50 simple blends.....	195
7.18 DSC (a) cooling and (b) heating sweeps for PVDF/ENR-50 blends.....	197
7.19 Thermal characteristics from DSC curves as a function of ENR-50 content.....	198
7.20 Temperature dependence of E' and $\tan \delta$ for PVDF/ENR-50 blend with different blend ratios	199
7.21 Glass transition temperature (T_g) of PVDF and ENR-50 phases as a function of ENR-50 content in PVDF/ENR-50 blend.....	201
7.22 Storage modulus and $\tan \delta$ as a function of ENR-50 content in PVDF/ENR-50 blends.....	202
7.23 Temperature dependence of (a) ϵ' and (b) ϵ'' of 80/20 PVDF/ENR-50 blend at frequency (\square) 1, (\circ) 10, (\triangle) 100, (∇) 1k and (\diamond) 10k Hz.....	203
7.24 Temperature dependence of (a) ϵ' and (b) ϵ'' of 30/70 PVDF/ENR-50 blend at frequency (\square) 1, (\circ) 10, (\triangle) 100, (∇) 1k and (\diamond) 10k Hz.....	203
7.25 Temperature dependence of $\tan \delta$ obtained from DMA and DEA for the blend with different blend compositions.....	204
7.26 Temperature dependence of M'' of (a) 80/20 and (b) 30/70 PVDF/ENR-50 blends at several frequency (\square) 1, (\circ) 10, (\triangle) 100, (∇) 1k and (\diamond) 10k Hz.....	205
7.27 Relaxation time of glass rubber transitions and conductivity process as a function of reciprocal temperature for PVDF/ENR-50 blends with various blend ratios.....	206

LIST OF FIGURES

Figures	Page
CHAPTER 8: Selective Localization of Barium Titanate in PVDF/ENR-50	
Blends.....	215
8.1 SEM micrographs of PVDF/ENR-50 simple blends (a) 80/20-0BT, (b) 80/20-5BT, (c) 50/50-0BT and (d) 50/50-5BT.....	217
8.2 Mixing torque of pure PVDF and ENR-50 at a rotor speed 50 rpm and temperature 180°C.....	218
8.3 Schematic diagram illustration of selective localization of BT in PVDF/ENR-50 simple blends.....	219
8.4 SEM micrographs of dynamically cured PVDF/ENR-50 blend at blend ratio (a) 80/20 and (b) 50/50.....	220
8.5 SEM micrographs of dynamically cured PVDF/ENR-50 blend containing 5 vol% BT prepared by BDV method with (a and c) PVDF/ENR-50 = 80/20 and (b and d) PVDF/ENR-50 = 50/50.....	221
8.6 SEM micrographs of dynamically cured PVDF/ENR-50 blend containing 5 vol% BT prepared by ADV method for (a) PVDF/ENR-50 = 80/20 and (b) PVDF/ENR-50 = 50/50.....	222
8.7 Schematic diagram for dynamically cured of BT/PVDF/ENR-50 blend prepared by BDV method.....	223
8.8 Schematic diagram for dynamically cured of BT/PVDF/ENR-50 blend prepared by ADV method.....	224
8.9 Stress-strain curves of (a) simple and (b) dynamically cured PVDF/ENR-50 blends with and without BT at 80/20 and 50/50 blend ratios.....	225
8.10 Temperature dependence of E' and $\tan \delta$ of 80/20 PVDF/ENR-50 (a) simple blend and (b) dynamically cured blend with and without BT.....	227
8.11 Temperature dependence of E' and $\tan \delta$ of 50/50 PVDF/ENR-50 (a) simple blend and (b) dynamically cured blend with and without BT.....	228
8.12 Frequency dependence of (a, b) ϵ' and (c, d) ϵ'' at room temperature of simple blends (SB) and dynamically cured PVDF/ENR-50 blends (DV) with the blend ratios of (a, c) 80/20 and (b, d) 50/50.....	231
8.13 Loss factor (ϵ'') of PVDF and ENR-50 at room temperature.....	233

LIST OF FIGURES

Figures	Page
8.14 Permittivity (ϵ') at 1 kHz of PVDF/ENR-50 (a) simple blend and (b) dynamically cured blend with and without BT.....	233
8.15 SEM micrographs of dynamically cured PVDF/ENR-50 blend containing various amounts of BT.....	235
8.16 Stress-strain curves of dynamically cured PVDF/ENR-50 blend with blend ratios of (a) 80/20 and (b) 50/50 containing various BT loadings.....	237
8.17 (a) Tensile strength and (b) elongation at break of dynamically cured 80/20 and 50/50 PVDF/ENR-50 blend containing various BT loadings.....	237
8.18 Temperature dependence of E' and $\tan \delta$ of dynamically cured (a) 80/20 and (b) 50/50 PVDF/ENR-50 blends with various BT loadings.....	240
8.19 Relative storage modulus at 25°C as a function of BT loading.....	241
8.20 Frequency dependence of ϵ' and ϵ'' at room temperature of dynamically cured PVDF/ENR-50 blends with various BT loadings	243
8.21 (a) Permittivity (b) loss factor and (c) loss tangent at frequency 1 kHz of dynamically cured PVDF/ENR-50 blends as a function of BT loading.....	244

LIST OF ABBREVIATIONS

Abbreviations	Description
AC	Alternative current
ACM	Acrylic rubber
ADS	Air dried sheets
ADV	After dynamic vulcanization
ASTM	American Society for Testing and Materials
ATR-FTIR	Attenuated total reflectance-Fourier transform infrared
BaCO₃	Barium carbonate
BaTiO₃	Barium titanate
BDS	Broadband dielectric spectroscopy
BDV	Before dynamic vulcanization
BET	Brunauer–Emmett–Teller theory
BSE	Back-scattering electron
BN-BT	Bismuth sodium barium titanate
BT	Barium titanate
CB	Carbon black
CCB	Conductive carbon black
CNT	Carbon nanotube
CPC	Conductive polymer composites
CR	Chloroprene rubber
CRI	Cure rate index
DBP	Dibutyl phthalate
DC	Direct current
DEA	Dielectric analysis
DMA	Dynamic mechanical analysis
DMF	Dimethylformamide
DSC	Differential scanning calorimeter

LIST OF ABBREVIATIONS

Abbreviations	Description
DV	Dynamically vulcanized blend
ECF	Extra conductive furnace
EMA	Ethylene methyl acrylate
ENR	Epoxidized natural rubber
EPDM	Ethylene propylene diene rubber
EPR	Ethylene propylene rubber
ETD	Everhart-Thornley detector
EVA	Ethylene vinyl acetate
FTIR	Fourier transform infrared
FWHM	Full width at half maximum
HAF	High abrasion furnace
JCPDS	Joint committee on powder diffraction standards
LEDPNR	Deproteinized epoxidized natural rubber
MBT	Mercaptobenzothiazole
MEMS	Microelectromechanical systems
MLCC	Multi-layer ceramics capacitors
MNR	Maleated natural rubber
MWCNT	Multiwall carbon nanotube
MWS	Maxwell-Wagner-Sillars
NBR	Acrylonitrile butadiene rubber
NMR	Nuclear magnetic resonance
NR	Natural rubber
PA-6	Polyamide-6
PA-12	Polyamide-12
PBT	Poly(butylene terephthalate)
PbO	Lead oxide
PCL	Poly(ϵ -caprolactone)
PE	Polyethylene
PEI	Polyetherimide

LIST OF ABBREVIATIONS

Abbreviations	Description
Phr	Part per hundred
PLA	Poly lactide
PLLA	Poly(L-lactide)
PMMA	Poly(methyl methacrylate)
PMN-PT	Lead magnesium niobate-lead titanate
PP	Polypropylene
PS	Polystyrene
PT	Lead titanate
PU	Polyurethane
PVA	Poly(vinyl alcohol)
PVC	Poly(vinyl chloride)
PVDF	Poly(vinylidene fluoride)
P(VDF-HFP)	Poly[(vinylidene fluoride)-co-hexafluoro-propylene]
P(VDF-TrFE)	poly[(vinylidene fluoride)-co-trifluoroethylene]
PZT	Lead zirconate titanate
SB	Simple blends
SE	Secondary electron
SEM	Scanning electron microscope
TEM	Transmission electron microscope
TiO₂	Titanium(IV) oxide
TPE	Thermoplastic elastomers
TPNR	Thermoplastic natural rubber
TPO	Thermoplastic polyolefin
TPU	Thermoplastic polyurethane
TPV	Thermoplastic vulcanizates
vCD	Low voltage high contrast detector
VFT	Vogel-Fulcher-Talman
XRD	X-ray diffraction technique
ZnO	Zinc oxide

LIST OF SYMBOLS

Symbols	Description	Unit
χ	Flory-Huggins interaction parameter	-
δ	Solubility parameter	MPa
ϵ_B	Strain at break (elongation at break)	%
ϵ_c	Dielectric permittivity of ceramic	-
ϵ_{eff}	Dielectric permittivity of composite	-
ϵ_p	Dielectric permittivity of polymer	-
ϵ^*	Complex permittivity	-
ϵ'	Dielectric permittivity (dielectric constant)	-
ϵ''	Dielectric loss	-
ϵ''_{dc}	Dielectric loss due to conduction loss	-
ϵ''_D	Dielectric loss due to dipole orientation	-
ϵ''_{MW}	Dielectric loss due to interfacial polarization	-
ϵ_0	Vacuum permittivity (8.854×10^{-12} F/m)	F/m
γ	Interfacial tension	mN/m
γ^d	Dispersive part of surface tensions	mN/m
γ^p	Polar part of surface tensions	mN/m
φ_c	percolation threshold	vol%
φ	Volume fraction of filler	vol%
ρ	Density	g/cm ³
σ_{AC}	AC conductivity	S/cm
σ_B	Stress at break (Tensile strength)	MPa
σ_c	Conductivity of the conductive filler	S/cm
σ_{DC}	DC conductivity	S/cm
σ_{eff}	Effective conductivity of the composite	S/cm
σ_m	Conductivity of the polymer	S/cm
τ	Relaxation time	s
ω	Angular frequency	rad/s

LIST OF SYMBOLS

Symbols	Description	Unit
B	Activation temperature	K
C	Capacitance	F
E	Young's modulus	MPa
E_a	Activation energy	eV
E'	Storage modulus	MPa
E''	Loss modulus	MPa
F_B	Force at break	N
ΔG_m	Free energy of mixing	-
ΔH_m	Change in enthalpy of mixing	J
ΔH_m	Melting enthalpy of sample	J/g
ΔH_0	Theoretical enthalpy for 100 % crystalline	J/g
k	Boltzmann constant (8.617×10^{-5} eV/K)	eV/K
L_0	Initial length	mm
ΔL	Change in length	mm
M^*	Complex electric modulus	-
M'	Real part of electric modulus	-
M''	Imaginary part of electric modulus	-
M_H	Maximum torque	dN.m
$M_H - M_L$	Torque difference or delta torque	dN.m
M_L	Minimum torque	dN.m
p	Filler concentration	phr
p_c	percolation threshold	phr
R	Gas constant	J/K.mol
ΔS_m	Change in entropy of mixing	J/K
$\tan \delta$	Loss tangent	-
t_{c90}	Optimum time	min
T_c	Crystallization temperature	°C
T_m	Melting temperature	°C
T_g	Glass transition temperature	°C
t_{st}	Scorch time	min

CHAPTER 1

INTRODUCTION

The research described here was performed according to the frame work “Agreement for international joint supervision of a thesis” between the Prince of Songkla University (PSU, Thailand) and the University Claude Bernard Lyon 1 (UCBL, France). The research was performed in a collaboration between Department of Rubber Technology and Polymer Science, Faculty of Science and Technology, Prince of Songkla University (PSU, Thailand) and Le laboratoire IMP@Lyon1 (Ingénierie des Matériaux Polymères), UMR CNRS 5223, University Claude Bernard Lyon 1 (UCBL, France) with the financial support of the Royal Golden Jubilee Ph.D. Program (Grant No. PHD/0245/2549) and French Embassy in Thailand.

1.1 Introduction

Natural rubber (NR) based on the *Hevea brasiliensis* is an attractive material with the most valuable elastomer and a renewable resource. NR molecular chain consists of *cis*-1,4-polyisoprene which exhibit interesting physical properties, excellent flexibility and high mechanical strength. This is due to the ability to crystallize under stretching, leading to be typically used in industrial applications. However, NR contains conjugated double bonds with low polarity. Therefore, application of natural rubber is limited, mainly due to degradation and incompatibility of natural rubber with other materials. That is, NR has to be mixed with fillers and other polymers. To overcome these limitations, double bonds in NR molecules are replaced by polar functional groups. This causes to improvement of several properties while retaining the inherent excellent physical properties of NR. The modification leads to extending the usage of NR in many fields such as composites and blends. Epoxidized natural rubber (ENR) is one of the modified natural rubber by reacting NR with peracid in a latex state. The presence of epoxide groups in ENR molecules would improve the drawback of unmodified NR such as

enhanced polarity and compatibility with other polar materials, good oil resistance and low air permeability. Therefore, the use of epoxidized natural rubber instead of unmodified NR would be of interest in elaboration of polymer composites and polymer blends.

In recent years, polymer composites and polymer blends have been used extensively in various applications. Addition of filler into polymeric matrix and blending of polymers are well-established ways to improve the properties which cannot be achieved from the individual component. It is an effective cost and economic approach to produce a new material with desired properties.

Carbon black and silica are the most widely used fillers in thermoplastic and rubber industries to significantly improve modulus, tensile strength, tear resistance, abrasion resistance and dynamic mechanical properties. Recently, developments of polymer composites with high permittivity and high conductivity are attracting for electrical application. Such materials could be fabricated by using high permittivity ceramic and conductive fillers in the polymer matrix. Polymer composite based on ceramic has infrequently been reported and interested. Ceramic-polymer composite is a combination of inorganic piezoelectric ceramic and flexible polymer to form flexible piezoelectric composite. This provides unique material which exhibit high permittivity, low dielectric loss and good flexibility. Among ferroelectric ceramic, barium titanate (BaTiO_3) has been extensively employed as a ceramic filler as it can induce high permittivity in composite films. Meanwhile, the use of conductive filler such as carbon black can improve electrical conductivity when the filler concentration reach percolation threshold. At this concentration, the conductive cluster is connected as three-dimensional network in polymer matrix.

The blending of polymer has been studied extensively over the past decades in order to achieve a set of desired properties and high performances for specific applications. The thermoplastic elastomeric combination is an interesting and new class of material, so-called "Thermoplastic Elastomer" (TPE). The TPE consists of a rigid thermoplastic phase and a soft elastomer phase, resulting in a combination of the excellent elastic properties of rubber with melt processability of thermoplastic. The properties of TPE based on plastic-rubber blend depend on phase morphology and miscibility between two phases, mainly due to phase separation of the blend. There are

two types of blending technique to prepare TPE: simple blend and dynamic vulcanization. The simple blend (SB) means blending of plastic and rubber without cross-linker. The dynamic vulcanization is a blend with cross-linker to vulcanize rubber phase during melt mixing. The thermoplastic elastomer prepared by dynamic vulcanization is usually called *thermoplastic vulcanizate* (TPV).

1.2 Scope of thesis

The present work was focused on studying structure-properties relationship of the natural rubber filled with ceramic and carbon black fillers as well as thermoplastic elastomer based on blending of epoxidized natural rubber and poly(vinylidene fluoride). The research work was divided into two stages.

The first stage was to prepared gum and composite of natural rubber vulcanizate. Unmodified natural rubber and epoxidized natural rubber (ENR) were chosen to study molecular mobility and dielectric properties. The presence of polarity functional groups were speculated to affect the molecular dynamic of natural rubber. Furthermore, the enhancement for dielectric permittivity of epoxidized natural rubber was investigated by incorporation of barium titanate. Conductive elastomer composite based on epoxidized natural rubber was also prepared to obtain the conductive composite with high mechanical properties and low percolation threshold.

The second stage was to study blending of poly(vinylidene fluoride) (PVDF) and epoxidized natural rubber (ENR). The PVDF was chosen due to high dielectric constant of PVDF but the ENR was contributed to good compatibility with polar polymers. Effects of epoxidation level in ENR molecules and blend proportion on phase development and miscibility of thermoplastic elastomer were investigated. Furthermore, composite based on binary blend of PVDF/ENR-50 containing BT particles were also studied. The objective for incorporation of BT in the blend was to understand the selective localization of BT particle in the simple and dynamically cured PVDF/ENR-50 blends.

1.3 The aim of thesis

The aim of this research work was to develop a novel natural rubber composite based on ferroelectric ceramic and conductive carbon black, and a novel natural rubber blend based on fluoro-polymer by an understanding of the structure-properties relationship. The main aims of the project as listed follows:

1. To study influence of epoxide level in ENR molecules compared with unmodified natural rubber on vulcanizate properties.
2. To study influence of volume fraction for barium titanate on vulcanizate properties of epoxidized natural rubber (ENR-50) composite.
3. To study influence of surface area and structure of carbon black on reinforcement and formation of conductive path in the ENR-50 matrix.
4. To study influence of epoxide level in ENR molecules and blend proportion on various properties of PVDF/ENRs simple blend.
5. To study selective localization of barium titanate particles in simple blend and dynamically cure PVDF/ENR-50 blends with difference blend ratio.
6. To study influence of processing condition of dynamic vulcanization on selective localization of barium titanate particles in dynamically cure PVDF/ENR-50 blend.
7. To study influence of barium titanate loading on various properties of dynamically cure PVDF/ENR-50 blends.

1.4 Novelty of the work

- The molecular mobility and dynamic process of epoxidized natural rubber have been revealed by dielectric analysis. That is, the epoxide groups in the ENR significantly affected dielectric properties of ENR sample.

- The introduction of barium titanate (BT) particles in epoxidized natural rubber (ENR-50) resulted in an increase of dielectric permittivity as high as ceramic-polymer composite elsewhere in literature.

- Conductive elastomer composite based on extra conductive carbon black and epoxidized natural rubber with lowering percolation threshold was observed.

- Thermoplastic elastomer based on poly(vinylidene fluoride) and epoxidized natural rubber blend was prepared which found to be as a compatibilized blend.
- BT particles were incorporated into thermoplastic elastomer blend and the selective localization of BT in the blend is caused by kinetic effect and mixing sequence.

1.5 The thesis outline

This present thesis is concerned with the studies of the composites and blends based on natural rubber. The thesis is divided into several chapters which are structured to bring forth the structure-processing-property relationships, as follows:

Chapter 2 provides the theoretical background and fundamental understanding of ceramic-polymer composites, conductive polymer composites and thermoplastic-elastomer blends, particularly those forms using multiphase polymer matrices. The chapter also presents an introduction of natural rubber, epoxidized natural rubber, poly(vinylidene fluoride) and their composites and blends.

Chapter 3 describes the materials and experimental procedure that are used throughout the study. The material fabrication and characterization methods are presented. Also, the regarding microstructure analysis of the fabricated composites and blends study structure-properties relationship are described.

Chapter 4 discusses influence of epoxidation level in epoxidized natural rubber on the gum vulcanizate properties in terms of cure characteristic, mechanical properties, dynamic mechanical properties and dielectric analysis.

Chapter 5 describe the properties of flexible high permittivity materials based on ceramic-polymer composites of barium titanate (BT) and epoxidized natural rubber with 50 mol% epoxide (ENR-50). Mixture of BT and ENR-50 was prepared by melt mixing process to obtain the ceramic-polymer composites with 0-3 connectivity. The dielectric behavior of the composites with different proportions of the ceramic-polymer phases has been studied. The relative permittivity from the experiment was compared to the theoretical models. Furthermore, morphological, static and dynamic mechanical properties of the composites are discussed.

Chapter 6 is devoted to characterization of carbon black/epoxidized natural rubber composite with two types of carbon black. The role of surface area and structure of carbon black to form bound rubber at carbon black surface are related to mechanical properties (i.e., Young's modulus, tensile strength and elongation at break). The electrical properties of the conductive composites were also investigated over a wide ranges of composition. Influence of two different types of carbon black structures on percolation threshold of CB/ENR-50 composites was also discussed.

Chapter 7 describes the preparation of thermoplastic elastomer based poly(vinylidene fluoride) (PVDF) and epoxidized natural rubber blend. This deals with PVDF/ENRs simple blend using two different epoxide contents in ENR molecules (i.e., 25 and 50 mol%) with the same blend proportion (50/50). The effect of epoxidation level in ENR on morphological and other related properties is focused. Then, ENR-50 was selected to prepare PVDF/ENR-50 simple blend with different blend proportions. The phase development and miscibility of the blends are discussed.

Chapter 8 discusses the simple blend and dynamically vulcanized PVDF/ENR-50 blends containing BT particles by first focusing on selective localization of barium titanate particles (5 vol%) in the simple and dynamically vulcanized blends. The selective localization of particles are strongly dependent on viscosity of the blend components. Two different mixing sequences were exploited in dynamically cured blend. The morphological properties of the blend were also affected by localization of BT in the blend which was investigated by scanning electron microscopy (SEM). The dynamically vulcanized PVDF/ENR-50 blend with different volume fractions of BT is described in terms of morphological, mechanical, dynamic mechanical and dielectric properties of binary polymer composite.

CHAPTER 2

LITERATURE REVIEW

2.1 Polymer composites

Polymer composites are commonly defined as heterogeneous system of polymers containing inorganic or organic filler in various forms (i.e., spherical and fiber) with either micro or nano in size. The fillers are embedded into polymer to form material which consists of two or more components. This causes modifying of properties for individual component which provides opportunity to prepare new application and commercial value [1]. In the last decade, polymer composites are attractive materials and they have been intensively studied due to light weight, ease of processability and excellent properties. In fact, there are several reasons to apply fillers and reinforcements into the viscoelastic polymer materials. Firstly, incorporation of filler into polymer in order to upgrade product performance, including physical properties (i.e., conductivity, dielectric constant and density), mechanical properties (i.e., strength and modulus), rheological properties (i.e., viscosity and viscoelasticity). Polymer composites are widely used in several applications such as automotive, tires, packaging and electronic product [2, 3]. Incorporation of filler in polymer has been prepared and studied in the past for reinforcing polymer and elastomer. A variety of theoretical and experimental studies have been reported on the reinforcement effect in terms of macroscopic mechanical properties [4]. For example, reinforcement effect of carbon black and silica, the most commonly used reinforcing fillers, led to the development of many high engineering performance products for elastomers and plastic industries [2, 5-9]. Secondly, fillers are used for economic reason which is to reduce the cost of production [2, 3].

Recently, there has been an increasing interest in the preparation of polymer composites for electronic applications with high dielectric permittivity. These composite offers high and predictable dielectric permittivity, low dielectric loss, mechanical flexibility

as well as easy fabrication [4, 10]. Generally, polymers are materials with low dielectric permittivity ($\epsilon' = 2$ to 10) [10], as summarized in Table 2.1. They do not meet the application requirements of high capacity, especially non polar polymer which has no permanent dipole moments. The improvement in dielectric permittivity of polymer can be obtained by mixing the insulating polymer with high permittivity ceramics fillers ($\epsilon' \cong 1000$ to 2000) and very low loss factor (i.e., barium titanate (BT) [11], bismuth sodium barium titanate [12] and lead zirconate titanate (PZT)) [13] etc. Another approach to increase permittivity of polymer is to utilize conductive fillers such as carbon black, metal particle and carbon nanotube. However, this approach gets very high dielectric loss because the filler particles can easily form a conductive path in the composite. Conductive polymer composites (CPC) can be obtained when the filler concentration approaches the percolation threshold [14].

Table 2.1 Dielectric constant (ϵ') and loss tangent ($\tan \delta$) of some polymers

Polymers	Frequency	ϵ'	$\tan \delta$	Ref.
Poly(vinylidene fluoride) PVDF	1 kHz	10.5	0.026	[15]
Poly(vinylidene fluoride-co-trifluoro ethylene) ^a	1 kHz	11.0	0.184	[12]
Polyethylene (PE)	1 MHz	2.3	0.0001	[16]
Epoxy*	-	4.2	0.0082	[17]
Nylon-6 (PA6)	1 kHz	8.0	0.10	[18]
Natural rubber (NR)	1 kHz	2.7	0.002	[19]
Ethylene propylene rubber (EPR)	1 kHz	3.2	0.0066	[19]
Chloroprene rubber (CR)	1 kHz	6.5	0.03	[19]
Polyurethane (PU)	1 kHz	5.0	0.015	[19]

^a P(VDF-TrFE) VDF/TrFE : 70/30 mol%, * no record of frequency

2.1.1 Ceramic-polymer composites

Nowadays, ceramic-polymer composites have been developed to improve dielectric permittivity of the individual polymers because they generally suffer from low dielectric permittivity. However, they are easily processed with high ability to stretch [4, 10]. These types of composites are possible to combine desirable characteristics such as mechanical flexibility, chemical stability and processing possibilities of the polymer and the high dielectric constant (permittivity), piezoelectricity and stiffness of ceramics [20-22].

2.1.1.1 Ferroelectric ceramics

Ferroelectric ceramics were first discovered in the early 1940s with the discovery of high dielectric constant in barium titanate. Ferroelectric materials have permanent dipoles that usually interact to give a polarization in the absence of an applied electric field. They do not lose all of their ionic polarization when the field is removed due to the coupling between adjacent dipoles. This behavior is a key role for the ferroelectricity. While paraelectric materials cannot be left with a residual polarization once the field is removed due to the lack of mobile charged atoms. Ferroelectric ceramic based on perovskite structure is the most important category i.e., Barium titanate (BaTiO_3 , BT), lead zirconate titanate (PZT) and lead titanate [23, 24]. Barium titanate is the first compound with formula ABO_3 , which called perovskite mineral which exhibits ferroelectric behavior. The other ceramics in the perovskite families include SrTiO_3 , PbTiO_3 and KNbO_3 . The structure of perovskite structure (ABO_3) (i.e., BaTiO_3) is given in Figure 2.1. Ceramic materials with a perovskite structure are very significant electronic materials because they are ferroelectric, piezoelectric and have high dielectric constant [23, 25].

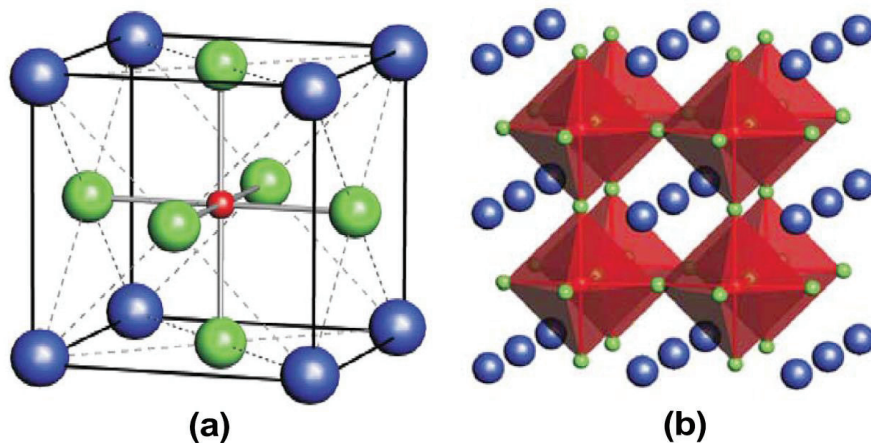


Figure 2.1 (a) Cubic perovskite-type structure ABO_3 (b) another view of the ABO_3 structure [25]

For example, BaTiO_3 unit cell consists of a network of oxygen octahedral with Ti^{4+} ion in the center of the cube, Ba^{2+} ion on the cube corners and O^{2-} ions at the face centers (Figure 2.1(a)) [24]. Ferroelectric BaTiO_3 possesses a high dielectric constant at room temperature which is higher than 1500 and a low dielectric loss. BaTiO_3 -based composition has been achieved by addition of special additive to increase dielectric

constant in the range of 100000. Because of these good characteristics, BT nowadays has become more and more important ceramics materials [24, 25].

2.1.1.2 Connectivity of ceramic and polymer in composites

In order to meet desired properties of ceramic-polymer composites, it is usually not only means to choose the appropriate pair materials in a particular way, but their properties are also governed by the composite structure arrangement or connectivity concept. The connectivity of the two-component composites with planar interfaces was first introduced by Newnham *et al.* [26]. Connectivity concept describes the spatial arrangement of two components in a composite and each phase could be self-connected in either one, two or three dimensions. Two digits of $\alpha\beta$ were used to indicate phase connectivity of ceramic-polymer composites. The first digit refers to the number of directions in which the piezoelectrically active phase (filler) and the second shows the continuity directions of an inactive phase (polymer). There are 10 connectivity patterns for a two-phase (diphasic) system; (0-0), (0-1), (0-2), (0-3), (1-1), (1-2), (2-2), (1-3), (2-3), and (3-3). Based on this connectivity concept, an array of piezoelectric ceramic/polymer composites has been developed, as shown in Figure 2.2 [20, 27-29].

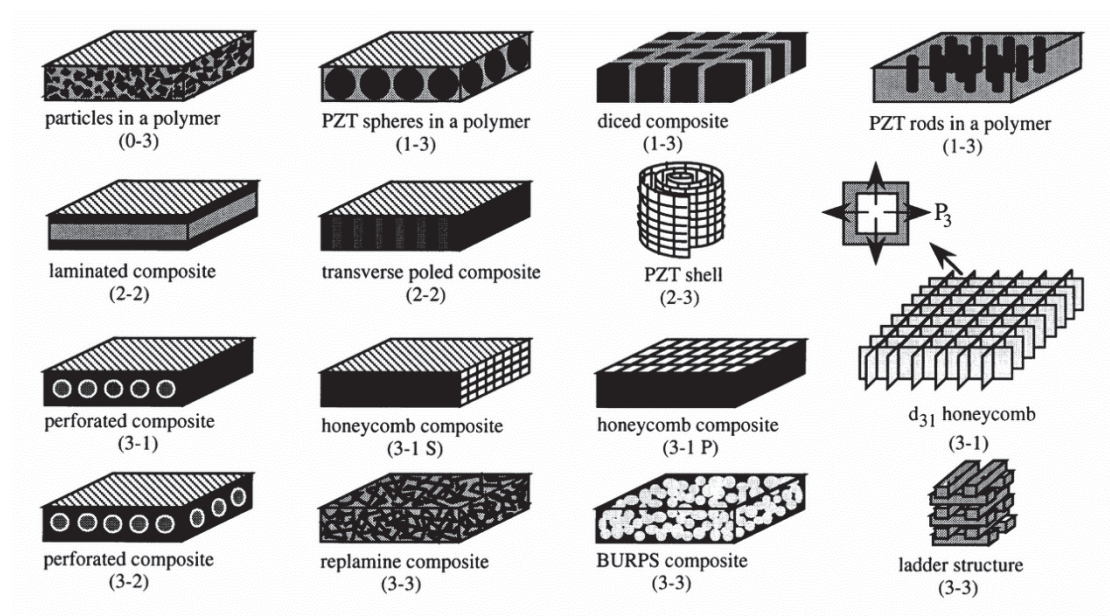


Figure 2.2 Connectivity of constituent phases in piezoelectric ceramic-polymer composites [28, 29]

2.1.1.3 0-3 connectivity composite and their fabrication

The 0-3 composite consists of random ceramic particles embedded in the three-dimensionally connected polymer matrix. This connectivity can be easily prepared and is one of the most common composites type. Its ease fabrication in a variety of forms including large flexible sheets allows mass production at a relatively low cost [11, 20, 27, 28]. The compounding can be prepared by first melting or softening polymer in a hot rolling machine. Ceramic powder is then gradually added during mixing until a reasonable blend is obtained. This composite can also be prepared through the solution containing polymer and ceramic with dispersed using an ultrasonic homogenizer. The composite film is finally fabricated by casting and then evaporation solution of mixture on the plates [20].

There are several reports on the dielectric properties of ceramic–polymer composites. Poly(vinylidene fluoride) or (PVDF) [11, 30-32] and its copolymer i.e., poly(vinylidene fluoride-co-trifluoroethylene) or P(VDF-TrFE) [12, 33] and poly(vinylidene fluoride-co-hexafluoro-propylene) or P(VDF-HFP) [13, 34, 35] have been recognized as the polymer matrix due to their relatively high dielectric and piezoelectric properties. Dielectric properties of the composites have been studied in order to establish the mixing rules of the dielectric activity of the composites which is dependent on the volumetric fraction. Mao *et al.* [11] demonstrated that dielectric permittivity of BT/PVDF reached a maximum value of 93 by using the particle size around 80-100 nm and 60 vol% of BT. Dang *et al.* [30] studied 0-3 BT/PVDF nanocomposites which were prepared via natural adsorption on the dielectric properties of the system. The dielectric permittivity of nanocomposites was found to increase with increasing loading of barium titanate. The dielectric permittivity of the composite with 50 vol% of BT measured at 1 kHz was 40.74. Furthermore, a relative high permittivity of 5000 has been reported by Ghallabi *et al.* [36] for addition of BT and multiwall carbon nanotubes (MWCNT) into PVDF matrix. This material is a good candidate for embedded capacitor applications. Wegener *et al.* [13] prepared 0-3 PZT/P(VDF-HFP) composites by solvent casting method. The improvement in permittivity and piezoelectric coefficient were observed with incorporation of PZT. The maximum of both values was 64.2 (0.58 PZT) and 11.3 pC N⁻¹ (0.48 PZT), respectively. Besides, the ceramic-polymer composite based soft elastomer was also studied by using silicone rubber as polymer matrix. Gallone *et al.* [37] studied on dielectric and mechanical properties of lead magnesium niobate–lead titanate (PMN-PT)/silicone rubber. The

dielectric constant and loss factor regularly increase with increasing the filler content, while a good stretchability is still retained. However, the use of lead-based ceramics i.e., lead titanate (PT), PZT and PMN-PT is not environmentally friendly ceramic. The toxicity of PbO in their main components either during the manufacturing process or after making the device is serious concerns [38]. Several types of ceramic and polymer used for preparation of ceramic-polymer composite have been employed to increase the dielectric permittivity of polymer with the volume fraction of ceramic, as summarized in Table 2.2.

Table 2.2 The dielectric permittivity of 0-3 ceramic polymer composites. The value with “~” is obtained from the graphical representations

Ceramic-polymer composites		Ceramic loading (vol%)	Frequency		ϵ'	$\tan \delta$	Ref.
Ceramic	Polymer						
BT	PVDF	60	1.14 kHz	93	<0.2	[11]	
BT	PVDF	50	10 MHz	~30	0.11	[30]	
BT	P(VDF-HFP)	60	1 kHz	~38	<0.04	[34]	
BT	P(VDF-HFP)	50	1 MHz	37	<0.07	[35]	
BN-BT ^a	P(VDF-TrFE)	30	1 kHz	~30	<0.05	[12]	
PMN-PT	P(VDF-TrFE)	40	1 kHz	~50	-	[33]	
BT	Polyimide	90	1 kHz	125	0.04	[39]	
BT	Polyetherimide	50	1 kHz	37	0.0052	[40]	
PZT	Poly(vinyl chloride)	50	1 kHz	43.7	0.0202	[41]	
BT	Ethylene-vinyl acetate elastomer	50	1 kHz	~14	<0.04	[14]	
PMN-PT	Silicone rubber	30	100 Hz	23.8	-	[37]	
CCTO ^b	PVDF	55	1 kHz	69.4	<0.2	[42]	

^a Bismuth sodium barium titanate ((Bi_{0.5}Na_{0.5})_{0.94}Ba_{0.06}TiO₃), ^b CaCu₃Ti₄O₁₂

2.1.2 Conductive polymer composites

The conductive polymer composite (CPC) is produced from incorporation of conducting filler into insulating polymer matrix. The polymer will become a conductor with addition of a sufficient amount of conductive filler to form a percolating network in the matrix [43, 44]. Electrical conductive fillers used are primarily divided into two groups: metal based filler (i.e., nickel, copper and iron) and carbon based filler (i.e., carbon black, graphite, graphene and carbon nanotube). Conductive polymer composites are widely used in many applications such as electromagnetic interference shielding, electrical industries, electrostatic charge dissipation and other electrical applications [45].

2.1.2.1 Theory of electrical percolation

Dispersion of conductive particles plays an important role in electrical conductivity in CPC. The electrical conductivity as a function of volume fraction of conductive filler is shown in Figure 2.3. The characteristic of conduction depends on the formation of a percolating path of conductive filler through the polymer matrix. The minimum volume fraction of dispersed filler in a polymer matrix to obtain a percolating network is called "*percolation threshold (φ_c)*". After this, the conductivity exhibits a plateau manner (Figure 2.3, Zone III) which corresponds to small increase of conductivity with increasing filler content.

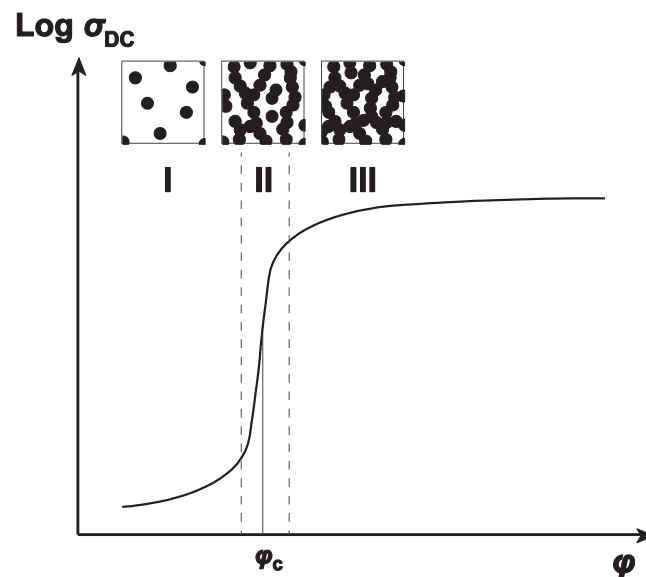


Figure 2.3 Dependence of electrical conductivity (σ) on the volume fraction (φ) of conductive fillers

To explain the percolation threshold phenomena, several models were proposed in literatures. The model proposed by Kirckpatrick [46] and Zallen [47] is quite often used.

- Zone I

Below the percolation threshold ($\varphi < \varphi_c$), the conductive particles remain isolated within the polymer matrix, and the number of contacts between them does not allow the passage of electric current continuously through the sample. The electric conductivity of the composite (σ_{eff}) depends only on the conductivity of the polymer (σ_m), according to the following equation:

$$\sigma_{\text{eff}} = \sigma_m (\varphi_c - \varphi)^{-s} \quad (2.1)$$

where s is a critical exponent whose value depends on the size of the network.

- Zone II

At percolation threshold (φ_c), the conductive particles begin to connect and form conducting paths which improve the flow of current in the composite. This cause a shape increase in conductivity and materials become conductor. The electrical conductivity is expressed by the factor of the matrix (σ_m) and the filler (σ_c):

$$\sigma_{\text{eff}} = \sigma_c \left(\frac{\sigma_m}{\sigma_c} \right)^{\frac{t}{s+t}} \quad (2.2)$$

where t is the critical exponent after percolation

- Zone III

Above percolation threshold ($\varphi > \varphi_c$), the great amount of conductive filler can multiply the number of conductive domain without any significant increase in the path way of electron. Then electrical conductivity reaches a maximum, or the conductivity depends only on the intrinsic electrical conductivity of fillers (σ_c).

$$\sigma_{\text{eff}} = \sigma_c (\varphi - \varphi_c)^t \quad (2.3)$$

The exponent depends on the critical t , which is the same as dimension s in the network.

2.1.2.2 Carbon black

Carbon black (CB) consists of agglomerates of small assemblies of carbon particles called aggregates. The CB structure is similar to disordered graphite that is formed in the incomplete combustion processes of hydrocarbon oil or a gas by which solid carbon condenses from the vapor. Carbon atoms and aromatic radicals react to form layer structures composed of hexagonal carbon rings, which tend to stack in three to four layers, forming crystallographic structures. An agglomerate consists of a number of aggregates hold together with physical interaction as distinguished from the continuous pseudo-graphitic structure of the aggregates [44, 48], as shown in Figure 2.4.

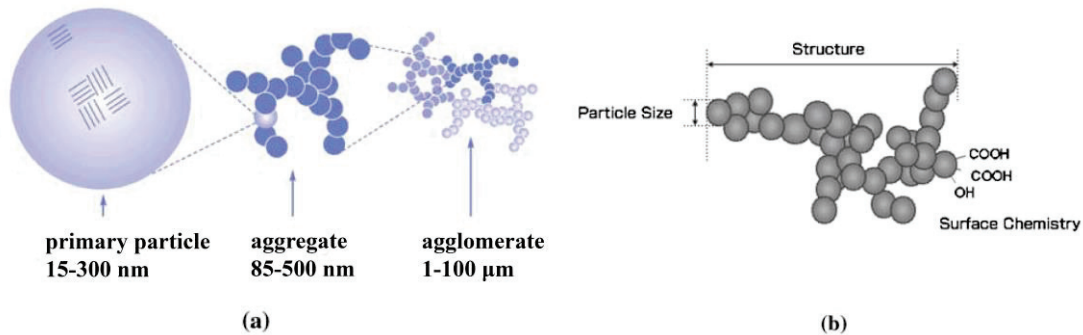


Figure 2.4 Structure of carbon black [49]

An important characteristic of CBs is the diameter of the primary particles which is extremely small (typically less than 300 nm), in particular CBs, may even be up to 500 nm (Figure 2.4). A further characteristic feature is the CB structure. CBs are variously described as “*high structure*” or “*low structure*” that correlates with their spatial extent, the former having larger dimensions than the latter. The CB characterized by primary aggregates composed of many prime particles, with considerable branching and chaining, is referred to as a high-structure CB. If the primary aggregates consist of relatively few prime particles, the CB is referred to as a low-structure CB (Figure 2.5). Their structures are further characterized by the adsorption of dibutyl phthalate (DBP), which measures the amount of oil that can be absorbed by CB. The higher value of DBP absorption indicates “higher structure” [44, 48].

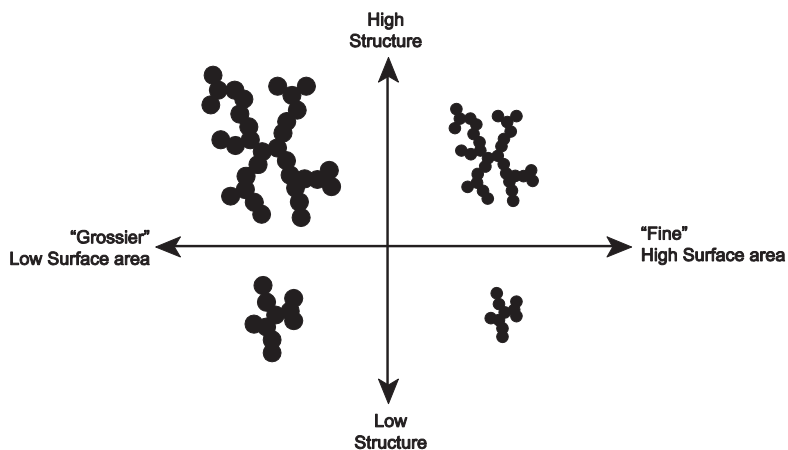


Figure 2.5 Schematic of the concept of CB structure and surface area

When CB is used as a conductive filler, it is characterized by three major properties: particle size (surface area), structure, and surface chemistry. The surface area

can be determined by the BET gas adsorption method or the iodine number test. The higher gas adsorption of the CB particles, the larger the surface area and porosity. High surface area and high porosity are the characteristics of conductive carbon black (CCB) that significantly improve the electric conductivity. In particular, the percolation threshold decreases with increasing specific surface area and/or structure of the CB particles [9, 44]. The particle diameter and the other characteristic (i.e., surface area and DBP absorption) of some types of carbon black that have been used in conducting applications are shown in Table 2.3.

Table 2.3 Properties of selected CBs for electric conductivity [44]

Name	Diameter (nm)	Nitrogen Surface Area (m ² /g)	DBP Absorption (cm ³ /100g)	Volatiles (%)
Black Pearls 2000	12	1500	330	2.0
Vulcan XC 72	30	254	178	1.5
Elftex TP	20	130	98	1.5
Vulcan P	20	140	116	1.4

Generally, percolation threshold of CB filler in elastomer is around 25-30 phr, which is higher as compared with the carbon nanotube (CNT) due to low aspect ratio of CB particle. Ghosh and Chakrabarti [45] found that the conductivity of CCB filled ethylene-co-propylene rubber (EPDM) undergoes a sharp transition over a carbon black loading range of 20 to 35 phr which is taken as the percolation concentration range. Sohi *et al.* [43] also showed that the percolation threshold of CCB filled ethylene vinyl acetate copolymer (EVA) was observed at 30 phr or 0.14 volume fraction of CCB.

Carbon black (CB) also plays an important role in the improvement of the mechanical properties of high performance rubber materials. The reinforcing potential in rubber is mainly attributed to two effects: (i) the formation of a physically bonded flexible filler network and (ii) strong polymer filler couplings. Both of these effects refer to a high surface activity and specific surface of the filler particles. The rubber chains are directly bounded to the CB surface by chemical and physical interaction. These strong bonds are formed very rapidly during mixing of the two components. As displayed in Figure 2.6(a), the rubber chains of the bound rubber are in a transition region (transition layer) connected by entanglements with those of the completely unbound polymer (mobile rubber). The

mobility of polymer segments is greatly restricted near the surface of filler [8, 9, 50]. The polymer chains have been highly immobilized with thicknesses of the bound rubber layers around 0.7 nm surrounding the CB particles [51]. The fillers covered by the immobilized rubber interface, can be considered as physical cross-links. This provides network chains for the rubber matrix in the proximity of carbon black particles [8, 52], as shown in Figure 2.6(b).

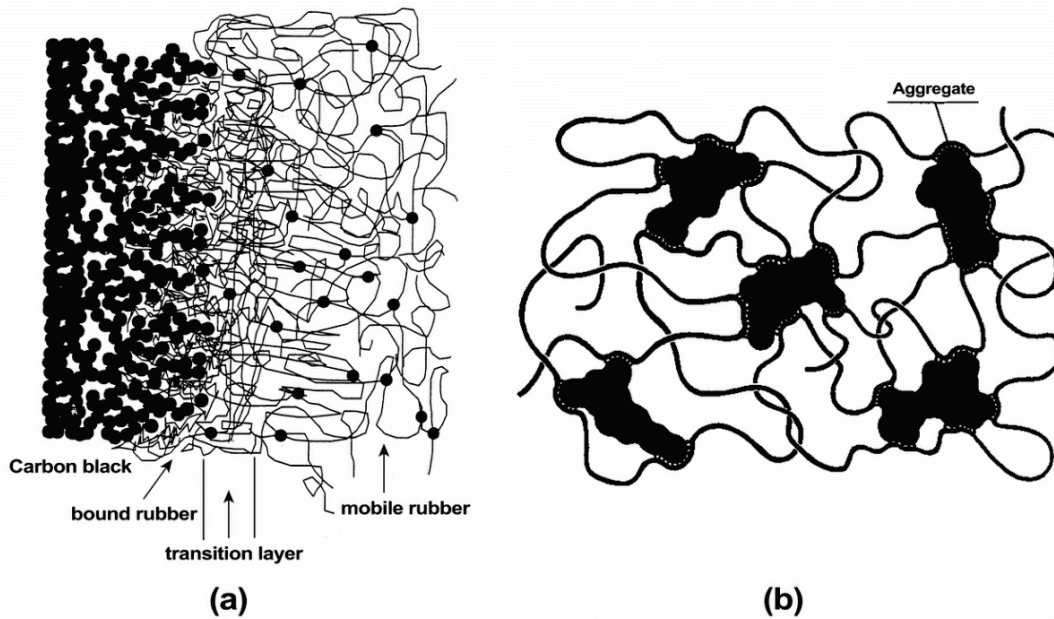


Figure 2.6 (a) Interface between the carbon black and the polymer [51]. (b) A schematic diagram of the physical network in a carbon black filled elastomer [52].

The mobility of the polymer chains is restricted to some extent due to filler-polymer interaction, depending on type of the polymers and fillers, and fillers distance which is mainly controlled by the specific surface area and filler loading [50]. The amount of immobilized rubber increases with the increasing content of carbon black. Stronger polymer-filler interaction would result in a thicker rubber shell for small particle-sized CB which is in combination with a larger interfacial area in the unit volume compound at the same loading. This gives more immobilized rubber shell in comparison with large particle-sized CB. It is well established that the immobilized rubber content of higher-structure carbon black is significantly higher than its low-structure counterpart. This is probably due to high structure CB is certainly related to the increased polymer-filler interfacial area and greater adsorption ability of the freshly built surface during mixing [53].

2.2 Thermoplastic elastomer blends

Blending of polymers is an attractive way to develop new material by combining two or more polymers in order to combine important characteristics of individual polymers, resulting in improvements in mechanical strength, toughness, thermal stability, aging resistance, etc [54, 55]. However, the difference in molecular structure and affinity of blend component results in the immiscible blend. This has been recognized to cause both inferior mechanical properties such as poor tensile strength, elongation at break and compression set. For the immiscible blend, the blend morphology determines the physical properties of the blend. The miscibility of the blend component is an important factor to proper control the blend morphology which plays an important role in controlling the final properties of the blend.

2.2.1 The miscibility of polymer blend

Basically, the interpenetration of polymer chains at the interfaces is very low due to large interfacial tension or poor adhesion between two phases, resulting in a macroscopic phase separation between the components. The concept of miscibility is connected to the second law of thermodynamics, through the variation of free energy of mixing ΔG_M , which is defined as follows [56]:

$$\Delta G_m = \Delta H_m - T\Delta S_m \quad (2.4)$$

where ΔH_M is the change in enthalpy of mixing and ΔS_M is the change in entropy of mixing and T is absolute temperature. For the miscibility of the mixture, it is necessary that ΔG_M is negative ($\Delta G_M < 0$).

For polymer blends, the free energy of mixing is given by;

$$\Delta G_m = RT \left(\underbrace{\frac{\varphi_1}{N_1} \ln \varphi_2 + \frac{\varphi_2}{N_2} \ln \varphi_2}_{\Delta S_M; \text{ trends to } 0} + \underbrace{\chi_{12} \varphi_1 \varphi_2}_{\Delta H_M} \right) \quad (2.5)$$

where R is the gas constant, φ_i is volume fraction of component i , N_i is degree of polymerization for component i and χ_{ij} is Flory interaction parameter.

Polymers generally have high degree of polymerization, N_i , and high molecular weight. This contributes that ΔS_M is small and close to zero in most cases. When they are blended together to form a blend, therefore, a phase-separated blend in terms of thermodynamic occurs. Miscibility is an exception and exists only for very few polymer combinations. The interaction parameter χ_{12} , can be determined by using solubility parameters [57-59]:

$$\chi_{12} = \frac{V}{RT} (\delta_1 - \delta_2)^2 \quad (2.6)$$

where R is the gas constant, V is volume and δ_i is solubility parameter of component i . The enthalpy of mixing is expressed as follows by the energetic interactions between the blend components:

$$\Delta H_m = RT \chi_{12} \phi_1 \phi_2 \quad (2.7)$$

Then, the enthalpic contribution part can be calculated through the difference in solubility parameter of blend component [58, 60]:

$$\Delta H_m = V (\delta_1 - \delta_2)^2 \phi_1 \phi_2 \quad (2.8)$$

For better miscibility, the polymers should have similar solubility parameters. This is in accordance with the general rule that chemical and structural similarity favors solubility. The difference in the solubility parameters δ_{12} must be that $\Delta\delta < 0.2 \text{ (J/cm}^3\text{)}^{1/2}$ for mixing to take place on a molecular level [59, 61].

The miscibility can be achieved through stabilization of the morphology by using compatibilizer or reactive blending. They can produce specific interaction such as covalent bond or ionic bond formation at interface, or by attractive intermolecular interaction, e.g., dipole-dipole, ion-dipole, charge-transfer, H-bonding, van der Waals forces, etc. These interactions promote interfacial adhesion and stabilize phase morphology. Thus, the compatibilization either by compatibilizing agent and reactive blending can promote optimum particle size formation of dispersed phase and prevent phase coalescence of the dispersed phase during blending [56, 62], as shown in Figure 2.7.

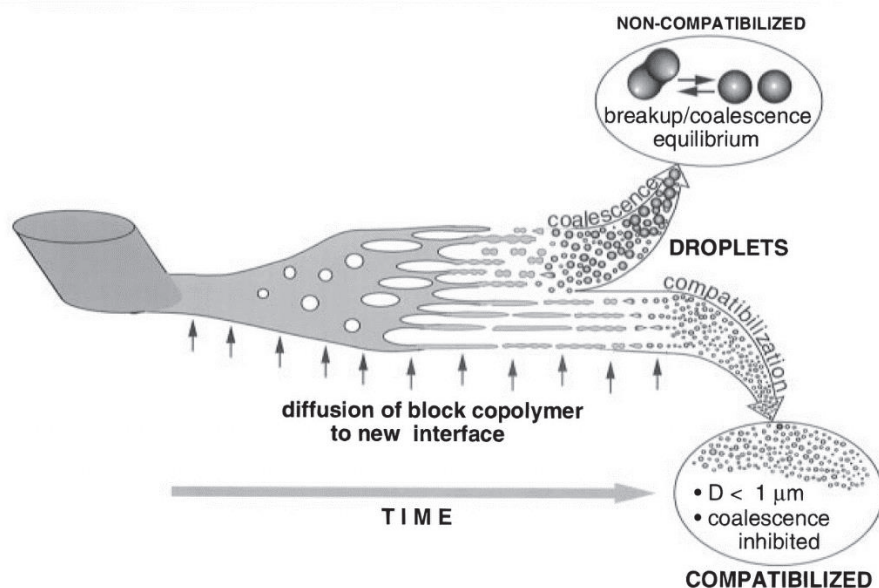


Figure 2.7 Formation mechanism of the morphology in the polymer blends [63]

Material based on blending of thermoplastic and elastomer is a combination of melt processability of thermoplastics and good elastic behavior of rubber, so-called *thermoplastic elastomers (TPEs)*. The TPE is an interesting class of polymer materials which consist of rigid thermoplastic phase (hard phase) and soft elastomer phase (soft phase) [64]. The soft phase provides rubber-like properties such as elasticity, compression set and flexibility. The physical network and strength are given by hard phase which is thermal reversible. This allows TPE to melt and flow, providing thermoplastic characteristics such as processability and recyclability. Therefore, the TPE scrap can be reprocessed. The use of TPE materials for industrial application, such as, automotive industries, household appliances, medical apparatus, cable and wire, has grown steadily due to their excellent performance. TPE based on blending of rubber and thermoplastic is one of the most commonly used method of obtaining thermoplastic elastomer. Recently, TPEs based on heterogeneous polymer blends have attracted wide interest in scientific research and industry because its properties and performance can be tailored by blend composition and morphology. TPE based on blending can be divided into two groups: *simple blend (SB)* or *thermoplastic polyolefin (TPO, TPE-O)* containing non-cross-link elastomer and *dynamically vulcanized blend (DV)* or *thermoplastic vulcanizate (TPV, TPE-V)* consisting of dispersed cross-linked elastomer in thermoplastic matrix.

2.2.2 Simple blend

Simple blend thermoplastic elastomer can be prepared by melt mixing of the elastomer and thermoplastic without cross-linker. They are heterogeneous blend or phase-separated system due to their large interfacial tension and different affinity. Differently possible morphologies can be observed in a two-phase system, as shown in Figure 2.8. This depends on blend composition, viscosity ratio, elasticity ratio and interfacial tension.

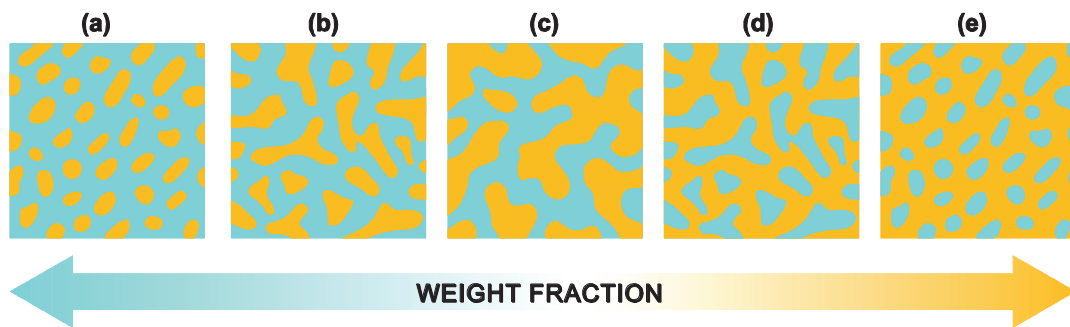


Figure 2.8 The evolution of the morphology of simple blend with different blend compositions

At a low concentration of the minor phase, the dispersion of minority in the matrix is observed (Figure 2.8(a)). When quantity of the dispersed fraction increases, the morphology changes from a dispersion of spherical drops in the matrix to interconnected drops (Figure 2.8(b)). Increasing amount of the minor phase causes the first phase inversion and there is no dispersed phase in the blend and the two phases become co-continuous (Figure 2.8(c)). Further increases in the minor phase, the second phase inversion occurs in which the minor phase becomes a matrix while the major phase becomes a dispersed phase (Figure 2.8(d) and (e)). However, the co-continuous structure provides the material with characteristics of thermoplastic elastomer based on the simple blend. This can be explained in the terms of properties of the blend. In the case of a dispersed elastomer in a continuous hard phase, the properties of the blend are dominated by the plastic phase. Therefore, a brittle and tough polymer blends are obtained. The co-continuous structure yields the product with characteristic of TPE that offers strength and processability and the continuous soft phase offers the flexibility. While a hard plastic dispersed in an elastomer phase, the blend has very low strength because of the unvulcanized rubber and this blend is not strong enough for practical application.

2.2.3 Thermoplastic vulcanizate

Thermoplastic vulcanizates (TPVs) are prepared by a dynamic vulcanization technique by adding curative during a mixing operation. The TPVs consist of dispersion of vulcanized rubber domains in thermoplastic matrix, which differs from the simple blends. The dynamic vulcanization occurs through two stages: first, a blending step without crosslinking or simple blend, and second, a superimposed cross-linking and mixing steps. The viscosity plays a significant role on formation of TPV morphology. When the degree of vulcanization is high, the rubber particles may be broken into micron size of elastomeric particles. The dynamic vulcanization of rubber phase in the plastic matrix leads to formation of materials with improved properties of high elasticity, while thermoplastic phase provides the melt processing. The varieties of TPVs have already found commercial applications, especially in the automotive sector [59, 65, 66].

In the first blending step, the morphology of both phases changes to co-continuous structure (Figure 2.9(a)). The continuous mixing leads to formation of smaller grains of co-continuous structure under the action of shear and elongational stresses on a highly viscous co-continuous structure (Figure 2.9(b)). After addition of curatives, viscosity of the rubber phase quickly increases and the co-continuous structure is deformed by shearing process (Figure 2.9(c)). The break-up mechanism of the highly deformed co-continuous structure happens after the blend reached a critical stress from increased viscosity, which results in dispersion of the cross-linked rubber phase in the thermoplastic matrix. With the high amount of crosslinks in rubber, the rubber phase will break up into a finely dispersed particles morphology (Figure 2.9(d) and (e)) [59, 66, 67]. This is the moment where the co-continuous morphology is transformed into a dispersed-matrix phase, which depends on blend composition, viscosity and elasticity ratio, processing condition and cross-linking condition. Therefore, TPV morphology typically consists of the cross-linked rubber particles finely dispersed in the thermoplastic matrix. However, at high content of rubber phase or rubber-rich TPV, the cross-linking is insufficient to enforce phase inversion and it is commonly difficult to separate rubber particles in rubber-rich TPV.

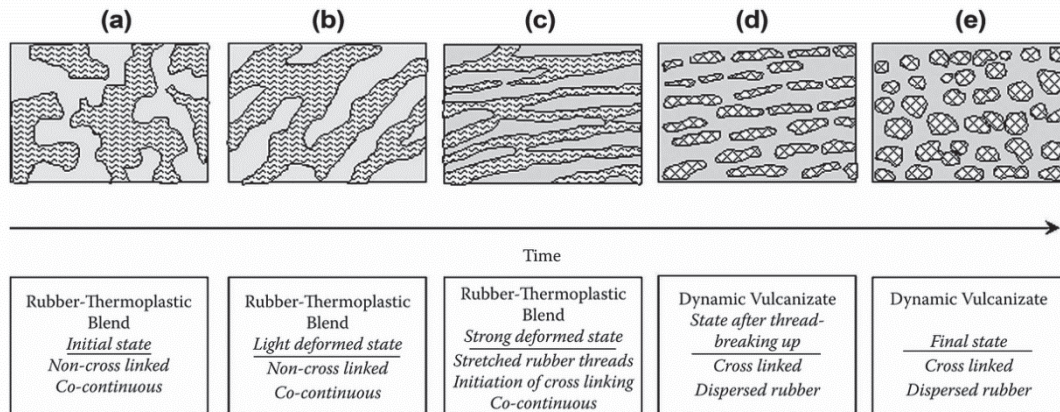


Figure 2.9 Schematic diagram of morphology transformation during the dynamic vulcanization of polymer blends [59]

The vulcanization system is one the important factor in determining physical properties of the dynamic vulcanizates. TPVs have been extensively investigated by using various types of the vulcanization system such as phenolic resin [67-71], sulfur [72, 73], peroxide [74, 75], and mixed curative (sulfur and peroxide) [70, 76]. Recently, the phenolic cured system has received more attention in TPVs. This is because the fine dispersion of rubber particles in the matrix is obtained. As a consequence, improvement in mechanical properties of TPV was achieved [70]. Abdou-Sabet and Fath [68] obtained TPV with good compression set, oil resistance and processing characteristics by using phenolic resin as a curing agent. The sulfur cured TPV provided superior mechanical properties in terms of tensile strength and elongation at break as compared with peroxide cure but it always gives an unpleasant smell during processing [76]. TPV based on the peroxide cured system showed good elastic behavior in particular the compression set, heat resistance and no discoloration of the final products. However, peroxide cured material shows a blooming effect and decomposes of peroxide into smelly by products along with β -chain scission reaction of the PP [70, 74]. The use of multifunctional peroxide may overcome the drawbacks and provide PP-based TPV with appropriate mechanical properties [77, 78]. Furthermore, the mixed cured system (sulfur and peroxide) caused minimize the degradation reaction in PP and showed higher mechanical properties than the individual system [70, 76]. Moreover, the optimum vulcanization system depends on type of rubber such as acrylic rubber (ACM) must employ hexamethylene diamine carbamate crosslinking agent [79, 80].

2.3 Binary polymer composites

Polymer blends containing fillers have been the subject of intense investigation in scientific and industrial exploitation during the last decade. They present a challenge and complexity of polymer composite and polymer blend fields, as many factors have the potential to impact their morphology and final properties. The filler dispersion and blend microstructure are the main considerations to control obtained properties [55, 81]. The main objective of adding fillers to the blend is to study the role of filler in the blend which affects the final properties. Several researchers have demonstrated that the addition of particles in the blend caused improvement of mechanical properties [82-84]. Recently, investigations of the effects of particles in immiscible blend focus on selective localization of filler in the blend. Particularly, the interfacial localization is possible to enhance the compatibility between the two phases and reduce the domain size in polymer blend.

2.3.1 Filler localization

In the immiscible blend, the particles generally distribute unevenly in the two phases that significantly affects the morphology and the physical properties of the blend. When a filler is incorporated in polymer blend, three possibilities of filler location are possibly to occur, as shown in Figure 2.10; particles locate uniformly in both phases, particles locate only in one phase, and particles remain at the interface. The existence of different filler distribution in immiscible polymer blends is governed by [55]:

- (i) *Thermodynamic effect*; relating to the surface properties of all components
- (ii) *Kinetic effect*; relating to viscosity of polymer components.
- (iii) *Processing procedure*; relating to mixing sequence.

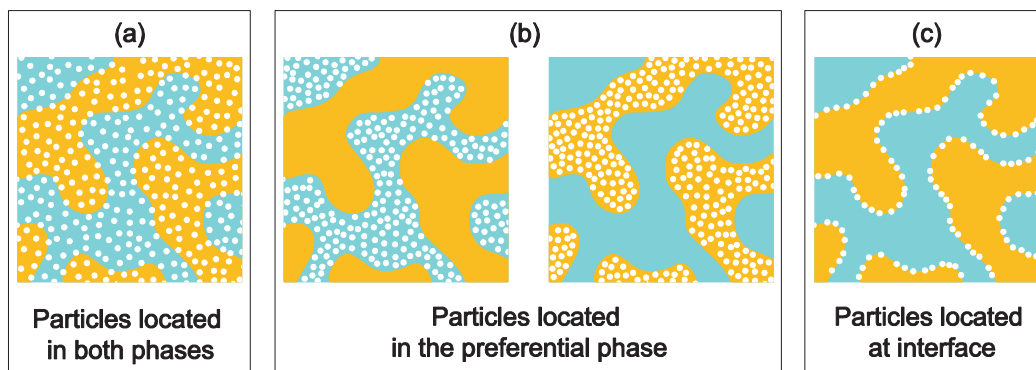


Figure 2.10 Selective localization of particles in polymer blends

2.3.1.1 Thermodynamic effect

When fillers are introduced into a polymer blend, they generally tend to migrate to the phase which have the better affinity, in a thermodynamic sense. The affinity between filler and polymer is considered by using the concept of surface tension, which contributes to the localization of the filler in the blend [55]. Sumita *et al.* [85] applied the wettability coefficient to predict the phase for which the filler would have the greatest affinity. This coefficient reflects the ability of filler to be wetted by one or the other of the polymer phases. The wetting can be calculated from the following equation [86, 87];

$$\omega = \frac{\gamma_{\text{filler-2}} - \gamma_{\text{filler-1}}}{\gamma_{1-2}} \quad (2.9)$$

where $\gamma_{\text{filler-2}}$ and $\gamma_{\text{filler-1}}$ are the interfacial tension between filler and polymer 2, and between filler and polymer 1, γ_{1-2} is the interfacial tension between polymer 1 and polymer 2. The localization of filler depends on the value of ω , three cases are possible.

- If $\omega > 1$, the filler preferentially locates in the polymer 1
- If $\omega < -1$, the filler preferentially locates in the polymer 2
- If $-1 < \omega < 1$, the filler locates at interface between two phases

The values of interfacial tensions of component can be evaluated by using the Harmonic-mean equation [87]:

$$\gamma_{12} = \gamma_1 + \gamma_2 - 4 \left(\frac{\gamma_1^d \gamma_2^d}{\gamma_1^d + \gamma_2^d} + \frac{\gamma_1^p \gamma_2^p}{\gamma_1^p + \gamma_2^p} \right) \quad (2.10)$$

where γ_i is the surface tension of component i, γ_i^d and γ_i^p are the dispersive and polar part of surface tension of component i, respectively.

Experimentally, the localization of silica particles in polystyrene (PS) and polypropylene (PP) blends [88] and in EVA/PP blends [89] have been successfully predicted by wetting coefficient. Wetting parameter (ω) is equal to 4.87 and 8.0 for the hydrophilic silica in PS/PP and EVA/PP, respectively. Therefore, the particles should be preferentially located in the PS and EVA. These predictions are confirmed by transmission electron microscopy. Martin *et al.* [90] also studied the localization of silica in PP/EPDM blends. It was found that hydrophilic silica particles migrate within the elastomeric phase,

whereas hydrophobic particles can be found at the interface and EPDM phase. The good agreements between thermodynamic prediction and morphology observation of particle localization in the immiscible blend were also observed in the blending of polylactide (PLA) and poly(ϵ -caprolactone) (PCL) containing organoclay [91] and in the blending of polypropylene (PP) and poly(ethylene terephthalate) (PET) with organoclay [92].

2.3.1.2 Kinetic factor

Surface tension has been an important parameter of the blend components to control the location of particles in the two phases. That is, fillers should localize within the phase which has the largest affinity. However, the localization of filler does not only depends on interfacial energy of polymer and filler. In some cases, the physical properties of polymer contribute to selective localization of filler in the blend. This factor is classified as “kinetic effect”, which is directly related to the shear viscosity of polymer during the blends. When the difference of viscosity of polymer is very large, the filler is preferentially located within the lower viscosity polymer [55, 86]. Wu *et al.* [91] found that the selective localization of clay in the blend of polylactide/poly(ϵ -caprolactone) or PLA/PCL agrees with thermodynamically prediction. In TEM observation of CNT, it located in the PCL phase. However, this is contrary to the thermodynamically prediction because high viscosity ratio between PLA and PCL is the dominant driving force of the PCL localization despite higher affinity to the PLA phase. However, with reduced viscosity ratios, the thermodynamical aspects become the dominant role, and the CNTs change their localization from the PCL to the PLA phase. It is noted that the viscosity effect dominate only when small difference of affinity between two polymers and filler is encountered. Particle-polymer affinity is considered as the dominate factor only when the viscosity ratio of both polymer phase is nearly one [86, 93].

2.3.1.3 Processing factor

Processing factor related to the sequence of addition of the component. There are three main mixing procedures which are commonly used in the literatures [55, 86]. First, the most commonly method is incorporation of the two polymers and filler together in the mixing. The second method is mixing of two polymers prior to adding filler in the blender. The third method is preparation of filler masterbatch in one polymer before mixing with the second polymer. Shi *et al.* [87] prepared CNT/EVA and CNT/poly(L-lactide)

(PLLA) master batches for diluting in PLLA and EVA, respectively. The result showed that CNT located in EVA phase when using CNT/EVA master batch even the proposed thermodynamic prediction resulted in a localization of CNTs in PLLA phase. The localization at interface of CNTs was observed if CNT/PLLA master batch was used. This is attributed to high viscosity of PLLA, which led to preventing the migration of particles into PLLA phase. They also found that the localization of CNTs at interface results in lower electrical resistivity than the localization in the one phase. Baudouin *et al.* [94] observed that morphology of the polyamide/ethylene and methyl acrylate or PA/EMA blend filled with MWCNT depended on the mixing sequence. MWCNTs should be localized at the interface between both polymers as predicted by thermodynamics. However, the MWCNTs are localized in the PA phase when they are premixed with the PA and they are localized at the interface when MWCNTs are premixed with EMA. There are two possible reasons, either the system did not reach the thermodynamic equilibrium or the thermodynamic is modified during the premixing step. This indicates that the mixing sequence play a role for to localization of particle in immiscible blends.

2.3.2 Compatibilization effect of particles

It has been well-known that the compatibilization of multi-phases can be achieved by using block copolymer to act as emulsifier in the blend, leading to an improved dispersion and the interfacial adhesion between two immiscible polymers. In addition, the use of nanoparticles in polymer blend can act as compatibilizing agents with reducing domain size in immiscible polymer blends. The fillers presented at the interface between two phases are evident compatibilizing effect for using filler as compatibilizer. This also enhances the interfacial adhesion which is very important for mechanical properties of the blend. Elias *et al.* [81] introduced nano-silica in PP/EVA to study domain size of polymer blend. A significant reduction of the EVA droplet size was observed in the presence of hydrophilic and hydrophobic silica. The volume droplet radius decreases from 2.2 μm to nearly 0.5 μm for filled blends with 3 wt% silica. Hong *et al.* [95] also found that the domain size PE phase in polybutylene terephthalate (PBT)-rich blend was reduced upon addition of organoclay in PBT/PE blend. The localization of organoclay at the interface hydrodynamically stabilized the blend morphology by suppressing the coalescence of the droplet. However, in the PBT/clay droplet, the domain size tends to increase with increasing addition of organoclay, because the likelihood of breakup of the

droplets against hydrodynamic force is decreased by the consequent reduction in deformability of the droplets. The reduction in domain size in the blend containing carbon nanotube was also reported by Wu *et al.* [83]. With addition of MWCNT in PCL/PLA blend, the size of the discrete PLA domain was reduced remarkably. The interface localization of MWCNT can improve mechanical properties of immiscible PCL/PLA blend. Bitinis *et al.* [96] reported that organoclay preferentially located at the polymer interface in the PLA/NR blend. This localization of organoclay acted as compatibilisers for the blend, which prevent the coalescence of NR droplets.

2.4 Natural rubber

Europeans discovered the use of rubber in Central American and South American Indians in the sixteenth and seventeenth centuries. The first scientific study of rubber was undertaken by Charles de la Condamine, when he encountered it during his trip to Peru in 1735. He also creates the French word rubber from the "cao-tchu" which means "wood crying" for Indian expression. The tree called *Hevea brasiliensis* is the world's number one source for natural rubber (NR) which has unique in its chemical structure and cannot be replaced by synthetic rubber. Nowadays, NR is the most well-known rubber and exhibits an excellent in mechanical properties, including good resilience, very low heat build-up, good electrical insulation and good resistance to abrasion, tear and fatigue. Consequently, it is a strategically important raw material used in tire, automotive, adhesive, footwear and other typical elastomer applications including medical devices. NR molecules can crystallize when stretched, so-called stress-induced crystallization due to high degree of stereo-regularity in NR structure. This contributes to enhance modulus on the stretching process. However, like most of hydrocarbon diene-based rubbers, NR is easily attacked by ozone and organic solvent, being unsuitable properties in specific industrial applications [97]. Therefore, it is well established that the properties of rubber can be improved either by chemically modifying or blending with specific elastomer or polymer. Modification of natural rubber by introducing new atom can be prepared such as epoxidized natural rubber (ENR), chlorinated natural rubber, maleated natural rubber (MNR) and natural rubber grafted polystyrene as well as changing of intermolecular chain of NR without new atom such as hydrogenated natural rubber [98].

2.4.1 Epoxidized natural rubber

The epoxidation of NR and unsaturated polymer was stated to increase solvent resistance and mechanical properties. It is one of the most promising methods to modify chemical structure of polydiene by transforming double bond into epoxy-group. The *in situ* epoxidation of NR latex using peracid with elevated temperature to yield epoxidized natural rubber (ENR) [99], as shown in Figure 2.11. The epoxidation method commonly used today is addition of formic acid and hydrogen peroxide to form performic acid *in situ* in the latex solution. The relative low cost of reagents and latex state reaction make epoxidation is an attractive route for rubber modification.

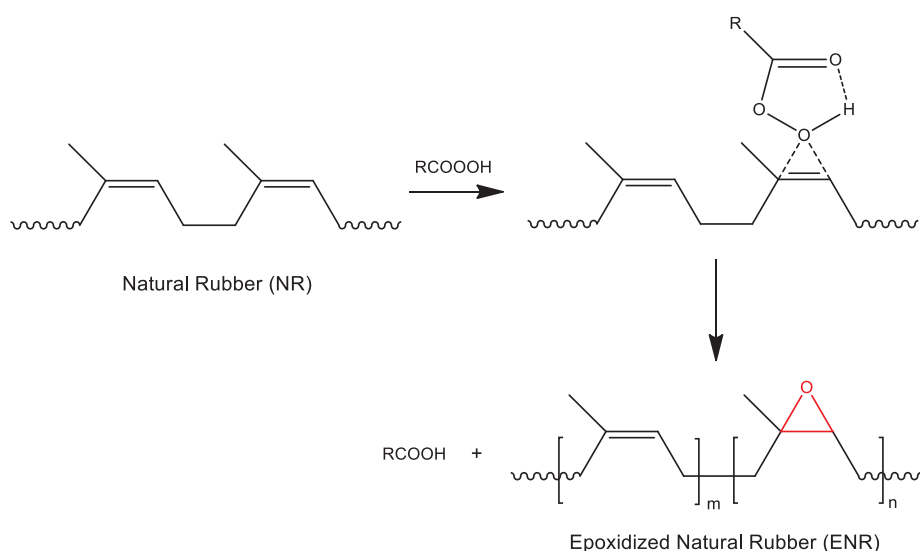


Figure 2.11 The mechanism for epoxidation of natural rubber [100]

Two grades of commercially available ENR have 25 mol % and 50 mol% of modification. The properties of natural rubber are changed gradually as one increases the degree of epoxidation. The glass transition temperature increased linearly with increasing of epoxidation level. Gelling [99] reported that every mole percent increase in epoxidation, the glass transition temperature increased by 0.93°C. The modification of epoxy-group into NR molecular also improves oil resistance and low permeability of gas. The presence of oxirane ring in ENR significantly increases polarity and solubility parameter, which are important factors for oil resistance and compatibility in polymer having polar groups [98]. The solubility parameters of NR and ENR with 25 and 50 mo% epoxide are reported as 16.5, 17.4, and 18.2 (J/cm³)^{1/2}, respectively [101, 102]. Furthermore, The ENR is one of the modified natural rubber which retains strain-induced

crystallization process for excellent physical properties. A strain induced crystallization of ENRs remains almost constant up to 50 mol% of epoxidation level. This is explained by the fact that ENRs are stereoregular, the *cis* configuration being preserved during the epoxidation process. It is also reported that oil resistance of ENR-50 in hydrocarbon fluid is between polychloroprene (CR) and acrylonitrile butadiene rubber (NBR). Hence, the ENR-50 can be used to replace NBR in many applications such as oil suction hose, seals, oil-well pipe protectors and so on [98, 99].

2.4.2 Composites and polymer blends based on ENR

ENR consists of epoxide groups which are reactive to polar functional group of filler. Thus, ENR is widely used in polymer composite to improve mechanical properties and dispersion of filler [103]. It is well-known that ENR has the ability to be reinforced with silica and carbon black due to the chemical bond formation between epoxy group in ENR and functional group on surface of silica and carbon black. This leads to increases storage modulus, which corresponds to restricted movement of polymer chain at filler surface [104].

Blending of thermoplastic and natural rubber is well known to prepare thermoplastic natural rubber (TPNR) materials [105]. A variety of thermoplastics have been selected to blend with NR and its modified forms (i.e., MNR and ENR). These are polypropylene (PP) [69, 70, 77], polyethylene (PE) [106, 107], poly(vinyl chloride) (PVC) [108], poly(methylmethacrylate) (PMMA) [72], polyamide (PA) [109] and thermoplastic polyurethane (TPU) [110, 111]. The TPNR based on ENR has been demonstrated to improve compatibility with polar polymer and its oil resistance. Narathichat *et al.* [109] prepared the reactive blending of ENR with Nylon-12. The strong interaction between epoxide group in ENR and polar functional group in Nylon-12 leads to enhanced mechanical properties and obtained finer grain morphology as compared with the use of unmodified natural rubber. Kalkornsurapranee *et al.* [110] reported that the blending of ENR and PU exhibited excellent in oil and heat resistance as compared with super TPV and EPDM/PP TPV in the market.

2.5 Poly(vinylidene fluoride)

Poly(vinylidene fluoride), or poly(1,1-difluoroethylene) is known by its acronym PVDF. The repeating pattern of PVDF is presented in Figure 2.12. PVDF is prepared in aqueous medium by polymerization of vinylidene fluoride ($\text{CH}_2=\text{CF}_2$). Polymerization procedures, temperatures, pressure, recipe ingredients, monomer feeding strategy, and post polymerization are variables influencing product characteristics and quality [15, 16]. Addition of monomeric units in a 'head-to-head' or 'tail-to-tail' defects is out of control during the polymerization which is caused by temperature of polymerization. The defect structure around 3-6% affects the crystallinity and mechanical properties PVDF [112].

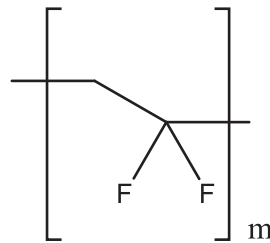


Figure 2.12 Chemical structure of PVDF

PVDF has semi-crystalline structure, its properties are strongly related to its degree of crystallinity. In general, the PVDF has a significant degree of crystallinity, of the order of 50-70% with four distinct crystalline forms: α , β , γ and δ [15]. Generally, the dynamic mechanical spectra of PVDF indicated four relaxations [112]; γ -relaxation (-70°C) is attributable to restricted motions of chains or to chain rotations in the amorphous regions. The β -relaxation (-40°C) corresponds to micro-Brownian motions of amorphous segments which is related to the glass transition (T_g). The β' -relaxation (50°C) has been attributed to fold motions. Regarding the α -relaxation (100°C), it has been attributed to segmental motion in the crystalline phase. The melting temperatures (T_m) of crystalline PVDF regions are in the range $155\text{-}192^\circ\text{C}$. The high level of intrinsic crystallinity of PVDF provides the toughness and mechanical strength as well as the impact resistance. It has also excellent thermal stability and resists damage from most chemicals and solvents as well as from ultraviolet and high energy radiation [15, 113]. The spatial arrangement of the alternating CH_2 and CF_2 groups along the PVDF chain and the strong dipole moment of the CF_2 accounts for the unique polarity, unusually high dielectric constant, and high piezoelectric and pyroelectric activity of the polymer [15, 16].

2.5.1 Composites and polymer blends based on PVDF

PVDF and its copolymer have been extensively used for composites and blend because of its potential applications to high dielectric permittivity, and unique piezoelectric, and ferroelectric properties. As mentioned above, a lot of investigations have been focused on the development of polymer/ceramics composites by using ferroelectric ceramics as fillers in PVDF to increase dielectric permittivity of composite [11, 30, 32]. Incorporation of other types of fillers into PVDF matrix has been studied with the objective to improve its properties, such as mechanical and thermal properties. Priya and Jog [114] prepared PVDF/clay nanocomposite by melt intercalation with organophilic clay. The addition of clay significantly enhanced rate of crystallization and storage modulus. He *et al.* [115] reported that incorporation of graphite in PVDF might act as a nucleating agent and accelerated the overall non-isothermal crystallization process of PVDF. The storage modulus and the dielectric constant of the composites increased linearly with graphite concentration.

PVDF exhibits thermodynamic compatibility with other polymers and blends of PVDF with various other homopolymers were extensively investigated. It has been reported that PVDF was miscible with polymethylmethacrylate (PMMA) [116, 117]. Pimbert *et al.* [117] revealed miscibility of PVDF/PMMA which is confirmed by DSC and DMA. They supposed that specific interaction between PMMA and PVDF were consistent with strong dipole-dipole interaction between the carbonyl group of PMMA and 'acidic' hydrogen atom in PVDF. PVDF was also used to prepare thermoplastic elastomer blend including simple blend and dynamically vulcanized blend. Li *et al.* [79] prepared thermoplastic elastomer based on PVDF/ACM blend which showed only one glass transition temperature due to single-phase nature. It was also found that thermoplastic elastomer based on PVDF/ACM blends showed excellent elongation at break, strain recovery, and heat and oil resistances. Wang *et al.* [113] studied the blends of poly(vinylidene fluoride) (PVDF) and silicone rubber, which were prepared through dynamic vulcanization. It was found that the cross-linked spherical SR particles with an average diameter of 2-4 μm formed a "network" in the PVDF continuous phase.

2.6 Conclusions

The first part of this literature review indicates the importance of polymer composites which are widely used in many applications. The incorporation of fillers in polymer can achieve higher levels of performance than those of the unfilled matrix (increased modulus, increased strength, increased conductivity and increased permittivity). Recently, the preparation of polymer composites for electronic applications has received great interest. The improvement of dielectric permittivity and electrical conductivity can be obtained by using ceramic and carbon black as fillers, respectively. The challenge is to increase permittivity and reduce percolation threshold of composites as much as possible for financial reasons and physical properties.

The second part shows the advantage of thermoplastic elastomer (TPE) blends for being good elasticity and processability. The simple blend can be prepared by melt mixing of the elastomer and thermoplastic without cross-linker whereas the preparation of thermoplastic vulcanizates uses cross-linker during blending process. Their properties mainly depended on phase development and miscibility of the blend. The TPE based on natural rubber has been studied extensively over the past decades, which is well known as thermoplastic natural rubber (TPNR). Furthermore, the addition of filler in immiscible blends is considered to bring new properties to the material. Many researchers demonstrated that the particles distribute unevenly in binary system. Three possibilities of filler location are possibly to occur in the blends. That is, particles locate uniformly in both phase, particles locate only in one phase and particles remain at the interface. Selective localization of filler in the blend requires a good understanding, which is govern by thermodynamic effect, kinetic effect and processing procedure. It would be interesting to study incorporation of particles in immiscible blends. Particularly, interfacial localization caused improvement compatibility and mechanical properties of the blends.

2.7 References

- [1] Xanthos, M. 2010. *Polymers and polymer composites*, in *Functional Fillers for Plastics*, M. Xanthos, ed. Wiley-VCH Verlag GmbH & Co. KGaA, Weinheim.
- [2] Leblanc, J.L. 2009. *Filled Polymers: Science and Industrial Applications*. CRC Press, Boca Raton.
- [3] Tjong, S.C. 2006. *Structural and mechanical properties of polymer nanocomposites*. Mater. Sci. Eng. R. 53, 73-197.
- [4] Abraham, R., Thomas, S.P., Kuryan, S., Isac, J., Varughese, K.T. and Thomas, S. 2009. *Mechanical properties of ceramic-polymer nanocomposites*. Express Polym. Lett. 3, 177-189.
- [5] Choi, S.S. and Kim, I.S. 2002. *Filler-polymer interactions in filled polybutadiene compounds*. Eur. Polym. J. 38, 1265-1269.
- [6] Luo, Y.Y., Wang, Y.Q., Zhong, J.P., He, C.Z., Li, Y.Z. and Peng, Z. 2011. *Interaction between fumed-silica and epoxidized natural rubber*. J. Inorg. Organomet. P. 21, 777-783.
- [7] Ten Brinke, J.W., Litvinov, V.M., Wijnhoven, J.E.G.J. and Noordermeer, J.W.M. 2002. *Interactions of Stober silica with natural rubber under the influence of coupling agents, studied by ^1H NMR T_2 relaxation analysis*. Macromolecules. 35, 10026-10037.
- [8] Litvinov, V.M., Orza, R.A., Klüppel, M., Van Duin, M. and Magusin, P.C.M.M. 2011. *Rubber-filler interactions and network structure in relation to stress-strain behavior of vulcanized, carbon Black filled EPDM*. Macromolecules. 44, 4887-4900.
- [9] Klüppel, M., Schroöder, A. and Heinrich, G. 2007. *Carbon black*, in *Physical Properties of Polymers Handbook*, J.E. Mark, ed. Springer, New York.
- [10] Dang, Z.M., Yuan, J.K., Zha, J.W., Zhou, T., Li, S.T. and Hu, G.H. 2012. *Fundamentals, processes and applications of high-permittivity polymer matrix composites*. Prog. Mater. Sci. 57, 660-723.
- [11] Mao, Y.P., Mao, S.Y., Ye, Z.G., Xie, Z.X. and Zheng, L.S. 2010. *Size-dependences of the dielectric and ferroelectric properties of $\text{BaTiO}_3/\text{polyvinylidene fluoride}$ nanocomposites*. J. Appl. Phys. 108, 014102.

-
- [12] Wang, X.X., Lam, K.H., Tang, X.G. and Chan, H.L.W. 2004. *Dielectric characteristics and polarization response of lead-free ferroelectric $(\text{Bi}_{0.5}\text{Na}_{0.5})_{0.94}\text{Ba}_{0.06}\text{TiO}_3\text{-P(VDF-TrFE)}$ 0-3 composites*. Solid State Commun. 130, 695-699.
- [13] Wegener, M. and Arlt, K. 2008. *PZT/P(VDF-HFP) 0-3 composites as solvent-cast thin films: preparation, structure and piezoelectric properties*. J. Phys. D: Appl. Phys. 41, 165409.
- [14] Huang, X., Xie, L., Jiang, P., Wang, G. and Liu, F. 2009. *Electrical, thermophysical and micromechanical properties of ethylene-vinyl acetate elastomer composites with surface modified BaTiO_3 nanoparticles*. J. Phys. D: Appl. Phys. 42, 245407.
- [15] Ameduri, B. 2009. *From vinylidene fluoride (VDF) to the applications of VDF-containing polymers and copolymers: recent developments and future trends*. Chem. Rev. 109, 6632-6686.
- [16] Mark, H.F. 2007. *Encyclopedia of Polymer Science and Technology*. 3rd ed. Wiley-Interscience, New York.
- [17] Ramajo, L., Reboredo, M. and Castro, M. 2005. *Dielectric response and relaxation phenomena in composites of epoxy resin with BaTiO_3 particles*. Compos. Part A: Appl. S. 36, 1267-1274.
- [18] Shonaike, G.O. 2003. *Gas Barrier properties of polymeric materials*, in *Advanced Polymeric Materials : Structure Property Relationships*, G.O. Shonaike and S.G. Advani, eds. CRC Press, Boca Raton.
- [19] Nam, J.D., Choi, H.R., Koo, J.C., Lee, Y.K. and Kim, K.J. 2007. *Dielectric elastomers for artificial muscles*, in *Electroactive Polymers for Robotic Applications: Artificial Muscles and Sensors*, K.J. Kim and S. Tadokoro, eds. Springer, London.
- [20] Dias, C.J. and Das-Gupta, D.K. 1996. *Inorganic ceramic/polymer ferroelectric composite electrets*. IEEE T. Dielect. El. In. 3, 706-734.
- [21] Dias, C.J., Igreja, R., Marat-Mendes, R., Inacio, P., Marat-Mendes, J.N. and Das-Gupta, D.K. 2004. *Recent advances in ceramic-polymer composite electrets*. IEEE T. Dielect. El. In. 11, 35-40.
- [22] Sebastian, M.T. and Jantunen, H. 2010. *Polymer-ceramic composites of 0-3 connectivity for circuits in electronics: a review*. Int. J. Appl. Ceram. Technol. 7, 415-434.
-

- [23] Carter, C.B. and Norton, M.G. 2007. *Ceramic Materials: Science and Engineering*. Springer, New York.
- [24] Haertling, G.H. 1999. *Ferroelectric ceramics: history and technology*. J. Am. Ceram. Soc. 82, 797-818.
- [25] Vijatovic, M.M., Bobic, J.D. and Stojanovic, B.D. 2008. *History and challenges of barium titanate: part I*. Sci. Sinter. 40, 155-165.
- [26] Newnham, R.E., Skinner, D.P. and Cross, L.E. 1978. *Connectivity and piezoelectric-pyroelectric composites*. Mater. Res. Bull. 13, 525-536.
- [27] Topolov, V.Y. and Bowen, C.R. 2008. *Electromechanical Properties in Composites based on Ferroelectrics*. Springer, London.
- [28] Tressler, J.F., Alkoy, S., Dogan, A. and Newnham, R.E. 1999. *Functional composites for sensors, actuators and transducers*. Compos. Part A: Appl. S. 30, 477-482.
- [29] Tressler, J.F., Alkoy, S. and Newnham, R.E. 1998. *Piezoelectric sensors and sensor materials*. J. Electroceram. 2, 257-272.
- [30] Dang, Z.M., Wang, H.Y., Zhang, Y.H. and Qi, J.Q. 2005. *Morphology and dielectric property of homogenous BaTiO₃/PVDF nanocomposites prepared via the natural adsorption action of nanosized BaTiO₃*. Macromol. Rapid Commun. 26, 1185-1189.
- [31] Li, Y.C., Tjong, S.C. and Li, R.K.Y. 2011. *Dielectric properties of binary polyvinylidene fluoride/barium titanate nanocomposites and their nanographite doped hybrids*. Express Polym. Lett. 5, 526-534.
- [32] Chanmal, C.V. and Jog, J.P. 2008. *Dielectric relaxations in PVDF/BaTiO₃ nanocomposites*. Express Polym. Lett. 2, 294-301.
- [33] Lam, K.H. and Chan, H.L.W. 2005. *Piezoelectric and pyroelectric properties of 65PMN-35PT/P(VDF-TrFE) 0-3 composites*. Compos. Sci. Technol. 65, 1107-1111.
- [34] Kim, P., Doss, N.M., Tillotson, J.P., Hotchkiss, P.J., Pan, M.J., Marder, S.R., Li, J., Calame, J.P. and Perry, J.W. 2009. *High energy density nanocomposites based on surface-modified BaTiO₃ and a ferroelectric polymer*. ACS Nano. 3, 2581-2592.

-
- [35] Kim, P., Jones, S.C., Hotchkiss, P.J., Haddock, J.N., Kippelen, B., Marder, S.R. and Perry, J.W. 2007. *Phosphonic acid-modified barium titanate polymer nanocomposites with high permittivity and dielectric strength*. *Adv. Mater.* 19, 1001-1005.
- [36] Ghallabi, Z., Arous, M., Kallel, A., Royaud, I., Boiteux, G. and Seytre, G. 2010. *Giant permittivity in three-phase PVDF composites*. in *Proceedings of the 2010 IEEE International Conference on Solid Dielectrics, ICSD 2010*. 1-3.
- [37] Gallone, G., Carpi, F., De Rossi, D., Levita, G. and Marchetti, A. 2007. *Dielectric constant enhancement in a silicone elastomer filled with lead magnesium niobate-lead titanate*. *Mater. Sci. Eng., C* 27, 110-116.
- [38] Lau, S.T., Cheng, C.H., Choy, S.H., Lin, D.M., Kwok, K.W. and Chan, H.L.W. 2008. *Lead-free ceramics for pyroelectric applications*. *J. Appl. Phys.* 103.
- [39] Devaraju, N.G., Kim, E.S. and Lee, B.I. 2005. *The synthesis and dielectric study of BaTiO₃/polyimide nanocomposite films*. *Microelectron. Eng.* 82, 71-83.
- [40] Choudhury, A. 2010. *Dielectric and piezoelectric properties of polyetherimide/BaTiO₃ nanocomposites*. *Mater. Chem. Phys.* 121, 280-285.
- [41] Xiaofang, L., Chuanxi, X., Huajun, S., Lijie, D., Rui, L. and Yang, L. 2005. *Characterization of PZT/PVC composites added with carbon black*. *J. Wuhan Univ. Technol.-Mat. Sci. Edit.* 20, 60-64.
- [42] Thomas, P., Varughese, K.T., Dwarakanath, K. and Varma, K.B.R. 2010. *Dielectric properties of poly(vinylidene fluoride)/CaCu₃Ti₄O₁₂ composites*. *Compos. Sci. Technol.* 70, 539-545.
- [43] Sohi, N.J.S., Bhadra, S. and Khastgir, D. 2011. *The effect of different carbon fillers on the electrical conductivity of ethylene vinyl acetate copolymer-based composites and the applicability of different conductivity models*. *Carbon.* 49, 1349-1361.
- [44] Huang, J.C. 2002. *Carbon black filled conducting polymers and polymer blends*. *Adv. Polym. Tech.* 21, 299-313.
- [45] Ghosh, P. and Chakrabarti, A. 2000. *Conducting carbon black filled EPDM vulcanizates: assessment of dependence of physical and mechanical properties and conducting character on variation of filler loading*. *Eur. Polym. J.* 36, 1043-1054.
- [46] Kirkpatrick, S. 1973. *Percolation and conduction*. *Rev. Mod. Phys.* 45, 574-588.
-

- [47] Zallen, R. 1983. *The Physics of Amorphous Solids*. John Wiley & Sons, New York.
- [48] Davidson, T. 2010. *Conductive and magnetic fillers*, in *Functional Fillers for Plastics*, M. Xanthos, ed. Wiley-VCH Verlag GmbH & Co. KGaA, Weinheim.
- [49] Samarzija-Jovanovic, S., Jovanovic, V., Markovic, G. and Marinovic-Cincovic, M. 2009. *The effect of different types of carbon blacks on the rheological and thermal properties of acrylonitrile butadiene rubber*. J. Therm. Anal. Calorim. 98, 275-283.
- [50] Fröhlich, J., Niedermeier, W. and Luginsland, H.D. 2005. *The effect of filler–filler and filler–elastomer interaction on rubber reinforcement*. Compos. Part A: Appl. S. 36, 449-460.
- [51] Heinrich, G. and Vilgis, T.A. 1993. *Contribution of entanglements to the mechanical properties of carbon black-filled polymer networks*. Macromolecules. 26, 1109-1119.
- [52] Litvinov, V.M. and Steeman, P.A.M. 1999. *EPDM-carbon black interactions and the reinforcement mechanisms, as studied by low-resolution ^1H NMR*. Macromolecules. 32, 8476-8490.
- [53] Wang, M.-J. 1998. *Effect of polymer-filler and filler-filler interactions on dynamic properties of filled vulcanizates*. Rubber Chem. Technol. 71, 520-589.
- [54] Utracki, L.A. 2002. *Introduction to polymer blends*, in *Polymer Blends Handbook*, L.A. Utracki, ed. Springer, Dordrecht.
- [55] Bailly, M. and Kontopoulou, M. 2010. *Nanocomposite blends containing polyolefins*, in *Advances in Polyolefin Nanocomposites*, V. Mittal, ed. CRC Press, Boca Raton.
- [56] White, J.L. and Yang, J. 2007. *Miscibility and characteristics of polyolefin blends*, in *Polyolefin Blends*, D. Nwabunma and T. Kyu, eds. John Wiley & Sons, New Jersey.
- [57] Mohanty, S., Nando, G.B., Vijayan, K. and Neelakanthan, N.R. 1996. *Mechanical and dynamic mechanical properties of miscible blends of epoxidized natural rubber and poly(ethylene-co-acrylic acid)*. Polymer. 37, 5387-5394.
- [58] Utracki, L.A. 2003. *Thermodynamics of polymer blends*, in *Polymer Blends Handbook*, L.A. Utracki, ed. Springer, Dordrecht.

- [59] Radusch, H.-J. 2005. *Phase morphology of dynamically vulcanized thermoplastic vulcanizates*, in *Micro- and Nanostructured Multiphase Polymer Blend Systems*, S. Thomas, G. Groeninckx and C. Harrats, eds. CRC Press, Boca Raton.
- [60] Zeng, W., Du, Y., Xue, Y. and Frisch, H.L. 2007. *Solubility parameters*, in *Physical Properties of Polymers Handbook*, J.E. Mark, ed. Springer, New York.
- [61] Xavier, S.F. 2003. *Properties and performance of polymer blends*, in *Polymer Blends Handbook*, L.A. Utracki, ed. Springer, Dordrecht.
- [62] Brown, S.B. 2002. *Reactive compatibilization of polymer blends*, in *Polymer Blends Handbook*, L.A. Utracki, ed. Springer, Dordrecht, The Netherlands.
- [63] Macosko, C.W., Guégan, P., Khandpur, A.K., Nakayama, A., Marechal, P. and Inoue, T. 1996. *Compatibilizers for melt blending: premade block copolymers*. *Macromolecules*. 29, 5590-5598.
- [64] Holden, G. and Quirk, R.P. 2004. *Thermoplastic Elastomers*. Hanser, New York.
- [65] Bhadane, P.A., Virgilio, N., Favis, B.D., Champagne, M.F., Huneault, M.A. and Tofan, F. 2006. *Effect of dynamic vulcanization on co-continuous morphology*. *AIChE J.* 52, 3411-3420.
- [66] Martin, G., Barrès, C., Sonntag, P., Garois, N. and Cassagnau, P. 2009. *Morphology development in thermoplastic vulcanizates (TPV): Dispersion mechanisms of a pre-crosslinked EPDM phase*. *Eur. Polym. J.* 45, 3257-3268.
- [67] Antunes, C.F., Machado, A.V. and Van Duin, M. 2011. *Morphology development and phase inversion during dynamic vulcanisation of EPDM/PP blends*. *Eur. Polym. J.* 47, 1447-1459.
- [68] Abdou-Sabet, S., Puydak, R.C. and Rader, C.P. 1996. *Dynamically vulcanized thermoplastic elastomers*. *Rubber Chem. Technol.* 69, 476-494.
- [69] Nakason, C. and Kaewsakul, W. 2010. *Influence of oil contents in dynamically cured natural rubber and polypropylene blends*. *J. Appl. Polym. Sci.* 115, 540-548.
- [70] Nakason, C., Worlee, A. and Salaeh, S. 2008. *Effect of vulcanization systems on properties and recyclability of dynamically cured epoxidized natural rubber/polypropylene blends*. *Polym. Test.* 27, 858-869.
- [71] Machado, A. and Van Duin, M. 2005. *Dynamic vulcanisation of EPDM/PE-based thermoplastic vulcanisates studied along the extruder axis*. *Polymer.* 46, 6575-6586.

- [72] Nakason, C., Tobprakhon, A. and Kaesarnan, A. 2005. *Thermoplastic vulcanizates based on poly(methyl methacrylate)/epoxidized natural rubber blends: mechanical, thermal, and morphological properties*. J. Appl. Polym. Sci. 98, 1251-1261.
- [73] Mousa, A., Ishiaku, U.S. and Mohd Ishak, Z.A. 2000. *Rheological properties of dynamically vulcanized poly(vinyl chloride)/epoxidized natural rubber thermoplastic elastomers: effect of processing variables*. Polym. Test. 19, 193-204.
- [74] Thitithammawong, A., Nakason, C., Sabakaro, K. and Noordermeer, J.W.M. 2007. *Thermoplastic vulcanizates based on epoxidized natural rubber/polypropylene blends: Selection of optimal peroxide type and concentration in relation to mixing conditions*. Eur. Polym. J. 43, 4008-4018.
- [75] Mani, S., Cassagnau, P., Bousmina, M. and Chaumont, P. 2011. *Morphology development in novel composition of thermoplastic vulcanizates based on PA12/PDMS reactive blends*. Macromol. Mater. Eng. 296, 909-920.
- [76] Nakason, C., Wannavilai, P. and Kaesaman, A. 2006. *Effect of vulcanization system on properties of thermoplastic vulcanizates based on epoxidized natural rubber/polypropylene blends*. Polym. Test. 25, 34-41.
- [77] Thitithammawong, A., Nakason, C., Sahakaro, K. and Noordermeer, J.W.M. 2009. *Multifunctional peroxide as alternative crosslink agents for dynamically vulcanized epoxidized natural rubber/polypropylene blends*. J. Appl. Polym. Sci. 111, 819-825.
- [78] Babu, R.R., Singha, N.K. and Naskar, K. 2009. *Dynamically vulcanized blends of polypropylene and ethylene octene copolymer: influence of various coagents on mechanical and morphological characteristics*. J. Appl. Polym. Sci. 113, 3207-3221.
- [79] Li, Y., Oono, Y., Kadowaki, Y., Inoue, T., Nakayama, K. and Shimizu, H. 2006. *A novel thermoplastic elastomer by reaction-induced phase decomposition from a miscible polymer blend*. Macromolecules. 39, 4195-4201.
- [80] Jha, A., Dutta, B. and Bhowmick, A.K. 1999. *Effect of fillers and plasticizers on the performance of novel heat and oil-resistant thermoplastic elastomers from nylon-6 and acrylate rubber blends*. J. Appl. Polym. Sci. 74, 1490-1501.

- [81] Elias, L., Fenouillot, F., Majeste, J.C., Alcouffe, P. and Cassagnau, P. 2008. *Immiscible polymer blends stabilized with nano-silica particles: rheology and effective interfacial tension*. Polymer. 49, 4378-4385.
- [82] Lee, S.H., Kontopoulou, M. and Park, C.B. 2010. *Effect of nanosilica on the co-continuous morphology of polypropylene/polyolefin elastomer blends*. Polymer. 51, 1147-1155.
- [83] Wu, D.F., Zhang, Y.S., Zhang, M. and Yu, W. 2009. *Selective localization of multiwalled carbon nanotubes in poly(ϵ -caprolactone)/polylactide blend*. Biomacromolecules. 10, 417-424.
- [84] Calcagno, C.I.W., Mariani, C.M., Teixeira, S.R. and Mauler, R.S. 2008. *The role of the MMT on the morphology and mechanical properties of the PP/PET blends*. Compos. Sci. Technol. 68, 2193-2200.
- [85] Sumita, M., Sakata, K., Asai, S., Miyasaka, K. and Nakagawa, H. 1991. *Dispersion of fillers and the electrical conductivity of polymer blends filled with carbon black*. Polym. Bull. 25, 265-271.
- [86] Fenouillot, F., Cassagnau, P. and Majeste, J.C. 2009. *Uneven distribution of nanoparticles in immiscible fluids: morphology development in polymer blends*. Polymer. 50, 1333-1350.
- [87] Shi, Y.Y., Yang, J.H., Huang, T., Zhang, N., Chen, C. and Wang, Y. 2013. *Selective localization of carbon nanotubes at the interface of poly(L-lactide)/Ethylene-co-vinyl acetate resulting in lowered electrical resistivity*. Compos. Part B: Eng. 55, 463-469.
- [88] Elias, L., Fenouillot, F., Majeste, J.C. and Cassagnau, P. 2007. *Morphology and rheology of immiscible polymer blends filled with silica nanoparticles*. Polymer. 48, 6029-6040.
- [89] Elias, L., Fenouillot, F., Majeste, J.C., Martin, G. and Cassagnau, P. 2008. *Migration of nanosilica particles in polymer blends*. J. Polym. Sci. Pol. Phys. 46, 1976-1983.
- [90] Martin, G., Barres, C., Sonntag, P., Garois, N. and Cassagnau, P. 2009. *Co-continuous morphology and stress relaxation behaviour of unfilled and silica filled PP/EPDM blends*. Mater. Chem. Phys. 113, 889-898.

- [91] Wu, D.F., Lin, D.P., Zhang, J., Zhou, W.D., Zhang, M., Zhang, Y.S., Wang, D.M. and Lin, B.L. 2011. *Selective localization of nanofillers: effect on morphology and crystallization of PLA/PCL blends*. *Macromol. Chem. Phys.* 212, 613-626.
- [92] Entezam, M., Khonakdar, H.A., Yousefi, A.A., Jafari, S.H., Wagenknecht, U. and Heinrich, G. 2013. *Dynamic and transient shear start-up flow experiments for analyzing nanoclay localization in PP/PET blends: correlation with microstructure*. *Macromol. Mater. Eng.* 298, 113-126.
- [93] Feng, J.Y., Chan, C.M. and Li, J.X. 2003. *A method to control the dispersion of carbon black in an immiscible polymer blend*. *Polym. Eng. Sci.* 43, 1058-1063.
- [94] Baudouin, A.C., Bailly, C. and Devaux, J. 2010. *Interface localization of carbon nanotubes in blends of two copolymers*. *Polym. Degrad. Stab.* 95, 389-398.
- [95] Hong, J.S., Namkung, H., Ahn, K.H., Lee, S.J. and Kim, C. 2006. *The role of organically modified layered silicate in the breakup and coalescence of droplets in PBT/PE blends*. *Polymer.* 47, 3967-3975.
- [96] Bitinis, N., Verdejo, R., Maya, E.M., Espuche, E., Cassagnau, P. and Lopez-Manchado, M.A. 2012. *Physicochemical properties of organoclay filled polylactic acid/natural rubber blend bionanocomposites*. *Compos. Sci. Technol.* 72, 305-313.
- [97] Cardarelli, F. 2008. *Materials Handbook: A Concise Desktop Reference*. Springer, New York.
- [98] Baker, C.S.L. 2001. *Modified natural rubber*, in *Handbook of Elastomers*, A.K. Bhowmick and H.L. Stephens, eds. Marcel Dekker, New York.
- [99] Gelling, I.R. 1991. *Epoxidised natural rubber*. *J. Nat. Rubber Res.* 6, 21.
- [100] Hashim, A.S. and Kohjiya, S. 1993. *Preparation and properties of epoxidized natural rubber*. *Kaut. Gummi Kunstst.* 46, 208.
- [101] Brydson, J.A. 1988. *Rubbery Materials and Their Compounds*. Springer, London.
- [102] Chee, K.K. 1995. *Solubility parameters of polymers from swelling measurements at 60°C*. *J. Appl. Polym. Sci.* 58, 2057-2062.
- [103] Rajasekar, R., Pal, K., Heinrich, G., Das, A. and Das, C.K. 2009. *Development of nitrile butadiene rubber-nanoclay composites with epoxidized natural rubber as compatibilizer*. *Mater. Design.* 30, 3839-3845.

- [104] Manna, A.K., De, P.P., Tripathy, D.K. and De, S.K. 1998. *Hysteresis and strain-dependent dynamic mechanical properties of epoxidized natural rubber filled with surface-oxidized carbon black*. J. Appl. Polym. Sci. 70, 723-730.
- [105] Ibrahim, A. and Dahlan, M. 1998. *Thermoplastic natural rubber blends*. Prog. Polym. Sci. 23, 665-706.
- [106] Pechurai, W., Nakason, C. and Sahakaro, K. 2008. *Thermoplastic natural rubber based on oil extended NR and HDPE blends: blend compatibilizer, phase inversion composition and mechanical properties*. Polym. Test. 27, 621-631.
- [107] Pichaiyut, S., Nakason, C., Kaesaman, A. and Kiatkamjornwong, S. 2008. *Influences of blend compatibilizers on dynamic, mechanical, and morphological properties of dynamically cured maleated natural rubber and high-density polyethylene blends*. Polym. Test. 27, 566-580.
- [108] Varughese, K.T., Nando, G.B., De, P.P. and De, S.K. 1988. *Miscible blends from rigid poly(vinyl chloride) and epoxidized natural rubber*. J. Mater. Sci. 23, 3894-3902.
- [109] Narathichat, M., Kummerlöwe, C., Vennemann, N., Sahakaro, K. and Nakason, C. 2012. *Influence of epoxide level and reactive blending on properties of epoxidized natural rubber and nylon-12 blends*. Adv. Polym. Tech. 31, 118-129.
- [110] Kalkornsurapranee, E., Nakason, C., Kummerlöwe, C. and Vennemann, N. 2013. *Development and preparation of high-performance thermoplastic vulcanizates based on blends of natural rubber and thermoplastic polyurethanes*. J. Appl. Polym. Sci. 128, 2358-2367.
- [111] Pichaiyut, S., Nakason, C. and Vennemann, N. 2012. *Thermoplastic elastomers-based natural rubber and thermoplastic polyurethane blends*. Iran Polym. J. 21, 65-79.
- [112] Lovinger, A.J. 1982. *Poly(vinylidene fluoride)*, in *Developments in Crystalline Polymers*, D.C. Bassett, ed. Applied Science Publishers, London.
- [113] Wang, Y.P., Fang, L.M., Xu, C.H., Chen, Z.H. and Chen, Y.K. 2013. *Preparation and properties of dynamically cured poly(vinylidene fluoride)/silicone rubber blends*. Polym. Test. 32, 1072-1078.

- [114] Priya, L. and Jog, J.P. 2002. *Poly(vinylidene fluoride)/clay nanocomposites prepared by melt intercalation: crystallization and dynamic mechanical behavior studies*. J. Polym. Sci., Part B: Polym. Phys. 40, 1682-1689.
- [115] He, F.A., Fan, J.T. and Lau, S.T. 2008. *Thermal, mechanical, and dielectric properties of graphite reinforced poly(vinylidene fluoride) composites*. Polym. Test. 27, 964-970.
- [116] Sy, J.W. and Mijovic, J. 2000. *Reorientational dynamics of poly(vinylidene fluoride)/poly(methyl methacrylate) blends by broadband dielectric relaxation spectroscopy*. Macromolecules. 33, 933-946.
- [117] Pimbert, S., Avignon-Poquillon, L. and Levesque, G. 2002. *Calorimetric study of fluorinated methacrylic and vinyl polymer blends: part 2: correlation between miscibility, chemical structure and χ_{12} interaction parameter in binary systems*. Polymer. 43, 3295-3302.

CHAPTER 3

MATERIALS AND EXPERIMENT METHODOLOGY

This chapter provides information on the materials used, as well as descriptions of sample preparations and the characterization techniques used throughout the project. The section covering sample preparation is divided into two sections; natural rubber vulcanizates and PVDF/ENR blends.

3.1 Materials

The thesis work involves rubber vulcanizates and blends of poly(vinylidene fluoride) (PVDF) and epoxidized natural rubber (ENR). The details of materials used in this study are listed below:

3.1.1 Natural rubber

Natural rubber (NR) in the form of air dried sheet (ADS) was used to prepare rubber vulcanizate. It was manufactured by a local factory, Khuan Pun Tae Farmer Cooperation, Phattalung, Thailand.

3.1.2 Epoxidized natural rubber

Epoxidized natural rubber (ENR) with two levels of epoxidation in the ENR (i.e., 25 and 50 mol% epoxide or ENR-25 and ENR-50, respectively) were used to prepare rubber vulcanizate and used as blend component in PVDF/ENR blends. ENR-25 and ENR-50 are available in commercial grade as Epoxyprene 25 and Epoxyprene 50, respectively. They were manufactured by Muang Mai Guthrie, Phuket, Thailand.

3.1.3 Poly(vinylidene fluoride)

Homopolymer poly(vinylidene fluoride) or PVDF, KYNAR 740 in the form of pellet was used as a blend component in PVDF/ENR blends. The specific gravity of PVDF

CHAPTER 3

was 1.78 g/cm³ and melting temperature 168°C. It was purchased from Arkema Inc., France.

3.1.4 Zinc oxide

Zinc oxide (ZnO) was used as an activator in sulfur vulcanization system. It is a white powder with a density of 5.606 g/cm³ and a melting point of 419°C. It was manufactured by Metoxide Thailand Co., Ltd., Pathumthani, Thailand.

3.1.5 Stearic acid

Stearic acid (C₁₈H₃₆O₂) was used as an activator in sulfur vulcanization system. It is a waxy white solid with a density, melting point and boiling point of 0.847 g/cm³, 69.6°C and 383°C, respectively. It was manufactured by Imperial Chemical Co., Ltd., Pathumthani, Thailand.

3.1.6 Mercaptobenzothiazole

Mercaptobenzothiazole (MBT), Perkasis MBT, was used as an accelerator in sulfur vulcanization system. It is a cream color powder with a density of 1.52 g/cm³ and was manufactured by Flexsys, Termoli, Italy.

3.1.7 Sulfur

Sulfur was used as a vulcanizing agent. It is a yellow powder with a density of 2.00 g/cm³. It was manufactured by Ajax Chemicals Pty. Co., Ltd., Sydney, Australia, Thailand.

3.1.8 Phenolic resin

Phenolic resin, HRJ-10518 was used as vulcanizing agent in phenolic cure system to perform dynamic vulcanization in PVDF/ENR blends. It contains 6-9% active hydroxymethyl (methylol) groups with a density of 1.05 g/cm³. It was manufactured by the Schenectady International Inc., New York, USA. The molecular structure of HRJ-10518 is shown in Figure 3.1.

3.1.9 Titanium(IV) oxide

Titanium(IV) oxide (TiO₂) was used to prepare barium titanate. It is white powder form with a density of 3.9 g/cm³. It was manufactured by Fluka Co. Ltd, Switzerland.

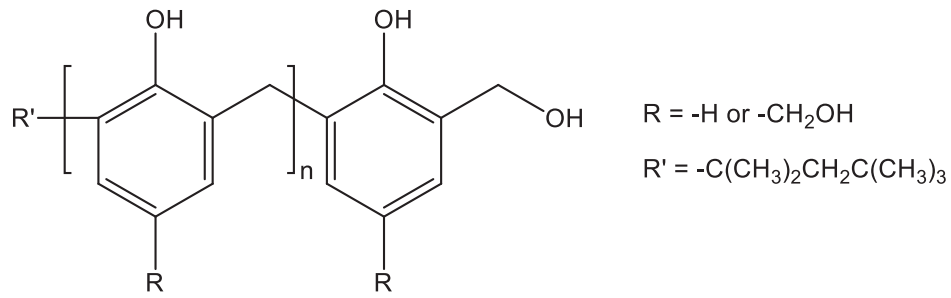


Figure 3.1 Molecular structure of HRJ-10518

3.1.10 Barium carbonate

Barium carbonate ($BaCO_3$) was used to prepare barium titanate with solid state technique. It is a white powder with a density of 4.29 g/cm^3 . It was manufactured by Ajax Finechem Pty Ltd., Australia.

3.1.11 Carbon black

Carbon black (CB) with two different surface areas and structures was used to prepare conductive ENR-50 composite. These are high abrasion furnace (HAF) and extra conductive furnace (ECF). HAF in a trade name of Thaiblack N330 was manufactured by Thai Carbon Black Public Co., Ltd, Ang Thong, Thailand. ECF in a trade name of Vulcan XC72R was manufactured by Cabot Corporation, Texas, USA. The characteristics of HAF and ECF are summarized in Table 3.1.

Table 3.1 Characteristics of used carbon black

Carbon black	Diameter (nm)	Iodine adsorption (mg/g)	Nitrogen Surface Area (m^2/g)	DBP Absorption ($\text{cm}^3/100\text{g}$)
HAF	29	82	80	102
ECF	30	235	254	192

3.1.12 Barium titanate

Barium titanate ($BaTiO_3$ or BT) is a ferroelectric ceramic, which was used as filler in PVDF/ENR blend. It is a white powder with a density of 5.85 g/cm^3 . It was manufactured by Alfa Aesar GmbH & Co. KG, Germany.

3.2 Experimental procedure

3.2.1 Preparation of natural rubber vulcanizate

The three types of natural rubbers (i.e., NR, ENR-25 and ENR-50) were cross-linked with sulfur vulcanization system to study effect of epoxidation level on cure characteristic, mechanical properties, dynamic mechanical properties and dielectric properties. Mixing process was carried out using Brabender Plasticoder PLE 331 (Brabender OHG Duisburg, Germany) with a mixing chamber of 80 cm³ at 60°C and a rotor speed of 60 rpm. The compounding formulation is shown in Table 3.2. NR was first masticated for 5 min. Zinc oxide and stearic acid were then added and mixed for 2 and 1 min, respectively. After dumping the mixes out of the mixing chamber, MBT and sulfur were added, respectively and mixed using a two-roll mill for 1 and 2 min, respectively. The rubber compound was then sheeted out and left at room temperature for 12 h before testing and vulcanizing.

Table 3.2 Compounding formulation used to prepare rubber vulcanizate

Ingredients	Quantities (phr)
Rubber ^a	100
ZnO	0.6
Stearic acid	0.5
MBT	0.5
Sulfur	3.5

^a NR, ENR-25 and ENR-50, phr = Parts per Hundred of Rubber

3.2.2 Preparation of barium titanate

There are several techniques available in the literature for ceramic preparation. The mechanical method (i.e., solid state reaction) is one of the successful methods for a large-scale production of bulk ceramic powders because of its low cost and easy adaptability. In this work, barium titanate was prepared by using the mixed oxide process i.e., high temperature solid state reaction techniques. This is a conventional method in which oxides and carbonates are used as precursors. Barium titanate (BaTiO₃) was synthesized by the conventional solid state reactions of BaCO₃|TiO₂, consisting of the following steps. Starting materials (i.e., BaCO₃|TiO₂) were first weighed with a molar ratio

of 1:1. They were then incorporated into a 1 liter ball-mill jar and thoroughly mixed for 1 min. Isopropanol was used as a medium in the system. It was added until 75 vol% of the jar. The mixing was continued for 5 min. The mixture was then ball-milled for another 24 h using zirconia balls with a half capacity of the jar. Isopropanol was thereafter separated by rotary evaporator. The remaining product was then dried at 120°C for 12 h in a hot air oven. The mixed powder was then ground, sieved through 120 mesh screen, and then incorporated into the alumina crucible. Calcination was then performed at 1100°C for 2 h in the muffle furnace (Thermolyne 6000 furnace, Barnstead International, Dubuque, USA). The structural characterization and particles size of barium titanate were studied by X-ray diffraction technique (XRD), dielectric spectroscopy and particle size analysis. The calcined powders were mixed with poly(vinyl alcohol) (PVA) as a binder and were then pressed into cylindrical pellets of 16 mm in diameter and 1-2 mm thick under a uniaxial pressure. The pellets were then sintered for 4 h at 1300°C in air atmosphere. PVA Binder removal was carried out by heating the pellets at 550°C for 1 h. These pellets were then sintered at 1300°C for 4 hr dwell time with a heating/cooling rate of 5°C/min. The sintered pellets were polished by using fine-grit sandpaper. The both sides of pellet were painted with silver paste and cured at 600°C for 30 min to form perfect electrodes on the sample surfaces. Dielectric properties of specimens were characterized at room temperature.

3.2.3 Preparation of BT/ENR-50 and CB/ENR-50 composites

BT/ENR-50 and CB/ENR-50 composites were prepared in an internal mixer with 80 cm³ capacity (Brabender Plasticorder, model PLE331, Brabender OHG Duisburg, Germany), at 60°C with a rotor speed of 60 rpm. The influence of BT loading (i.e., 0, 5, 10, 15, 20, 30, 40 and 50 vol%) and CB loading (i.e., 0, 5, 10, 15, 20, 25, 30, 40, 50 and 60 phr) on the properties of composites was studied. Two types of CB (i.e., HAF and ECF) were used in this investigation. The conversion from volume to weight of BT in ENR-50 can be expressed by:

$$m_c = m_p \times \frac{\rho_c}{\rho_p} \times \frac{\varphi}{1 - \varphi} \quad (3.1)$$

where m_c is weight of BT, m_p is weight of ENR-50, ρ_c is density of BT (5.85), ρ_p is density of ENR-50 (0.97) and φ is volume fraction of BT.

The ingredients for vulcanization (i.e., ZnO, stearic acid, MBT and sulfur) in part per hundred (phr) of rubber were listed in Table 3.2. ENR-50 was first masticated for 5 min. Zinc oxide was added and mixed for 2 min and then mixed with stearic acid for 1 min. The BT or CB filler was finally added into the mixing chamber. After dumping the mixes out, MBT was added and mixed in a two-roll mill for 1 min, then sulfur was added similarly with 2 min mixing. The rubber compound was then sheeted out and left at room temperature for 12 h before testing and vulcanizing. Furthermore, cure characteristic, mechanical properties, dynamic mechanical analysis and dielectric analysis of composites based on BT and CB were investigated.

3.2.4 Preparation of PVDF/ENR simple blends

PVDF/ENR simple blends were prepared using an internal mixer HAAKE rheomix R600 with a mixing chamber of 50 cm³. The mixing was performed at 180°C with a rotor speed of 50 rpm. All components were incorporated step by step into the mixer. PVDF was first incorporated into the mixing chamber for 3 min and ENR was then added with a total mixing time of 8 min, as shown in Figure 3.2. At the end of the mixing cycle, the materials were collected and fabricated into a sheet form by using a compression molding machine (Polystat 200 T, Servitec Maschinenservice GmbH, Wustermark, Germany). Morphological, mechanical properties and thermal properties (i.e., differential scanning calorimetry or DSC analysis, dynamic mechanical analysis (DMA) and dielectric analysis (DEA)) of the blends were later investigated.

3.2.4.1 Effect of epoxidation level

Two levels of epoxidation in ENR (i.e., ENR-25 and ENR-50 with 25 and 50 mole % epoxide, respectively) were used to prepare PVDF/ENR simple blends at a fixed blend ratio 50/50 wt%.

3.2.4.2 Effect of blend ratio

ENR-50 was selected to be a representative ENR to study influence of proportions on PVDF/ENR simple blends. Various weight ratios of PVDF/ENR-50 at 20/80, 30/70, 40/60, 50/50, 60/40, 70/30 and 80/20 were studied.

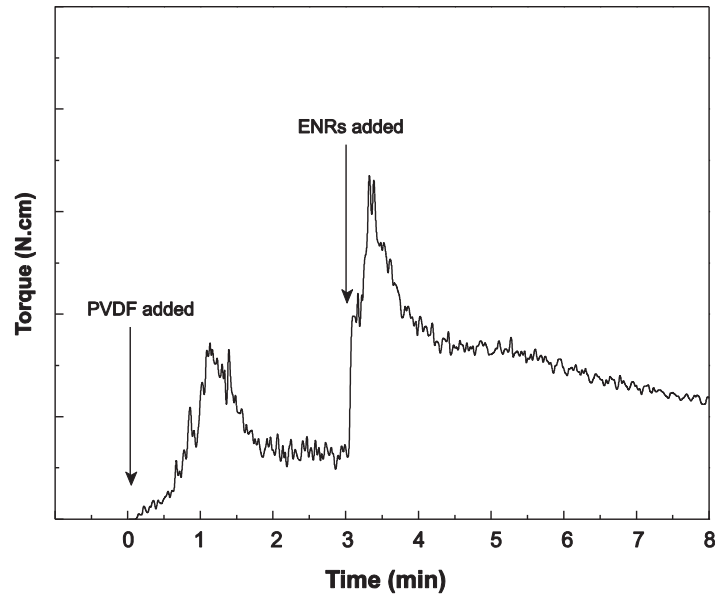


Figure 3.2 Mixing torque-time graph for PVDF/ENR simple blend

3.2.5 Preparation of BT/PVDF/ENR-50 composites

PVDF/ENR simple blends were prepared using an internal mixer HAAKE rheomix R600, with a mixing chamber of 50 cm³. The mixing was performed at 180°C with a rotor speed of 50 rpm. All components were incorporated step by step into the mixer. At the end of the mixing cycle, the materials were collected and fabricated into a sheet form by using a compression molding machine (Polystat 200 T, Servitec Maschinenservice GmbH, Wustermark, Germany). Morphological, mechanical properties and dynamic mechanical analysis and dielectric properties of the blends with the presence BT were examined.

3.2.5.1 Effect of incorporation of barium titanate into PVDF/ENR-50 simple blends and dynamic vulcanized blends

Two different blend ratios of PVDF/ENR-50 (i.e., 80/20 and 50/50 wt%) with BT concentration of 5 vol% were used in this study, as shown in Table 3.3. The blends without BT particle was prepared for comparison.

For BT filled simple blend, PVDF was first incorporated into the mixing chamber for 3 min mixing and ENR was then added for 5 min mixing. BT particles were then added into mixing chamber and mixed for another 10 min. The total mixing time was 18 min.

CHAPTER 3

For dynamic vulcanizate blend, the dynamic vulcanization was carried out by addition of HRJ-10518 (5 phr) into the chamber for 20 min mixing. Two mixing sequences (i.e., BDV and ADV methods) were used in order to study localization of BT particles in dynamically cured PVDF/ENR-50 blends. BDV is the addition of BT before dynamic vulcanization. In contrast, ADV is the addition of BT after dynamic vulcanization. The details of the mixing sequences are shown in Figure 3.3.

Table 3.3 Composition of simple and dynamically cured PVDF/ENR-50 blends with addition of BT

	Composition (wt%)		BT loading (vol%)	HRJ-10518 (phr)
	PVDF	ENR-50		
Simple blend	80	20	5	
	50	50	5	
dynamically cured blend	80	20	5	5
	50	50	5	5

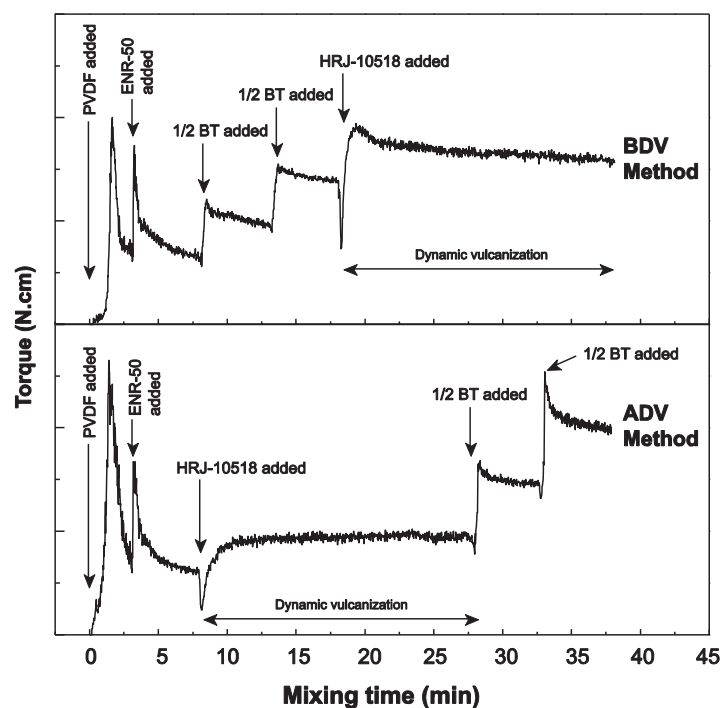


Figure 3.3 Mixing torque-time graph for dynamically cured PVDF/ENR-50 blends with different methods to introduce BT particles in the blends

3.2.5.2 Effect of BT loading in BT/PVDF/ENR-50 dynamically cured blends

Variation of BT contents of 0, 5, 12, 25 and 35 vol% was added into two different blend ratios of PVDF/ENR-50 TPVs (i.e., 80/20 and 50/50 wt%). The addition of BT after the dynamic vulcanization (ADV) was used for the mixing procedure. The composition of dynamically cured blend containing various BT loadings are listed in Table 3.4.

Table 3.4 Composition of dynamically cured PVDF/ENR-50 blend with various BT loadings

Composition (wt%)		BT loading (vol%)	HRJ-10518 (phr)
PVDF	ENR-50		
80	20	0, 12, 25 and 35	5
50	50	0, 12, 25 and 35	5

3.3 Testing and characterization

The objectives of this section are to gather information about the physical and chemical phenomena that will be needed in the interpretation of experimental results developed in the following chapters.

3.3.1 Cure characteristic

The cure characteristic is different for each formulation. A rotorless rheometer (rheoTECH MD+, Tech Pro, Cuyahoya Falls, OH, USA) was used to determine cure characteristic of rubber compound. The mixture is placed and vulcanized in the chamber which is oscillated through 0.5 arc at a frequency of 1.7 Hz and at 160°C according to ASTM D5289. The resistance of deformation or torque is measured as a function of time at the fixed amplitude and frequency, so-called rheometer chart. The typical changes in the torque versus time are shown in Figure 3.4.

The first region is induction period, the torque does not change in the induction period that occurs the most of the accelerator reactions for a safe processing time. The second period is the curing time, the torque rises due to beginning of vulcanization and reaches the equilibrium state when rubber is fully vulcanized. A decrease in torque value or reversion indicates a breakage of the crosslink bonds caused by the temperature, while an increase in torque or marching is related to a further cross-linking of the material [1].

From rheometer chart, it can be characterized a minimum torque (M_L), a maximum torque (M_H), and delta torque ($M_H - M_L$). Furthermore, scorch time (t_{s1}) is the time required for the onset of crosslink formation. This is generally taken as a time for one-point rise from minimum torque. The optimum cure time (t_{c90}) is determined based on the time to develop 90% of the difference in force or torque from the minimum to the maximum, as calculated according to Equation 3.2. Cure rate index were calculated using Equation 3.3.

$$t_{c90} \text{ (min)} = M_L + \frac{90}{100}(M_H - M_L) \quad (3.2)$$

and

$$\text{Cure rate index (CRI)} = \frac{100}{t_{c90} - t_{s1}} \quad (3.3)$$

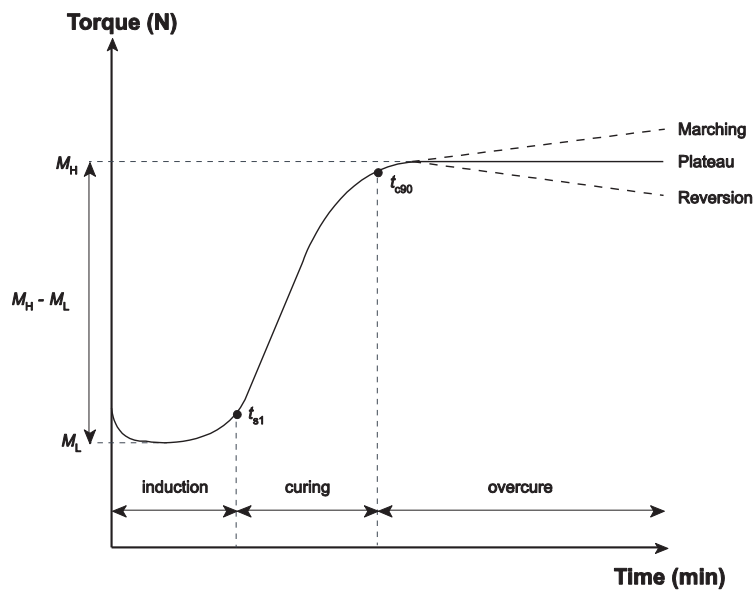


Figure 3.4 Torque as a function of time during vulcanization

3.3.2 Morphological properties

The scanning electron microscopy is a very useful technique based on the principle of electron-matter interactions. An electron beam is used to excite the atoms in the surface of the sample. The interaction of the beam results mainly in an emission of secondary electrons, backscattered electron and X-ray emitted by the surface, as shown in Figure 3.5. They are collected and then analyzed by different detectors for reconstructing a topographical image of the surface studied.

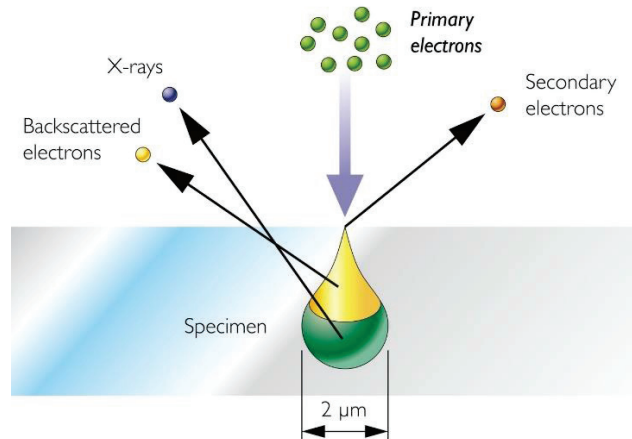


Figure 3.5 Schematic diagram of the various signals generated by the interaction of the electron beam with the sample

Two different scanning electron microscopes were used in this study. In the first step, morphological properties of BT/ENR-50 were observed with SEM (Hitachi SEM model S800, Hitachi, Tokyo, Japan) to characterize dispersion of BT particles in ENR-50. In the case of PVDF/ENR blends, morphological properties were determined by using SEM (Quanta 400, FEI company, OR, USA). The latter SEM is equipped with two different detectors: Everhart-Thornley Detector (ETD) and low voltage high contrast detector (vCD). The SEM imaging is normally used with the ETD as a standard detector by detecting the emission of secondary electron from sample. The detection of secondary electrons (SE) of low energy is used to obtain a topographic image of the surface. Alternatively, the vCD was installed in the chamber for detection of back scattering electron (BSE) to obtain images of the composition and topography of the surface but it gave poorer resolution than the secondary electrons. The contrast between the blend components in SEM based on BSE is relatively high compared to one seen with SE. The high phase contrast of topography of BSE-SEM is attributed to backscattered electron, which is emitted from the beam that has been elastically scattered by nuclei in the sample and escape from the surface. Therefore, backscattered electron imaging reveals better contrast between blend components, which relates to atomic number of element in the blend because these electrons are sensitive to the atomic number of the atoms in the sample. The increasing of brightness in the image can be interpreted as regions of different composition with high average atomic number as the image gets brighter. The strong dependence of the backscattered electron yield with atomic number of sample provides more phase

information about the composition and surface topography as compared with secondary electron [2].

In all cases, the samples are cryo-fractured after immersion in liquid nitrogen. The fractured surface of rubber composites and PVDF/ENR-50 TPV are metallized with a thin layer of gold without extraction. However, the cryo-fractured PVDF/ENR simple blends were immersed in toluene for 72 h to extract ENR phase in the blend, which contains ENR concentration lower than 60 wt%. When ENR-50 becomes the matrix, it is impossible to extract ENR-50 phase. Thus, dimethylformamide (DMF) was used to extract PVDF phase for ENR-50-rich blend. The samples were then dried under vacuum to remove the selective solvent.

3.3.3 Mechanical properties

3.3.3.1 Tensile properties

The purpose of the tensile tests is to determine the breaking strength and elongation at break of a material. This allows to evaluate and compare the mechanical behavior of various polymer composites and blends. Schematic tensile stress-strain behavior of polymeric materials is shown in Figure 3.6.

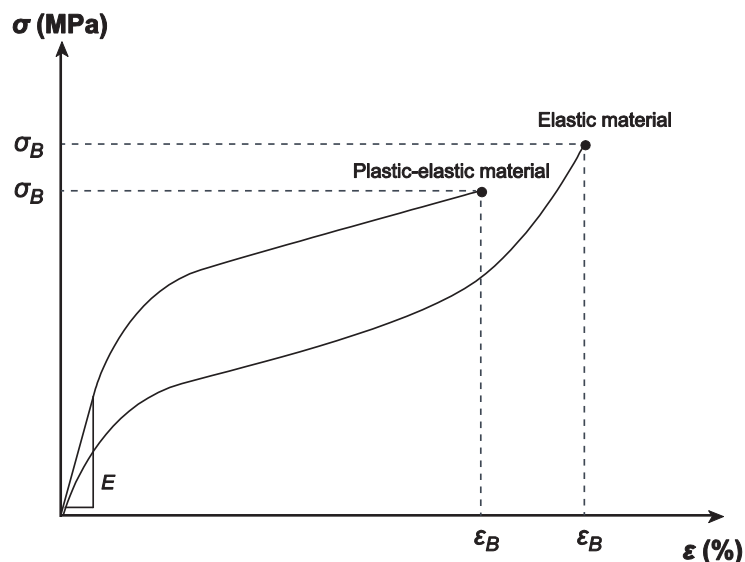


Figure 3.6 Typical stress–strain curve for polymeric materials

The polymeric material deforms irreversibly and non-linear function in the applied stress. The Hooke's law is valid only in a so-called linear region and reversible deformation curve [3]. Thus, the slope of the uniaxial stress-strain (response in the linear region is Young's modulus (also called modulus of elasticity (E)). The value is determined by calculating the slope of the stress-strain curve in the elastic area, The Young's modulus (E) is obtained as follows:

$$E \text{ (MPa)} = \frac{\sigma}{\varepsilon} = \frac{F/A}{\Delta L/L_0} \quad (3.4)$$

where σ is stress, ε is strain, F is force (N), A is cross-section area (mm^2), L_0 is initial length (mm) and ΔL is change in length (mm).

The stress at break (σ_B) or tensile strength is calculated in units of force at break (F_B) per initial cross-section area (A) of test specimen as follows:

$$\sigma_B \text{ (MPa)} = \frac{F_B}{A} \quad (3.5)$$

Elongation at break (ε_B) is the percentage elongation at the rupture of the test piece, expressed as change in length (ΔL) at the rupture compared to initial length (L):

$$\sigma_B \text{ (\%)} = \frac{\Delta L}{L_0} \times 100 \quad (3.6)$$

The stress-strain curves of rubber vulcanizate were measured from the dumb-bell shaped specimens of ASTM die type C, with a universal tensile testing machine (Hounsfield Tensometer, model H 10KS, Hounsfield Test Equipment Surrey, U.K.). The grip separation speed was set at 500 mm/min and initial gauge length was 25 mm, following the American standards (ASTM D412), as shown in Figure 3.7 and Table 3.5. Tensile testing is performed by elongating a specimen and measuring the load carried by the specimen. Tensile properties can be extracted from the stress-strain curve.

Mechanical behavior of the simple blend and dynamically cured of PVDF/ENR blend was measured with a universal tensile testing machine (MTS Q test 25, MTS Systems Corporation, North Carolina, USA). The grip separation speed was set at 500 mm/min, following the French standards (NFT 51 034), as shown in Figure 3.7 and Table 3.5.

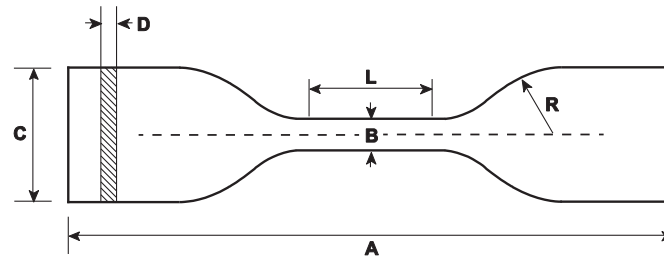


Figure 3.7 Standard die shape for cutting dumbbell specimens

Table 3.5 Dimensions of dumbbell test specimens

Positions	Dimension (mm)	
	ASTM D412	NFT 51 034
A: Overall length	115	50 (±2.00)
B: Width of narrow parallel	6 (±0.05)	4 (±0.10)
C: Width at ends	25 (±1.00)	8.5 (±1.00)
D: Thickness	2.0 (±1.00)	1.5 to 3
L: Gauge length	25 (±0.25)	10
R: Large radius	25 (±2.0)	10

3.3.3.2 Tension set

Tension set is the extent to which a specimen is permanently deformed after being stretched at a specified amount (typically 100% elongation) for a short time (10 min). After 10 min of elongation, the specimens are allowed to relax for 10 min. After the 10 min retraction, tension set is measured from the distance between bench marks and expressed as a percentage of a final distance between the bench marks after 10 min to original distance on the specimens as follows:

$$\text{Tension set (\%)} = \frac{(L - L_0)}{L_0} \times 100 \quad (3.7)$$

where L is final distance between the bench marks after 10 min retraction (mm) and L_0 is original distance between the bench marks (mm).

3.3.3.3 Hardness

Hardness test method is based on the penetration of a specific type of indenter when forced into the material under specified conditions. The indentation hardness is inversely related to the penetration and is dependent on the elastic modulus and viscoelastic behavior of the material. The test result is influenced by orientation, residual stresses and morphology (supermolecular structure, filler and reinforcement) [3].

Hardness of the sample in this study was measured using an indentation durometer shore A, according to ASTM 2240. The dimension of test specimen was at least 6.0 mm in thickness. The test was performed at room temperature. Five measurements at different positions on the same specimen were carried out and arithmetic mean of the five values were reported.

3.3.4 Differential scanning calorimetry analysis

Differential scanning calorimetry (DSC) is a technique that measures the difference in heat flow rate between a substance and a reference as a function of time and temperature. This technique can determine various characteristic temperatures, heat capacity, melting and crystallization temperatures, and heat of fusion, as well as the various thermal parameters of chemical reactions at constant heating or cooling rates [4]. A DSC system consists of a sample holder and a reference which are connected with a separate heater. In order to maintain at the same temperature, the difference in thermal power uptake between the sample and reference pans is measured and plotted as a function of temperature or time. When specific heat capacity of a sample changes, more (in endothermic processes) or less (in exothermic processes) heating power is transferred to the sample to avoid difference in temperature.

In this study, differential scanning calorimeter (DSC 2920 TA instrument, New Castle, DE, USA) was used to determine crystallization temperature (T_c) and melting temperature (T_m) of PVDF and its blends. The sample (around 10 mg) was sealed in aluminum hermetic pan. The sample was first heated to 200°C to eliminate possible thermal-mechanical histories. Measurements were carried out under helium gas atmosphere at a scanning rate of 10°C/min in the temperature range -90 to 200°C. The crystallization temperature (T_c) and melting temperature (T_m) were determined by cooling

and heating thermograms, respectively. The degree of crystallinity (X_c) of PVDF in the blend has been quantitatively calculated with the following formula:

$$X_c (\%) = \frac{\Delta H_m(m_c/m_p)}{\Delta H_0} \times 100 \quad (3.8)$$

where ΔH_m is melting enthalpy of the sample, ΔH_0 the theoretical enthalpy for 100% crystalline PVDF (104.5 J/g) [5], m_c is weight of the sample and m_p is weight of PVDF in the blends.

3.3.5 Dynamic mechanical properties

The dynamic mechanical analysis (DMA) is used to study the viscoelastic properties of a material by measuring the dynamic modulus properties as a function of time and temperature. A sinusoidal strain is applied on the sample, ε (or stress σ) and the corresponding stress, σ (or strain, ε) developed was measured. Due to the phase (δ) shift between stress and strain, the strain and stress can be written as [3, 6].

$$\varepsilon (t) = \varepsilon_0 \sin (\omega t) \quad (3.9)$$

and

$$\sigma (t) = \sigma_0 \sin (\omega t + \delta) \quad (3.10)$$

Accordingly, the dynamic behavior of a polymer material can be expressed by complex modulus (E^*) which may be divided into real and imaginary components:

$$E^* = \frac{\sigma (t)}{\varepsilon (t)} = E' + iE'' \quad (3.11)$$

where a real part (E') and an imaginary part (E'') can be distinguished:

$$E' = \frac{\sigma_0}{\varepsilon_0} \cos \delta \quad \text{and} \quad E'' = \frac{\sigma_0}{\varepsilon_0} \sin \delta \quad (3.12)$$

The real part (E') is known as the storage modulus and is a measure of the elastic character or solid-like nature of the material. The imaginary part (E'') or the loss modulus is a measure of the viscous character and is related to energy dissipated during oscillation period.

Alternatively the material damping coefficient or loss tangent ($\tan \delta$) can be calculated by:

$$\tan \delta = \frac{E''}{E'} \quad (3.13)$$

Dynamic mechanical analysis of natural rubber composites and blends were characterized using a TA instrument dynamic mechanical analyzer (DMA; model Q800 New Castle, DE, USA). The storage modulus (E') and $\tan \delta$ were measured in a tension mode under the test temperature range of -90 to 100°C at a frequency of 1 Hz under stream of liquid nitrogen. The glass transition temperature was evaluated from the maximum position peak in $\tan \delta$ versus temperature plots.

3.3.6 Dielectric analysis

The term dielectric analysis (DEA) refers to a group of techniques that measure changes in different physical properties, such as polarization, permittivity, and conductivity, with temperature or frequency. The reorientation of dipoles and the translational diffusion of charged particles in an oscillating electric field provide the basis of the analysis based on alternating current (AC) dielectric methods [3, 7].

The electrical properties of dielectric materials, placed between the two electrodes, and a sinusoidal voltage is applied to one of the electrodes. The capacitance (C) is related to the quantity of storage charges:

$$C = \epsilon \epsilon_0 \frac{A}{d} \quad (3.14)$$

where ϵ is the relative permittivity or the dielectric constant, where ϵ_0 is the vacuum permittivity (8.854×10^{-12} F/m).

The dielectric constant or permittivity is related to polarization ability by an applied electric field to dielectric materials. The relationship between the induced dielectric polarization density (P) and electric field (E) are defined by following equation:

$$P = (\epsilon^* - 1)\epsilon_0 E \quad (3.15)$$

where ϵ^* is complex permittivity of the investigated materials which can be divided into a real part (ϵ') and an imaginary part (ϵ'') of the dielectric permittivity:

$$\varepsilon^* = \varepsilon' - i\varepsilon'' \quad (3.16)$$

where ε' is proportional to the energy reversibly stored per period in the materials, also known as the relative dielectric permittivity. ε'' is proportional to the energy dissipation per period, also known as the dielectric loss. Furthermore, the tangent of the phase angle between applied voltage and resulting current also term dissipation factor, result from:

$$\tan \delta = \frac{\varepsilon''}{\varepsilon'} \quad (3.17)$$

where $\tan \delta$ is a factor which provides information on the energy loss and is highly dependent on physical conditions of the insulating material.

3.3.6.1 Polarization in polymer

The polymers are polarizable insulating materials. The polarization is the result of load distribution mechanisms under the influence of an electric field. There are different types of polarization along the polar or nonpolar character of the material and depending on the frequency of the applied electric field stress. The total polarization can usually be mainly divided into three parts: electronic, atomic and orientation (or dipole) [8], which will depend on the applied frequency and temperature. Frequency and temperature dependence of dielectric permittivity and loss in the presence of different polarizability are shown in Figure 3.8.

- (i) Electronic polarization results from the deformation of the electron cloud around the core with respect to the positive nucleus of any atom by the applied field.
- (ii) Atomic polarization relates to the movement of ions and molecules. When applying the electric field induces a dipole, the atoms move relative to each other, giving rise to an atomic polarization.
- (iii) Orientation polarization is found in certain molecules having a permanent electric dipole moment that can change orientation in an applied electric field.

At very low frequency and high temperature, the polarization processes are additionally obscured by the effect of interfacial polarization and conduction

- (iv) The interfacial polarization or Maxwell-Wagner-Sillars (MWS) is due to impurities and lattice defects which introduce discontinuities polarization. This type of bias occurs when the material has several phases of different conductivity and permittivity.
- (v) Conductivity originates from charge carrier mobility in the system at a low frequency and high temperature. This can be considered as a DC conduction.

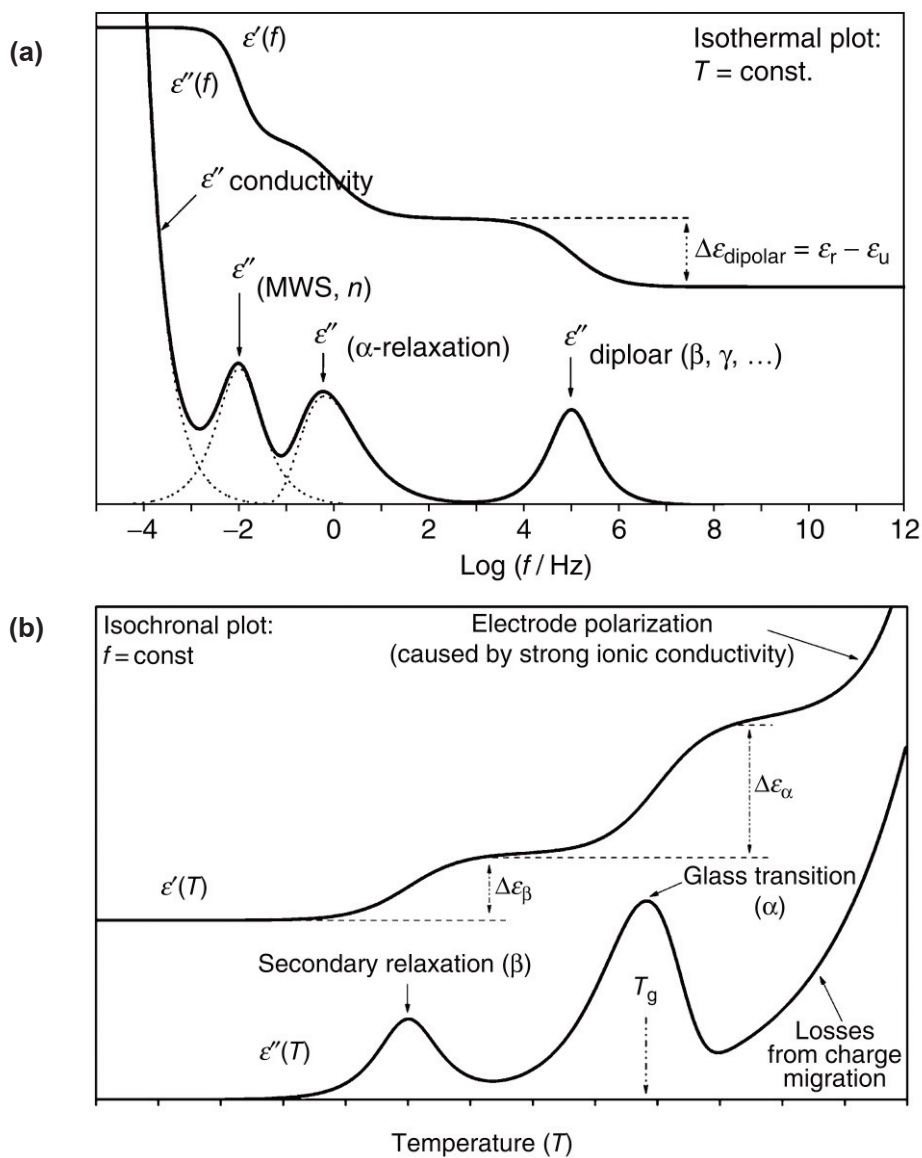


Figure 3.8 Schematic presentation of the (a) frequency and (b) temperature dependences of ϵ' and ϵ'' for typical dielectric relaxation in polymers [7]

Generally, interfacial polarization is masked by conduction at lower frequencies and high temperature. McCrum *et al.* [9] introduced the electric modulus formalism to overcome this difficulty in evaluating interfacial polarization. Complex electric modulus M^* is defined as the reciprocal of the complex relative permittivity:

$$M^* = M' + iM'' = \frac{1}{\epsilon^*} = \frac{\epsilon'}{(\epsilon')^2 + (\epsilon'')^2} + i \frac{\epsilon''}{(\epsilon')^2 + (\epsilon'')^2} \quad (3.18)$$

The M'' plots effectively suppress large contributions of non-local relaxations at low frequencies. Very important is the suppression of the strong DC conductivity signal, appearing in the ϵ'' spectrum.

3.3.6.2 Dielectric relaxation

The relaxation phenomena are generally accelerated by increasing of temperature (in isothermal plot) and frequency (in isochronal plot). In the polymers, the temperature dependence of the relaxation time not only depends on the nature of relaxation but also depend on the temperature and frequency range studied. Two types of behavior are generally observed in the analysis of molecular mobility of polymers [7].

When relaxing entities associated with relaxation mode are small (fashion secondary), the temperature dependence of $\log(\tau)$ is a linear function of $1/T$, it follows Arrhenius's law [10].

$$\tau = \tau_0 \exp\left(\frac{E_a}{kT}\right) \quad (3.19)$$

where τ_0 is the pre-exponential factor, E_a is the activation energy and k is the Boltzmann constant (8.617×10^{-5} eV/K) and T is the absolute temperature

For the main mode of relaxation associated with glass rubber transition (T_g), the dependence temperature $\log(\tau)$ is a non-linear function of $1/T$ leading to the equation of Vogel-Fulcher-Talmann (VFT) [10-12].

$$\tau = \tau_0 \exp\left(\frac{B}{T - T_0}\right) \quad (3.20)$$

where B is an activation temperature with units of temperature and T_0 is Vogel temperature which is generally 30-70 K below T_g .

The temperature dependence of permittivity (ϵ') and loss factor (ϵ'') of rubber vulcanizates and polymer blends were performed by using dielectric analyzer (DEA) from TA instrument (model DEA 2970, New Castle, DE, USA). The samples were measured between the ceramic parallel plate with the diameter of 25 mm and thickness around 1 mm. The experiment procedures were performed at various frequencies in the temperature range -90 to 150°C with a heating rate of 3°C. The DEA cell was purged with nitrogen gas.

The frequency dependence of permittivity (ϵ') and loss factor (ϵ'') of rubber vulcanizates and polymer blends were performed by using broadband dielectric spectroscopy (BDS) (Novocontrol, Germany). The samples were measured between two electrodes with the diameter of 30 mm and thickness around 1 mm. The experiment procedures was performed at room temperature in the frequency range 10^{-1} to 10^7 Hz. Both sides of a sample were coated with circular 30 mm diameter aluminum electrodes by vacuum evaporation and deposition.

3.4 References

- [1] Coran, A.Y. 1995. *Vulcanization: conventional and dynamic*. Rubber Chem. Technol. 68, 351-375.
- [2] Sawyer, L.C., Grubb, D.T. and Meyers, G.F. 2008. *Polymer Microscopy*. Springer, New York. 568.
- [3] Grellmann, W. and Seidler, S. 2007. *Polymer Testing*. Hanser, Munich.
- [4] Menczel, J.D., Judovits, L., Prime, R.B., Bair, H.E., Reading, M. and Swier, S. 2009. *Differential scanning calorimetry (DSC)*, in *Thermal Analysis of Polymers: Fundamentals and Applications*, J.D. Menczel and R.B. Prime, eds. John Wiley & Sons, New Jersey.
- [5] Xia, Q., Zhao, X.J., Chen, S.J., Ma, W.Z., Zhang, J. and Wang, X.L. 2010. *Effect of solution-blended poly (styrene-co-acrylonitrile) copolymer on crystallization of poly (vinylidene fluoride)*. Express Polym. Lett. 4, 284-291.
- [6] Chartoff, R.P., Menczel, J.D. and Dillman, S.H. 2009. *Dynamic mechanical analysis (DMA)*, in *Thermal Analysis of Polymers: Fundamentals and Applications*, J.D. Menczel and R.B. Prime, eds. John Wiley & Sons, New Jersey.

- [7] Vassilikou-Dova, A. and Kalogeras, I.M. 2009. *Dielectric analysis (DEA)*, in *Thermal Analysis of Polymers: Fundamentals and Applications*, J.D. Menczel and R.B. Prime, eds. John Wiley & Sons, New Jersey.
- [8] Kao, K.-C. 2004. *Dielectric Phenomena in Solids: with Emphasis on Physical Concepts of Electronic Processes*. Academic Press, San Diego.
- [9] MacCrum, N.G., Read, B.E. and Williams, G. 1967. *Anelastic and Dielectric Effects in Polymeric Solids*. Dover Publications, New York.
- [10] Nikaj, E., Stevenson-Royaud, I., Seytre, G., David, L. and Espuche, E. 2010. *Dielectric properties of polyamide 6-montmorillonite nanocomposites*. *J. Non-Cryst. Solids*. 356, 589-596.
- [11] Pluta, M., Jeszka, J.K. and Boiteux, G. 2007. *Poly(lactide)/montmorillonite nanocomposites: Structure, dielectric, viscoelastic and thermal properties*. *Eur. Polym. J.* 43, 2819-2835.
- [12] Hernández, M., Carretero-González, J., Verdejo, R., Ezquerra, T.A. and López-Manchado, M.A. 2010. *Molecular dynamics of natural rubber/layered silicate nanocomposites as studied by dielectric relaxation spectroscopy*. *Macromolecules*. 43, 643-651.

CHAPTER 4

CHARACTERIZATION OF NATURAL RUBBER AND EPOXIDIZED NATURAL RUBBER

4.1 Introduction

Natural rubber (NR) or *cis*-1,4-polyisoprene is a renewable source material used in tremendous quantities by the medical, transportation, and defense industries because it has excellent mechanical properties such as elasticity, resilience and abrasion resistance. The excellence in mechanical properties of NR resulted from strain-induced crystallization with increasing modulus on the stretching process [1, 2]. However, they are easily attacked by oxidizing reagent, highly sensitive to sunlight exposure and they have also poor chemical resistance to petroleum. These drawbacks are major obstruction for using NR in many industrial applications. Thus, NR has been chemically modified to improve these properties [3]. One of well-known alternative method for modification of diene polymer through double bond is epoxidation. Epoxidized natural rubber (ENR) is obtained from using hydrogen peroxide and formic acid with elevated temperature to NR latex. The properties of NR are significant improved with degree of epoxidation. The presence of epoxide groups in rubber molecules increases solvent resistance, wear resistance and mechanical properties and decrease air permeability [4, 5]. Besides, the ENR containing 50 mol% of epoxide group or ENR-50 is still a strain-induced crystallizable rubber for giving high tensile strength and elongation at break.

In this chapter, the influence of epoxide groups in natural rubber on cure characteristic, mechanical, dynamic mechanical and dielectric properties was studied. Two types of epoxidized natural rubber (ENR) with 25 and 50 mol% epoxide or ENR-25 and ENR-50, respectively, were used in this study in comparison with the virgin natural rubber (NR) without modification.

4.2 Effect of natural rubber types on properties of vulcanizate

The three types of natural rubber vulcanizate (i.e., NR, ENR-25 and ENR-50) were prepared using methodology described in section 3.2.1. Curing characteristic, static and dynamic mechanical properties, and dielectric analysis were then investigated.

4.2.1 Cure characteristic

The curing characteristic of elastomer yields cross-link behavior at certain curing temperature. Figure 4.1 shows the rheograph of three types of natural based rubbers: NR, ENR-25 and ENR-50. The plateau curing curve was observed in the gum compound of unmodified NR but reversion phenomenon (i.e., decreasing of torque with increasing testing time) was observed in the ENR gum compounds. This is attributed to breakdown of monosulfidic and ether linkages, which contributes to the higher reversion in the ENR networks [6]. The scorch time, cure time, cure rate index, maximum torque, minimum torque and delta torque are obtained from the curing curve of elastomer. Cure characteristics of three types of rubbers are summarized in Table 4.1. It is seen that the ENR compounds showed shorter cure and scorch times but higher cure rate index compared to the NR compound. This may be attributed to higher reactivity of the double bonds adjacent to the epoxide groups in the ENR molecules [7, 8]. Furthermore, the delta torque increased with increasing epoxide groups in the ENR molecules. The delta torque typically relates to crosslink density in the rubber vulcanizate [9]. This indicates that ENRs have higher crosslink density than NR vulcanizate. The high cross-link density of ENRs is attributed to acidic byproducts containing sulfur, which induce epoxide ring-opening reactions via ether crosslinks [9, 10].

Table 4.1 Cure characteristic of NR, ENR-25 and ENR-50 compounds

Properties	Type of NR		
	NR	ENR-25	ENR-50
Min. torque, M_L (dN.m)	1.70	1.12	1.37
Max. torque, M_H (dN.m)	8.80	14.69	15.41
Δ Torque, $M_H - M_L$ (dN.m)	7.11	13.58	14.05
Scorch time, t_{s1} (min)	1.00	0.43	0.43
Cure time, t_{90} (min)	7.00	2.67	2.57
Cure rate index, (CRI)	16.67	44.64	46.73

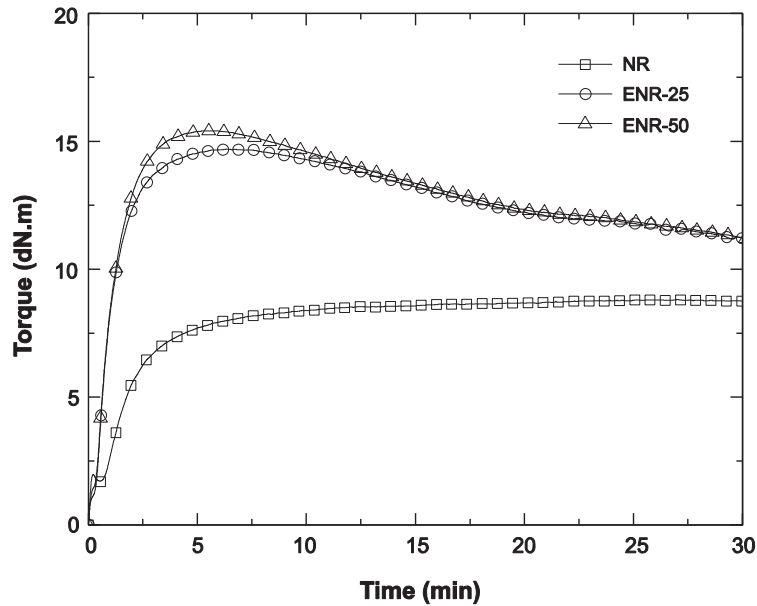


Figure 4.1 Rheograph of gum vulcanizates of NR, ENR-25 and ENR-50 at 160°C

4.2.2 Mechanical properties

Figure 4.2 shows stress–strain curves of NR, ENR-25 and ENR50 vulcanizates. As usual, stress increased with increasing strain. However, the stress drastically increase at higher strain (~500%) means rubber becomes “self-reinforcing” without reinforcing filler. This is attributed to perfect stereospecific chains of NR that the network chains of NR tend to orient themselves in the direction of stretching and this typically leads NR to the formation of crystallites or called as “strain-induced crystallization”. This phenomenon results to excellent mechanical properties (i.e., high tensile strength and elongation at break) for all types of natural rubbers [11-13]. Young’s modulus, tensile strength, elongation at break (i.e., at ultimate positions) and hardness of the vulcanizates are summarized in Table 4.2. The ENRs exhibited higher modulus, tensile strength but lower elongation at break than that of NR. The high mechanical properties of ENRs originate from two aspects related: the strain-induced crystallization and high crosslink density of ENRs as linked to delta torque value in the earlier results of section 4.2.1. This reveals that the ENR with 50 mol% epoxide groups (ENR-50) is still able to perform strain-induced crystallization, which causes an improvement of the mechanical properties. Furthermore, ENRs show higher hardness than the unmodified NR due to high crosslink density in ENR that resists to the penetration of indenter under the load.

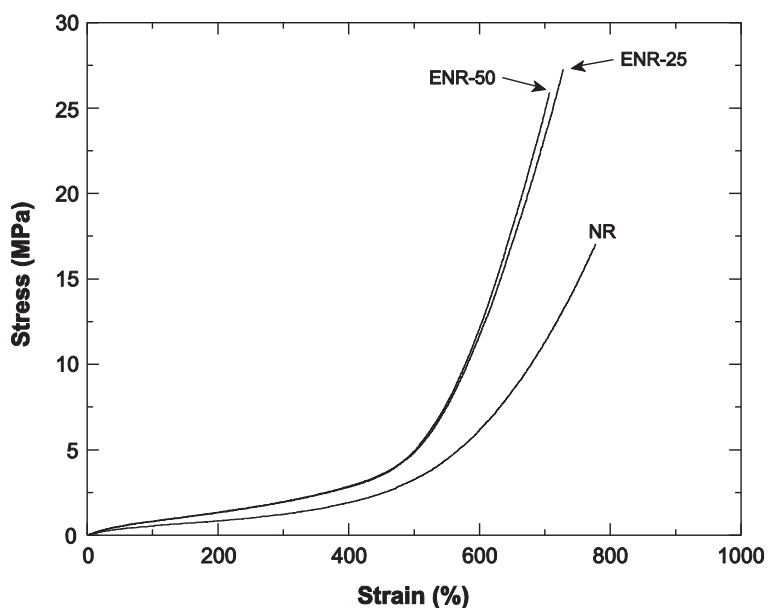


Figure 4.2 Stress-strain curves of NR, ENR-25 and ENR-50 gum vulcanizates

Table 4.2 Mechanical properties of NR, ENR-25 and ENR-50 gum vulcanizates

Type of NR	Young's modulus (MPa)	Tensile strength (MPa)	Elongation at break (%)	Hardness (Shore A)
NR	1.3 (± 0.1)	17.1 (± 0.8)	778 (± 25)	30.0 (± 0.61)
ENR-25	2.0 (± 0.2)	27.3 (± 1.6)	728 (± 23)	34.0 (± 0.79)
ENR-50	1.9 (± 0.2)	26.0 (± 1.5)	707 (± 37)	38.0 (± 0.57)

4.2.3 Dynamic mechanical analysis

Figure 4.3 shows temperature dependence of storage modulus (E') and loss tangent ($\tan \delta$) of NR, ENR-25 and ENR-50 vulcanizates. It is observed that the storage modulus curve of all types of NR is divided into three regions. First, a high storage modulus value (3000 to 7000 MPa) is observed at very low temperature period, which is called glassy state. Second, a sharp decrease of storage modulus by three decades is defined as glass transition region. Third, the storage modulus exhibited plateau curve which is called rubbery state. The main data from DMA curves are presented in Table 4.3.

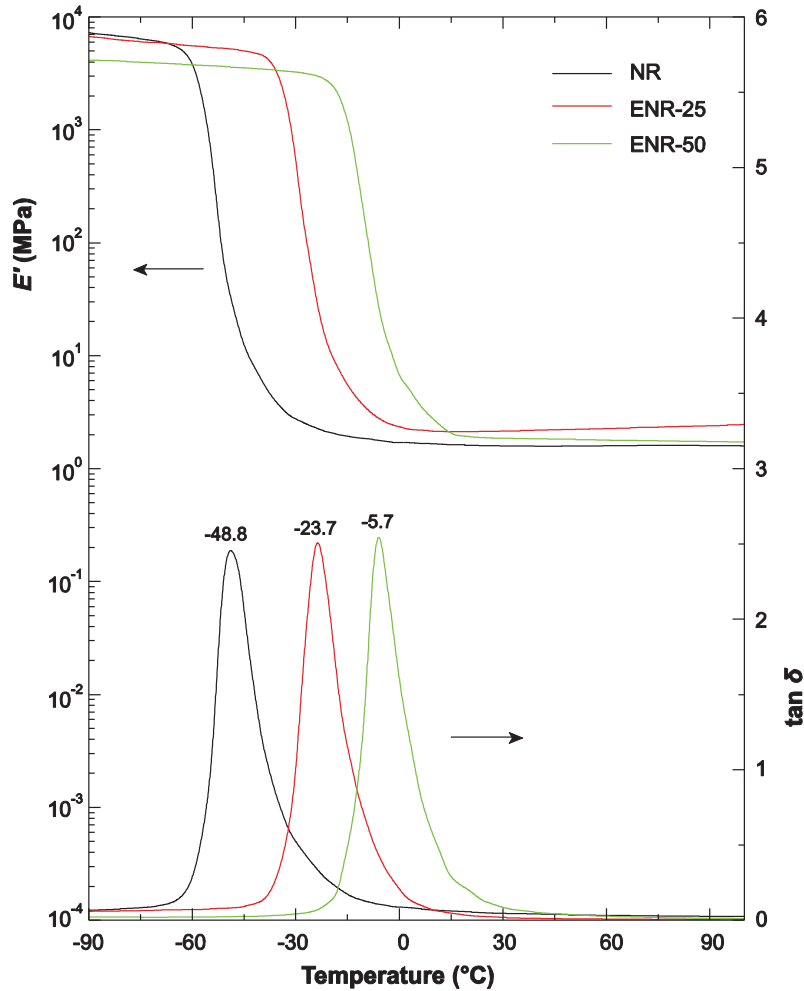


Figure 4.3 Temperature dependence of E' and $\tan \delta$ of NR, ENR-25 and ENR-50 gum vulcanizates

Table 4.3 Storage modulus and $\tan \delta$ of NR, ENR-25 and ENR-50 gum vulcanizates

Type of NR	Storage modulus, E' (MPa)		Loss tangent, $\tan \delta$	
	at -80°C	at 25°C	$\tan \delta_{\max}$	$T_g (^{\circ}\text{C})$
NR	6700	1.6	2.48	-48.8
ENR-25	6200	2.1	2.62	-23.7
ENR-50	3800	1.9	2.70	-5.7

At room temperature, all rubber vulcanizates showed storage modulus in the range of 1.5-2.0 MPa. The $\tan \delta$ peak is observed by the decreasing of storage modulus at transition region. The maximum position of $\tan \delta$ peak is commonly taken to determine the glass transition temperature (T_g) of polymer [14], which is attributed to micro-Brownian

motion of main chain or also called α -relaxation [15]. The transition region of storage modulus and position of $\tan \delta$ peak shifted to higher temperature with increasing epoxide group as clearly seen in Figure 4.3. This indicates that glass transition temperature increased with increasing epoxide group content because polar elastomers tend to have relatively high T_g [16]. The relative high T_g of ENR is mainly caused by the steric interference of the epoxide group, resulting in restriction of chain mobility because the intermolecular forces exerted on the ENR molecules [4, 17]. The level of intermolecular forces depends on the concentration of polar groups in the ENR molecules; higher epoxide contents caused lower chain mobility and hence higher T_g s. The results correspond to the work of Gelling [18] and Baker *et al.* [19]. Gelling [5] reported for every mole percent increase in epoxidation, the glass transition temperature (T_g) increases by 0.93°C.

4.2.4 Dielectric analysis

The temperature dependence of permittivity (ϵ') and loss factor (ϵ'') of NR, ENR-25 and ENR-50 vulcanizates are shown in Figures 4.4 - 4.6, respectively. Molecular relaxation is observed for NR and ENRs. At low temperature, there is a slight dependence of permittivity on frequency and low permittivity is observed. The permittivity increases at temperature near glass transition temperature, that corresponding to the segmental motion of the rubber chain. At glass transition temperature, the dipoles begin to have enough mobility to contribute to the permittivity, indicating a relaxation process. Segmental mobility of the polymer molecules increased with increasing temperature, leading to the increase in permittivity [20]. The step-like in ϵ' and ϵ'' peak reveal relaxation in the materials. The ϵ' and ϵ'' are strongly depend on temperature and frequency. A drastic increase of permittivity and appearance of loss factor peak is attributed to α -relaxation which associated to the glass transition region. The transition region and loss factor peak shifted to the higher temperature with increasing frequency, because the increased frequency results in faster movement of polymer chains, which leads to increase in relaxation temperature, consequently shifting the maximum peak to higher temperature.

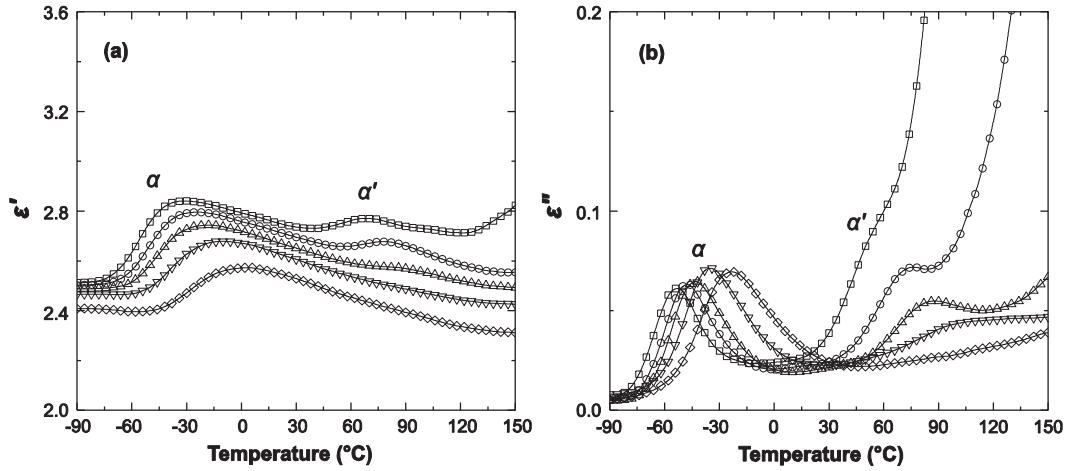


Figure 4.4 Temperature dependence of (a) ϵ' and (b) ϵ'' of vulcanized NR at several frequencies (\square) 1, (\circ) 10, (\triangle) 100, (∇) 1k and (\diamond) 10k Hz

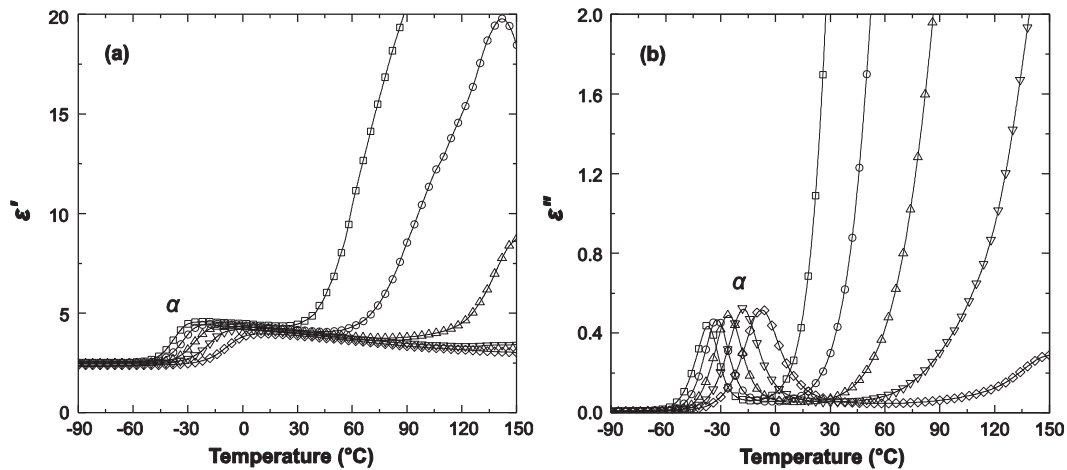


Figure 4.5 Temperature dependence of (a) ϵ' and (b) ϵ'' of vulcanized ENR-25 at several frequencies (\square) 1, (\circ) 10, (\triangle) 100, (∇) 1k and (\diamond) 10k Hz

Dielectric spectroscopy of *cis*-1,4 polyisoprene has been widely revealed by many researchers to study molecular dynamics [21-24]. They reported that polyisoprene is a type-A polymer because the lack of symmetry in its chemical structure of polyisoprene non-zero components of the dipole moment both perpendicular and parallel to the chain axis, as shown in Figure 4.7. Thus, the two dielectric relaxation can be observed in unvulcanized polyisoprene, those are a segmental (220 K, local motions of the perpendicular dipole moment) and a normal mode process (fluctuations of the dipole components parallel to the chain contour). When polyisoprene is vulcanized the normal

mode process will be suppressed as a consequence of the cross-linking [23]. In Figure 4.4, NR vulcanizate showed two relaxation processes: at low temperature and high temperature. A sharp relaxation peak around -50°C corresponds to segmental motion of the polymer chain which has its origin to local motion of perpendicular dipole moment [24]. This relaxation process can be assigned to α -relaxation which is associated to glass-rubber transition temperature (T_g) of NR [25]. A broader relaxation peak at higher temperature might be due to impurity (non-rubber) in NR and an additive such as stearic acid, which is not attributed to normal mode process. However, second relaxation can be labelled as α' -relaxation.

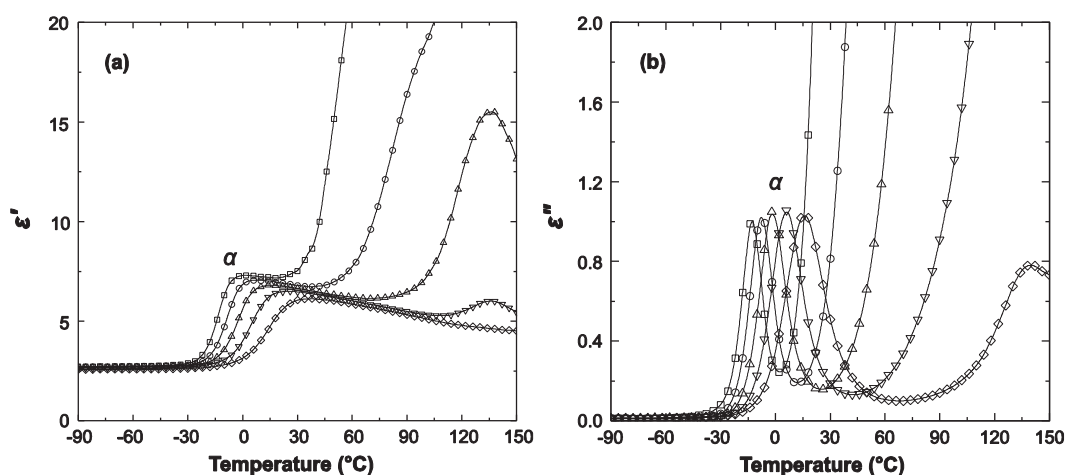


Figure 4.6 Temperature dependence of (a) ϵ' and (b) ϵ'' of vulcanized ENR-50 at several frequencies (\square) 1, (\circ) 10, (\triangle) 100, (∇) 1k and (\diamond) 10k Hz

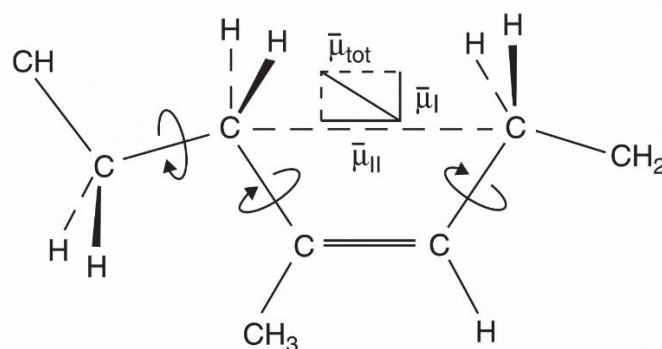


Figure 4.7 Chemical structure and dipole moment of poly(*cis*-1,4-isoprene) [26]

In Figures 4.5 and 4.6, ENR-25 and ENR-50 showed only one main relaxation that associated to α -relaxation or glass transition temperature (T_g). The second relaxation as found in NR was not observed in ENR. This process may be masked by the effect of charge carrier mobility in high temperature range, resulting in increased the permittivity and dielectric losses. The relaxation peaks move to higher temperature with increasing frequency. It is well known that the segmental motion for α -relaxation can be well fitted with the Vogel-Tamman-Fulcher (VFT) model. The reciprocal temperature dependence of the relaxation time for α -process in NR, ENR-25 and ENR-50 are shown in Figure 4.8. All fitted parameters are given in Table 4.4.

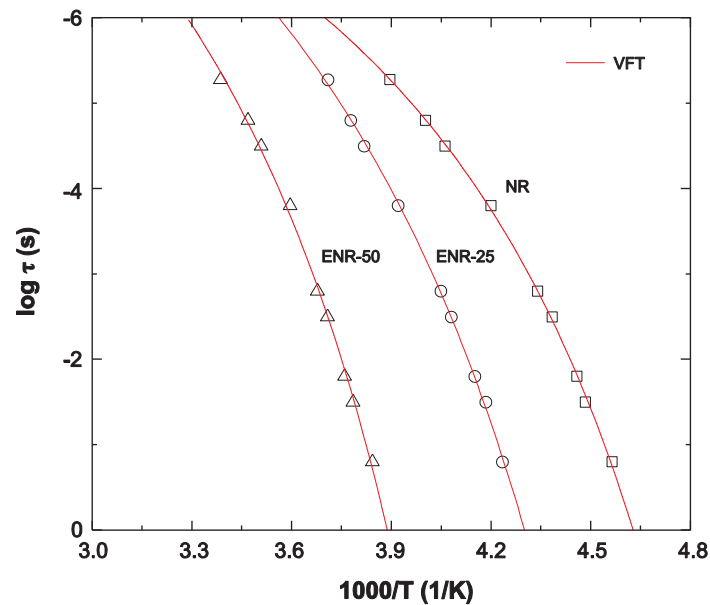


Figure 4.8 Relaxation time at maximum of ϵ'' for α -relaxation of NR, ENR-25 and ENR-50 as a function of reciprocal temperature. Solid line represent the overall best fits according to Equation 3.20

Table 4.4 Fitting parameters of VFT equation to the experimental data

Type of NR	Fitting parameter		
	$\log \tau_0$	B (K)	T_0 (K)
NR	-10.18	893	178
ENR-25	-11.95	1329	185
ENR-50	-12.04	1328	210

In Figure 4.8, it is observable that α -relaxation of all types of rubbers was well described with VFT plot. The B value of ENR is higher than unmodified NR. This result is in good agreement with the work of Klinklai *et al.* [27], who stated that B value was dependent on epoxide groups in deproteinized epoxidized natural rubber (LEDPNR): the B value increased from 942 K for 16 mol% epoxide group in LEDPNR to 2500 K for 57 mole % epoxide group in LEDPNR. The B parameter is likely deconstructed into an activation energy. Liao [4] showed that the activation energy of ENR is higher than the NR at the same concentration of curing agent because the epoxide group is classified as heterocyclic group in NR, leading to increase the energy barrier of molecular motions. Therefore, it is consistent that the molecular motions of ENR have higher activation energy. Vogel temperature (T_0) increased with increasing epoxide groups that correlates with the increase of the glass transition temperature of rubber. This result indicates that the molecular mobility of each polymer is different to the others depending on their chemical and physical structure.

For comparison, loss factor of DMA and DEA at 1 Hz as a function temperature are illustrated in Figure 4.9. It can be seen that the loss tangent peak from both technique shifted to higher temperature with increasing epoxide group contents. This is due to the steric interference caused by the presence of epoxide groups and the restriction of chain mobility due to the intermolecular forces exerted on the ENR molecules as mentioned earlier. However, the maximum peak from the both techniques is not exhibited at the same temperature. This might be due to the difference of measurement technique.

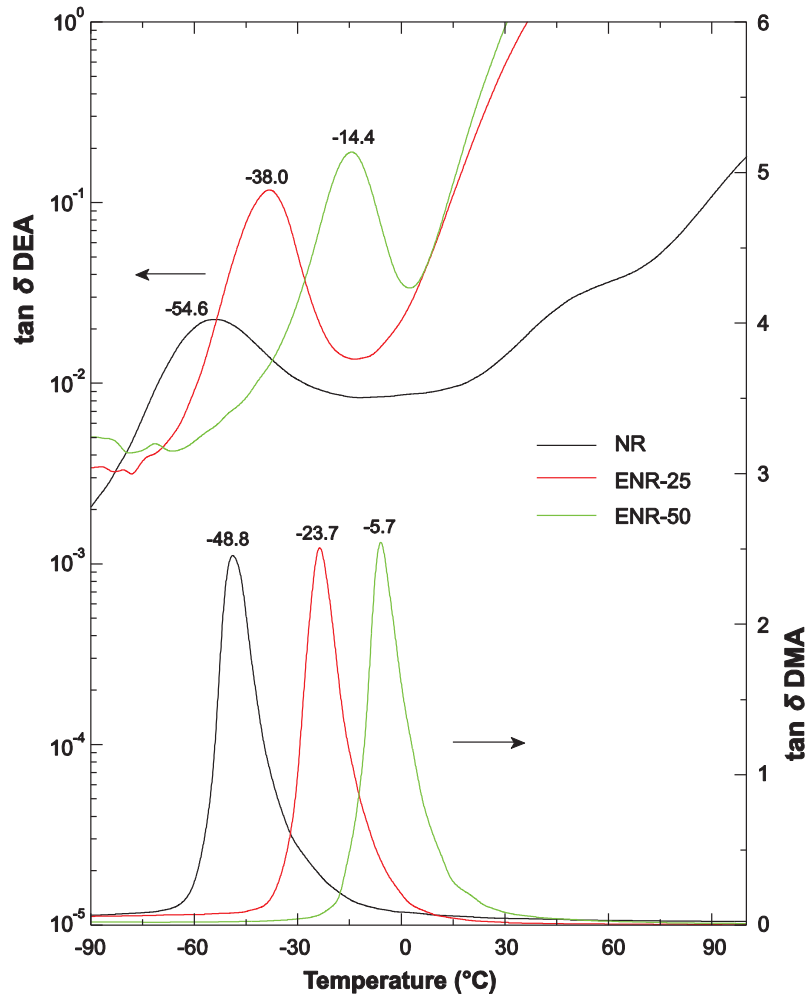


Figure 4.9 Temperature dependence of $\tan \delta$ of NR, ENR-25 and ENR-50 vulcanizates obtained from DMA and DEA techniques at frequency 1 Hz

The frequency dependence permittivity (ϵ') and loss factor (ϵ'') of different rubber vulcanizates are shown in Figure 4.10. Permittivity decreased with increasing frequency due to the dipole orientation and displacement polarization cannot rapidly follow the change in alternation electric field at sufficiency high frequency. Moreover, permittivity decreased very fast in the range of 10^4 to 10^6 Hz, which related to apparent of loss factor peak. Generally, one relaxation peak in loss factor at room temperature corresponds to α -relaxation. The relaxation peak shifted to lower frequency as epoxide group increased, suggesting a restricted dynamics motion of natural rubber with the presence of epoxide group [24]. The ϵ' , ϵ'' and $\tan \delta$ at 1 kHz of different types of natural rubbers are summarized in Table 4.5. It can be seen that the values of ϵ' and ϵ'' of NR are significantly

lower compared to ENRs one. This is attributed to difference in polarity of chain segments. The NR segments have no polar group. Therefore, NR is a very low polarity rubber. Naturally, the ENR-50 has much more polar than the ENR-25 due to the presence of a larger number of epoxide groups in its structure. Generally, the high polarity in molecular structure leads to the increase of the dielectric permittivity [28-30]. Hence, the ENR-50 shows the highest ϵ' , ϵ'' and $\tan \delta$ as it has the highest concentration of dipole. The increase of dipole in ENR also leads to increase the amplitude of loss factor peak as observed in temperature and frequency dependence curves. This has a good agreement with the work of Furukawa *et al.* [31]. They reported that the ϵ'' peak becomes higher as the maleic anhydride fraction increased because the dipole moment of maleic anhydride groups contributed to the relaxation strength.

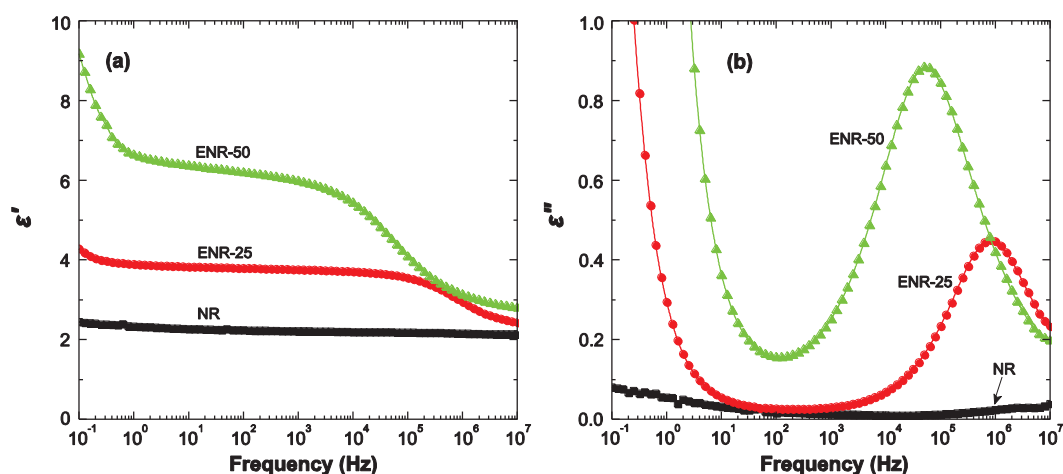


Figure 4.10 Frequency dependence of (a) ϵ' and (b) ϵ'' of NR, ENR-25 and ENR-50 vulcanizates at room temperature

Table 4.5 Dielectric properties at frequency 1 kHz of NR, ENR-25 and ENR-50 vulcanizates

Type of NR	Permittivity, ϵ'	Loss factor, ϵ''	Loss tangent, $\tan \delta$
NR	2.22	0.01	0.006
ENR-25	3.76	0.03	0.008
ENR-50	6.00	0.25	0.042

At low frequency and high temperature, a sharp increase of permittivity and loss factor was observed in ENR-25 and ENR-50 (Figure 4.5, 4.6 and 4.10) confirming the existence of conduction loss due to thermally excited ionic species which can accumulate and become trapped at the electrode and/or at local heterogeneous interface within the material. The interfacial polarization may arise from the additive, fillers, impurities and heterogeneous system having different permittivity and conductivity in polymer and polymer composites [20, 32, 33]. The high values of ϵ' at high temperatures and low frequencies can be attributed to the charge in carriers accumulating at interfaces within the bulk of the sample (interfacial or Maxwell-Wagner-Sillars (MWS) polarization phenomenon) and/or at the interface between the sample and the electrodes (electrode or space charge polarization phenomenon). At high temperatures, the ϵ'' mainly exhibits an increase with decreasing frequency due to the contribution of DC conductivity (σ_{dc}) indicating the existence of space charge polarization [32]. The electric modulus formalism can be used to exclude the electrode polarization and space charge injection phenomena. The relaxation process is hidden by high permittivity and the loss factor can be revealed and explained by applying electric modulus (see Equation 3.18) [20, 33, 34].

The imaginary part (M'') versus temperature with various frequencies for NR, ENR-25 and ENR-50 are shown in Figure 4.11. It can be seen that a new peak was observed in experimented temperature range of M'' plot, which indicates the relaxation processes. NR showed two relaxation peaks corresponded to α and α' -relaxation as observed in dielectric loss factor (Figure 4.4). The two M'' relaxation peaks were clearly observed at lower and higher temperature for ENR-25 and ENR-50 vulcanizates. The relaxation at low temperature corresponded to α -relaxation process which is related to segmental motion of molecular chain. The relaxation at high temperature was not visibly evident in ϵ'' spectrum but appear in M'' spectrum. This relaxation is attributed to the conductivity (σ) because at sufficient temperature and low frequency charge transfer in conductivity process sharply increases the dielectric value [20, 35].

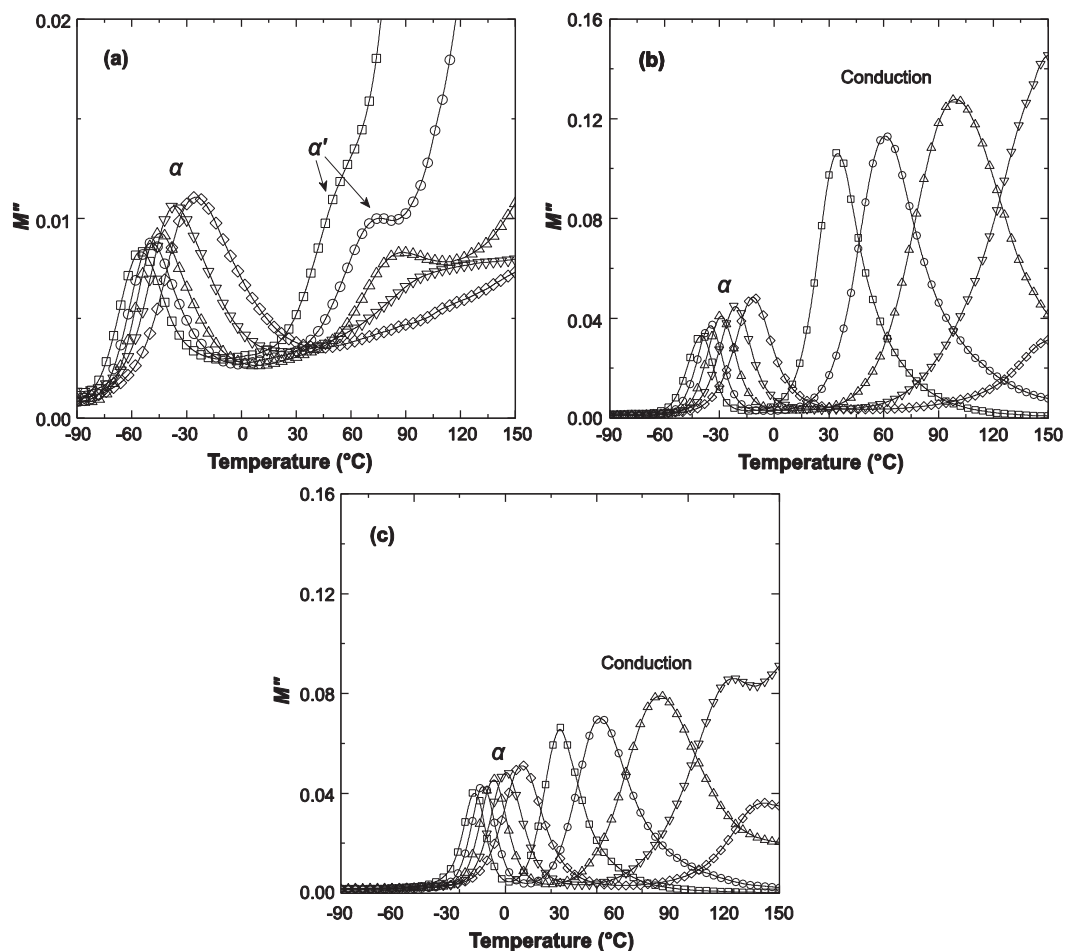


Figure 4.11 Temperature dependence of M'' of (a) NR, (b) ENR-25 and (c) ENR-50 vulcanizates at several frequencies (\square) 1, (\circ) 10, (\triangle) 100, (∇) 1k and (\diamond) 10k Hz

Furthermore, the conductivity relaxation can also be observed in frequency domain of M'' as depicted in Figure 4.12. ENR-50 shows two relaxation peaks at low and high frequency. The narrow peak at frequency 1 Hz is associated with conductivity relaxation. Second relaxation peak at higher frequency can be ascribed to α -relaxation process generally associated with segmental motion [35]. Nevertheless, ENR-25 shows only one relaxation peak in experimented frequency. Therefore, conductivity peak of ENR-25 may be observed at very low frequency ($<10^{-1}$ Hz). Meanwhile, relaxation of NR in M'' as a function of frequency was not clearly observed.

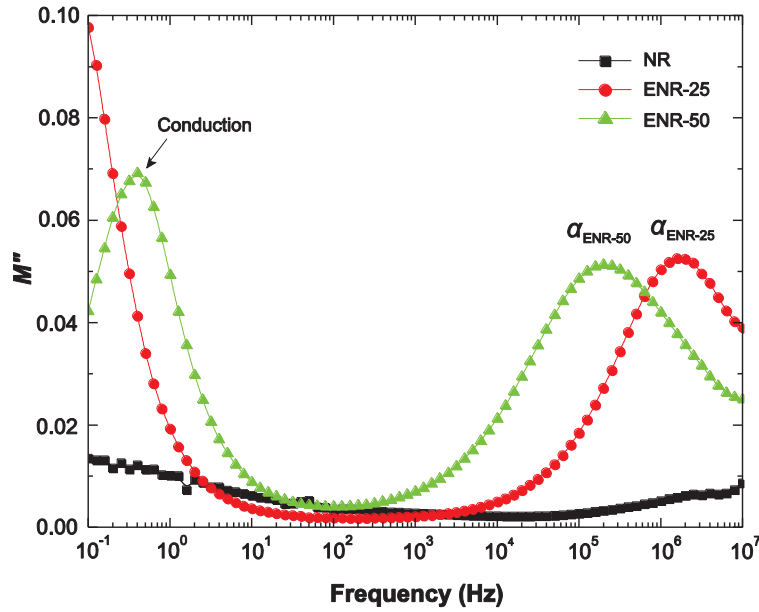


Figure 4.12 Frequency dependence of M'' of NR, ENR-25 and ENR-50 vulcanizates

Conduction process at low frequency is confirmed by AC conductivity (σ_{AC}) plot as shown in Figure 4.13. The σ_{AC} has been analyzed to study charge carrier movement on polarization and calculated from dielectric loss using equation:

$$\sigma = \omega \epsilon_0 \epsilon'' \quad (4.1)$$

where ϵ_0 is the permittivity of the free space ($\epsilon_0 = 8.854 \times 10^{-12}$ F/m) and ω is the angular frequency ($\omega = 2\pi f$).

Figure 4.13, NR shows frequency dependence of AC conductivity in the observed frequency range. However, frequency dependence of electrical conductivity of ENRs (i.e., ENR-25 and ENR-50) can be divided into two regions: First, conductivity pattern shows frequency independence at low frequency, exhibiting plateau region, and second region exhibits dispersion at higher frequencies. The plateau region in AC conductivity can be considered as real conductivity (ionic/electronic conductivity process) because σ_{DC} is the frequency independent conductivity (DC conductivity at $\omega \rightarrow 0$) [36]. This proves the existence of conductivity process in ENRs at low frequency and high temperature. It can also be seen that conductivity increases with increasing epoxide group content, therefore, the conductivity of ENR-50 is higher than that of NR for 3 decades and higher than ENR-25 for 1 decade. Conductivity is generally reflecting the mechanism

of charge transport behavior of charge carriers. It can be concluded that at low frequency and sufficient temperature, an ion can jump successfully from one site to its neighboring vacant site, hence contributing to DC conductivity. The enhancement in conductivity with epoxide group may be due to an increase in number of ions transportation.

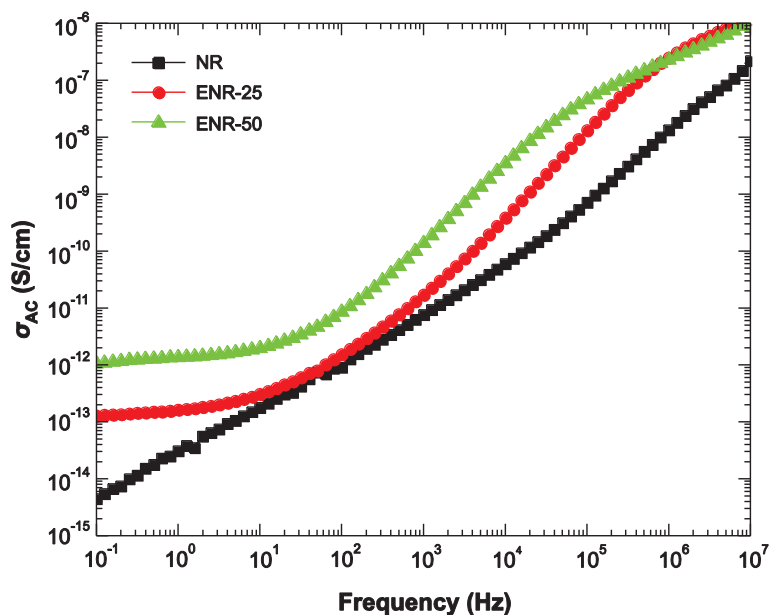


Figure 4.13 Frequency dependence of AC conductivity of NR, ENR-25 and ENR-50 vulcanizates

The temperature dependence of M'' for peak related to the conductivity process at high temperature, can provide information of charge transport mechanisms within the materials. Figure 4.14 shows relaxation time of conductivity process as a function of reciprocal of temperature where solid line least square fits to experimental data points. The conductivity relaxation shows Arrhenius type behavior indicating that relaxation is thermally activated process. The relaxation time decreases with increasing temperature due to enhancement of mobility of charge carriers at high temperature; the movement of ions by hopping mechanism is more favored and leads to increase conductivity. For Arrhenius relationship, it is stated that the nature of transportation charge carrier is similar with the migration in ionic crystal [37]. Existence of hopping process in ENRs resulting from oxirane ring may act as a vacant site or empty voids in the polymer chains. Therefore, the ions tend to occupy these neighboring vacant sites. This transportation of charge carriers increases the conductivity and it also increases with increasing epoxide content. The temperature dependence of dielectric relaxation time is well described by

the Arrhenius type behavior. The activation energy calculated from slope of plot around 0.70 eV for ENR-25 and 0.75 eV for ENR-50.

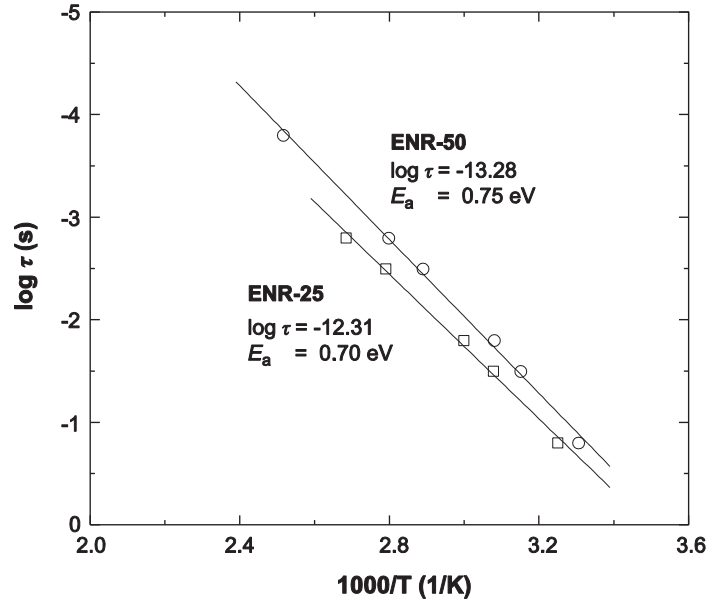


Figure 4.14 Relaxation time at maximum of M'' for conduction process of NR, ENR-25 and ENR-50 as a function of reciprocal temperature. Solid lines represent the overall best fits according to Equation 3.19

4.3 Conclusions

The natural rubber vulcanizates with different epoxide groups were prepared by melt mixing process. Based on the results, it can be concluded that polymer molecular structure has a significant influence on polymer characteristics. The unmodified NR shows plateau curing curves and ENRs show reversion phenomenon. The ENRs have shorter scorch time and cure time but higher cure rate index compared to NR. An increase in modulus at high strain was observed and it is attributed to stress-induced crystallization of natural rubber. The ENRs exhibited higher modulus, tensile strength but lower elongation at break than that of NR. The contribution to the lower modulus of NR comes from the fact that the double bond in NR are partly replaced by epoxide group. The dynamic mechanical analysis (DMA) and dielectric analysis (DEA) revealed that the molecular mobility between unmodified and modified NR are different due to difference in their chemical and physical structures. The NR, ENR-25 and ENR-50 showed drastically

decrease in storage modulus when reaching their glass transition temperature. The relaxation peak which correspond to glass rubber transition in DMA and DEA shifts to higher temperature as epoxide group content increased. The ENRs show conduction process at low frequency and high temperature which was revealed by electric modulus formalism. The relaxation time for segmental motion or α -relaxation and conductivity can be well fitted with the Vogel-Tamman-Fulcher (VFT) and Arrhenius equation, respectively. The B and T_0 were dependent on epoxide groups content in molecular chains while activation energy of conductivity is around 0.70 eV. Furthermore, dielectric parameter (i.e. ϵ' , ϵ'' and $\tan \delta$) and conductivity increased with increasing epoxide groups concentration and ENR-50 shows the highest value. This result indicated that ENR-50 was suitable polymer for preparation of high permittivity composite due to its higher mechanical properties and dielectric permittivity than those of ENR-25 and NR.

4.4 References

- [1] Mark, H.F. 2007. *Encyclopedia of Polymer Science and Technology*. 3rd ed. Wiley-Interscience, New York.
- [2] Eng, A.H. and Ong, E.L. 2001. *Hevea natural rubber*, in *Handbook of elastomers*, A.K. Bhowmick and H.L. Stephens, eds. Marcel Dekker, New York.
- [3] Cardarelli, F. 2008. *Materials Handbook: A Concise Desktop Reference*. Springer, New York.
- [4] Liau, W.B. 1999. *Dynamic mechanical relaxation of lightly cross-linked epoxidized natural rubber*. *Polymer*. 40, 599-605.
- [5] Gelling, I.R. 1991. *Epoxidised natural rubber*. *J. Nat. Rubber Res.* 6, 21.
- [6] Poh, B.T., Kwok, C.P. and Lim, G.H. 1995. *Reversion behaviour of epoxidized natural rubber*. *Eur. Polym. J.* 31, 223-226.
- [7] Sadequl, A.M., Ishiaku, U.S., Ismail, H. and Poh, B.T. 1998. *The effect of accelerator/sulphur ratio on the scorch time of epoxidized natural rubber*. *Eur. Polym. J.* 34, 51-57.
- [8] Poh, B.T., Chen, M.F. and Ding, B.S. 1996. *Cure characteristics of unaccelerated sulfur vulcanization of epoxidized natural rubber*. *J. Appl. Polym. Sci.* 60, 1569-1574.

- [9] Ismail, H. and Chia, H.H. 1998. *The effects of multifunctional additive and vulcanization systems on silica filled epoxidized natural rubber compounds*. Eur. Polym. J. 34, 1857-1863.
- [10] Gelling, I.R., Porter, M. and Ad, R. 1990. *Chemical modification of natural rubber*. Natural rubber science and technology, AD Roberts (ed.), Malaysian Rubber Producers Research Association, Oxford University Press, Oxford.
- [11] Trabelsi, S., Albouy, P.A. and Rault, J. 2004. *Stress-induced crystallization properties of natural and synthetic cis-polyisoprene*. Rubber Chem. Technol. 77, 303-316.
- [12] Tripathy, A.R., Morin, J.E., Williams, D.E., Eyles, S.J. and Farris, R.J. 2002. *A novel approach to improving the mechanical properties in recycled vulcanized natural rubber and its mechanism*. Macromolecules. 35, 4616-4627.
- [13] Ozbas, B., Toki, S., Hsiao, B.S., Chu, B., Register, R.A., Aksay, I.A., Prud'homme, R.K. and Adamson, D.H. 2012. *Strain-induced crystallization and mechanical properties of functionalized graphene sheet-filled natural rubber*. J. Polym. Sci. Pol. Phys. 50, 718-723.
- [14] Zhang, X.G. and Loo, L.S. 2009. *Study of glass transition and reinforcement mechanism in polymer/layered silicate nanocomposites*. Macromolecules. 42, 5196-5207.
- [15] Grellmann, W. and Seidler, S. 2007. *Polymer Testing*. Hanser, Munich.
- [16] Groves, S. 1998. *Natural rubber/ENR-25 blends*, in *Blends of Natural Rubber*, A.J. Tinker and K.P. Jones, eds. Springer.
- [17] Nakason, C., Panklieng, Y. and Kaesaman, A. 2004. *Rheological and thermal properties of thermoplastic natural rubbers based on poly(methyl methacrylate)/epoxidized-natural-rubber blends*. J. Appl. Polym. Sci. 92, 3561-3572.
- [18] Gelling, I.R. 1985. *Modification of natural rubber latex with peracetic acid*. Rubber Chem. Technol. 58, 86-96.
- [19] Baker, C.S.L., Gelling, I.R. and Newell, R. 1985. *Epoxidized natural rubber*. Rubber Chem. Technol. 58, 67-85.

- [20] Hammami, H., Arous, M., Lagache, M. and Kallel, A. 2007. *Study of the interfacial MWS relaxation by dielectric spectroscopy in unidirectional PZT fibres/epoxy resin composites*. J. Alloys Compd. 430, 1-8.
- [21] Ortiz-Serna, P., Díaz-Calleja, R., Sanchis, M.J., Floudas, G., Nunes, R.C., Martins, A.F. and Visconte, L.L. 2010. *Dynamics of natural rubber as a function of frequency, temperature, and pressure. a dielectric spectroscopy investigation*. Macromolecules. 43, 5094-5102.
- [22] Ortiz-Serna, P., Díaz-Calleja, R., Sanchis, M.J., Riande, E., Nunes, R., Martins, A. and Visconte, L. 2011. *Dielectric spectroscopy of natural rubber-cellulose II nanocomposites*. J. Non-Cryst. Solids. 357, 598-604.
- [23] Fragiadakis, D., Bokobza, L. and Pissis, P. 2011. *Dynamics near the filler surface in natural rubber-silica nanocomposites*. Polymer. 52, 3175-3182.
- [24] Hernández, M., Ezquerra, T.A., Verdejo, R. and López-Manchado, M.A. 2012. *Role of vulcanizing additives on the segmental dynamics of natural rubber*. Macromolecules. 45, 1070-1075.
- [25] Hernández, M., López-Manchado, M.A., Sanz, A., Nogales, A. and Ezquerra, T.A. 2011. *Effects of strain-induced crystallization on the segmental dynamics of vulcanized natural rubber*. Macromolecules. 44, 6574-6580.
- [26] Kremer, F. 2007. *Broadband dielectric spectroscopy to study the molecular dynamics of polymers having different molecular architectures*, in *Physical Properties of Polymers Handbook*. Springer, New York.
- [27] Klinklai, W., Kawahara, S., Marwanta, E., Mizumo, T., Isono, Y. and Ohno, H. 2006. *Ionic conductivity of highly deproteinized natural rubber having various amount of epoxy group mixed with lithium salt*. Solid State Ionics. 177, 3251-3257.
- [28] Madbouly, S.A. and Otaigbe, J.U. 2007. *Broadband dielectric spectroscopy of nanostructured maleated polypropylene/polycarbonate blends prepared by in situ polymerization and compatibilization*. Polymer. 48, 4097-4107.
- [29] Popielarz, R., Chiang, C.K., Nozaki, R. and Obrzut, J. 2001. *Dielectric properties of polymer/ferroelectric ceramic composites from 100 Hz to 10 GHz*. Macromolecules. 34, 5910-5915.

- [30] Leu, C.M., Chang, Y.T. and Wei, K.H. 2003. *Polyimide-side-chain tethered polyhedral oligomeric silsesquioxane nanocomposites for low-dielectric film applications*. Chem. Mater. 15, 3721-3727.
- [31] Furukawa, T., Yuruzume, H., Kimura, T. and Matsuura, S. 1994. *Dielectric investigation of polypropylene grafted with maleic anhydride*. 8th International Symposium on Electrets (ISE 8), 450-454.
- [32] Khazaka, R., Locatelli, M.L., Diaham, S., Bidan, P., Dupuy, L. and Grosset, G. 2013. *Broadband dielectric spectroscopy of BPDA/ODA polyimide films*. J. Phys. D: Appl. Phys. 46.
- [33] Wang, M.-J. 1998. *Effect of polymer-filler and filler-filler interactions on dynamic properties of filled vulcanizates*. Rubber Chem. Technol. 71, 520-589.
- [34] Kontos, G.A., Soulintzis, A.L., Karahaliou, P.K., Psarras, G.C., Georga, S.N., Krontiras, C.A. and Pisanias, M.N. 2007. *Electrical relaxation dynamics in TiO₂-polymer matrix composites*. Express Polym. Lett. 1, 781-789.
- [35] Adohi, B.J.P. and Brosseau, C. 2009. *Dielectric relaxation in particle-filled polymer: Influence of the filler particles and thermal treatments*. J. Appl. Phys. 105.
- [36] Sohi, N.J.S., Bhadra, S. and Khastgir, D. 2011. *The effect of different carbon fillers on the electrical conductivity of ethylene vinyl acetate copolymer-based composites and the applicability of different conductivity models*. Carbon. 49, 1349-1361.
- [37] Ramesh, S., Liew, C.W. and Ramesh, K. 2013. *Ionic conductivity, dielectric behavior, and HATR-FTIR analysis onto poly(methyl methacrylate)-poly(vinyl chloride) binary solid polymer blend electrolytes*. J. Appl. Polym. Sci. 127, 2380-2388.

CHAPTER 5

FLEXIBLE CERAMIC-POLYMER COMPOSITES

BASED ON BT/ENR-50 COMPOSITES

5.1 Introduction

Polymer composites incorporating reinforcing and non-reinforcing fillers have been consistently investigated to create useful property of the combinations. Their typical modified characteristics include stiffness, stability, coloring and anti-static properties. Ferroelectric ceramics are one type of filler which can be used to prepare ceramic-polymer composites for dielectric permittivity improvement. They have been used in various applications: multi-layer ceramics capacitors (MLCC), piezoelectric sensors, transducers, actuators, and microelectromechanical systems (MEMS) because they typically exhibit high dielectric constant and piezoelectric coefficient [1]. On the other hand polymers provide excellent flexibility and are easy to process, but generally have low dielectric constant. The synthesis of ferroelectric ceramic-polymer composites strives to combine some electrical properties of the ceramic with the viscoelastic properties of the polymer matrix. In prior studies, such 0-3 structured hybrid materials have provided stiffness and high permittivity from the ceramic part and excellent flexibility and strength from the polymer part. These composites are essential in various applications such as flexible capacitors, sensors, and piezoelectric and pyroelectric devices [2-4]. Recently, ferroelectric ceramic-polymers based on poly(vinylidene fluoride) and its copolymers have been reported that these materials have high permittivity and dielectric strength [5, 6]. Some other semi-crystalline and amorphous polymers, such as polyimide [7], and poly(methyl methacrylate) (PMMA) [8] have also been used to prepare ceramic-polymer composite. The fabrication of ceramic-containing composites based on thermoset polymers such as epoxy [9, 10], cross-linked silicone rubber [11], and ethylene-vinyl acetate elastomer (EVA) [12] have been prepared and reached relatively low degradation

and high flexibility. Besides, epoxidized natural rubber (ENR) is a modified natural rubber containing epoxide groups in its molecular backbone. In our previous chapter and work, the presence of epoxide groups in isoprene units was found to enhance mechanical properties and dielectric permittivity of ENR. ENR-50 (containing 50 mol% epoxide) has the highest dielectric constant in comparison with unmodified natural rubber and ENR-25 (containing 25 mol% epoxide) [13]. Therefore, the high mechanical strength, flexibility and high dielectric permittivity of ENR-50 make it a prime candidate for the synthesis of ceramic-polymer composites with high dielectric constant.

The aim of this chapter is to investigate the use of barium titanate (BT) particle, which was prepared through solid state reaction technique. The XRD, microstructure and dielectric properties were used to verify the BT characteristics for fabricating ceramic-polymer composite. The composites of BT with ENR-50 were prepared by melt-mixing method. The effect of loading level of BT particle in ENR-50 on curing, morphological, static and dynamic mechanical, dielectric properties was investigated and discussed.

5.2 Barium titanate characterization

Preparation of barium titanate ceramic (BaTiO_3 or BT) has been described in section 3.2.2. Microstructure and dielectric properties of prepared barium titanate were investigated.

5.2.1 XRD pattern

The BT were prepared by using solid state technique. The phases involved in formation of the BT were examined by XRD technique as the patterns shown in Figure 5.1. It can be seen that the mixed powders of $\text{BaCO}_3|\text{TiO}_2$ exhibited the different XRD patterns compared to the BT product. The structure of BT was found at peak of 22.02° , 22.23° , 31.49° , 31.65° , 38.89° , 44.90° , 45.37° , 50.98° , 55.27° , and 56.27° which corresponded to the (0 0 1), (1 0 0), (1 0 1), (1 1 0), (1 1 1), (0 0 2), (2 0 0), (2 0 1), (1 1 2), and (2 1 1) planes of perovskite structure, respectively. Furthermore, the results in Figure 5.1 agreed with the XRD data of BT reported in the JCPDS (Joint Committee on Powder Diffraction Standards) file number 01-075-0583, which is proved that the reaction of BaCO_3 and TiO_2 at 1100°C yielded BT product.

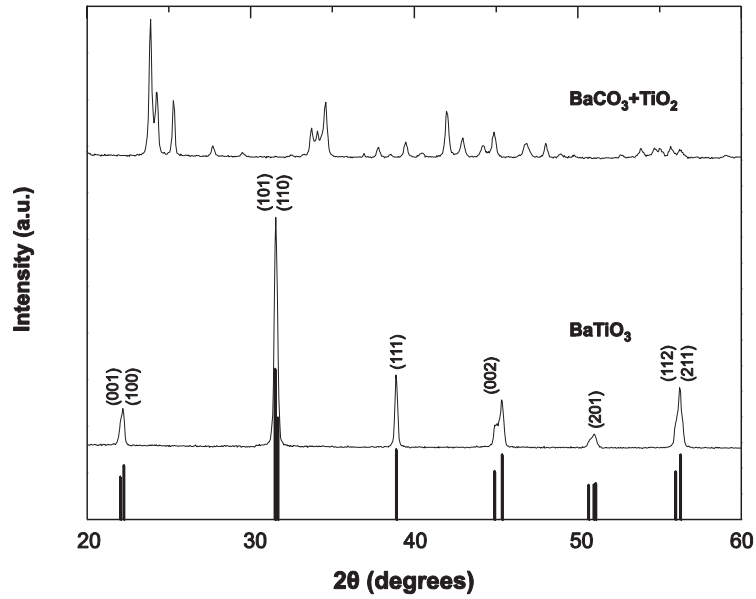


Figure 5.1 XRD patterns of mixed $\text{BaCO}_3+\text{TiO}_2$ and BaTiO_3

5.2.2 Microstructure of barium titanate

The microstructure of BT was investigated using scanning electron microscope (SEM) and particle size distribution studies as the results shown in Figure 5.2. The SEM and particle size distribution studies on the powder prepared BT show that agglomerate size distribution of the prepared powder is large distribution and the powder crushed by conventional ball mill consists of agglomerated particles with an average particle size of about $4.5 \mu\text{m}$.

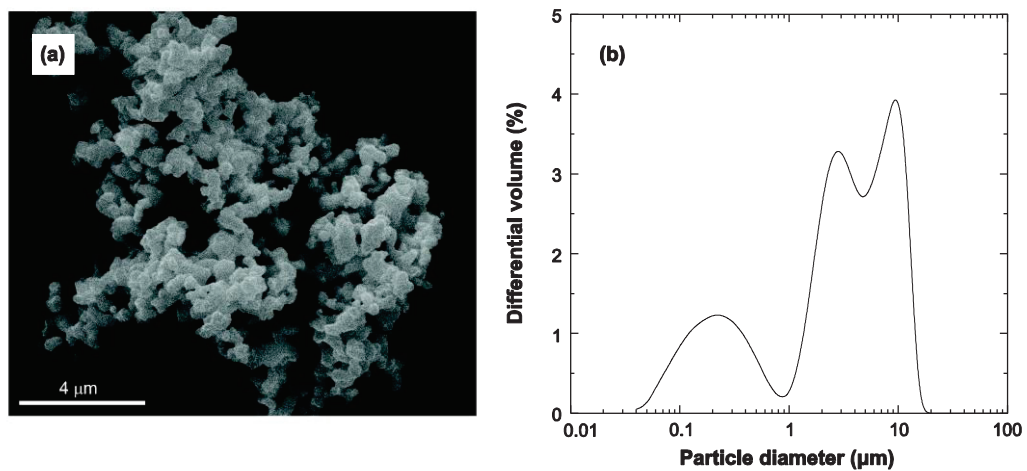


Figure 5.2 (a) SEM micrograph and (b) particle size distribution of BT powders

5.2.3 Dielectric properties

The permittivity (ϵ'), loss factor (ϵ'') and loss tangent ($\tan \delta$) of the BT pellets sintering from the powder were studied. The investigation were done in the frequency range of 0.1 Hz to 10 MHz at room temperature with silver electrodes on both sides of the circular disc. A function of ϵ' , ϵ'' and $\tan \delta$ with frequency is shown in Figure 5.3. It can be seen that the ϵ' was almost constant in the frequency range while ϵ'' and $\tan \delta$ was significant varied with frequency. The values of permittivity, loss factor and loss tangent of synthesized barium titanate at 1 kHz were 2400, 94 and 0.04, respectively. The permittivity or dielectric constant is related to electrical energy stored in a material by an applied voltage. Dielectric losses occur due to DC conductivity and dipole relaxation. The loss factor ($\tan \delta$) is a useful indicator of the energy loss of materials. The high permittivity and low loss tangent of barium titanate is due to the characteristic of ferroelectric ceramic. The high dielectric constant or permittivity and low loss factor make it being an excellent material for many applications, such as capacitors, multilayer capacitors and energy storage devices. Our synthesized barium titanate has high permittivity and low loss factor as doped-barium titanate [14] and barium titanate from precipitate method [15].

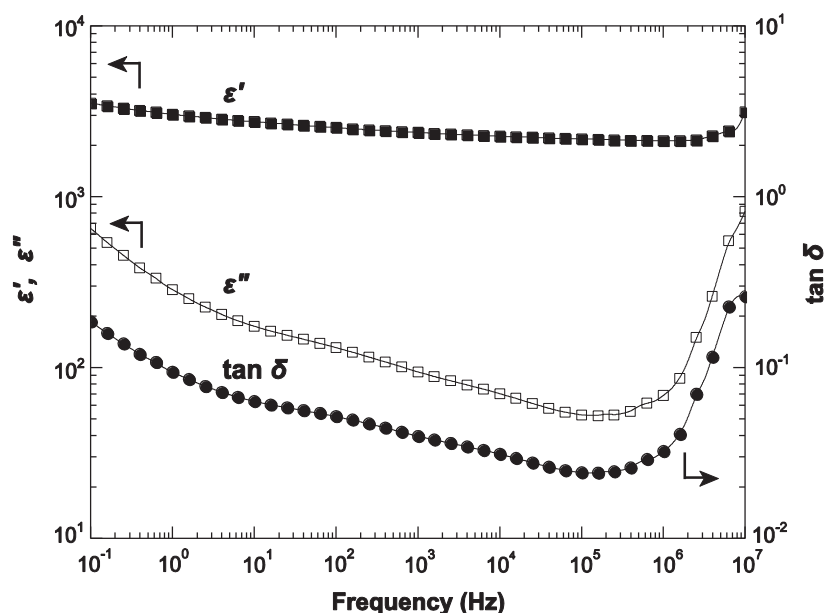


Figure 5.3 Permittivity (ϵ'), loss factor (ϵ'') and loss tangent ($\tan \delta$) as function of frequency of synthesized barium titanate

5.3 Effect of BT loading level on properties of BT/ENR-50 composites

Ceramic-polymer composites based on BaTiO₃/ENR-50 or BT/ENR-50 with different BT loading in ENR-50 phase were prepared according to method describing in section 3.2.3. Effect of BT loading (i.e., 0, 5, 10, 15, 20, 30, 40 and 50 vol%) on cure characteristic, morphological, mechanical and thermal properties (determined by dynamic mechanical analysis and dielectric analysis) were investigated.

5.3.1 Cure characteristic

Curing characteristics of ENR-50 filled with various amounts of BT are shown in Figure 5.4. It is observable that the torque increases because of the formation of crosslinking bonds. It is clear that the maximum torque (M_H) increased with increasing amount of BT. A reversion, a decreasing trend after the maximum is observed which is due to the low thermal stability of sulfidic bonds (C-S_x-C) in the rubber network, and their degradation [16]. The reversion behavior is more pronounced with increasing BT content, due to the changes in cross-link structures of the vulcanizates after the maximum vulcanization [17]. Curing characteristics in terms of minimum torque, maximum torque and delta torque, scorch time, and cure time of the gum rubber and the BT/ENR-50 compounds are summarized in Table 5.1. Basically, the minimum torque is related to the viscosity of rubber compound, while maximum torque is related to magnitude of crosslink reaction and interaction in vulcanizate rubber. The maximum torque and torque difference increased with increasing BT loading due to an increase of filler-polymer and filler-filler interactions and also restriction of the rubber chain mobility with the loaded filler. Thus, the torque difference ($M_H - M_L$) is an indirect measurement of network density in the crosslink system, increases with the loading level of BT. In Table 5.1, both scorch and cure times became shorter as BT content increases. This is due to the fact that incorporation of BT in ENR-50 could accelerate the reaction rate of vulcanization. Therefore, both scorch time and cure time decreased.

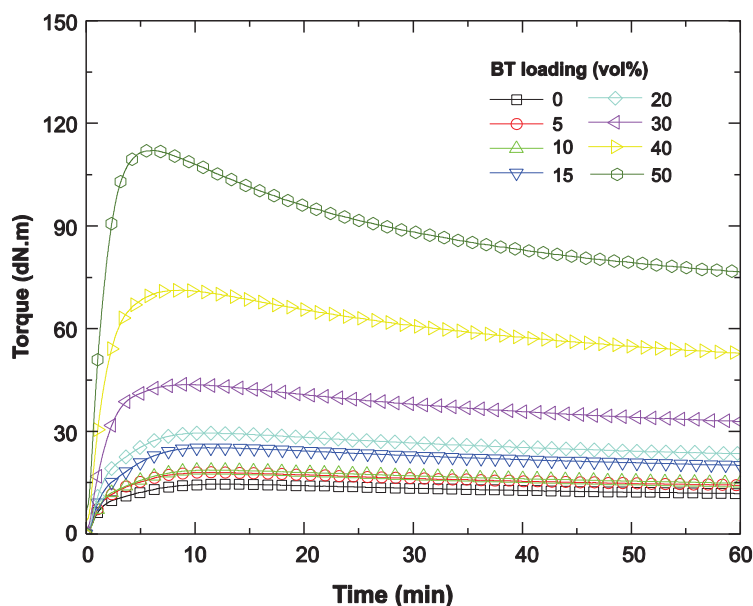


Figure 5.4 Rheographs of BT/ENR-50 composites with various BT loadings

Table 5.1 Cure characteristic of BT/ENR-50 composites with various BT loadings

Properties	Barium titanate loading (vol%)							
	0	5	10	15	20	30	40	50
Min. torque, M_L (dN.m)	0.99	0.78	0.84	0.92	1.10	1.59	3.72	7.55
Max. torque, M_H (dN.m)	14.53	17.97	18.66	25.22	29.50	43.68	71.23	112.08
Δ Torque, $M_H - M_L$ (dN.m)	13.54	17.19	17.82	24.30	28.40	42.09	67.51	104.53
Scorch time, t_{s1} (min)	0.46	0.41	0.39	0.36	0.34	0.33	0.31	0.29
Cure time, t_{90} (min)	6.49	6.23	6.22	6.19	5.73	3.99	3.70	3.05
Cure rate index, (CRI)	16.58	17.18	17.15	17.15	18.55	27.32	29.50	36.23

5.3.2 Morphological properties

SEM micrographs of the fractured surfaces of the composites with various amounts of BT, are shown in Figure 5.5. In gum vulcanizate, a dispersion of ZnO in cross-linked ENR-50 matrix is clearly observed. A compact and homogeneous microstructure of the BT/ENR-50 composites can be comprehended which means that the mixing process and parameters used for composite manufacturing are appropriate. The BT particles are embedded in the ENR-50 matrix, which establishes microstructure (0-3) connectivity of the composite, with unconnected particles in the continuous ENR-50 matrix. The thickness of the ENR-50 matrix layer, surrounded by BT particles, decreased

when the BT concentration increased. Enlarged image in Figure 5.6 shows that the average diameter of BT particles in ENR-50 matrix was less than 1 μm (1000 nm) and their agglomerate formation was visibly observed particularly at high loading level. At low particle loadings (10 and 15 vol%), the ceramic powder is uniformly dispersed in the ENR-50 matrix without apparent agglomeration. However, at higher loading levels, agglomeration of BT in composites was observed (encircled in Figures 5.5(f), (g) and (h)) due to decreasing of inter-particle distance and thus filler particles become closer. At 40 and 50 vol% loading level of BT (arrows in Figure 5.5(g) and (h)) the thin film becomes porous. This is due to poor adhesion between the polymer matrix and the ceramic particles. The particle dispersion, volume percent of particle, connectivity of phase and particle-matrix reinforcement play important roles in both electrical and mechanical properties of the composites.

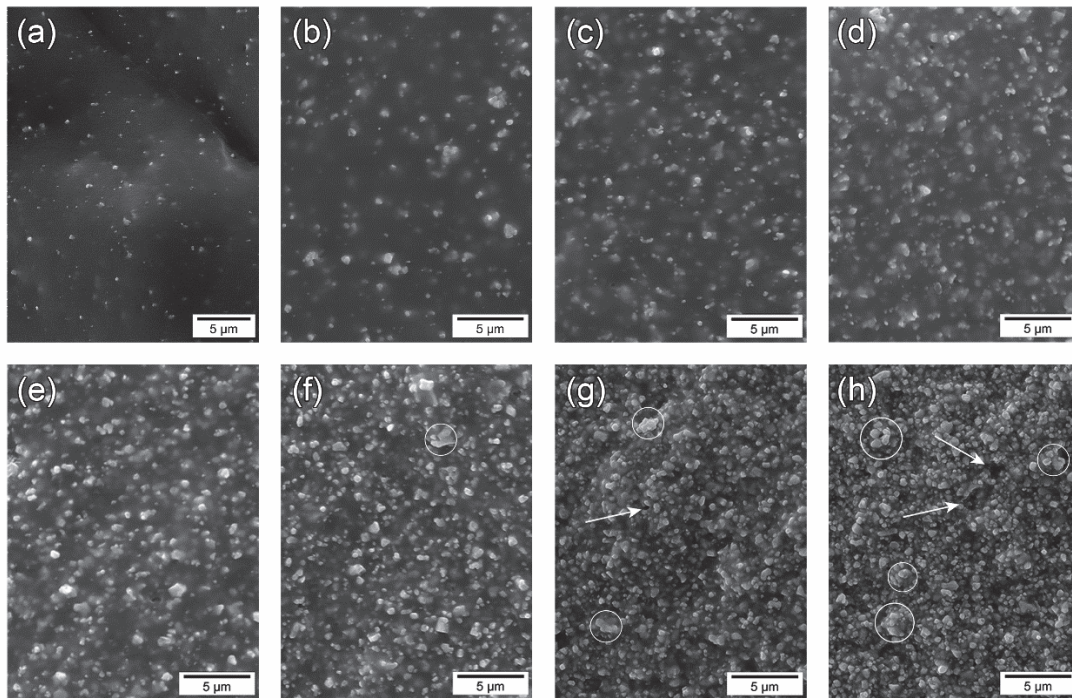


Figure 5.5 SEM micrographs of BT/ENR-50 composites with various BT loadings (a) 0, (b) 5, (c) 10, (d) 15, (e) 20, (f) 30, (g) 40 and (h) 50 vol%

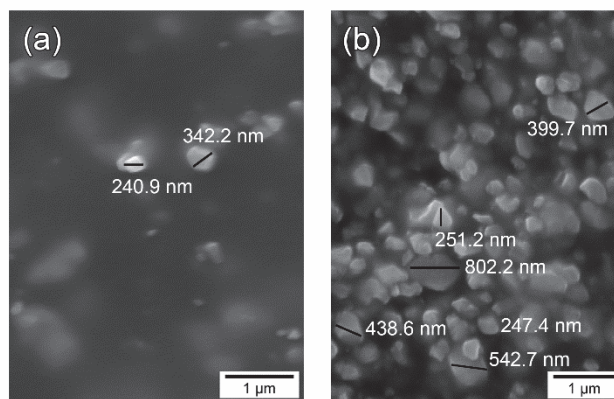


Figure 5.6 Enlarged SEM micrographs of BT/ENR-50 composites with (a) 10 and (b) 50, vol% of BT

5.3.3 Mechanical properties

The stress-strain curves of gum and BT filled ENR-50 vulcanizates are shown in Figure 5.7. The ENR-50 gum vulcanizate exhibited flexibility (i.e., high elongation at break) and high mechanical strength (i.e., high stress at break) due to the typical orientation of natural rubber molecules. Incorporation of filler particles in ENR-50 enhanced the material stiffness (i.e., increasing initial slope of the curves) however, it reduced the flexibility (decreases in elongation at break) due to poorer molecular chains mobility. Therefore, the stiffness of composites is higher than that of the gum vulcanizate which can be estimated from Young's modulus and hardness, as shown in Table 5.2. Both the Young's modulus and hardness increased with increasing BT content. This is attributed to the filler-polymer and filler-filler interactions in the composite that limit mobility of polymer molecules. This result agrees well with increasing of delta torque in Table 5.1. In Figure 5.7, it is seen that the composites retained good flexibility even at a loading level of 40 vol%: the elongation at break is higher than 100%. However, at a loading level of 50 vol%, flexibility became low and the material was ductile. Mechanical properties in terms of tensile strength and elongation at break, based on the failure points of stress-strain curves in Figure 5.7, are graphed in Figure 5.8. An increasing volume fraction of BT was associated with decreasing tensile strength and elongation at break. In summary, BT particles in ENR-50 matrix enhanced modulus or stiffness but deteriorated tensile strength and elongation at break. Especially, at BT content higher than 30 vol%, elongation at break drastically decreased from 508% (for 30 vol%) to 114% (for 40 vol%).

Due to high volume of ceramic particles in ENR-50 matrix, reducing the deformation area in the matrix and connectivity in the polymer led to reduction of the tensile strength and elongation at break [18]. At an excessive filler loading, the particles have the tendency to form cluster and cavities in the composites (as shown in Figure 5.5(g) and (h)) which is from lack of adhesion between matrix and filler. The non-uniform distribution of BT powder and cavities in composites caused decreases of mechanical properties in term of tensile strength and elongation at break [11]. Moreover, the necking behavior in stress-strain curve is observed in the composite with high BT content at 40 and 50 vol% BT.

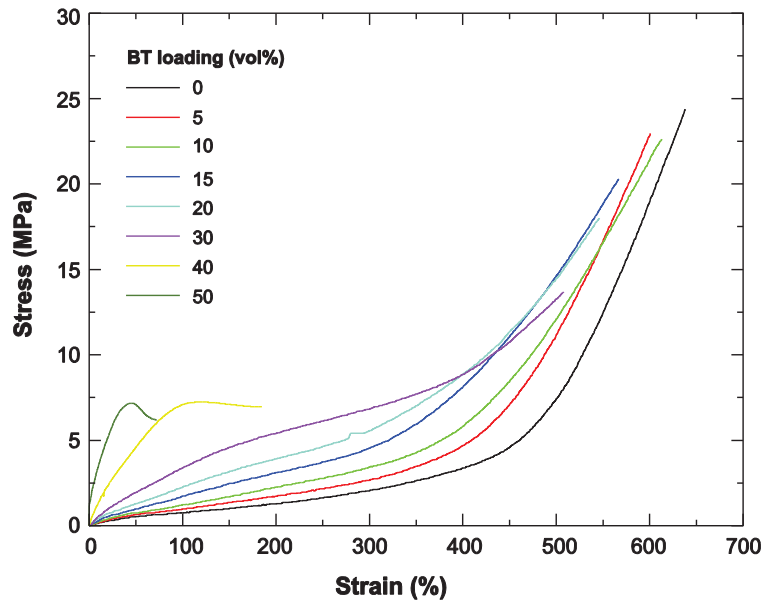


Figure 5.7 Stress-strain curves of BT/ENR-50 composites with various BT loadings

Table 5.2 Mechanical properties of BT/ENR-50 composites with various BT loadings

BT loading (vol%)	Young's modulus (MPa)	Tensile strength (MPa)	Elongation at break (%)	Hardness (Shore A)
0	1.2 (± 0.1)	24.4 (± 1.0)	645 (± 8)	42 (± 0.8)
5	1.5 (± 0.1)	23.0 (± 1.77)	620 (± 19)	47 (± 0.7)
10	1.8 (± 0.2)	22.8 (± 0.87)	620 (± 7)	49 (± 0.9)
15	2.7 (± 0.2)	20.3 (± 0.62)	570 (± 10)	50 (± 1.0)
20	3.5 (± 0.1)	18.0 (± 0.58)	550 (± 6)	52 (± 0.7)
30	5.8 (± 0.3)	13.7 (± 0.56)	510 (± 15)	55 (± 0.8)
40	13.4 (± 0.3)	7.0 (± 0.31)	110 (± 21)	59 (± 1.1)
50	33.6 (± 0.8)	6.2 (± 0.18)	60 (± 12)	63 (± 0.8)

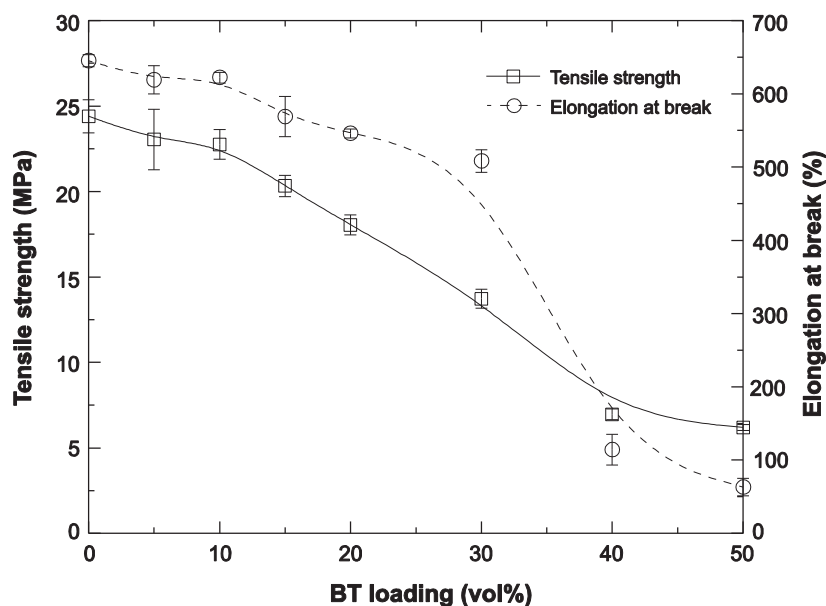


Figure 5.8 Tensile strength and elongation at break as a function of BT loading in BT/ENR-50 composites

5.3.4 Dynamic mechanical analysis

The dependence of the storage modulus (E') and loss tangent ($\tan \delta$) on temperature, at various BT contents, is shown in Figure 5.9. It can be seen that the storage modulus of all samples dropped drastically at glass transition temperature, indicating apparent transition from glassy state to rubbery state. The addition of BT strongly increased the storage modulus of composites: the E' increased with increasing BT loading over glassy (-60°C) and rubbery states (25°C) of the studied temperature range, as summarized in Table 5.3. An incorporation of BT particle in ENR-50 matrix leads to restriction of polymer chain around filler particle. Therefore, the reduction of chain mobility results in the increase of storage modulus. This increase correlates well with the increase of mechanical properties: modulus and hardness as mentioned in section 5.3.3. Both gum vulcanizate and the composites show one primary relaxation or α -relaxation. This is attributed to the initiation of micro-Brownian motion of the macromolecular chain segments in the ENR-50 molecule [19], which mainly related to the glass transition temperature (T_g). When BT particles were added, the relaxation peak had a very small shifting as compared with gum vulcanizate, but the amplitude of relaxation was influenced by loading level of BT. At glass-rubber transition, polymer chain segments began to gain

mobility and dissipated a great amount of energy through viscous movement. Therefore, the intensity of damping peak provided information regarding to the mobility of chain segments during glass transition [20, 21]. The decrease in the amplitude of $\tan \delta$ peak indicates a reduction in the number of polymer chain segments undergoing the glass transition [22], leading to reduction in damping properties and heat build-up when increasing filler content, together with restriction of polymer chain by the filler-polymer interaction [23]. However, it was found that no changes in glass transition temperature for BT/ENR-50 composites

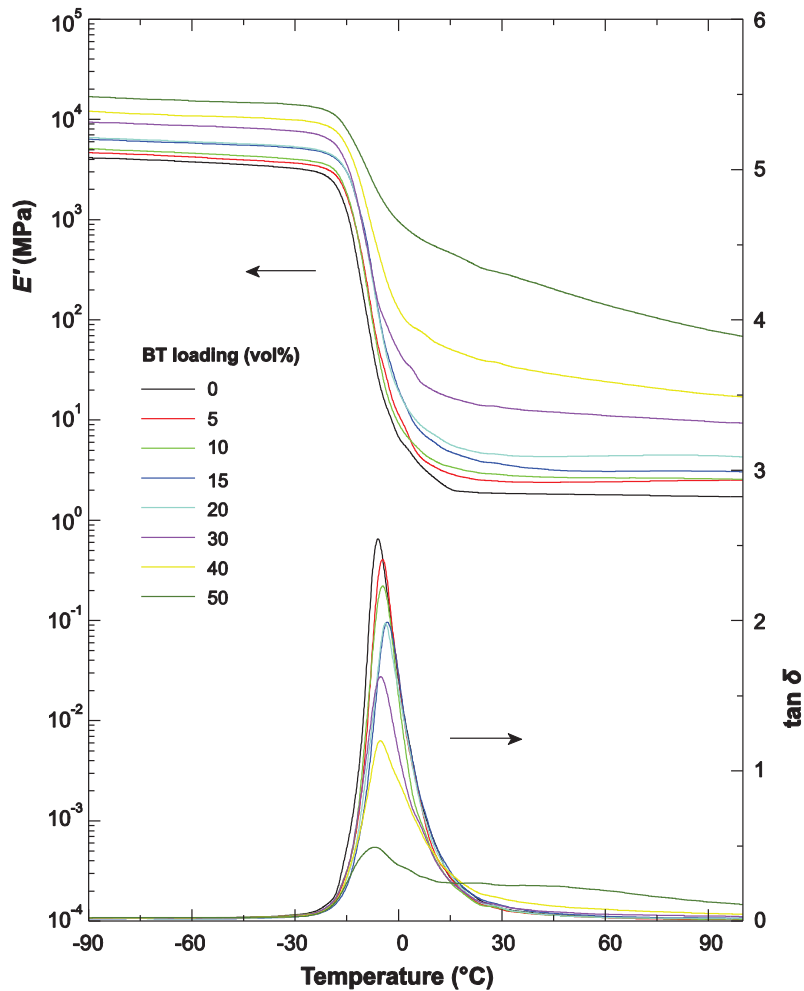


Figure 5.9 Temperature dependence of E' and $\tan \delta$ of BT/ENR-50 composites with various BT loadings

Table 5.3 Storage modulus (E') and loss tangent ($\tan \delta$) of BT/ENR-50 with various BT loadings

BT loading (vol%)	Storage modulus, E' (MPa)		Loss tangent, $\tan \delta$	
	at -60°C	at 25°C	$\tan \delta_{\max}$	T_g (°C)
0	3800	1.9	2.7	-5.7
5	4200	2.5	2.5	-4.7
10	4610	2.9	2.3	-4.6
15	5800	3.8	2.1	-3.3
20	6000	4.6	2.1	-3.8
30	8700	13.9	1.7	-5.3
40	10900	38.8	1.2	-5.5
50	15300	319.8	0.5	-7.4

5.3.5 Dielectric analysis

Temperature dependence of permittivity (ϵ') and loss factor (ϵ'') of BT/ENR-50 composites with 10, 20, 30 and 50 vol% of BT in ENR-50 matrix are shown in Figure 5.10, 5.11, 5.12 and 5.13, respectively. All composites demonstrated similar dielectric relaxation to gum ENR-50 as described in section 4.2.4. At low temperature, the permittivity and loss factor slightly depend on frequency. Molecular chains have enough mobility to contribute to the permittivity, leading to the increase in permittivity. At high temperature, the permittivity is higher and strongly depends on frequency. The step-like in ϵ' and the ϵ'' peak represents relaxation in the materials which corresponds to micro-Brownian cooperative motions of the polymer chain segment or α -relaxation and associated to glass transition temperature (T_g). The gradual increase in permittivity with the increasing ceramic volume fraction can also be clearly seen from the curves.

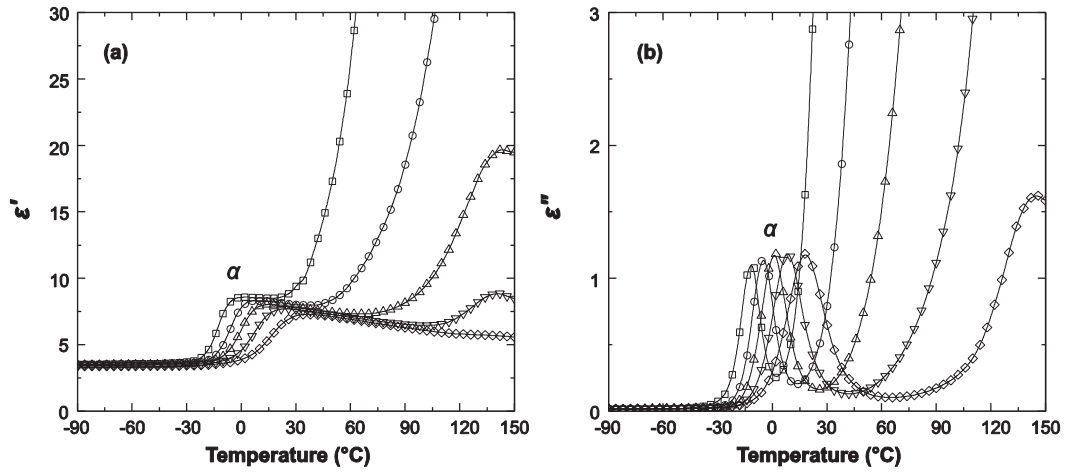


Figure 5.10 Temperature dependence of (a) ϵ' and (b) ϵ'' of BT/ENR-50 composite with 10 vol% BT at several frequencies (\square) 1, (\circ) 10, (\triangle) 100, (∇) 1k and (\diamond) 10k Hz

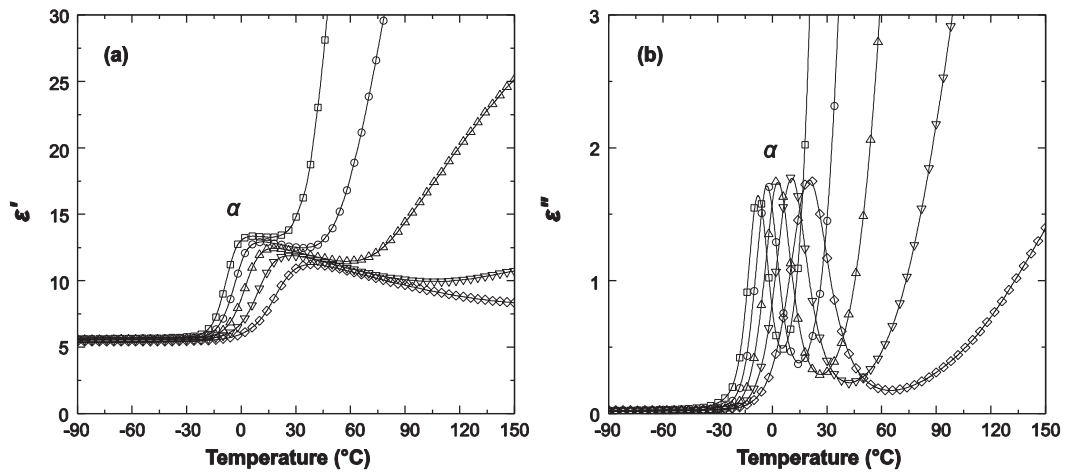


Figure 5.11 Temperature dependence of (a) ϵ' and (b) ϵ'' of BT/ENR-50 composite with 20 vol% BT at several frequencies (\square) 1, (\circ) 10, (\triangle) 100, (∇) 1k and (\diamond) 10k Hz

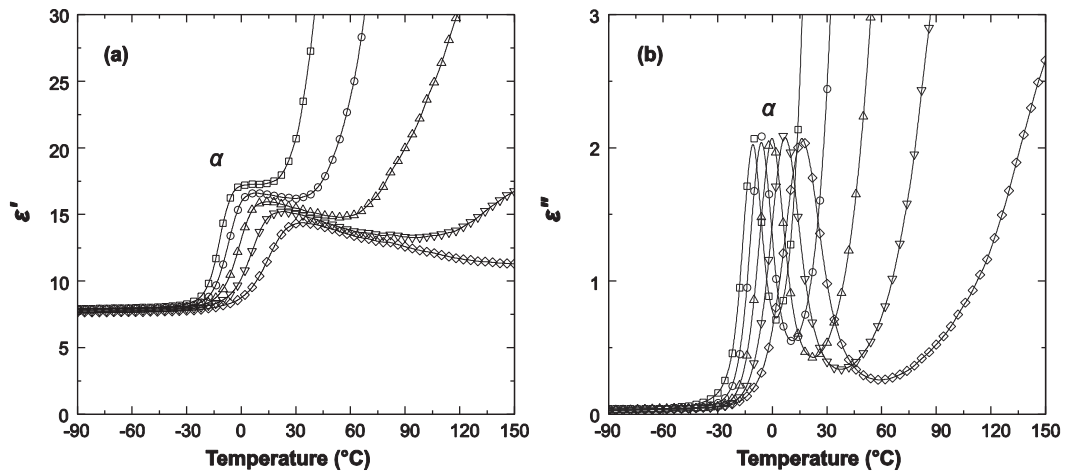


Figure 5.12 Temperature dependence of (a) ϵ' and (b) ϵ'' of BT/ENR-50 composite with 30 vol% BT at several frequencies (\square) 1, (\circ) 10, (\triangle) 100, (∇) 1k and (\diamond) 10k Hz

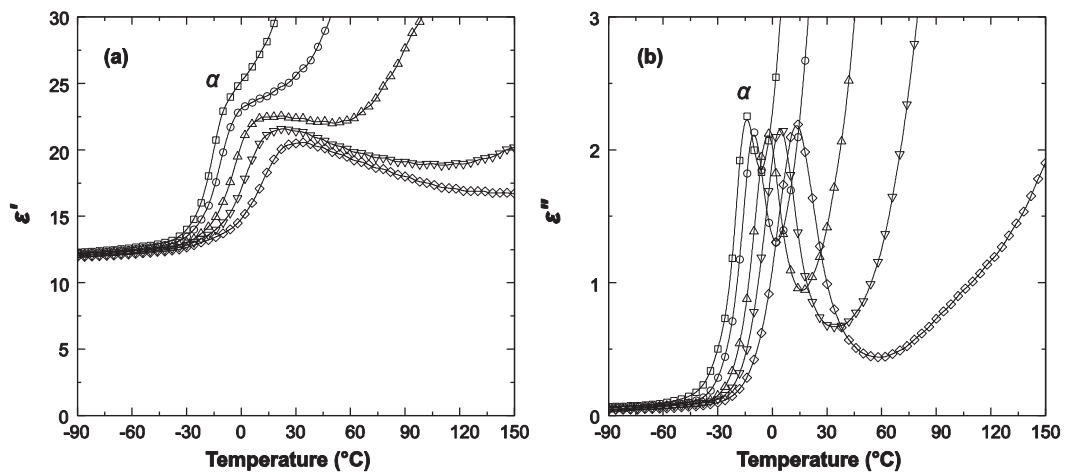


Figure 5.13 Temperature dependence of (a) ϵ' and (b) ϵ'' of BT/ENR-50 composite with 50 vol% BT at several frequencies (\square) 1, (\circ) 10, (\triangle) 100, (∇) 1k and (\diamond) 10k Hz

The permittivity (ϵ') and loss factor (ϵ'') as a function of frequency (at room temperature) of BT/ENR-50 composites with various amounts of BT are shown in Figure 5.14. The permittivity, loss factor and loss tangent at the frequency of 1 kHz are summarized in Table 5.4. It can be seen that addition of BT caused increase of permittivity, loss factor and amplitude of the loss factor of the composites. The increase of permittivity of the composites is due to relatively high permittivity or dielectric constant

of ceramic filler compared to the single polymer. In addition, as BT content increased, the interfacial area between ceramic phase and polymer phase was increased that resulted in interfacial polarization. Both factors significantly influence the dielectric permittivity and dielectric loss, according to the increase of permittivity and dielectric loss [4]. It can also be seen that for each sample the permittivity was nearly constant in the frequency range of 1 to 10^4 Hz, then decreased with a higher the frequency, and drops drastically between 10^5 and 10^6 Hz; which is also indicated by apparent relaxation peaks in the loss factor curves. This is attributed to segmental motion of ENR-50 backbone or α -relaxation of ENR-50.

For composite systems, loss factor might originate from the contributions of dipole orientation, conduction loss and interfacial polarization. The measurement results of dielectric loss are helpful to confirm the polarization mechanism [12, 24]. The ϵ'' of composite systems could be expressed as a sum of three distinct effects, that is:

$$\epsilon'' = \epsilon''_{dc} + \epsilon''_{MW} + \epsilon''_D \quad (5.1)$$

where ϵ''_{dc} is due to conduction loss contribution, ϵ''_{MW} is due to interfacial polarization (Maxwell–Wagner) contribution and ϵ''_D is the dipole orientation or Debye loss factor.

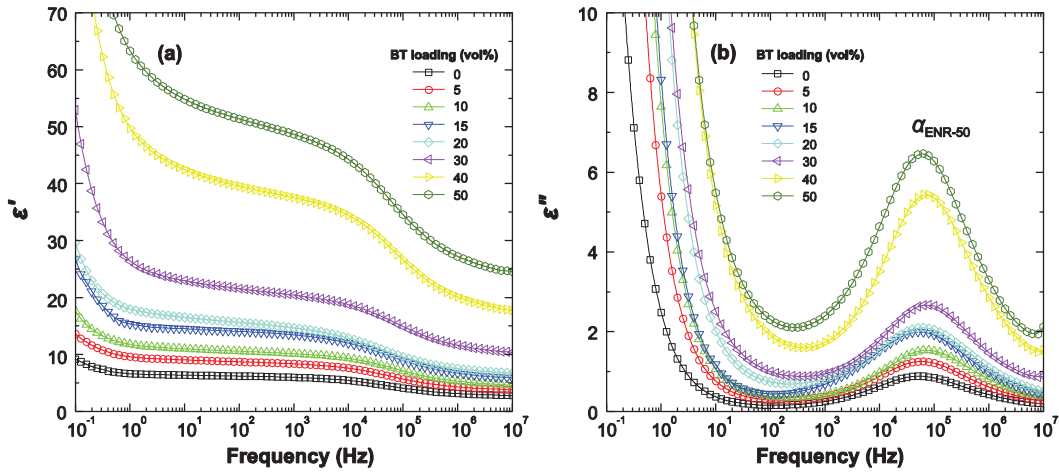


Figure 5.14 Frequency dependence of (a) ϵ' and (b) ϵ'' of BT/ENR-50 composites with various BT loadings

Table 5.4 Permittivity (ϵ'), loss factor (ϵ'') and loss tangent ($\tan \delta$) at fixed frequency 1 kHz of BT/ENR-50 composites with various BT loadings

BT loading (vol%)	Permittivity, ϵ'	Loss factor, ϵ''	Loss tangent, $\tan \delta$
0	6.00	0.25	0.042
5	8.36	0.38	0.045
10	10.13	0.42	0.042
15	13.14	0.68	0.051
20	14.66	0.82	0.055
30	20.41	0.94	0.046
40	33.35	1.73	0.046
50	48.65	2.40	0.079

There are several models that have been proposed to fit or predict the permittivity of ceramic-polymer composites of 0-3 connectivity. Key factors include the permittivity and volume fraction of each component, and the spatial arrangement in the mixture [7]. The permittivity of composite can be obtained from the pertinent values for the ceramic and polymer because ceramic-polymer composite consists of spherical inclusions of ceramic embedded in a polymer matrix that in turn is covered with a homogeneous medium whose properties average approximately the average composite properties [25], as shown in Figure 5.15.

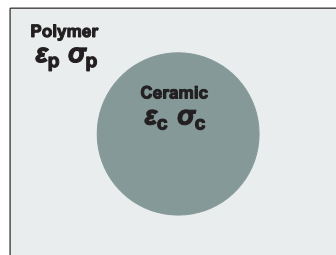


Figure 5.15 Schematic representations the structure of ceramic-polymer composite

The logarithmic model is well-known, and predicts the permittivity of a two-component system [7, 9, 26, 27]:

$$\log \epsilon_{\text{eff}} = v_c \log \epsilon_c + (1-v_c) \log \epsilon_p \quad (5.2)$$

where ϵ_{eff} is the effective permittivity of a binary composite, ϵ_c is the permittivity of ceramic (ϵ_c of BT = 2400), ϵ_p is the permittivity of polymer (ϵ_p of ENR-50 = 6.0) and v_c is the volume fraction of ceramic particles in the polymer matrix.

The modified Lichtenecker's equation with a fitting factor k can be applied to calculate permittivity of composites. It is reported that $k = 0.3$ is the best suited for a well-dispersed system [7, 28]:

$$\log \varepsilon_{\text{eff}} = \log \varepsilon_p + v_c(1-k)\log \left(\frac{\varepsilon_c}{\varepsilon_p} \right) \quad (5.3)$$

The effective medium theory (EMT) model has been used to calculate the permittivity of composites [6, 27, 29, 30]:

$$\varepsilon_{\text{eff}} = \varepsilon_p \left[1 + \frac{v_c(\varepsilon_c - \varepsilon_p)}{\varepsilon_p + n(1 - v_c)(\varepsilon_c - \varepsilon_p)} \right] \quad (5.4)$$

where n is a shape factor of the ceramic particles. A small value of n corresponds to near-spherical shape, while a high value of n is used for elongated particle shapes.

Jayasundere and Smith (J-S) developed a model by modifying the well-known Kerner equations to include interactions between neighboring spheres, for calculation the permittivity of composites [6, 7, 11, 31]:

$$\varepsilon_{\text{eff}} = \frac{\varepsilon_p(1 - v_c) + \varepsilon_c v_c(A)(B)}{(1 - v_c) + v_c(A)(B)} \quad (5.5)$$

where

$$A = \frac{3\varepsilon_p}{\varepsilon_c + 2\varepsilon_p} \quad \text{and} \quad B = 1 + \left[\frac{3\varepsilon_c(\varepsilon_c - \varepsilon_p)}{\varepsilon_c + 2\varepsilon_p} \right] \quad (5.6)$$

The theoretical model of Bruggeman has the form [10, 11, 32, 33]:

$$\frac{\varepsilon_c - \varepsilon_{\text{eff}}}{(\varepsilon_{\text{eff}})^{1/3}} = (1 - v_c) \frac{\varepsilon_c - \varepsilon_p}{(\varepsilon_p)^{1/3}} \quad (5.7)$$

A comparison of the experimental values of permittivity, obtained from dielectric spectra at 1 kHz, and the above equations is shown in Figure 5.16. The effective permittivity has a nonlinear nature and most prediction models showed a matching result at a low ceramic content up to 15 vol% of BT. Some of them deviate from experiment at high ceramic content. The Jayasundere and Smith (J-S) and modified Lichtenecker's models performed the best for lower and higher particle loadings. This is due to the fact

that J-S model includes field interactions between neighboring spheres, which gain importance when a high volume fraction of the ceramic phase is used. The good correspondence of modified Lichtenecker's model is due to including fitting factor k in equation which represents the interaction between the filler and the matrix. Moreover, it was found to be sensitive to both the filler and the matrix [34]. In this work, $k=0.3$ was obtained that means a well dispersion of ceramic-polymer composites. As for the earlier reports, Choudhury [7] obtained Jayasundere and Smith model for better correlation in polyetherimide/BaTiO₃ (PEI/BT) nanocomposites and Hu *et al.* [26] obtained modified Lichtenecker's model with a k value of 0.37 for a better fit result for barium strontium titanate/poly(phenylene sulfide). Therefore, Jayasundere and Smith and modified Lichtenecker's model could be used to predict the dielectric constant of BT/ENR-50 composite.

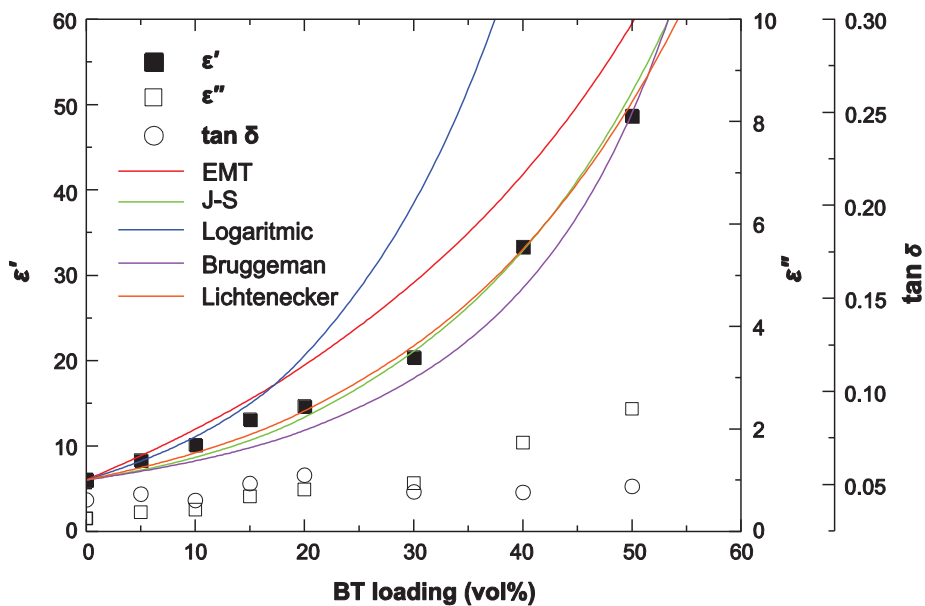


Figure 5.16 Experimental and theoretical values from different models of permittivity (at 1 kHz) of composite as a function of BT content in BT/ENR-50 composites

There are two reasons for a slight difference between theoretical model and experimental observation. First, poor dispersion of ceramic particles and the presence of air (i.e., cavitation) in the composites at high loadings. This is due to that the permittivity of air is low and that violate idealized assumptions on deriving model [4, 35]. Second, it is difficult to obtain the correct permittivity of the ceramic powders. Instead, permittivity of the bulk ceramic is used. The permittivity of powder may be different from that of the bulk

[35]. Many theoretical models suggested that fillers in a material should be ideally separated, non-interactive and roughly spherical shape. However, in a practical way they are not in such a case. Hence, the effective permittivity of the composites depends on the permittivity of each phase in the mixture, their volume fractions, shape and size of fillers, morphology, dispersion, porosity, interphase polarizability and interphase volume fractions [4, 18, 35]. Levassort *et al.* [36] reported that at high volume fractions of ferroelectric ceramic, there will be some degree of particle-particle contact that induces a change in connectivity. In such a case, some particles are in contact, and 3-3 connectivity must be considered at different locations in the composite. The composite is then no longer the 0-3 connectivity type but a mixture of 0-3 and 3-3 connectivities are taken place. The corresponding composite representation is given in Figure 5.17.

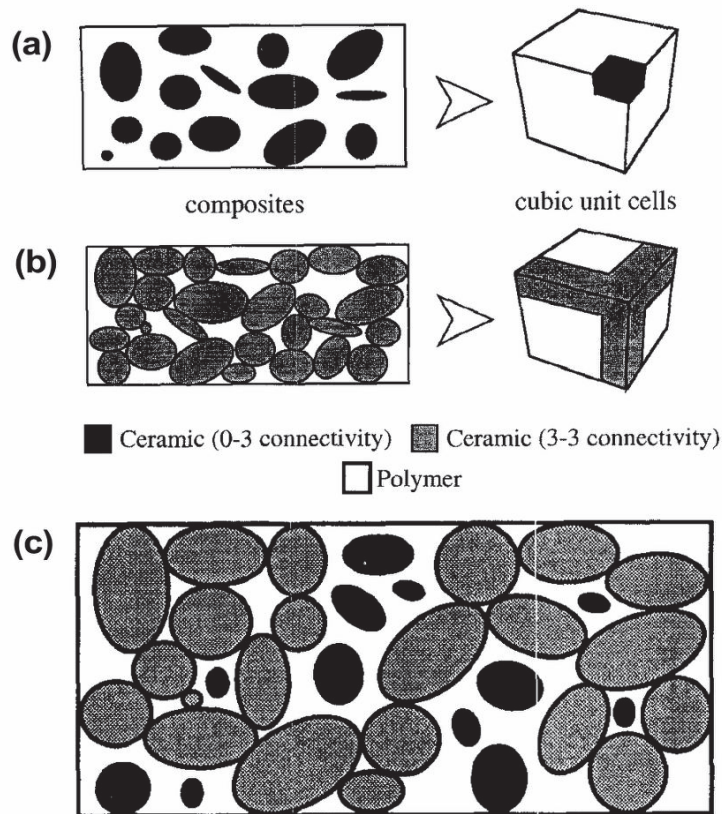


Figure 5.17 Unit cell representations for composites (a) 0-3 connectivity (b) 3-3 connectivity and (c) containing both 0-3 and 3-3 connectivity

Our BT/ENR-50 composites at 50 vol% of BT nearly reached the values of permittivity, loss factor and loss tangent of 48.7, 2.4 and 0.05, respectively, at 1 kHz. These values matched the values obtaining from PVDF and its co-polymer as matrix, [5, 37] and exceeding the permittivity of some polyimide/BT composites [7, 38] and epoxy/BT [9] at the same loading and same measured frequency as summarized in Table 2.2. This can be concluded that high permittivity (high- ϵ') and low loss tangent (low-tan δ) composite are successfully prepared by filling BT in ENR-50. Furthermore, all types of composites showed a sharp increasing of permittivity and loss factor at high temperature and low frequency, which is rather due to conductivity as described earlier. The imaginary part (M'') as a function of temperature of BT/ENR-50 composite at different amounts of BT is shown in Figure 5.18.

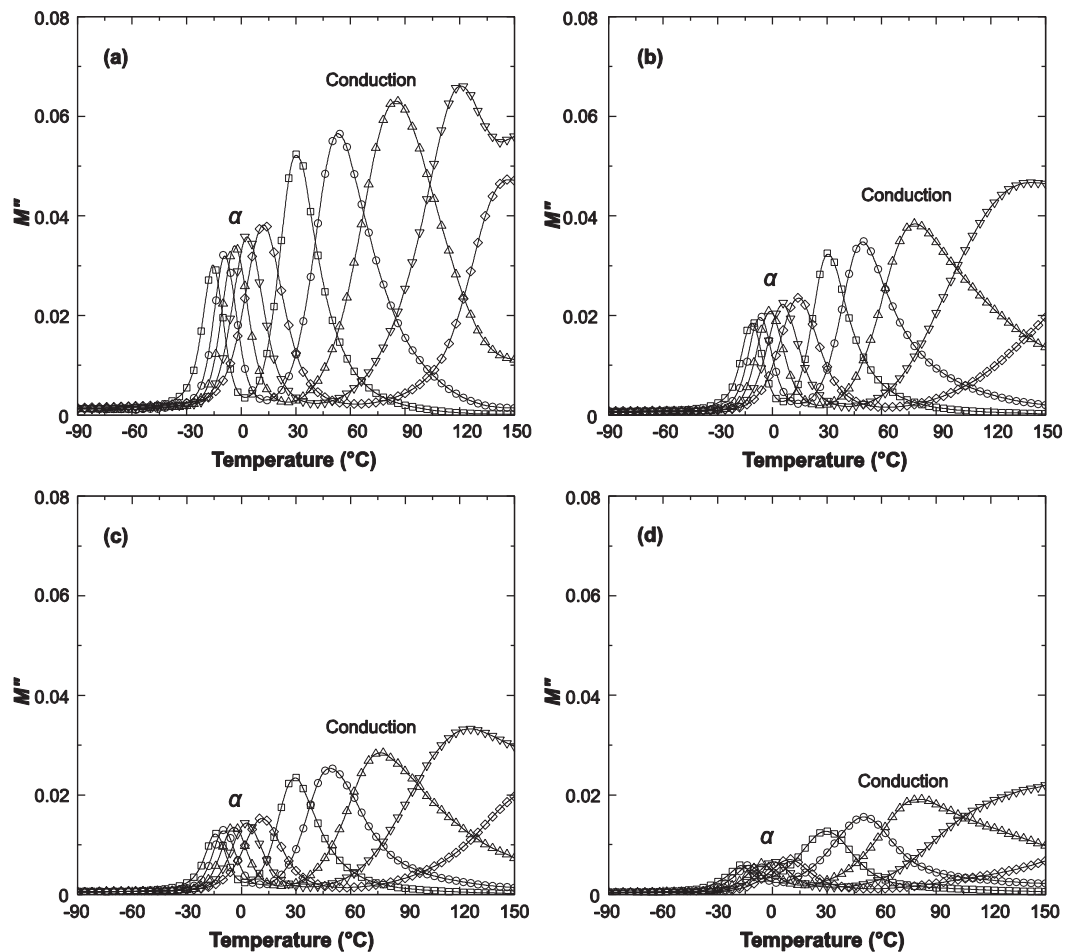


Figure 5.18 Temperature dependence of M'' of ENR-50 composites with (a) 10, (b) 20, (c) 30 and (d) 50 vol% BT at (\square) 1, (\circ) 10, (\triangle) 100, (∇) 1k and (\diamond) 10k Hz

In Figure 5.18, it is clear that all types of composites revealed two relaxations at lower and higher temperatures. The relaxation peak at low temperature corresponds to α -relaxation process which mainly related to segmental motion of molecule chain or glass transition temperature. The second relaxation peak cannot be observed in ϵ'' spectra however, using electric modulus formalism revealed a new relaxation peak at higher temperature. This relaxation peak attributed to the conductivity because at sufficient temperature and low frequency, charge transfer in conductivity process affects sharp increase of ϵ' and ϵ'' values [39, 40]. This relaxation is also attributed to the interfacial or Maxwell-Wagner-Sillars (MWS) polarization which is normally encountered in heterogeneous materials. Furthermore, the conduction process at low frequency can be confirmed by appearance of relaxation at low frequency in the plot of M'' in frequency domain as shown in Figure 5.19. The relaxation peak at low frequency related to conductivity and at high frequency related to α -process. It can also be seen that the intensity of relaxation peak decreased with increasing BT contents. These are due to the real permittivity was increased.

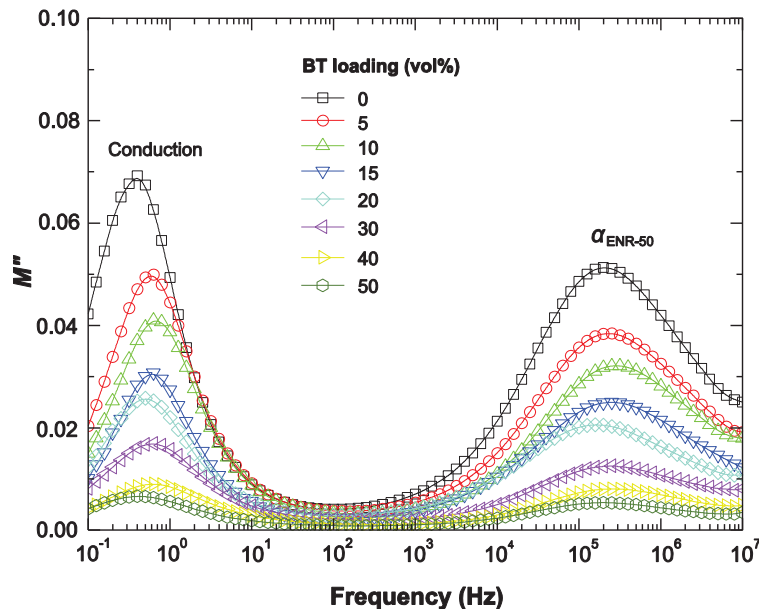


Figure 5.19 Frequency dependence of M'' of BT/ENR-50 composites with various BT loadings

The peak positions of α -relaxation and conductivity process move to higher temperature with increasing frequency. The reciprocal temperature dependence of the relaxation time for α and conductivity process in composites with various amounts of BT are shown in Figure 5.20. It can be seen that the α -relaxation is associated with the glass transition which can be well fitted with the Vogel-Tamman-Fulcher (VFT) (Equation 3.20). The conductivity process or MWS process have been described by Arrhenius equation (Equation 3.19). All fit parameters that obtained from fitting the experimental results are listed in Table 5.5. The B value of composites was slightly dependent in BT/ENR-50 composites and T_0 became higher than that of gum ENR-50. The different amount of BT can be evaluated as a very small effect to the dynamic mobility of segmental motion. However, the activation energy of conductivity process increased with BT content because the presence of BT caused increase of heterogeneity of the system. Then, activation energy tended to decrease which may be due to the formation of ceramic particle network or percolation threshold leading to increase in conductivity and transferring of charge.

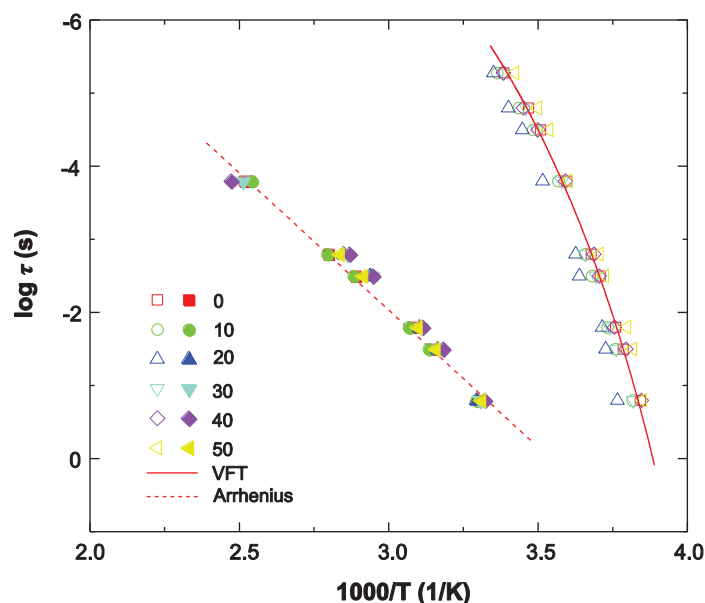


Figure 5.20 Relaxation time of α -process and conduction process as a function of reciprocal temperature for BT/ENR-50 with composites various amounts of BT. Dash and solid lines represent the overall best fits according to Equations 3.19 and 3.20, respectively

Table 5.5 Fitting parameters of VFT and Arrhenius equations to the experimental data

BT loading (vol%)	α -relaxation			Conductivity	
	$\log \tau_0$	B (K)	T_0 (K)	$\log \tau_0$	E_a (eV)
0	-12.04	1328	210	-13.28	0.75
10	-11.89	1305	212	-13.81	0.79
20	-12.02	1340	214	-15.57	0.89
30	-12.17	1320	212	-13.36	0.75
40	-11.90	1335	209	-12.65	0.70
50	-11.94	1256	211	-14.72	0.84

5.4 Conclusions

In this study, the homogeneous and fine BaTiO₃ or BT powders were prepared by using the mixed oxide process consisting of BaCO₃ and TiO₂ as a precursor. The XRD analysis of prepared BT powder confirmed the reaction of BaCO₃ and TiO₂. The average particle size characterized by particle size analyzer is 4.5 μm . The dielectric permittivity (ϵ') and dielectric loss (ϵ'') and loss tangent factor ($\tan \delta$) of the sintered BT pellet at 1 kHz measured at room temperature were 2400, 94 and 0.04, respectively.

Ceramic-polymer composites with 0–3 structure were prepared from prepared BT ceramic particles and ENR-50 as the polymer matrix. The composites showed a reduction in scorch time and cure time, and increased minimum and maximum torque with increasing concentration of BT. The reversion behavior is more pronounced with BT content, due to the changes in cross-link structures of the vulcanizates after the maximum vulcanization. The SEM micrograph revealed that the ceramic powder is uniformly dispersed in the ENR-50 matrix without apparent agglomeration, which establishes microstructure (0-3) connectivity of the composite. However, at higher loading levels, some degree of particle-particle contact or agglomeration of BT in composites was observed. The tensile strength and elongation at break decreased while the hardness and Young's modulus increased with the loading level. The dynamic mechanical properties showed that the storage modulus increased in over temperature range with increasing BT content. The small increase in storage modulus was more pronounced in rubber region due to restriction of polymer chain around filler particles. The dielectric permittivity increased with increasing BT content due to interfacial polarization and intrinsic high

permittivity of BT particle in ENR-50 matrix. The drastically decrease in permittivity between 10^5 and 10^6 Hz corresponds to segmental motion of ENR-50 backbone or α -relaxation of ENR-50 as evidenced by relaxations in the loss factor curves. The Jayasundere and Smith (J-S) and modified Lichtenecker's models performed the best fit to describe for fabricated BT/ENR-50 composite in over range of BT loading. BT/ENR-50 composites at 50 vol% of BT nearly reached value of permittivity, loss factor and loss tangent of 48.7, 2.4 and 0.05, respectively at 1 kHz. Therefore, it is concluded that addition of BT into ENR-50 matrix is suitable ceramic-polymer pairs and can be used to prepare ceramic-polymer composite with high permittivity and flexibility.

5.5 References

- [1] Carter, C.B. and Norton, M.G. 2007. *Ceramic Materials: Science and Engineering*. Springer, New York.
- [2] Patsidis, A. and Psarras, G.C. 2008. *Dielectric behaviour and functionality of polymer matrix-ceramic BaTiO₃ composites*. *Express Polym. Lett.* 2, 718-726.
- [3] Hsiang, H.-I., Lin, K.-Y., Yen, F.-S. and Hwang, C.-Y. 2001. *Effects of particle size of BaTiO₃ powder on the dielectric properties of BaTiO₃/polyvinylidene fluoride composites*. *J. Mater. Sci.* 36, 3809-3815.
- [4] Dang, Z.M., Yuan, J.K., Zha, J.W., Zhou, T., Li, S.T. and Hu, G.H. 2012. *Fundamentals, processes and applications of high-permittivity polymer matrix composites*. *Prog. Mater. Sci.* 57, 660-723.
- [5] Kim, P., Doss, N.M., Tillotson, J.P., Hotchkiss, P.J., Pan, M.J., Marder, S.R., Li, J., Calame, J.P. and Perry, J.W. 2009. *High energy density nanocomposites based on surface-modified BaTiO₃ and a ferroelectric polymer*. *ACS Nano*. 3, 2581-2592.
- [6] Ahmad, Z., Prasad, A. and Prasad, K. 2009. *A comparative approach to predicting effective dielectric, piezoelectric and elastic properties of PZT/PVDF composites*. *Physica B*. 404, 3637-3644.
- [7] Choudhury, A. 2010. *Dielectric and piezoelectric properties of polyetherimide/BaTiO₃ nanocomposites*. *Mater. Chem. Phys.* 121, 280-285.
- [8] Wang, H., Xiang, F. and Li, K.C. 2010. *Ceramic-polymer Ba_{0.6}Sr_{0.4}TiO₃/poly(methyl methacrylate) composites with different type composite structures for electronic technology*. *Int. J. Appl. Ceram. Technol.* 7, 435-443.

- [9] Cho, S.D., Lee, S.Y., Hyun, J.G. and Paik, K.W. 2005. *Comparison of theoretical predictions and experimental values of the dielectric constant of epoxy/BaTiO₃ composite embedded capacitor films*. J. Mater. Sci: Mater. El. 16, 77-84.
- [10] Peng, W., Huang, X., Yu, J., Jiang, P. and Liu, W. 2010. *Electrical and thermophysical properties of epoxy/aluminum nitride nanocomposites: Effects of nanoparticle surface modification*. Compos. Part A: Appl. S. 41, 1201-1209.
- [11] Gallone, G., Carpi, F., De Rossi, D., Levita, G. and Marchetti, A. 2007. *Dielectric constant enhancement in a silicone elastomer filled with lead magnesium niobate-lead titanate*. Mater. Sci. Eng., C. 27, 110-116.
- [12] Huang, X., Xie, L., Jiang, P., Wang, G. and Liu, F. 2009. *Electrical, thermophysical and micromechanical properties of ethylene-vinyl acetate elastomer composites with surface modified BaTiO₃ nanoparticles*. J. Phys. D: Appl. Phys. 42, 245407.
- [13] Salaeh, S., Muensit, N., Bomlai, P. and Nakason, C. 2011. *Ceramic/natural rubber composites: influence types of rubber and ceramic materials on curing, mechanical, morphological, and dielectric properties*. J. Mater. Sci. 46, 1723-1731.
- [14] Hsiang, H.I., Mei, L.T. and Chun, Y.J. 2009. *Dielectric properties and microstructure of Nb-Co codoped BaTiO₃-(Bi_{0.5}Na_{0.5})TiO₃ ceramics*. J. Am. Ceram. Soc. 92, 2768-2771.
- [15] Chen, J.F., Shen, Z.G., Liu, F.T., Liu, X.L. and Yun, J. 2003. *Preparation and properties of barium titanate nanopowder by conventional and high-gravity reactive precipitation methods*. Scripta. Mater. 49, 509-514.
- [16] González Hernández, L., Rodríguez Díaz, A., Valentín, J.L., Marcos-Fernández, Á. and Posadas, P. 2005. *Conventional and efficient crosslinking of natural rubber: effect of heterogeneities on the physical properties*. Kaut. Gummi Kunstst. 58, 638-643.
- [17] Kruzelák, J., Kysela, G. and Hudec, I. 2008. *Elastomeric magnetic composites curing and properties*. Kaut. Gummi Kunstst. 61, 424-428.
- [18] Rajesh, S., Murali, K.P., Rajani, K.V. and Ratheesh, R. 2009. *SrTiO₃-filled PTFE composite laminates for microwave substrate applications*. Int. J. Appl. Ceram. Technol. 6, 553-561.

- [19] Mohanty, S., Nando, G.B., Vijayan, K. and Neelakanthan, N.R. 1996. *Mechanical and dynamic mechanical properties of miscible blends of epoxidized natural rubber and poly(ethylene-co-acrylic acid)*. Polymer. 37, 5387-5394.
- [20] Rao, Y.Q. and Pochan, J.M. 2007. *Mechanics of polymer-clay nanocomposites*. Macromolecules. 40, 290-296.
- [21] Zhang, X.G. and Loo, L.S. 2009. *Study of glass transition and reinforcement mechanism in polymer/layered silicate nanocomposites*. Macromolecules. 42, 5196-5207.
- [22] Zhang, B.Q., Ding, Y.F., Chen, P., Liu, C.Y., Zhang, J., He, J.S. and Hu, G.H. 2005. *Fibrillation of thermotropic liquid crystalline polymer enhanced by nano-clay in nylon-6 matrix*. Polymer. 46, 5385-5395.
- [23] Rajasekar, R., Pal, K., Heinrich, G., Das, A. and Das, C.K. 2009. *Development of nitrile butadiene rubber-nanoclay composites with epoxidized natural rubber as compatibilizer*. Mater. Design. 30, 3839-3845.
- [24] Chen, Q., Xi, Y., Bin, Y. and Matsuo, M. 2008. *Electrical and dielectric properties in carbon fiber-filled LMWPE/UHMWPE composites with different blend ratios*. J. Polym. Sci. Pol. Phys. 46, 359-369.
- [25] Riande, E. and Díaz-Calleja, R. 2004. *Electrical Properties of Polymers*. Marcel Dekker Inc, USA.
- [26] Hu, T., Juuti, J. and Jantunen, H. 2007. *RF properties of BST-PPS composites*. J. Eur. Ceram. Soc. 27, 2923-2926.
- [27] George, S. and Sebastian, M.T. 2009. *Three-phase polymer-ceramic-metal composite for embedded capacitor applications*. Compos. Sci. Technol. 69, 1298-1302.
- [28] Sonoda, K., Juuti, J., Moriya, Y. and Jantunen, H. 2010. *Modification of the dielectric properties of 0-3 ceramic-polymer composites by introducing surface active agents onto the ceramic filler surface*. Compos. Struct. 92, 1052-1058.
- [29] Thomas, P., Varughese, K.T., Dwarakanath, K. and Varma, K.B.R. 2010. *Dielectric properties of poly(vinylidene fluoride)/CaCu₃Ti₄O₁₂ composites*. Compos. Sci. Technol. 70, 539-545.

- [30] Anjana, P.S., Uma, S., Philip, J. and Sebastian, M.T. 2010. *Thermal properties of low loss PTFE-CeO₂ dielectric ceramic composites for microwave substrate applications*. J. Appl. Polym. Sci. 118, 751-758.
- [31] George, S., Anjana, P.S., Sebastian, M.T., Krupka, J., Uma, S. and Philip, J. 2010. *Dielectric, mechanical, and thermal properties of low-permittivity polymer-ceramic composites for microelectronic applications*. Int. J. Appl. Ceram. Technol. 7, 461-474.
- [32] Wegener, M. and Arlt, K. 2008. *PZT/P(VDF-HFP) 0-3 composites as solvent-cast thin films: preparation, structure and piezoelectric properties*. J. Phys. D: Appl. Phys. 41, 165409.
- [33] Wang, X.X., Lam, K.H., Tang, X.G. and Chan, H.L.W. 2004. *Dielectric characteristics and polarization response of lead-free ferroelectric (Bi_{0.5}Na_{0.5})_{0.94}Ba_{0.06}TiO₃-P(VDF-TrFE) 0-3 composites*. Solid State Commun. 130, 695-699.
- [34] Thomas, S., Deepu, V., Uma, S., Mohanan, P., Philip, J. and Sebastian, M.T. 2009. *Preparation, characterization and properties of Sm₂Si₂O₇ loaded polymer composites for microelectronic applications*. Mater. Sci. Eng. B: Adv. 163, 67-75.
- [35] Sebastian, M.T. and Jantunen, H. 2010. *Polymer-ceramic composites of 0-3 connectivity for circuits in electronics: a review*. Int. J. Appl. Ceram. Technol. 7, 415-434.
- [36] Levassort, F., Lethiecq, M. and Desmare, R. 1999. *Effective electroelastic moduli of 3-3 (0-3) piezocomposites*. IEEE T. Ultrason. Ferr. 46, 1028-1034.
- [37] Dang, Z.M., Wang, H.Y., Zhang, Y.H. and Qi, J.Q. 2005. *Morphology and dielectric property of homogenous BaTiO₃/PVDF nanocomposites prepared via the natural adsorption action of nanosized BaTiO₃*. Macromol. Rapid Commun. 26, 1185-1189.
- [38] Xie, S.H., Zhu, B.K., Wei, X.Z., Xu, Z.K. and Xu, Y.Y. 2005. *Polyimide/BaTiO₃ composites with controllable dielectric properties*. Compos. Part A: Appl. S. 36, 1152-1157.
- [39] Chanmal, C.V. and Jog, J.P. 2008. *Dielectric relaxations in PVDF/BaTiO₃ nanocomposites*. Express Polym. Lett. 2, 294-301.

- [40] Hammami, H., Arous, M., Lagache, M. and Kallel, A. 2007. *Study of the interfacial MWS relaxation by dielectric spectroscopy in unidirectional PZT fibres/epoxy resin composites*. J. Alloys Compd. 430, 1-8.

CHAPTER 6

CONDUCTIVE ELASTOMER COMPOSITES BASED ON CB/ENR-50 COMPOSITES

6.1 Introductions

Carbon black (CB) is a reinforcing filler and also widely used as conductive filler to improve mechanical and electrical properties of high performance rubber materials. Different types of carbon black offer difference in mechanical and electrical properties which mainly depend on the specific surface area and/or structure of the primary aggregates [1, 2]. A high surface activity and specific surface area of the carbon black play an important role in reinforcement of elastomer by physically bound of the chain at the surface of CB particles. The strong interaction between filler and elastomer leads to increase in tensile strength, tear resistance, abrasion resistance and modulus [1, 3, 4]. The surface area of CB depends on primary particle size of filler which determines effective contact area between the filler and polymer matrix. Generally, structure of CB is related to the aggregate irregularity in shapes. High structure carbon blacks exhibit a high number of primary particles per aggregate but low structure carbon blacks show only a weak aggregation [3]. Conductivity of composite depends on the formation of a percolating path of conductive filler through the polymer matrix. The percolation threshold (p_c) is the minimum concentration of the filler that causes to form a continuous conducting structure. Hence, the composite is transferred from an insulator to conductor [5]. Generally, the CB with high surface area and high structure is generally considered as conductive carbon black (CCB) due to lower percolation threshold concentration. That is p_c decreases with the increasing of the surface area and/or structure of the CB particles. This leads to decrease in gaps between particles or particle clusters, which contributes to hopping of charge carriers across the gaps for conductivity of CB filled polymers [1, 2]. The percolation threshold of CB filler in elastomer is around 25 to 30 phr (~12 to 14 vol%) [6-

10], which is higher than carbon nanotube elastomer composites around 1 to 5 phr (~0.5 to 3 vol%) [7, 11-13]. However, utilization of carbon nanotube in elastomer resulted in poor dispersion in elastomer matrix [13]. Thus, the challenge is to reduce as much as possible the percolation threshold of CB in conductive composite. This is favored the financial reasons but inferior in mechanical properties is needed to compensate.

The main aim of this study was to prepare CB/ENR-50 composite with low percolation threshold. Two types of CBs; high abrasion furnace (HAF) and extra conductive furnace (ECF) were employed in the investigation. Effect of different types of CB (i.e., HAF and ECF) and CB loading (i.e., 0 to 60 phr) on the properties of CB/ENR-50 composite were elucidated. Cure characteristic, mechanical, dynamic mechanical properties and electrical properties of the prepared composite were investigated.

6.2 Effect of different carbon black structure and content on properties of carbon black filled ENR-50 composites

The study was performed with the ENR-50 using two types of carbon black (i.e., HAF and ECF with various CB loading (0 to 60 phr)). Various important properties were studied as follows:

6.2.1 Cure characteristic

Cure characteristics of the HAF and ECF filled ENR-50 compound are shown and summarized in Figure 6.1 and Table 6.1, respectively. It can be seen that torque is increased with increasing loading level of carbon black. This is due to the formation of crosslinks and filler-polymer interaction upon increasing content of fillers. A remarkable increase in minimum torque, maximum torque and delta torque with addition of CB particles. This might be attributed to the formation of physical bound rubber at the surface of CB particles in the matrix, as shown in Figure 2.6(b), resulting in hindrance in the mobility of rubber chains which restrict chains deformation. The delta torque or torque difference is related to cross-link density of rubber vulcanizates. In the Figure 6.1 and Table 6.1, the ECF composite showed higher delta torque than HAF composite. This is attributed to high surface area and structure of ECF (Table 3.1). This give rises to large number of rubber chains immobilized on the carbon black surfaces [4, 14]. This leads to enhancement of physical crosslink and hence the delta torque. Furthermore, the HAF

filled ENR-50 exhibited reversion phenomenon while the ECF higher than 25 phr shows marching phenomenon with ECF higher than 25 phr. This is due to high structure and surface area of ECF particles could be possibly absorbed accelerator and curing agent molecules during vulcanization [15]. This causes delayed of vulcanization reaction and hence increasing of the scorch time (t_{s1}), cure time (t_{c90}) and decreasing of cure rate index (Table 6.1). However, Li *et al.* [14] reported that the content of sulfur on CB surface was highly associated with the surface area of carbon black that the shorter scorch time and cure time can be observed in rubber filled with high structure CB.

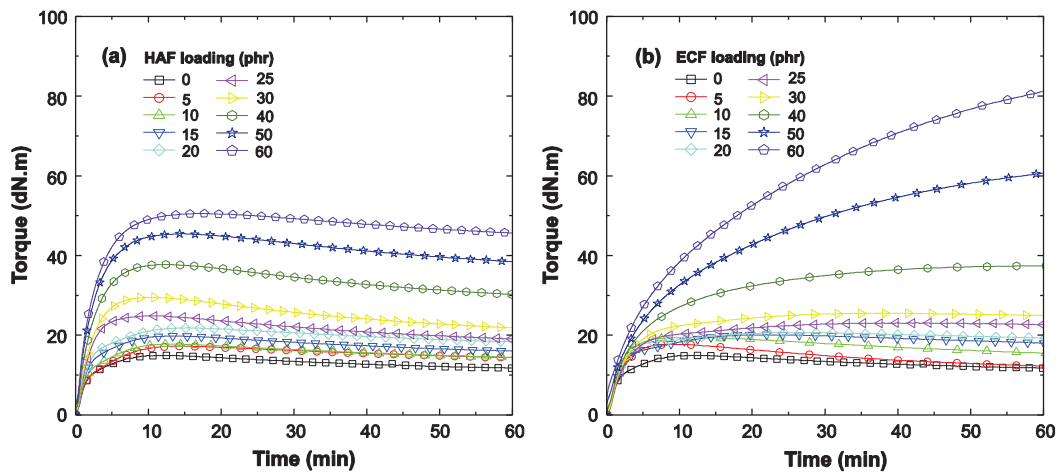


Figure 6.1 Rheographs of (a) HAF and (b) ECF filled ENR-50 at various CB loading levels

Table 6.1 Cure characteristic of HAF and ECF filled ENR-50 composites

Properties	Carbon black loading (phr)										
	0	5	10	15	20	25	30	40	50	60	
Min. torque, M_L (min)	HAF	0.91	0.93	0.94	0.95	0.99	1.23	1.42	2.00	2.45	
	ECF	0.99	0.93	0.94	0.96	0.97	1.10	1.26	1.80	3.63	6.13
Max. torque, M_H (min)	HAF	17.29	17.79	19.81	21.83	24.81	29.48	37.74	45.43	50.52	
	ECF	14.53	17.69	19.43	20.13	21.48	23.16	26.64	37.39	60.68	81.33
Δ torque, $M_H - M_L$ (dN.m)	HAF	16.38	16.86	18.87	20.88	23.82	28.25	36.32	43.43	48.07	
	ECF	13.54	16.76	18.49	19.17	20.51	22.06	25.38	35.59	57.05	75.20
Scorch time, t_{s1} (min)	HAF	0.46	0.45	0.42	0.41	0.40	0.37	0.34	0.28	0.26	0.25
	ECF	0.46	0.59	0.56	0.52	0.48	0.44	0.43	0.40	0.35	0.27
Cure time, t_{c90} (min)	HAF	6.49	7.78	6.93	6.63	6.60	4.11	4.77	5.62	6.22	6.69
	ECF	6.49	6.67	6.91	9.90	12.45	14.09	15.38	25.00	40.73	44.81
Cure rate index, (CRI)	HAF	16.58	13.64	15.36	16.08	16.13	26.74	18.73	18.73	16.78	15.53
	ECF	16.58	16.45	15.75	10.66	8.35	7.32	6.69	4.07	2.48	2.25

6.2.2 Mechanical properties

Stress–strain curves of HAF and ECF filled ENR-50 are shown in Figures 6.2. It is observable that increasing of carbon black content causes decreasing of failure strain along with an increase in modulus. The mechanical properties in terms of Young’s modulus, tensile strength, elongation at break and hardness of carbon black/ENR-50 composites are summarized in Table 6.2.

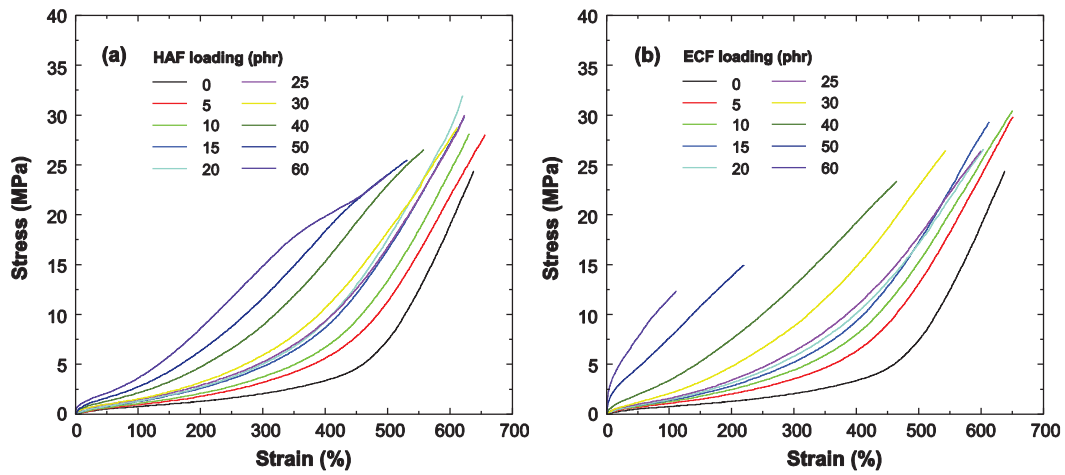


Figure 6.2 Stress-strain curves of (a) HAF and (b) ECF filled ENR-50 with various HAF and ECF loadings

Table 6.2 Young’s modulus (E), tensile strength (σ_B), elongation at break (ϵ_B) and hardness of HAF/ENR-50 and ECF/ENR-50 composites

CB loading (phr)	HAF/ENR-50				ECF/ENR-50			
	E (MPa)	σ_B (MPa)	ϵ_B (%)	Hardness (Shore A)	E (MPa)	σ_B (MPa)	ϵ_B (%)	Hardness (Shore A)
0	1.2 (± 0.1)	24.4 (± 1.0)	645 (± 8)	42 (± 0.8)	1.2 (± 0.1)	24.4 (± 1.0)	645 (± 8)	42 (± 0.8)
5	1.5 (± 0.2)	28.1 (± 0.6)	656 (± 26)	45 (± 1.1)	1.6 (± 0.1)	29.9 (± 1.7)	651 (± 16)	45 (± 0.6)
10	1.8 (± 0.1)	28.8 (± 1.1)	632 (± 14)	47 (± 0.8)	2.0 (± 0.1)	30.5 (± 1.3)	650 (± 13)	47 (± 1.2)
15	2.3 (± 0.1)	30.3 (± 0.4)	632 (± 14)	49 (± 0.9)	2.3 (± 0.2)	28.1 (± 1.8)	613 (± 20)	50 (± 1.3)
20	2.7 (± 0.2)	31.4 (± 1.0)	620 (± 8)	50 (± 0.9)	2.8 (± 0.2)	28.0 (± 2.2)	604 (± 20)	52 (± 1.1)
25	2.9 (± 0.3)	30.0 (± 1.1)	618 (± 13)	52 (± 0.7)	3.8 (± 0.2)	26.4 (± 1.3)	587 (± 15)	55 (± 1.1)
30	4.1 (± 0.5)	28.3 (± 1.5)	624 (± 18)	55 (± 0.8)	4.0 (± 0.2)	26.5 (± 1.3)	560 (± 13)	58 (± 1.3)
40	7.0 (± 0.9)	26.5 (± 1.1)	545 (± 19)	59 (± 1.4)	11.0 (± 1.7)	23.4 (± 1.1)	464 (± 14)	65 (± 1.1)
50	8.9 (± 1.0)	25.5 (± 1.5)	527 (± 24)	63 (± 0.8)	27.9 (± 4.9)	14.9 (± 1.0)	227 (± 13)	80 (± 0.7)
60	23.1 (± 5.1)	23.2 (± 1.5)	470 (± 32)	67 (± 1.3)	134.5 (± 16.2)	12.8 (± 0.4)	112 (± 8)	82 (± 0.8)

Improvement in mechanical properties was observed for addition of both CB in ENR-50, whilst the reduction trend was observed in elongation at break, as shown in Figure 6.3. Furthermore, the tensile strength of composite is increased with the maximum values at 10 phr and 20 phr for ECF/ENR-50 and HAF/ENR-50 composites, respectively, as shown in Figure 6.3(a). This is attributed to the high degree of reinforcement because of addition of CB particles into polymer matrix. Also, the specific surface area of CB determines physical absorption of the polymer chain units to the carbon black surface. The filler particles are hence covered by the semi-rigid interface can be considered as multifunctional physical cross-links, as shown in Figure 2.6 [16]. However, further increase of CB led to the decrease in tensile strength due to high degree of restriction, high cross-link density and smaller mobility of polymer chain. This is also attributed to formation of agglomerate of filler which could be possible acted as a weak point in composites [17, 18]. It can be noted that tensile strength increased with increase of cross-link density and tended to decrease at a certain level, as shown in Figure 6.4. Besides, the use of ECF reached a maximum value of tensile strength before HAF which indicates that the use of ECF can achieve maximum tensile strength at lower loading level (10 phr) than that of the use of HAF (20 phr). An increase in tensile strength is generally observed in rubber/CB composites because of reinforcement effect which is the contribution from small particle size, surface area and structure of CB. However, HAF and ECF used in this study have the similar particle size (~29 nm). Thus, the reinforcement of the composites is practically due to difference in surface area and structure. That is, the adsorbed rubber chains at surface of high surface area and structure of ECF is significantly higher than that of HAF with low surface area and structure [4]. This results in the ECF/ENR-50 composites contains higher polymer-filler interfacial area and mechanical properties at low loading level. It has also been established that the active functional groups on carbon black surfaces play an important role on level of mechanical properties of the carbon black composites [6, 19, 20].

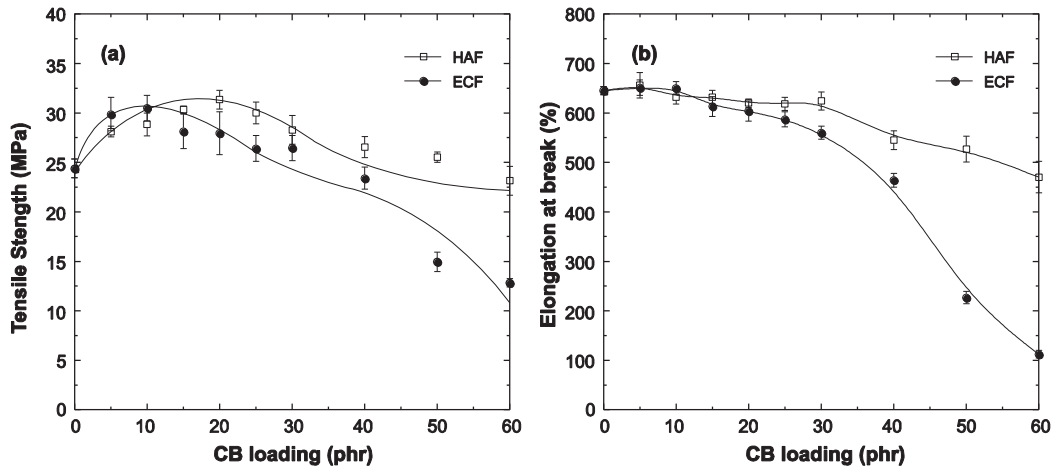


Figure 6.3 (a) Tensile strength and (b) elongation at break as a function of CB loading in ENR-50 vulcanizates

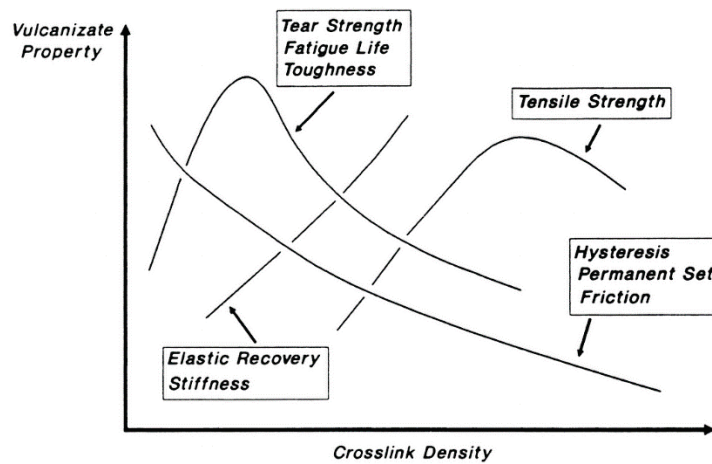


Figure 6.4 Vulcanizate properties as a function of the extent of vulcanization [21]

The contribution of polymer-filler at interface was investigated with swelling measurement by using Kraus's equation, which has been applied to follow the extent of filler reinforcement [22]:

$$\frac{V_{r0}}{V_{rf}} = 1 - m \left[\frac{\varphi}{(1 - \varphi)} \right] \quad (6.1)$$

where V_{r0} and V_{rf} are the volume fractions of the polymer in the fully swollen unfilled sample and in the fully swollen filled sample respectively. φ is the volume fraction of filler in the vulcanizates.

The volume fraction of rubber in the swollen vulcanizates was calculated by the equation as follows [23]:

$$V_r = \frac{(D - FT)\rho_r^{-1}}{(D - FT)\rho_r^{-1} + A_0\rho_s^{-1}} \quad (6.2)$$

where T is the weight of the sample, F is the weight fraction of insoluble components in the composites, D is the de-swollen weight of the specimen, A_0 is the weight of absorbed solvent, ρ_r and ρ_s are the density of rubber and solvent, respectively.

According to Equation 6.1, m will be obtained from slope of the plot between V_{r0}/V_{rf} and $\phi/(1-\phi)$, which related to an indication of reinforcement of filler in the matrix. Higher negative slope means greater degree of reinforcement [23-25]. The plot of V_{r0}/V_{rf} against $\phi/(1-\phi)$ of ENR-50 filled with HAF and ECF is shown in Figure 6.5.

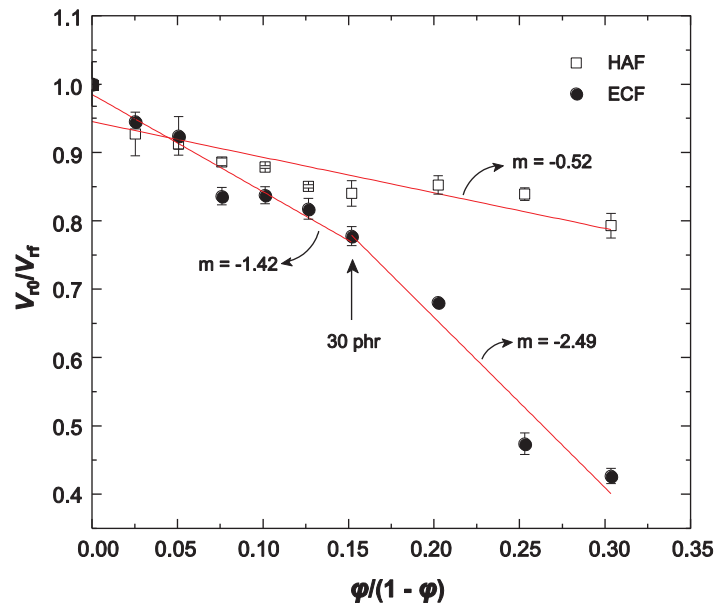


Figure 6.5 Kraus plot of HAF and ECF filled ENR-50

It can be seen that the slope (m) of the HAF/ENR-50 composite curve is -0.52. However, ECF/ENR59 composites showed two different slopes in composition range. That is, the slope of -1.42 for the composites with loading level of ECF of 0-30 phr and slope of -2.49 for the composites with ECF contents of 30-60 phr. Therefore, the higher slope of ECF/ENR-50 composites give a description that the degree of reinforcement in ECF/ENR-50 is more intensive than that of HAF/ENR-50 because higher negative slope. This is attributed to high structure and surface areas of ECF particle. It is interesting to

note that the abrupt change in V_{r0}/V_{rf} versus $\phi/(1-\phi)$ plot after addition 30 phr of ECF indicates abrupt change of structure within the material throughout filler-polymer network.

In Figure 6.3(b), it is seen that the CB/ENR-50 composites showed decreasing elongation at break with increasing loading levels of carbon black. This is typical phenomenon when incorporation of particulate fillers into the rubber matrix. This is attributed to greater degree of restricted chain and crosslink density in composites embedded the molecular chain from deformation [14, 17]. It is also seen that the elongation at break of HAF composites decreased gradually while rapidly decreasing trend was observed in ECF composites. Also, the ECF/ENR-50 composites showed lower elongation at break than that of HAF/ENR-50 composites with a given level of filler. This is due to higher number of rubber chain attached at the surface of ECF particles. Meanwhile, the higher surface area and structure of ECF lead to more interfacial interaction, therefore, locking in place the ECF carbon black particles in the rubber matrix is more rigid than HAF particles, as illustrated in Figure 6.6. This leads to decreasing extensibility of ECF composites. Moreover, an abrupt change in elongation at break was observed when the ECF content was higher than 30 phr. This is due to a great amount of restricted rubber chains on ECF surface as estimated by Kraus's relation (Figure 6.5).

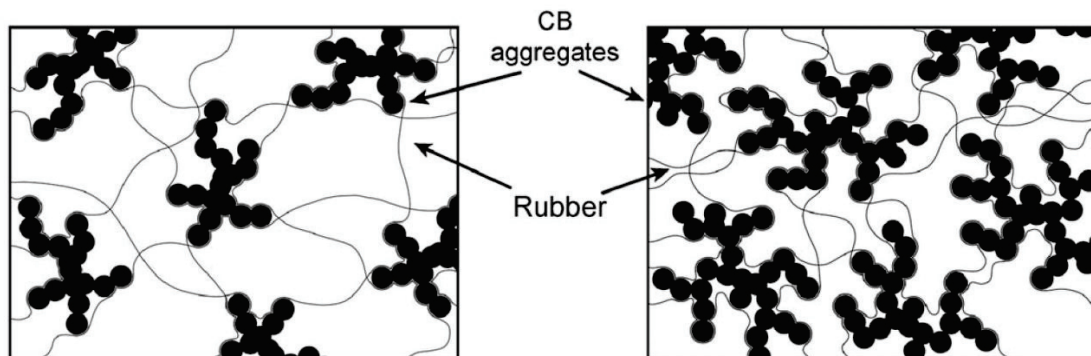


Figure 6.6 The physical network of (a) HAF and (b) ECF in rubber [20]

The variation of the Young's modulus and hardness of composites with different loading levels and types of carbon black is presented in Figure 6.7. It is clearly observed that both value are increased with increasing loading level of CB as consequence of a restriction in chain mobility with CB surface, resulting in an increase of the stiffness (i.e., Young's modulus and hardness) of ENR-50. It is interesting to note that two different slopes of Young's modulus and hardness versus CB loading plot are observed in the

ECF/ENR-50 composites. On the other hand, the HAF/ENR-50 composites showed a single slope of Young's modulus and hardness versus CB loading plot throughout the ranges of filler used. In Figure 6.7, it is also seen that the slope of Young's modulus and hardness of ECF/ENR-50 composite are larger than that of HAF/ENR-50 composites when the loading level of the ECF is higher than 30 phr. This confirmed the results of polymer–filler interaction based on Kraus's relation (Figure 6.5). This again may be attributed to high structure and surface area of the ECF particles.

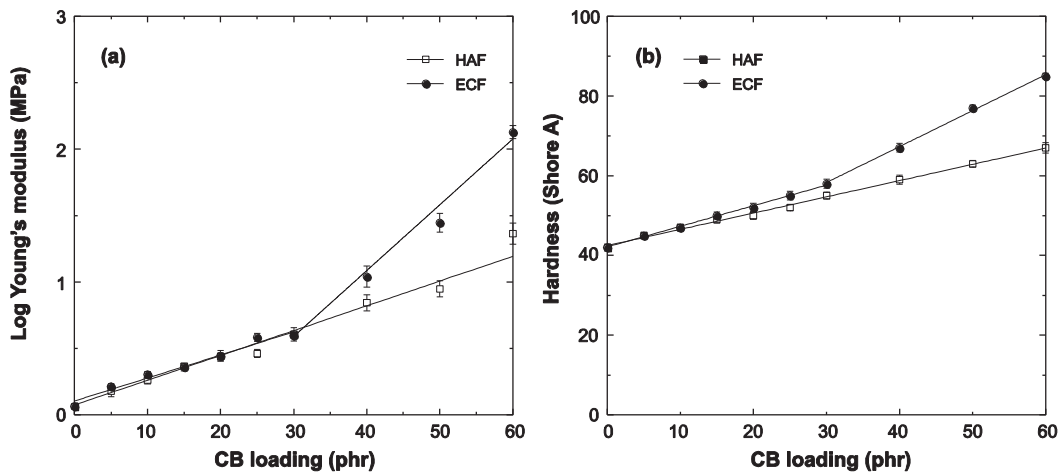


Figure 6.7 (a) Young's modulus and (b) hardness versus CB loading in ENR-50

6.2.3 Dynamic mechanical analysis

Effect of type and loading level of CB on dynamic properties in term of storage modulus (E') and loss tangent ($\tan \delta$) of CB filled ENR-50 as a function of temperature are shown in Figure 6.8. It can be seen that addition of CB led to a strong increasing E' in CB/ENR-50 composites in the tested temperature range. However, the increment of E' was more pronounced in the rubbery region. The increasing E' contributes from restricted movement of rubber molecule at carbon black surface, which plays a role in reinforcement of carbon black filler. The attachment of ENR-50 to the CB surfaces increase with higher CB content, resulting in an increased E' . As expected, the E' is abruptly decreased around three orders of magnitude when glass transition temperature (T_g) ranges of ENR-50 in each type of composites. These results in the composites are transitioned from glassy to rubber states. Loss tangent ($\tan \delta$) shows a peak at around -6°C which has been assigned to the α -relaxation or T_g of ENR-50. The representative values of the E' at -60 and 25°C including the maximum loss tangent and T_g of ENR-50 are listed in Table 6.3. At rubbery

plateau (25°C), the storage modulus increased from 1.9 (i.e., gum vulcanizate) to 86.6 MPa (i.e., loading of 60 phr) for HAF/ENR-50 composites and to 285.6 MPa (i.e., loading of 60 phr) for ECF/ENR-50 composites. However, slight increasing E' at -60°C was observed, as shown in Figure 6.9. Furthermore, sudden increase in E' at 25°C of ECF composites was observed with addition of ECF higher than 30 phr, while the E' at 25°C of HAF composites showed a linear increment in the composition range. This corresponds to the trend of the Young's moduli and hardness as described in Figure 6.7. The difference in E' between ECF and HAF composites can be explained in term of surface area and structure. That is, the high surface area and structure of ECF leads to a more immobilized rubber shell and significant increase in stiffness of ECF/ENR-50 composites [14]. Ha *et al.* [26] observed the sharp increase in storage modulus in the composites with carbon nanotube content of 0.05 to 0.1 wt%. They described that the composites have reached rheological percolation threshold with strong interaction between filler particles and impede the motion of polymer chain. In general, the rheological percolation threshold is higher than the electrical percolation threshold due to the filler's spherical shape and its low surface areas [27]. Thus, the sudden change in Young's modulus, hardness (Figure 6.7) and E' (Figure 6.9) after addition of 30 phr of ECF can be considered as a concentration for rheological percolation threshold to occur. It is noted that higher surface and structure of ECF to form filler-polymer easily at lower concentration than HAF. This why rheological percolation of HAF composites could not be observed in the composition range used in this work.

Table 6.3 Storage modulus (E') and loss tangent ($\tan \delta$) of HAF/ENR-50 and ECF/ENR-50 composites with various CB loadings

CB loading (phr)	HAF/ENR-50				ECF/ENR-50			
	E' (MPa)		$\tan \delta$		E' (MPa)		$\tan \delta$	
	-60°C	25°C	$\tan \delta_{\text{Max}}$	T_g (°C)	-60°C	25°C	$\tan \delta_{\text{Max}}$	T_g (°C)
0	3800	1.9	2.70	-6.0	3800	1.9	2.70	-6.0
10	4000	3.0	2.08	-5.2	4200	4.2	1.91	-4.8
20	4100	5.7	1.66	-4.2	4400	7.7	1.35	-3.1
30	4800	14.4	1.24	-7.6	4500	16.4	1.09	-3.1
50	5500	49.3	0.76	-7.9	5750	145.6	0.44	0.3
60	5750	86.6	0.72	-7.5	5100	285.6	0.32	0.3

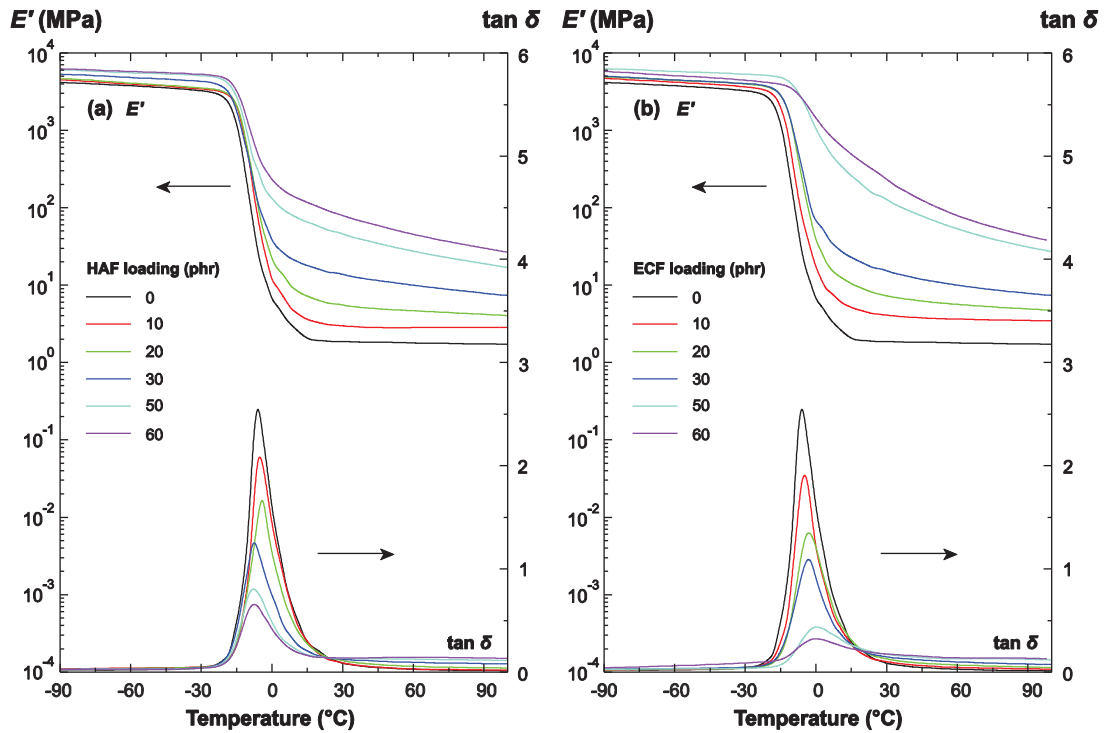


Figure 6.8 Temperature dependence of E' and $\tan \delta$ of (a) HAF and (b) ECF filled ENR-50 at various HAF and ECF loadings

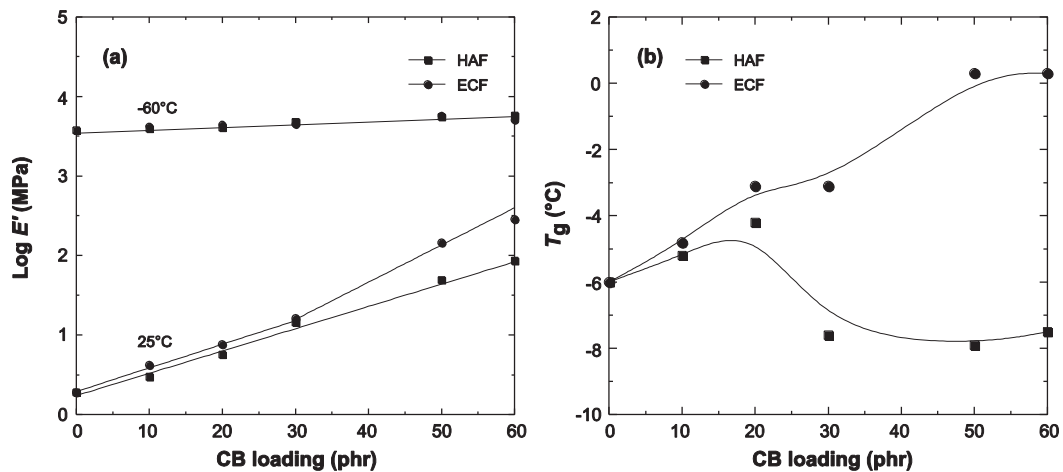


Figure 6.9 (a) E' at -60 and 25°C and (b) glass transition temperature as a function of CB content in HAF/ENR-50 and ECF/ENR-50 composites

In Figure 6.8, it is seen that the amplitude of $\tan \delta$ peak decreases with increasing carbon black content due to the limitation of the mobility of rubber molecules near the surface of CB particles. The reduction of $\tan \delta$ peak is related to minimize heat buildup as a result of lower damping characteristics of HAF and ECF filled ENR-50

vulcanizates. It is also seen that at a given loading of carbon black, the ECF/ENR-50 composites showed the lower $\tan \delta$ peak height than that of HAF/ENR-50 composites. This indicates a strong filler–rubber interactions and higher reinforcement capability of the ECF particles as compared with HAF counterpart. That is, high surface area and structure of ECF are responsible to cause very strong interaction between ECF and ENR-50 molecules, which contributed to reduction of the chain mobility and reduction of $\tan \delta$ peak height during dynamic mechanical deformation [25, 26, 28, 29]. In Figure 6.8 and Table 6.3, it is seen that increasing trend of T_g of ECF/ENR-50 composite was observed upon increasing loading level of ECF. That is, a shift in T_g by +6°C was observed in ECF/ENR-50 composite over the whole composition ranges. On the other hand, the T_g of HAF/ENR-50 composite increased until the maximum value at a loading level of HAF = 20 phr. Increasing higher loading level of HAF than 20 phr causes decreasing trend of T_g in HAF/ENR-50 composites. Therefore, the incorporation of carbon black filler could shift T_g of the matrix due to the strong interaction at filler surface that restricts the mobility of polymer chain segment [25, 30]. The immobilized rubber (occluded rubber) acts as a part of the filler rather than of the polymer, that increases the effective volume of the filler. The significant increase in T_g of ECF/ENR-50 composites is attributed to high structure and surface area of ECF particles. This results in greater immobilization of rubber molecules that restrict on the surface of ECF particles. However, addition of a much higher content of HAF (i.e., 30-60 phr) shows lower T_g than that of gum vulcanizate. This is believed that high content of filler prevents the packing of the polymer chain and consequently increases the free volume of molecular mobility. This results in the cooperative motion of the polymer chains at lower temperature [31, 32]. These results indicate a strong interfacial interaction between the CB and rubber matrix, in particular, by the incorporation of ECF.

6.2.4 Electrical properties

The variation of the dielectric permittivity (ϵ') at room temperature as a function of frequency for HAF and ECF filled ENR-50 is shown in Figure 6.10. At a given tested frequency, the value of the permittivity was significantly increased with increasing CB content. Since the permittivity is a measurement of the polarization in the sample. Hence, the amount of interfaces between CB and polymer is an important parameter to control

the level of permittivity [33]. In low frequency ranges, higher value of ϵ' is observed as compared to the high frequency ranges. This is originated from interfacial polarization and conduction process. The interfacial polarization or Maxwell-Wagner-Sillars polarization occurs in a dielectrically heterogeneous system because of the accumulation of charges at the interfaces. However, in the composites with higher content of CB, increasing of ϵ' is mainly due to conductivity. In Figure 6.10, it is also seen that increasing frequency causes continuously decrease of ϵ' . This is attributed to the dipole orientation and displacement polarization cannot rapidly follow the change in alternation electric field at sufficient high frequency. The relaxation was shifted towards the higher frequency with increasing loading of CB. This behavior has been observed in carbon-black and carbon nanotube filled polymers [11, 33]. Furthermore, the dielectric spectroscopy plots show that composites with high carbon black content exhibited a double-step behavior of ϵ' . In previous studies on carbon black filled elastomers, the low frequency transition has been related to percolation structure of the filler network and higher frequency transition has been assigned to a gap process. This referred to the tunneling or hopping of charge carriers over nano-scopeic gaps between adjacent particles of the CB network [11, 34].

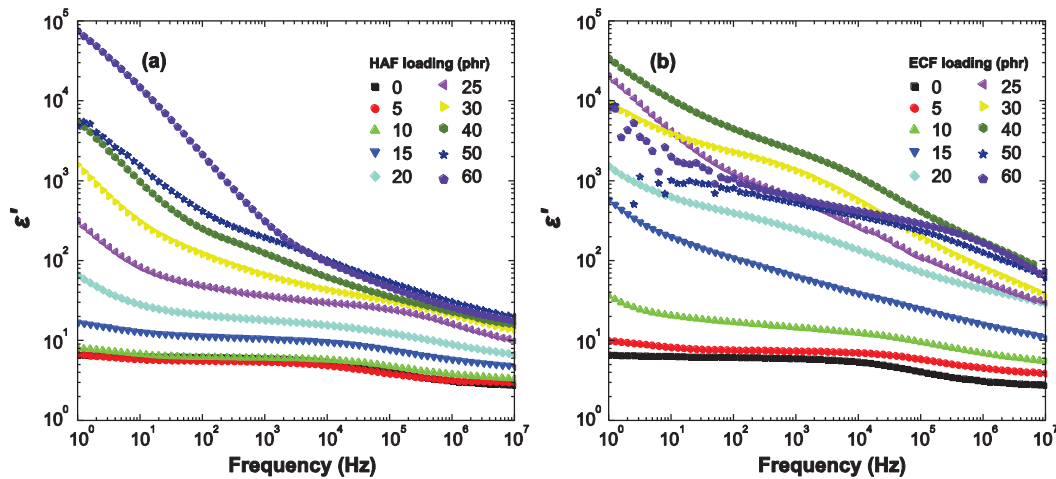


Figure 6.10 Dielectric permittivity (ϵ') at room temperature as a function of frequency for (a) HAF/ENR-50 (b) ECF/ENR-50 composites

Figure 6.11 shows dielectric loss (ϵ'') at room temperature as a function of frequency for HAF and ECF filled ENR-50. It can be seen that loss factor is increased with increasing filler content. This is originated from the contributions of dipole orientation, conduction loss and interfacial polarization as mentioned in previous chapter (Equation

5.1) [35, 36]. Furthermore, it is also visibly observed the relaxation peak in gum vulcanizate, which originates from the dipole relaxation in the polymer chain or α -relaxation of ENR-50. Also, the polymer chain relaxation peak is found in the HAF and ECF filled ENR-50 where the relaxation peaks are shifted to higher frequencies with the increasing CB content. However, the relaxation was masked and exhibited as a linear relation between ϵ'' and frequency when the CB content above 30 and 15 phr for HAF and ECF composites, respectively. This is attributed to predominating of DC conduction process in the composites with high CB loading. AC conductivity (σ_{AC}) of HAF and ECF composites as a function frequency with different amounts of carbon black is shown in Figure 6.12. It can be seen that the σ_{AC} of HAF and ECF composites is increased with increasing loading levels of CB in the vulcanizates. A significant increase in σ_{AC} was observed when introducing a high CB loading. This is attributed to the shorter distance between the charge carriers and flow of charges by hopping or tunneling [37, 38].

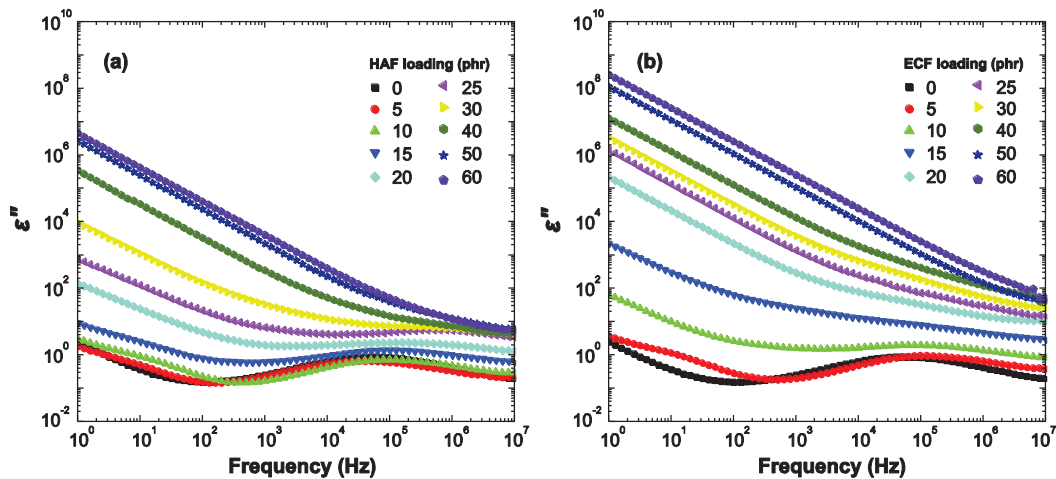


Figure 6.11 Dielectric loss factor (ϵ'') at room temperature as a function of frequency for (a) HAF/ENR-50 (b) ECF/ENR-50 composites

In general, the increase in σ_{AC} (real part, σ') with increasing frequency in isothermal condition can be expressed by the following equation [39, 40]:

$$\sigma'(\omega) = \sigma(0) + \sigma_{AC}(\omega) = \sigma_{DC} + A\omega^s \quad (6.3)$$

where ω is the angular frequency ($2\pi f$), σ_{DC} is the independent frequency conductivity or DC conductivity ($\omega \rightarrow 0$), A is a temperature-dependent constant and s is an exponent dependent on both frequency and temperature. This is a typical behavior for a wide variety

of materials and is called by Jonscher “universal dynamic response” (UDR) because of a wide variety of materials that displayed in such behavior [40].

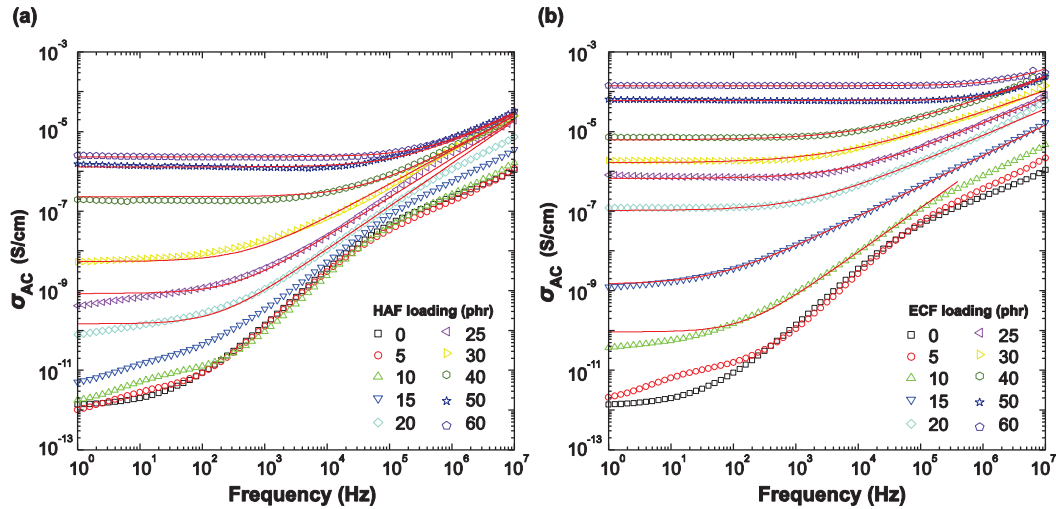


Figure 6.12 AC conductivity at room temperature as a function of frequency for (a) HAF and (b) ECF filled ENR-50 vulcanizate with various CB loading levels. The solid line is a fit of Equation 6.3

In Figure 6.12, the frequency dependence of AC conductivity of CB/ENR-50 composite can be divided into two regions. First region, conductivity pattern shows frequency independence at low frequency, exhibiting plateau region which can be considered as a truly DC conductivity σ_{DC} according to Equation 6.3. Second region, frequency dependence behavior is observed. This is generally attributed to the hopping transport phenomena, following a power law (ω^s) (Equation 6.3). In the conductive composite, the appearance of plateau region have been widely interpreted that the connective network or percolating paths of conductive clusters are formed in polymer matrix [7, 25, 41]. Furthermore, the DC plateau was seen to be broaden with increase in CB loading due to the increase in connected conductive networks within the insulating rubber together with the decreasing distance between the CB particles and clusters [42]. It is also seen that all the conductive composites showed plateau regions until some critical frequency (f_c). Above this frequency, conductivity is again increased with a power law. The transition region is therefore shifted to higher frequencies as increasing of CB content. The values of σ_{DC} , A , and s were obtained by fitting the power law equation are listed in Table 6.4.

Table 6.4 DC conductivity values obtained from the power law fitting curves of the conductivity plots

CB loading (phr)	HAF/ENR-50			ECF/ENR-50		
	σ_{DC}	A	s	σ_{DC}	A	s
0	9.29×10^{-13}			9.29×10^{-13}		
5	1.02×10^{-12}			2.11×10^{-12}		
10	1.75×10^{-12}			3.61×10^{-11}	4.17×10^{-14}	1.11
15	5.13×10^{-12}	5.96×10^{-14}	1.01	1.45×10^{-9}	1.49×10^{-11}	0.77
20	1.46×10^{-10}	7.37×10^{-14}	1.08	1.03×10^{-7}	2.22×10^{-10}	0.67
25	8.47×10^{-10}	4.49×10^{-13}	0.98	6.63×10^{-7}	5.28×10^{-10}	0.66
30	5.39×10^{-9}	4.95×10^{-12}	0.86	1.64×10^{-6}	5.40×10^{-9}	0.55
40	2.31×10^{-7}	7.87×10^{-12}	0.83	6.23×10^{-6}	9.26×10^{-9}	0.57
50	1.28×10^{-6}	3.30×10^{-11}	0.76	6.01×10^{-5}	4.92×10^{-12}	0.97
60	2.30×10^{-6}	9.18×10^{-12}	0.83	1.42×10^{-4}	5.31×10^{-11}	0.85

Also, the inferred conductivity to zero frequency was considered as DC conductivity ($\sigma_{DC} = \sigma_{AC} (\omega \rightarrow 0)$) according to Equation 6.3. The σ_{DC} of HAF/ENR-50 and ECF/ENR-50 composites with different CB content obtained from Figure 6.12 is summarized in Figure 6.13. At low CB content, the σ_{DC} is very low and increased slowly as carbon black content increases. This is due to the fact that conductivity was dominated by the matrix and conductive particles remain isolated from each other in the matrix. At the same loading level of CB, ECF composites show a higher conductivity than that of HAF composites. Further increasing CB content, the conductive structures are formed in the ENR-50 matrix. This causes the increasing electrical conductivity abruptly by several orders of magnitude. In Figure 6.13, it is clear that the percolation threshold is observed in the ranges of CB loading levels of 10 and 20 phr for ECF composites and between 15 and 30 phr for HAF composites. These critical regions of composites correspond to the formation of CB network in ENR-50 matrix and insulating composites become conducting composites at the percolation point. The high-structure of ECF in ENR-50 composite allows to achieve the percolation at lower content in comparison to low-structure HAF particle [43]. Then, the σ_{DC} does not increase significantly with increasing CB content above the percolation point. This is due to the conductive networks are already formed, the abundant of CB particles show little influence on conducting process.

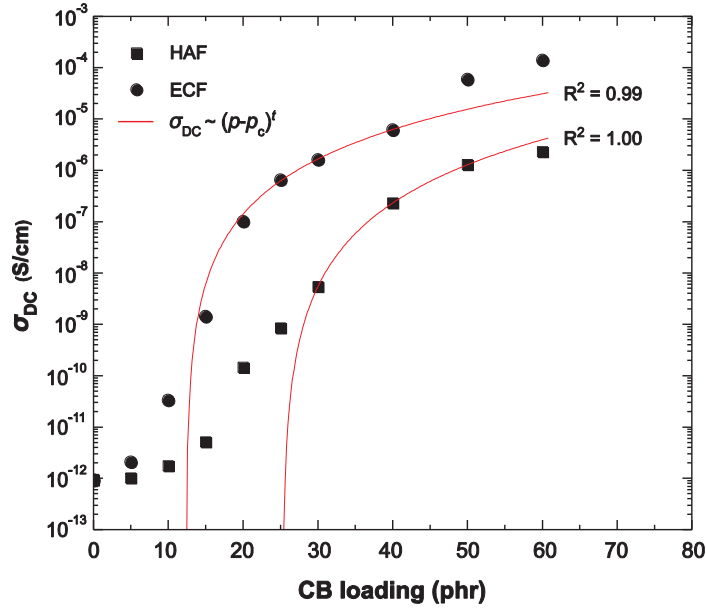


Figure 6.13 DC conductivity (σ_{DC}) versus CB loading levels of HAF and ECF composites

The classical relationship between the DC conductivity (σ_{DC}) of conductive particles filled polymer and conductive concentration (p) in the composite is well known as scaling law, which can be used to estimate percolation threshold (p_c) in the conductive composite [44]:

$$\sigma_{DC} = \sigma_0(p - p_c)^t \quad \text{for } p > p_c \quad (6.4)$$

where σ_0 is a constant, p is the filler concentration, p_c is the filler concentration at percolation threshold and t is the critical exponent. The electrical percolation threshold (p_c) was fitted the σ_{DC} data for $p > p_c$.

The p_c was determined from Figure 6.13, it was found that the best fitting for percolation threshold (p_c) in composites were 25.3 ± 0.4 and 12.4 ± 2.0 phr, respectively. A density of 1.8 g/cm^3 were employed to convert from phr to vol% [7]. Thus, the percolation threshold (p_c) of HAF and ECF composites are 12.0 vol% and 6.3 vol%, respectively. The ECF/ENR-50 composite show lower percolation threshold than that of HAF/ENR-50 composite due to high structure of ECF particles. The complex shape of ECF causes to form better conductive network which is formed through the spatial arrangement of carbon aggregate in the polymer matrix, as shown in Figure 6.14. It can be seen that high electrical contact of high-structure ECF are created in conductive

composite and electrical percolation reached at very low ECF content as compared with low-structure HAF. It was revealed that high structure CB exhibit more complex shapes, higher internal voids and large surface, leading to observed low percolation limit [7, 14, 43]. It is claimed that the estimated value of the percolation threshold for ECF/ENR-50 composite in this work is lower than those of conductive elastomer composites which have been reported in literature [6-8]. That is, Ghosh and Chakrabarti [6] obtained the percolation concentration zone over a carbon black loading range of 20-35 phr in ethylene-propylene diene copolymer (EPDM). Whereas, Reffae *et al.* [8] filled HAF in acrylonitrile butadiene rubber (NBR) by melt mixing technique and found the percolation threshold at approximately 30 phr of HAF. Furthermore, the high structure of ECF not only reduces percolation threshold concentration but it also increases the conductivity above percolation concentration. That is, the ECF composite reaches a value of 10^{-4} S·cm⁻¹, while HAF composite reaches a value of 10^{-6} S·cm⁻¹. This indicates that ECF composite is a conductive composite with low percolation threshold and high conductivity.

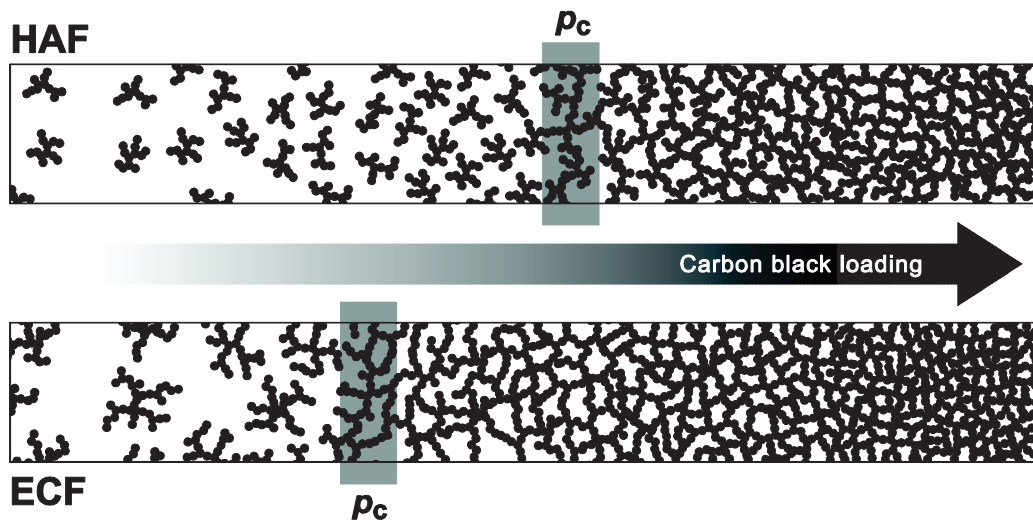


Figure 6.14 The formation of conductive network of two different CB structures

The t value can be obtained from the slope of σ_{DC} as a function of $(p - p_c)$ on a double logarithm scale, as shown in Figure 6.15. The t value of 3.3 ± 0.01 and 3.1 ± 0.16 are observed in HAF/ENR-50 and ECF/ENR-50 composites, respectively. Theoretically, a value of $t = 2.0$ is predicted for a statistical percolation network in three dimensions [45]. The t values based on our experiment are higher than theory, which might be probably due to the fact that wider inter-particle distance distribution yields a diverging

distribution of high-resistance element in the network. Inter-particle resistance bares the feature of exponential decay of tunneling conductivity with the inter-particle distance [43]. The high t value of 2.8 was also reported previously by Sohi *et al.* [7] for CB/EVA composite. Belaïd *et al.* [27] found $t = 4.1$ for EVA filled bamboo charcoal. Likewise, Levchenko *et al.* [46] found $t = 4.2$ in PP filled with CNT and organo-clay.

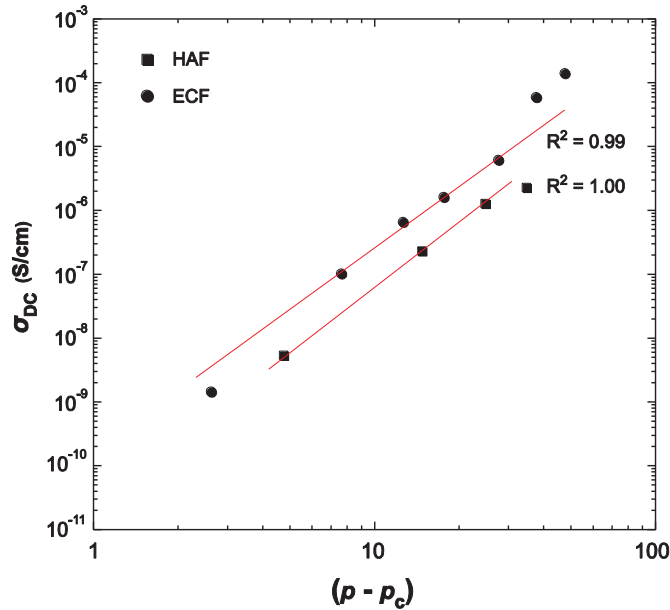


Figure 6.15 The conductivity for ENR-50 filled with HAF and ECF as function of ($\rho - \rho_c$)

6.3 Conclusions

In this chapter, cure characteristic, mechanical, dynamic mechanical and electrical properties of HAF/ENR-50 and ECF/ENR-50 composites were investigated. It was found that short scorch time and cure time but their delta torque were observed in HAF/ENR-50 compounds compared with ECF/ENR-50 compounds. Enhancement of tensile properties were observed in both HAF/ENR-50 and ECF/ENR-50 composites with the maximum tensile strength at loading level of CB of 20 and 10 phr, respectively. However, decreasing elongation at break was observed with increasing CB loading level. It was also found that incorporation of ECF particles in ENR-50 offered higher degree of reinforcement than that of HAF, as estimated by Krause's relation. This led to significantly increasing in Young's modulus and hardness of the ECF/ENR-50 composites.

Furthermore, dynamic mechanical properties revealed the significant improvement in storage modulus and reduction of $\tan \delta$ peak height of ECF composite due to the higher reinforcing efficiency of the ECF particles compared with HAF counterpart. The abruptly increase in Young's modulus, hardness and storage modulus with addition ECF above 30 phr might be attributed to the rheological percolation. Also, a shift in glass transition by +6°C was observed in ECF/ENR-50 composites over the whole composition range. On the other hand, the T_g of HAF composite increased until a loading level of 20 phr of HAF beyond this point the decreasing trend in T_g was observed. The electrical properties of CB/ENR-50 composites were also studied by employing dielectric spectroscopy. The incorporation of CB leads to increase permittivity, loss factor and conductivity of the composites. The use of ECF show higher conductivity than that of HAF at a given loading level of CB. The electrical percolation threshold (p_c) in HAF/ENR-50 and ECF/ENR-50 composites was found at 25.3 and 12.4 phr of CB, which are equivalent to 12.0 and 6.3 vol%, respectively. It is therefore concluded that the percolation threshold of ECF/ENR-50 composites is very low and it could be considered as high conductive elastomer material.

6.4 References

- [1] Klüppel, M., Schroöder, A. and Heinrich, G. 2007. *Carbon black*, in *Physical Properties of Polymers Handbook*, J.E. Mark, ed. Springer, New York.
- [2] Huang, J.C. 2002. *Carbon black filled conducting polymers and polymer blends*. Adv. Polym. Tech. 21, 299-313.
- [3] Fröhlich, J., Niedermeier, W. and Luginsland, H.D. 2005. *The effect of filler–filler and filler–elastomer interaction on rubber reinforcement*. Compos. Part A: Appl. S. 36, 449-460.
- [4] Wang, M.-J. 1998. *Effect of polymer-filler and filler-filler interactions on dynamic properties of filled vulcanizates*. Rubber Chem. Technol. 71, 520-589.
- [5] Zhang, W., Dehghani-Sanij, A.A. and Blackburn, R.S. 2007. *Carbon based conductive polymer composites*. J. Mater. Sci. 42, 3408-3418.
- [6] Ghosh, P. and Chakrabarti, A. 2000. *Conducting carbon black filled EPDM vulcanizates: assessment of dependence of physical and mechanical properties*

- and conducting character on variation of filler loading. *Eur. Polym. J.* 36, 1043-1054.
- [7] Sohi, N.J.S., Bhadra, S. and Khastgir, D. 2011. *The effect of different carbon fillers on the electrical conductivity of ethylene vinyl acetate copolymer-based composites and the applicability of different conductivity models.* *Carbon.* 49, 1349-1361.
- [8] Reffaae, A.S.A., El Nashar, D.E., Abd-El-Messieh, S.L. and Abd-El Nour, K.N. 2009. *Electrical and mechanical properties of acrylonitrile rubber and linear low density polyethylene composites in the vicinity of the percolation threshold.* *Mater. Design.* 30, 3760-3769.
- [9] Nanda, M. and Tripathy, D.K. 2008. *Physico-mechanical and electrical properties of conductive carbon black reinforced chlorosulfonated polyethylene vulcanizates.* *Express Polym. Lett.* 2, 855-865.
- [10] Sau, K.P., Chaki, T.K. and Khastgir, D. 1997. *Conductive rubber composites from different blends of ethylene-propylene-diene rubber and nitrile rubber.* *J. Mater. Sci.* 32, 5717-5724.
- [11] Das, A., Stöckelhuber, K.W., Jurk, R., Saphiannikova, M., Fritzsche, J., Lorenz, H., Klüppel, M. and Heinrich, G. 2008. *Modified and unmodified multiwalled carbon nanotubes in high performance solution-styrene-butadiene and butadiene rubber blends.* *Polymer.* 49, 5276-5283.
- [12] Bhattacharyya, S., Sinturel, C., Bahloul, O., Saboungi, M.L., Thomas, S. and Salvétat, J.P. 2008. *Improving reinforcement of natural rubber by networking of activated carbon nanotubes.* *Carbon.* 46, 1037-1045.
- [13] Bokobza, L. and Kolodziej, M. 2006. *On the use of carbon nanotubes as reinforcing fillers for elastomeric materials.* *Polym. Int.* 55, 1090-1098.
- [14] Li, Z.H., Zhang, J. and Chen, S.J. 2008. *Effects of carbon blacks with various structures on vulcanization and reinforcement of filled ethylene-propylene-diene rubber.* *Express Polym. Lett.* 2, 695-704.
- [15] Luo, Y.Y., Wang, Y.Q., Zhong, J.P., He, C.Z., Li, Y.Z. and Peng, Z. 2011. *Interaction between fumed-silica and epoxidized natural rubber.* *J. Inorg. Organomet. P.* 21, 777-783.

- [16] Litvinov, V.M. and Steeman, P.A.M. 1999. *EPDM-carbon black interactions and the reinforcement mechanisms, as studied by low-resolution ^1H NMR*. *Macromolecules*. 32, 8476-8490.
- [17] Dijkhuis, K.A.J., Noordermeer, J.W.M. and Dierkes, W.K. 2009. *The relationship between crosslink system, network structure and material properties of carbon black reinforced EPDM*. *Eur. Polym. J.* 45, 3302-3312.
- [18] Praveen, S., Chattopadhyay, P.K., Jayendran, S., Chakraborty, B.C. and Chattopadhyay, S. 2010. *Effect of rubber matrix type on the morphology and reinforcement effects in carbon black-nanoclay hybrid composites-a comparative assessment*. *Polym. Compos.* 31, 97-104.
- [19] Manna, A.K., De, P.P., Tripathy, D.K. and De, S.K. 1998. *Hysteresis and strain-dependent dynamic mechanical properties of epoxidized natural rubber filled with surface-oxidized carbon black*. *J. Appl. Polym. Sci.* 70, 723-730.
- [20] Salaeh, S. and Nakason, C. 2012. *Influence of modified natural rubber and structure of carbon black on properties of natural rubber compounds*. *Polym. Compos.* 33, 489-500.
- [21] Coran, A.Y. 2011. *Vulcanization*, in *Science and Technology of Rubber*, J.E. Mark, B. Erman and F. R. Eirich, eds. Elsevier, New York.
- [22] Kraus, G. 1963. *Swelling of filler-reinforced vulcanizates*. *J. Appl. Polym. Sci.* 7, 861-871.
- [23] Shanmugaraj, A.M. and Ryu, S.H. 2013. *Influence of aminosilane-functionalized carbon nanotubes on the rheometric, mechanical, electrical and thermal degradation properties of epoxidized natural rubber nanocomposites*. *Polym. Int.* 62, 1433-1441.
- [24] Stephen, R., Ranganathaiah, C., Varghese, S., Joseph, K. and Thomas, S. 2006. *Gas transport through nano and micro composites of natural rubber (NR) and their blends with carboxylated styrene butadiene rubber (XSBR) latex membranes*. *Polymer*. 47, 858-870.
- [25] Sahoo, B.P., Naskar, K. and Tripathy, D.K. 2012. *Conductive carbon black-filled ethylene acrylic elastomer vulcanizates: physico-mechanical, thermal, and electrical properties*. *J. Mater. Sci.* 47, 2421-2433.

- [26] Ha, M.L.P., Grady, B.P., Lolli, G., Resasco, D.E. and Ford, W.T. 2007. *Composites of single-walled carbon nanotubes and styrene-isoprene copolymer latices*. *Macromol. Chem. Phys.* 208, 446-456.
- [27] Belaïd, S., Boiteux, G. and Cassagnau, P. 2013. *Rheological and electrical properties of EVA copolymer filled with bamboo charcoal*. *Rheol. Acta.* 52, 75-84.
- [28] Teh, P.L., Ishak, Z.A.M., Hashim, A.S., Karger-Kocsis, J. and Ishiaku, U.S. 2004. *Effects of epoxidized natural rubber as a compatibilizer in melt compounded natural rubber-organoclay nanocomposites*. *Eur. Polym. J.* 40, 2513-2521.
- [29] Das, A., Costa, F.R., Wagenknecht, U. and Heinrich, G. 2008. *Nanocomposites based on chloroprene rubber: effect of chemical nature and organic modification of nanoclay on the vulcanizate properties*. *Eur. Polym. J.* 44, 3456-3465.
- [30] López-Manchado, M.A., Biagiotti, J., Valentini, L. and Kenny, J.M. 2004. *Dynamic mechanical and raman spectroscopy studies on interaction between single-walled carbon nanotubes and natural rubber*. *J. Appl. Polym. Sci.* 92, 3394-3400.
- [31] Logakis, E., Pandis, C., Peoglos, V., Pissis, P., Stergiou, C., Pionteck, J., Pötschke, P., Micusík, M. and Omastová, M. 2009. *Structure–property relationships in polyamide 6/multi-walled carbon nanotubes nanocomposites*. *J. Polym. Sci. Pol. Phys.* 47, 764-774.
- [32] Kosmidou, T.V., Vatalis, A.S., Delides, C.G., Logakis, E., Pissis, P. and Papanicolaou, G.C. 2008. *Structural, mechanical and electrical characterization of epoxy-amine/carbon black nanocomposites*. *Express Polym. Lett.* 2, 364-372.
- [33] Fritzsche, J., Lorenz, H. and Klüppel, M. 2009. *CNT based elastomer-hybrid-nanocomposites with promising mechanical and electrical properties*. *Macromol. Mater. Eng.* 294, 551-560.
- [34] Meier, J.G. and Klüppel, M. 2008. *Carbon black networking in elastomers monitored by dynamic mechanical and dielectric spectroscopy*. *Macromol. Mater. Eng.* 293, 12-38.
- [35] Chen, Q., Xi, Y., Bin, Y. and Matsuo, M. 2008. *Electrical and dielectric properties in carbon fiber-filled LMWPE/UHMWPE composites with different blend ratios*. *J. Polym. Sci. Pol. Phys.* 46, 359-369.

- [36] Huang, X., Xie, L., Jiang, P., Wang, G. and Liu, F. 2009. *Electrical, thermophysical and micromechanical properties of ethylene-vinyl acetate elastomer composites with surface modified BaTiO₃ nanoparticles*. J. Phys. D: Appl. Phys. 42, 245407.
- [37] Subramaniam, K., Das, A., Steinhäuser, D., Klüppel, M. and Heinrich, G. 2011. *Effect of ionic liquid on dielectric, mechanical and dynamic mechanical properties of multi-walled carbon nanotubes/polychloroprene rubber composites*. Eur. Polym. J. 47, 2234-2243.
- [38] Psarras, G.C., Manolakaki, E. and Tsangaris, G.M. 2002. *Electrical relaxations in polymeric particulate composites of epoxy resin and metal particles*. Compos. Part A: Appl. S. 33, 375-384.
- [39] Dyre, J.C. and Schrøder, T.B. 2000. *Universality of ac conduction in disordered solids*. Rev. Mod. Phys. 72, 873-892.
- [40] Jonscher, A.K. 1977. *The 'universal' dielectric response*. Nature. 267, 673-679.
- [41] Pötschke, P., Abdel-Goad, M., Alig, I., Dudkin, S. and Lellinger, D. 2004. *Rheological and dielectrical characterization of melt mixed polycarbonate-multiwalled carbon nanotube composites*. Polymer. 45, 8863-8870.
- [42] Al-Saleh, M.H., Al-Anid, H.K., Husain, Y.A., El-Ghanem, H.M. and Jawad, S.A. 2013. *Impedance characteristics and conductivity of CNT/ABS nanocomposites*. J. Phys. D: Appl. Phys. 46.
- [43] Balberg, I. 2002. *A comprehensive picture of the electrical phenomena in carbon black-polymer composites*. Carbon. 40, 139-143.
- [44] Barrau, S., Demont, P., Peigney, A., Laurent, C. and Lacabanne, C. 2003. *DC and AC conductivity of carbon nanotubes-polyepoxy composites*. Macromolecules. 36, 5187-5194.
- [45] Logakis, E., Pandis, C., Peoglos, V., Pissis, P., Pionteck, J., Pötschke, P., Micusik, M. and Omastova, M. 2009. *Electrical/dielectric properties and conduction mechanism in melt processed polyamide/multi-walled carbon nanotubes composites*. Polymer. 50, 5103-5111.
- [46] Levchenko, V., Mamunya, Y., Boiteux, G., Lebovka, M., Alcouffe, P., Seytre, G. and Lebedev, E. 2011. *Influence of organo-clay on electrical and mechanical properties of PP/MWCNT/OC nanocomposites*. Eur. Polym. J. 47, 1351-1360.

CHAPTER 7

PHASE DEVELOPMENT AND MISCIBILITY OF PVDF/ENR-50 SIMPLE BLENDS

7.1 Introduction

Blending of polymers is an attractive way to develop new materials by combining two or more polymers, resulting in improvements of properties which could not be obtained from the individual components [1, 2]. Most of polymer blends are generally immiscible and their properties are strongly dependent on phase structure. The morphology and physical properties of the blends can be tailored by adjusting blends ratio, viscosity, as well as the interfacial adhesion between their phases [3, 4]. Morphology of immiscible blends can be divided into two categories; dispersed and co-continuous structures. In the dispersed structure, the minor phase is generally dispersed in the major component, matrix that controls the physical properties of the blends. In the co-continuous phase structure, both components are interconnected in all directions, this could be fully contributing concurrently to the blends properties. Three dimensional co-continuous phase structure is a main criterion to form thermoplastic elastomer (TPE) materials based on blending of thermoplastic and elastomeric materials via a simple blend technique. The TPEs have attracted significant attention in polymer industries because they exhibit properties of elastomeric materials at room and ambient temperature together with the ability to process by using thermoplastic equipment. This is, the continuous hard plastic phase provides strength and processability while the continuous soft rubbery phase provides flexibility and elasticity of the materials [5].

Polymer blends generally exhibit high interfacial tension since it is only poor interfacial adhesion between blend components leading to poor physical properties. Therefore, compatibilization has been applied to improve interfacial adhesion or interaction and to stabilize the phase morphology. The blend components would be

stabilized by covalent bonds, ionic bonds or attractive intermolecular forces, e.g., dipole-dipole and ion-dipole interaction, charge-transfer, H-bonding, van der Waals forces, etc. The blends are usually compatibilized either by addition of compatibilizer or by reactive blending [6 - 9]. Miscibility and compatibility of polymer blends have been widely investigated by various techniques such as FTIR [4, 10], NMR [11], microscopy, dynamic mechanical properties [12-16] and dielectric properties [17-21].

Poly(vinylidene fluoride) (PVDF) molecules consist of alternating CH_2 and CF_2 groups in the carbon main chain. PVDF exhibits excellent mechanical properties and flexural modulus. Furthermore, the alternating CF_2 groups in PVDF molecules create dipole with high permittivity and exhibit ferroelectricity under certain conditions. Due to fluorine atoms in the molecular chain, PVDF has good chemical resistance and weatherability [9, 12, 22-24]. Blending of PVDF with other polymers have been extensively performed. It was found that the PVDF is miscible with poly(methyl methacrylate) (PMMA) [10, 17], poly(vinyl alcohol) (PVA) [19], and acrylic rubber (ACM) [25]. Furthermore, PVDF/ACM blend showed a single glass transition temperature (T_g), which indicates miscibility of the blend with excellent elongation at break, strain recovery, and heat and oil resistances [25]. However, the PVDF/polyamide-12 (PA-12) blend [26] and PVDF/thermoplastic polyurethane (TPU) blend [9] are partially compatible.

Epoxidized natural rubber (ENR) is chemically modified natural rubber (NR) by randomly replacement of epoxide groups to the double bond in *cis*-1,4-polyisoprene chains. ENR with low content of epoxide groups still exhibit strain-induced crystallization characteristics with high flexibility and mechanical properties in term of tensile strength and elongation at break. ENR has been used to enhance interfacial adhesion of polymer blends and to compatibilize filler-polymer composites. That is, high polarity of the epoxide rings in ENR molecules develop strong interactions between components in polymer blend and composite [27-29]. This evidences from blending of ENR with several polymers such as polyamide-12 (PA-12) [4], thermoplastic polyurethane (TPU) [28] and nitrile rubber (NBR) [29].

The main aim of this chapter is to prepare polymer blend based on PVDF/ENR by simple blend technique. Effects of different epoxide level in ENR molecules (i.e., ENR-25 and ENR-50 with 25 and 50 mol% epoxide, respectively) and various blend composition were investigated. Moreover, miscibility and phase development of

PVDF/ENR blends were determined. Furthermore, morphological properties, static and dynamic mechanical properties, differential scanning calorimetry, and dielectric analysis of the prepared blends were examined. Finally, the evolution of co-continuous structure of the blend was also investigated.

7.2 Effect of difference epoxidation level in ENR on the properties of PVDF/ENR simple blend

PVDF/ENRs blends were prepared by simple blend technique according to the methodology described in section 3.2.4. Two different types of ENRs (i.e., ENR-25 and ENR-50) were used to prepare the simple blend. Morphological and physical properties of the blends were analyzed. Further investigation have been done by dynamic mechanical properties, differential scanning calorimetry, and dielectric analysis. The evolution of co-continuous structure of the blend was also investigated.

7.2.1 Morphological properties

Figure 7.1 shows SEM micrographs of the PVDF/ENR-25 and PVDF/ENR-50 blends. It can be seen that the SEM micrographs showed the co-continuous phase structures with remained PVDF phase and cavitations were the former location of ENRs in the blends. Both blends exhibited the co-continuous structure, indicating 50/50 wt% is in the composition range for co-continuity of PVDF/ENR-25 and PVDF/ENR-50. It is clear that the PVDF/ENR-50 blend showed finer grain morphology of co-continuous phase structure compared with the PVDF/ENR-25 counterpart. The domain size in PVDF/ENR-25 blend developed with an average domain size of about 9.0 μm while average domain size of PVDF/ENR-50 was relatively small of about 3.7 μm . This indicates a higher interfacial adhesion and better miscibility between PVDF and ENR-50.

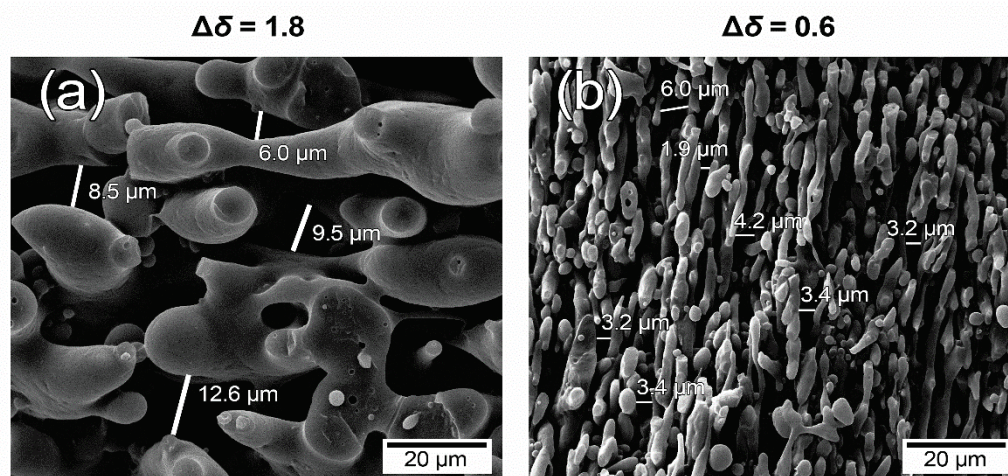


Figure 7.1 SEM micrographs of (a) PVDF/ENR-25 and (b) PVDF/ENR-50 blends

As discussed in section 2.2.1, phase separation can be caused by a high molecular weight of polymer and weak interaction between blend components. The miscibility contribution can be assessed in terms of solubility parameter [13, 30] (see Equation 2.8). The smaller the difference ($\Delta\delta = \delta_1 - \delta_2$) in solubility is the better miscibility. The solubility of polymers using in present work are listed in Table 7.1.

Table 7.1 Solubility parameter of PVDF, ENR-25 and ENR-50

Polymer	PVDF [31]	ENR-25 [32]	ENR-50 [32]
Solubility parameter, δ (MPa) ^{1/2}	19.2	17.4	18.6

On the basis of theoretical considerations interfacial tension arises mainly from the disparity between the polarities of the two polymer phases. The introduction of polar functional group causes to reduce interfacial tension between the components of the mixture. The difference between the solubility parameters ($\Delta\delta$) of the two polymer types increases as a consequence, interfacial tension increases as well [30]. Therefore, $\Delta\delta$ can be used to estimate interfacial tension in polymer blend. Based on data from Table 7.1, the solubility parameter of the ENR-50 is very close to PVDF as compared with ENR-25. The interfacial tension for the PVDF/ENRs blend is order as follows: PVDF/ENR-50 ($\Delta\delta = 0.6$) < PVDF/ENR-25 ($\Delta\delta = 1.8$). The small difference in solubility parameter of PVDF/ENR-50 is due to the presence of 50 mol% epoxide group in ENR chain, which increases solubility parameter and improve thermodynamic miscibility in PVDF/ENR-50. This supports the explanation on the decrease in domain size of PVDF/ENR-50 blends.

This is due to low interfacial tension and compatibility of PVDF/ENR-50 blend. Furthermore, the phase size reduction is also caused by the compatibilization between interface of the blend (i.e., via graft copolymer or reactive blending) which occurs during melt processing [4, 33-35]. This acts as emulsifier and reduce the interfacial tension between two phases [36]. The PVDF/ENR-50 blend shows parallel direction of elongated shape in blend components. An increase in the degree of elongation of co-continuous blend can be observed in the blend with high degree of compatibility. The lower interfacial tension in compatibilized PVDF/ENR-50 blend is expected to offer larger deformation of blend component and enhance their stability [36]. Therefore, increasing epoxide group content in ENR chains caused enhancement of blend compatibility between the two phases [4]. Hence, the strong interaction and interfacial adhesion between the two phases caused a formation of finer grain morphology in PVDF/ENR blends. The formation of a small structure by using ENR has also been reported in PA12/ENRs [4] and TPU/ENR blends [34].

7.2.2 Mechanical properties

Figure 7.2 shows stress-strain curve of PVDF/ENR blends with different types of ENRs. The mechanical properties in terms of tensile strength and elongation at break based on the failure point from Figure 7.2, tension set and hardness are summarized in Table 7.2. It can be seen that neat PVDF showed linear deformation up to maximum stress of 53 MPa. The modulus of linear part of the curve is dominated by the amorphous regions where tie chains bear the main load. When deformation is increased, the sample begins to flow, so that the stress remains nearly constant up to a high degree of elongation after the maximum point. This maximum stress is known as yield point. At the yield point the deformation becomes irrecoverable due to the change from the uniform elastic deformation mode to another one, which involves both elastic and plastic components [37]. The yield point was suppressed in the blends and the blends showed lower tensile strength and higher elongation at break than that of neat PVDF, which is a good characteristic for thermoplastic elastomer (TPE). It is also clear that the blend with higher epoxide group content in ENR (ENR-50) showed high tensile strength, elongation at break and hardness than the blend with low epoxide group content (ENR-25). As a result, PVDF/ENR-50 blends showed a fine co-continuous structure with good interfacial adhesion and miscibility between PVDF and ENR-50 phases. This could drive sufficient

stress transfer between the two phases, resulting in increased mechanical properties. This result is in good agreement with work presented by Ramesh and De [38]. Moreover, PVDF blends with ENR-50 showed lower tension set which is recovering from prolong extension and can be implied to better elastomeric behavior for thermoplastic elastomer materials.

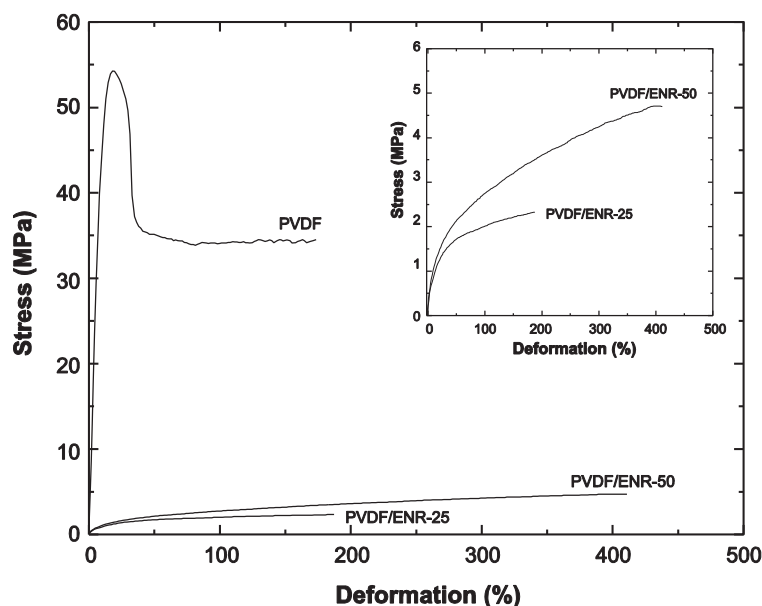


Figure 7.2 Stress-strain curves of PVDF, PVDF/ENR-25 and PVDF/ENR-50 blends

Table 7.2 Mechanical properties of PVDF, PVDF/ENR-25 and PVDF/ENR-50 blends

Sample	Young's Modulus (MPa)	Tensile strength (MPa)	Elongation at break (%)	Tension set (%)	Hardness (Shore A)
PVDF	496.7 (± 111.6)	34.3 (± 6.66)	120 (± 84)	-	94.0 (± 1.1)
PVDF/ENR-25	15.2 (± 1.6)	2.8 (± 0.43)	170 (± 53)	54.7 (± 1.0)	54.0 (± 1.5)
PVDF/ENR-50	19.0 (± 2.6)	4.8 (± 0.69)	440 (± 58)	45.0 (± 0.9)	58.5 (± 1.1)

7.2.3 Differential scanning calorimetry

Figure 7.3 shows DSC thermogram of PVDF and its blends (i.e., PVDF/ENR-25 and PVDF/ENR-50). It is clear that crystallization temperature (T_c) and melting temperature (T_m) of PVDF were observed in both pure PVDF and the blends. The DSC results are summarized in Table 7.3. PVDF showed a crystallization peak at 135.8°C with corresponding crystallinity of 50.3%. Addition of 50 wt% of ENRs (i.e., ENR-25 and ENR-50) increased crystallization temperature to 137.5°C for PVDF/ENR-25 blend and 139.3°C

for PVDF/ENR-50 blend, whereas the melting point slightly decreased from 168.4°C for PVDF to 167.4 and 167.0 °C for PVDF/ENR-25 and PVDF/ENR-50, respectively. The increased crystallization temperature in the blends of PVDF indicates that PVDF has a higher crystallization rate in the blends than in the neat polymer. The high crystallization process of the blend can be confirmed by full width at half maximum (FWHM) of crystallization peak which indicates the acceleration and growth of crystallization process [39]. It is clear that value of FWHM of the blend was lower than that of neat PVDF which indicates the acceleration of the nucleation in the presence of ENRs in the blends. Furthermore, the addition of ENRs also increased the degree of crystallinity of PVDF from 50.3% for the neat PVDF to 54.8 and 52.1% for PVDF/ENR-25 and PVDF/ENR-50, respectively. The increase of crystallinity of crystallizable polymer and amorphous blend can be explained that amorphous polymer (ENRs) acts as the nucleating agent for crystallization of semi-crystalline polymer (PVDF) in melt state [39].

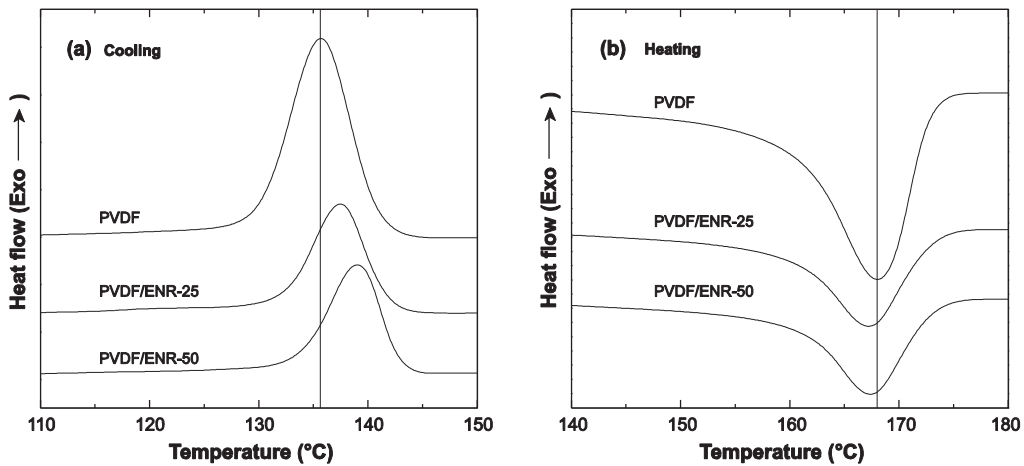


Figure 7.3 DSC (a) cooling and (b) heating sweeps for PVDF, PVDF/ENR-25 and PVDF/ENR-50 blends

Table 7.3 Thermal characteristics of PVDF and its blend during cooling and heating sweeps

Samples	T_c (°C)	FWHM ^a	T_m (°C)	ΔH_m (J/g)	X_c (%)
PVDF	135.8	5.72	168.4	52.55	50.3
PVDF/ENR-25	137.5	4.65	167.4	28.62	54.8
PVDF/ENR-50	139.3	4.55	167.0	27.22	52.1

^a Full Width at Half Maximum of crystallization peak

7.2.4 Dynamic mechanical analysis

DMA thermograms in terms of temperature dependence of storage modulus (E') and loss tangent ($\tan \delta$) of the neat PVDF in the temperature ranges of -90 to 100°C and a frequency 1 Hz are shown in Figure 7.4. It is seen that the neat PVDF exhibited high modulus in the glass transition region. The storage modulus then abruptly dropped in the glass transition region. The substantial decrease of E' indicates glass transition zone which is also associated to $\tan \delta$ relaxation. It is also clear that the PVDF showed three relaxations (i.e., $\tan \delta$ peak) around -39 , 25 and 85°C . The relaxation at lower temperature ($\sim 39^\circ\text{C}$) is related to β or α_a -relaxation which is attributed to segmental motion in the amorphous regions. This is typically assigned to the glass transition temperature (T_g) of PVDF. The relaxation at high temperature ($\sim 85^\circ\text{C}$) is related to α -relaxation that corresponds to segmental motion in crystalline region [40-44]. The weak relaxation between β and α relaxation ($\sim 25^\circ\text{C}$) is related to the β' -relaxation. This corresponds to fold motion in amorphous phase [44].

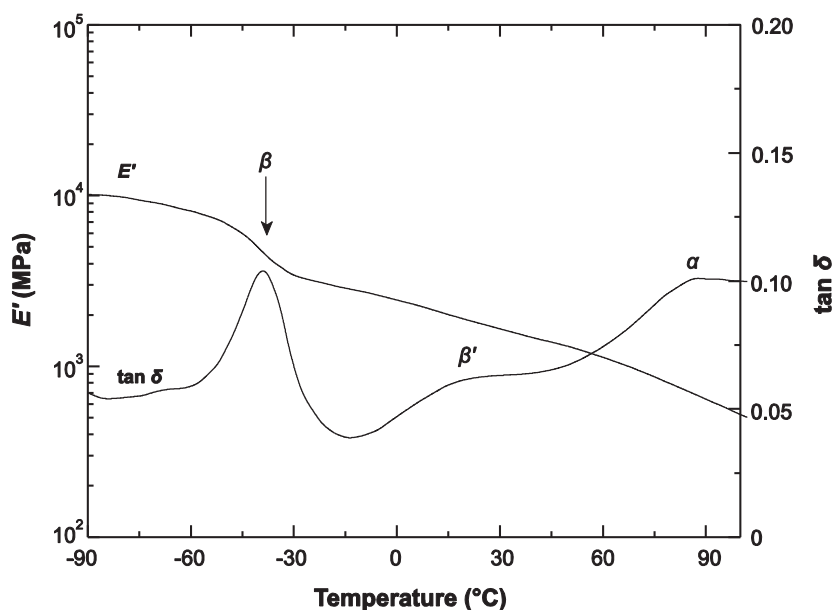


Figure 7.4 Temperature dependence of E' and $\tan \delta$ of PVDF at 1 Hz

Effects of epoxidation level on storage modulus (E') and loss tangent ($\tan \delta$) of PVDF/ENRs blends are shown in Figure 7.5. The dynamic mechanical properties of the blend are summarized in Table 7.4. It can be seen that all types of blends exhibited the lower magnitude of E' compared with the neat PVDF. This is due to addition of ENRs

which caused an increase of the chain mobility of the blends. The changes in the storage modulus at glass transition zone of PVDF are less drastic as compared with the blends due to semi-crystalline nature [45]. In the semi-crystalline polymer, the crystalline chains are regularly arranged and it will remain intact. Thus, the small amount of amorphous part undergoes segmental motion and leads to observing a small drop in storage modulus of semi-crystalline polymer (i.e., PVDF) at transition temperature. It is also seen that the higher storage modulus was observed in the PVDF/ENR-50 blend compared with PVDF/ENR-25 blend over the whole range of tested temperatures. As mentioned above, stress transfer was improved significantly, accompanied by an increase in interfacial adhesion, also resulting in an improved E' in dynamic mechanical properties.

In $\tan \delta$ plot, it is seen that the PVDF/ENR-25 blend showed a single relaxation peak or single glass transition temperature (T_g) at approximately -29.5°C . However, PVDF/ENR-50 showed double relaxation peaks at approximately -35.8 and -9.7°C , respectively. A single $\tan \delta$ peak or a single T_g in polymer blends might be presumably a proof of the miscible blends. However, in this type of blend, some degree of overlapping of β and α -relaxation which are related to glass transition temperatures of PVDF (i.e., $T_g = -39.1^\circ\text{C}$) and ENR-25 (i.e., $T_g = -23.9^\circ\text{C}$), respectively, might occur. This is the reason why the phase separation in the form of co-continuous phase structure is obviously observed in Figure 7.1. In the PVDF/ENR-50 blend, two relaxation peaks are associated to glass transition temperature of PVDF and ENR-50, respectively, the immiscible or partial miscible blend might occur. In this work, it is seen that the glass transition temperatures of PVDF and ENR-50 were shifted from -39.1°C to -35.8°C and from -5.7°C to -9.7°C , respectively. This indicates partial miscible blend where chemical interaction between the phases contributed to the shift of the glass transition temperature. It is also seen that the PVDF/ENR-25 blend showed lower glass transition temperature compared with the one of the PVDF/ENR-50 blend. This is attributed to the steric interference caused by the epoxide group and restriction of chain mobility due to the intermolecular forces exerted on the ENR molecules as observed in ENR-25 and ENR-50 vulcanizates [46, 47]. Higher epoxide contents caused lower chain mobility and hence higher T_g s. Furthermore, the β' and α -relaxation of PVDF could not be observed in all types of blends as marked by higher $\tan \delta$ of ENRs than that of the PVDF.

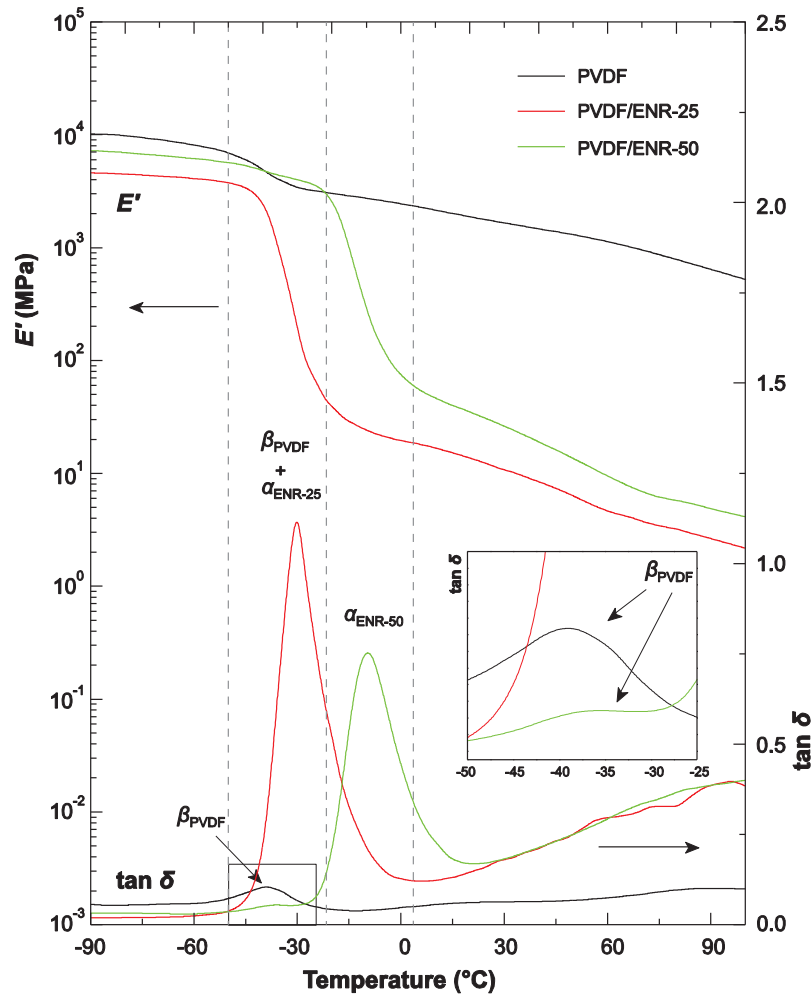


Figure 7.5 Temperature dependence of storage modulus and $\tan \delta$ of PVDF, PVDF/ENR-25 and PVDF/ENR-50 at 1 Hz

Table 7.4 Dynamic mechanical properties of PVDF and its blends

Samples	Storage Modulus, E' (MPa)		Loss tangent ($\tan \delta$)			
	-60°C	at 25°C	$\tan \delta_{\max}$		T_g (°C)	
			PVDF	ENR	PVDF	ENR
PVDF	8100	1765	0.10	-	-39.8	-
ENR-25	6220	2.1	-	2.62	-	-23.7
ENR-50	3800	1.9	-	2.70	-	-5.7
PVDF/ENR-25	4100	12.2	1.19		-29.6	
PVDF/ENR-50	6200	30.4	0.05	0.77	-35.8	-9.7

7.2.5 Consideration of physical properties improvement

Consideration of the physical property improvement can be regarded as the formation of compatibilization in the PVDF/ENRs blends. The morphology of compatibilized PVDF/ENRs blends is schematically illustrated in Figure 7.6. Chain entanglement in amorphous phase of each component results in strong intermolecular interactions, which are located between the two phases. This exhibits as miscible or compatibilized phase that prevents the coalescence of blend components during blending, resulting in reduction of the domain size in the blend. This lead to restriction of the molecular movement of the PVDF and ENRs chains with the consequence of the increase in tensile strength and T_g of blend components as observed earlier. The miscible phase may be reached through the chemical and physical interactions between opened ring of the epoxide group in ENR and C-F group in PVDF during high temperature mixing. The reaction between halogen group and ring-opened has been previously reported by Ramesh and De [38].

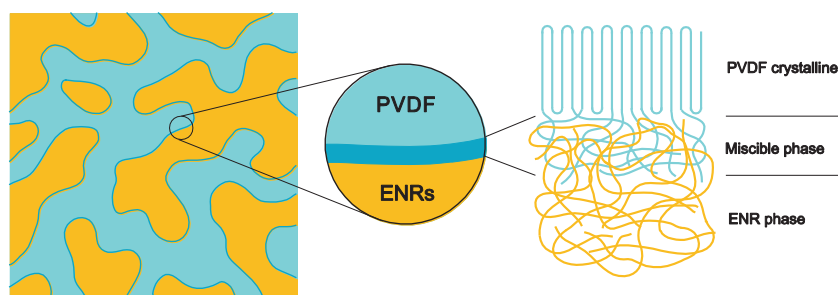


Figure 7.6 Schematic diagram of morphology of compatibilized PVDF/ENR blends

Figure 7.7 shows a proposed mechanism for formation of compatibilization at interface which is responsible for the enhanced interfacial adhesion in PVDF/ENRs blends. It occurred either through H-bonding or covalent bond resulting in formation of strong interaction for compatibilization. A high temperature and shearing force in an internal mixer allow a better reaction for reactive blending. As a consequence, a formation of miscible or compatibilized phase at interface leads to reduction of phase size and improves interfacial adhesion between PVDF and ENR phases. It is expected that the level of compatibilization rises with increasing epoxide group in ENR chain, resulting in increased mechanical properties for ENR with high epoxide group content.

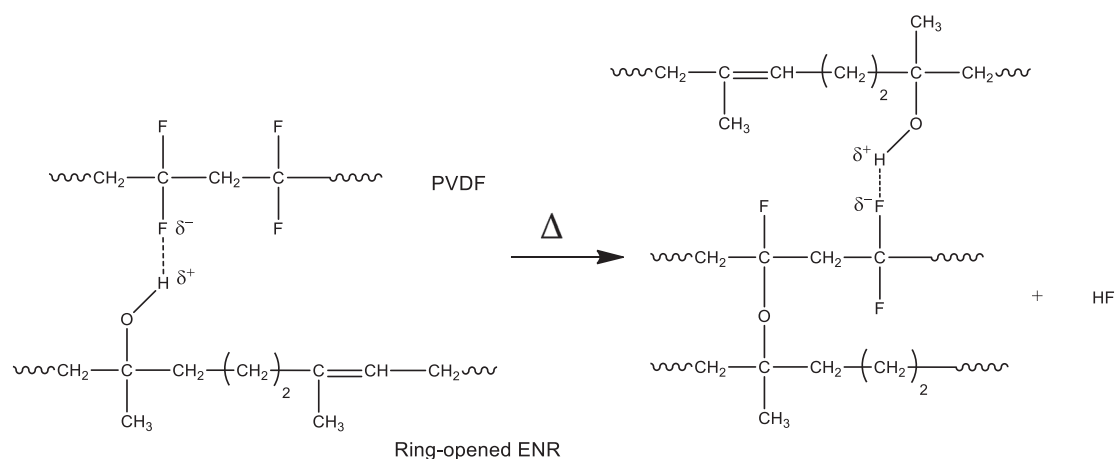


Figure 7.7 Proposed mechanism for interfacial reaction between PVDF and ENR

In order to investigate the formation of interfacial reactions in PVDF/ENRs blends, the blend sample was dissolved into toluene (good solvent for ENR) for 72 hr. The ENR solution was added into methanol to precipitate the ENR phase. The precipitated ENR was then dried in an oven at 50°C until a constant weight was obtained. ATR-FTIR was employed to elucidate the interaction between PVDF and ENRs. Figure 7.8 shows infrared spectra of the neat ENR-25, ENR-50 and PVDF as well as the extracted ENRs. It can be seen that the neat ENR-25 and ENR-50 show absorption peak at wave numbers 1450 cm^{-1} (C-H bending of CH_3) and 1250 cm^{-1} (full ring stretching vibrations of epoxy ring) [6]. In PVDF spectra, the major characteristic peaks of PVDF were found at 1212 and 1180 cm^{-1} (C-F stretching), 1151 cm^{-1} (CF_2 rocking), 1063 cm^{-1} (C-F stretching and C-C stretching) and 766 cm^{-1} (CF_2 bending and skeletal vibrations) [48-51]. The extracted ENR-25 and ENR-50 show absorption peaks from both components: ENR (1450 and 1250 cm^{-1}) and PVDF (1212, 1180, 1151, 1063 and 766 cm^{-1}). The presence of infrared characteristic of PVDF in the extracted ENRs support the formation of chemical reaction between epoxy groups of ENR and polar C-F groups of PVDF during blending process.

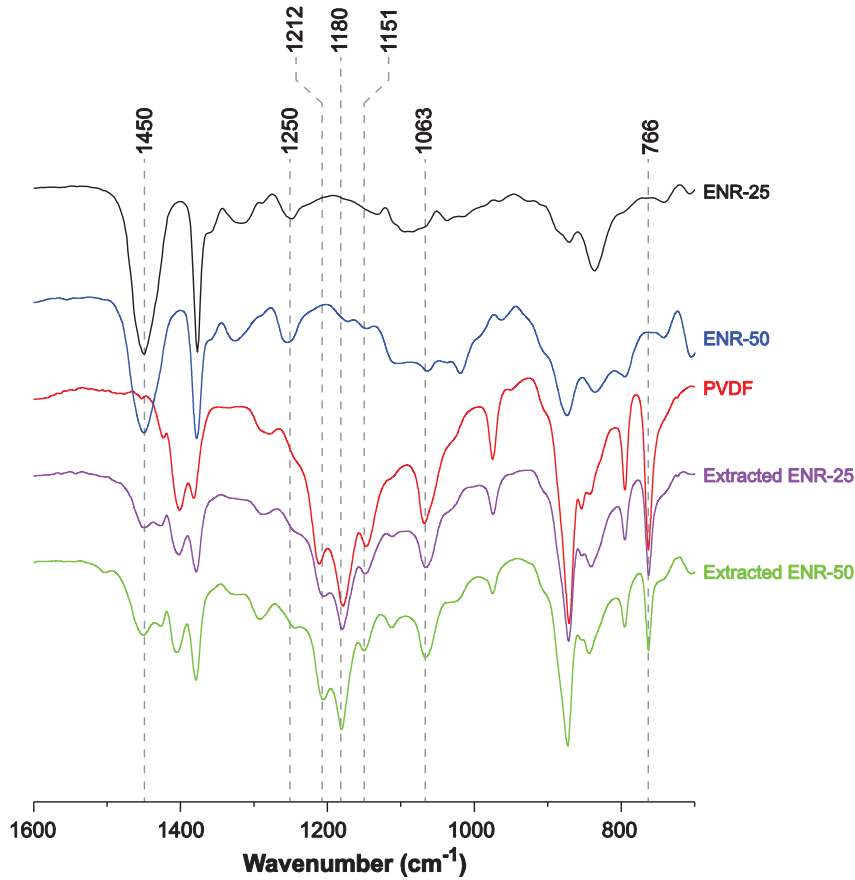


Figure 7.8 Infrared spectra of neat ENR-25, ENR-50, PVDF, extracted ENR-25 and extracted ENR-50

7.2.6 Dielectric analysis

The temperature dependence of permittivity (ϵ') and loss factor (ϵ'') in the frequency range (1 to 10^4 Hz) of PVDF is shown in Figure 7.9. The step in permittivity (ϵ') and the peak of loss factor (ϵ'') reveal relaxation in the materials. At low temperature ranges, there is slight dependence of permittivity on frequency and low permittivity value. A sharp increase in the permittivity is noticed at a temperature close to the glass transition temperature. At this temperature, the dipoles begin to have enough mobility to contribute the permittivity value, indicating a relaxation process. It is noted that segmental mobility of the polymer molecules increased with temperature, leading to the increase in permittivity [52, 53]. Dielectric spectra of PVDF shows two relaxations: in the domain (-45°C to -23°C), β or α_a -relaxation is associated to segmental motion in amorphous regions. While, in the domain (32°C to 144°C), α -relaxation is associated to segmental

motion in crystalline phase [53] which were also found earlier in dynamic mechanical analysis (DMA) in section 7.2.4.

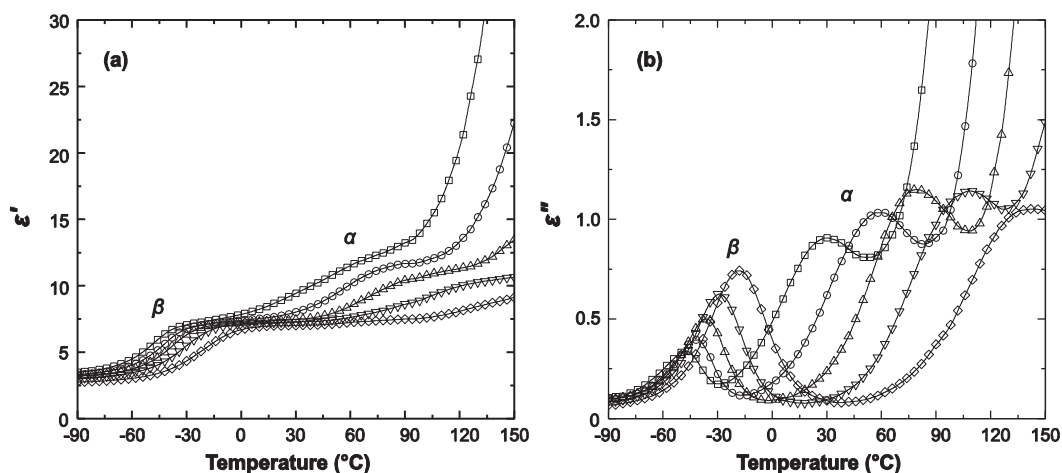


Figure 7.9 Temperature dependence of (a) ϵ' and (b) ϵ'' of PVDF at several frequencies (\square) 1, (\circ) 10, (\triangle) 100, (∇) 1k and (\diamond) 10k Hz

The permittivity and loss factor as a function of temperature for PVDF/ENR-25 and PVDF/ENR-50 blends are shown in Figure 7.10 and Figure 7.11, respectively. It can be seen that PVDF/ENR-25 showed one relaxation peak while PVDF/ENR-50 showed two relaxations peaks. The single relaxation peak in PVDF/ENR-25 is due to overlapping of β -relaxation of PVDF and α -relaxation of ENR-25 as mentioned earlier in DMA result. For PVDF/ENR-50, β -relaxation of PVDF appeared as a shoulder of ENR-50 relaxation. This indicates a phase separation of PVDF and ENR-50 phase. The α -relaxation was not observed among the blends due to overlapping with the conductivity contribution with increasing ϵ'' value that overlay α -process of PVDF.

The temperature dependence of the relaxation time (obtained from ϵ'' relaxation maximum) for segmental motion in amorphous phase or glass-rubber transition (α -relaxation for ENRs and β -relaxation for PVDF) and crystalline regions (α -relaxation) were examined and the results are plotted in Figure 7.12. It can be seen that β -relaxation of PVDF and α -relaxation of ENR have been described by VFT equation whereas conductivity current process has been described by Arrhenius equation. The fitting parameters are listed in Table 7.5. Furthermore, ENR-25 and ENR-50 relaxation moved to lower temperature with addition of PVDF, which can be assumed as compatibilized blend.

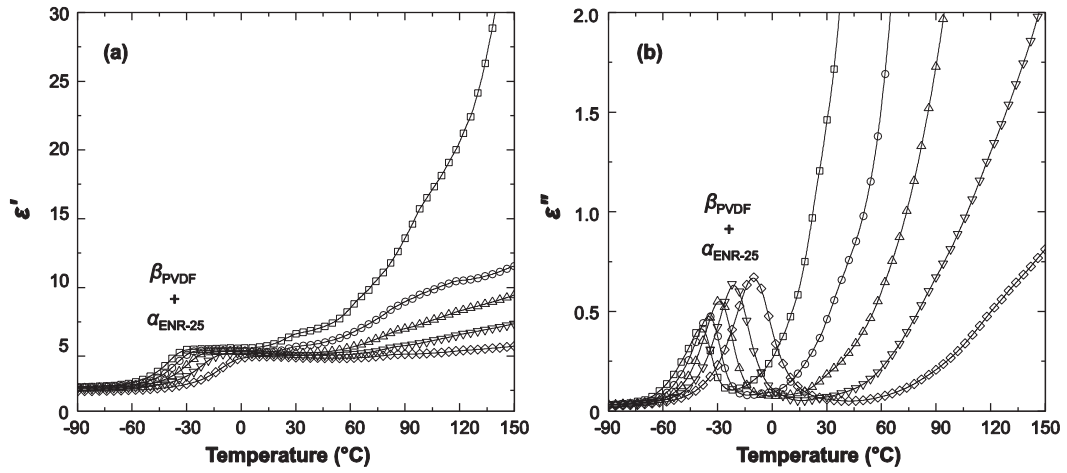


Figure 7.10 Temperature dependence of (a) ϵ' and (b) ϵ'' of PVDF/ENR-25 blend at several frequencies (\square) 1, (\circ) 10, (\triangle) 100, (∇) 1k and (\diamond) 10k Hz

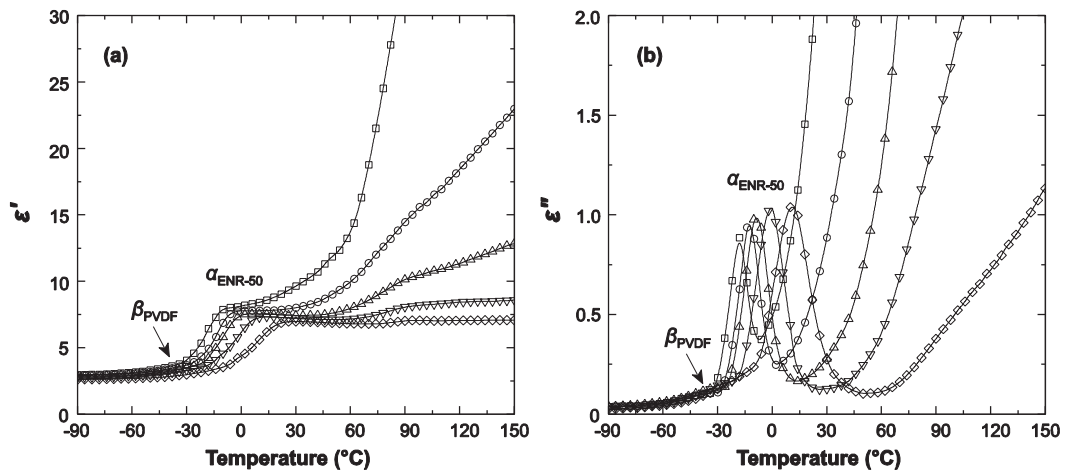


Figure 7.11 Temperature dependence of (a) ϵ' and (b) ϵ'' of PVDF/ENR-50 blend at several frequencies (\square) 1, (\circ) 10, (\triangle) 100, (∇) 1k and (\diamond) 10k Hz

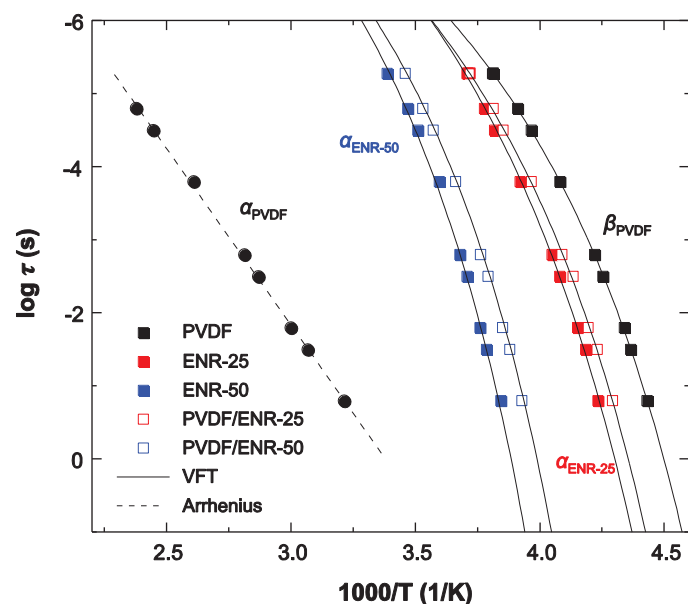


Figure 7.12 Activation plot for segmental motion (square symbols) of PVDF, ENR-25 and ENR-50 and α -relaxation (circle symbols) of PVDF

Table 7.5 Fitting parameters for PVDF, ENR-25, ENR-50 and their blends

Sample	Segmental motion			α -relaxation	
	$\log \tau_0$	B (K)	T_0 (K)	$\log \tau_0$	E_a (eV)
PVDF	-10.85	1067	180	-16.32	0.97
ENR-25	-11.95	1329	185		
ENR-50	-12.04	1328	210		
PVDF/ENR-25	-11.26	1168	185		
PVDF/ENR-50	-11.64	1237	205		

The sharp increase of permittivity and loss factor is observed at high temperature and low frequency. This is rather due to conductivity process which is contribution of ionic conductivity. This indicates the existence of space charge polarization and free charge motion within the blends. The electric modulus formalism (Equation 3.18) was employed to overcome the high temperature relaxation. The imaginary part of electric modulus (M'') of PVDF, PVDF/ENR-25 and PVDF/ENR-50 blends as a function of temperature at different frequencies are shown in Figure 7.13. It can be seen that PVDF shows three relaxations corresponding to β and α relaxation and conductivity, respectively, while ENR-25 and ENR-50 showed only two relaxations at low temperature

and high temperature. The relaxation at low temperature corresponds to segmental motion or α -relaxation, which is associated to glass-rubber transition. Another relaxation at high temperature corresponds to the contribution of the conductivity, so-called conductivity current relaxation [20]. Other phenomena might occur in the same temperature and frequency ranges, those are charge accumulation and interfacial polarization at boundaries between the two phases of polymer blends which is called as Maxwell-Wagner-Sillars (MWS) effect.

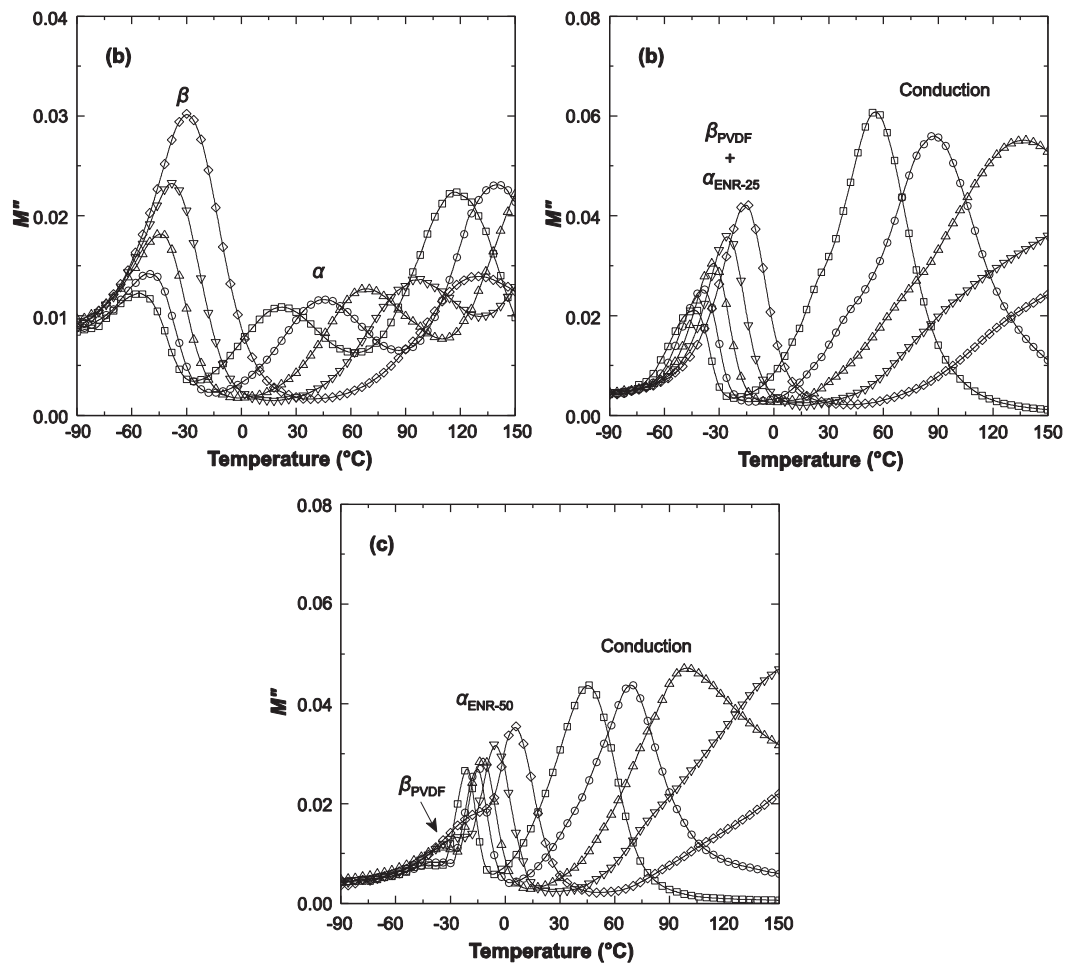


Figure 7.13 Temperature dependence of M'' of (a) PVDF (b) PVDF/ENR-25 and (c) PVDF/ENR-50 at several frequencies (\square) 1, (\circ) 10, (\triangle) 100, (∇) 1k and (\diamond) 10k Hz

Figure 7.14 presents the relaxation time of the conductivity process as a function of temperature for the PVDF blend with difference types of ENRs. The relaxation times of all samples are well fitted by the Arrhenius equation. The activation energy is provided in Table 7.6, which can also give information of the charge transport mechanism within the materials. The PVDF/ENR-50 blends have higher activation energy than that of PVDF/ENR-25. This might be attributed to the fine co-continuous structure of PVDF/ENR-50 as can be seen from Figure 7.1, which is more difficult for charge transport in the blend.

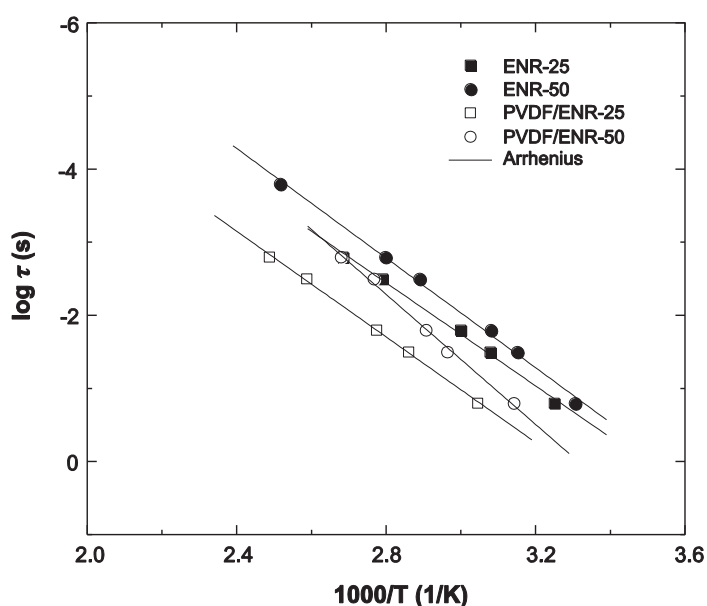


Figure 7.14 Activation plot for conductivity process for ENR-25, ENR-50 and their blends

Table 7.6 Fitting parameters of conductivity process for PVDF, ENR-25, ENR-50 and their blends

Sample	Conductivity	
	$\log \tau_0$	E_a (eV)
ENR-25	-12.30	0.71
ENR-50	-13.28	0.75
PVDF/ENR-25	-11.81	0.72
PVDF/ENR-50	-14.83	0.89

7.3 The effect of blend composition on the properties of PVDF/ENR-50 simple blend

PVDF/ENR-50 simple blend with different blend ratios were prepared, according to the experimental procedure as described in section 3.2.4. Their properties: morphological properties, mechanical properties, thermal behavior, dynamic mechanical analysis and dielectric analysis) were investigated and compared.

7.3.1 Morphological properties

Figure 7.15 shows SEM micrographs of PVDF/ENR-50 blends with various blend proportions. It is clearly seen that two apparent phase morphologies are distinguishable due to phase separation. In the blends with lower content of ENR-50 than 30 wt% (i.e., in Figure 7.15(a) and (b)), it can be seen that the minor ENR-50 component (i.e., cavitations) was dispersed in the major phase of PVDF. Also, the size of ENR-50 domains increased but PVDF phase decreased with increasing ENR-50 content until the fine co-continuous phase structures where dual dispersion phases is observed in the blends with PVDF/ENR-50 = 60/40, 50/50, and 40/60 (i.e., Figure 7.15(c), (d) and (e)), respectively. In Figure 7.15, it is clear that the first phase inversion occurred between the blend ratios of PVDF/ENR-50 = 70/30 and 60/40 where the dispersed ENR-50 in PVDF matrix was transformed to co-continuous phase structure. It is noted that the phase inversion occurs in a domain manner rather than at a single point [54]. It is also noted that increasing ENR content higher than 60 wt% causes the second phase inversion between the blend ratios of PVDF/ENR-50 = 40/60 and 30/70 where the co-continuous phase structure is modified leading to dispersion of PVDF in the ENR-50 matrix. This is due to the influence of different viscosity ratios and hence shearing forces of the blend components. Therefore, in the blends with ENR-50 content higher than 60 wt% (i.e., in Figure 7.15(f) and (g)), the PVDF phase remains as dispersed domains in the ENR matrix. Hence, phase separation between PVDF and ENR-50 was observed due to partly immiscible blends with the fully co-continuous phase structures. The phase inversion took place in the blend with ENR-50 beyond the weight content of 40 to 60%. Willemse *et al.* [55] reported that the composition range for full co-continuity not only depends on viscosity ratio but also depends on the interfacial tension. The increase of the interfacial tension

shifts the limiting composition for onset of co-continuity to higher concentrations, narrowing the composition range due to stability of the co-continuous morphology and the phase dimensions.

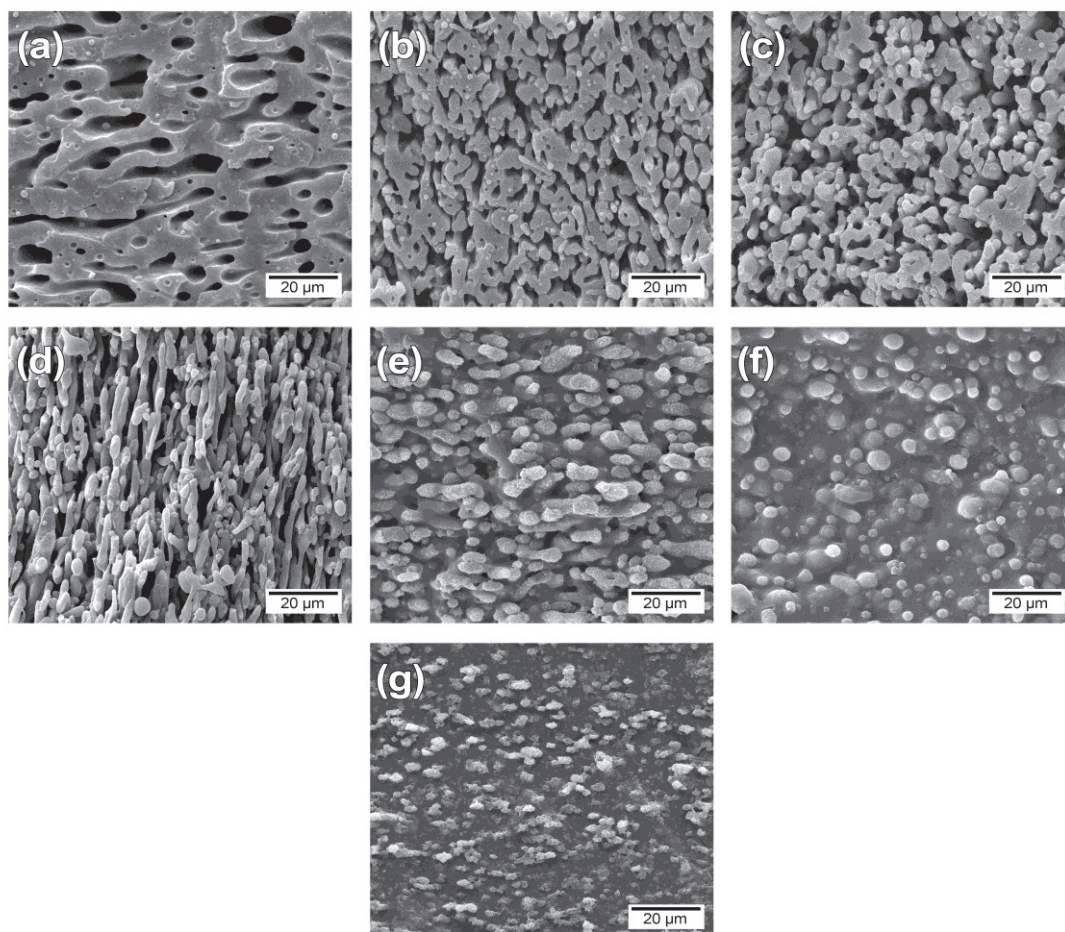


Figure 7.15 SEM micrographs of PVDF/ENR-50 simple blends with different blend ratios (a) 80/20, (b) 70/30, (c) 60/40, (d) 50/50, (e) 40/60, (f) 30/70 and (g) 20/80

7.3.2 Mechanical properties

Tensile measurements and hardness test were carried out to determine the mechanical properties of the PVDF/ENR-50 blends. The stress-strain curve of the PVDF/ENR-50 blends with various blend ratios are shown in Figure 7.16. The tensile strength and elongation at break were calculated from the stress-strain curves, tension set and hardness are shown in Table 7.7. It can be seen that necking was not observed in all blends. However, it was exhibited distinct regions such as yielding and plastic

deformation for the neat PVDF. Moreover, a significant difference of deformation characteristics was observed: The PVDF/ENR-50 (80/20) blend first showed very high tensile strength and quickly failed after slight stretching of 64%, indicating a brittle fracture behavior caused by PVDF matrix phase in the blend. Further increasing ENR-50 content, the blends break at elongation higher than 100% and represent like a typical elastomer deformation. This indicates that deformation ability of blend significantly changes from brittle plastic to elastomer characteristic with a larger strain. The phase morphology evolution of varying blend proportions can be used to describe tensile characteristics. Generally, the deformation characteristic is dominated by the matrix phase. The small addition of ENR-50 into PVDF showed high initial moduli, stiffness and strength but less capability for stretching due to the PVDF continuous matrix in the blend. Increasing ENR-50 concentration, the tensile strength decreased, while elongation at break increased, as shown in Figure 7.17. When ENR-50 become matrix phase, the blend showed superior elongation at break and flexibility but poor tensile strength. Hardness and tension set as a function of ENR-50 contents are shown in Figure 7.17. It can be seen that hardness and tension set decreased with increasing ENR-50 contents. This decreasing is attributed to incorporation of ENR-50 which increases chain mobility in the blend that less resists to deformation by indenter (low hardness). Furthermore, the tension set of the blends decreased with the addition of ENR-50, making high recovery of the blends after extension or better elasticity (low tension set). Although, the blends with ENR-50 matrix have superior extension and very low tension set which is expected for elastomeric material but they also exhibit very low tensile strength. Thus, 50/50 PVDF/ENR-50 blend presents an excellence balance of mechanical properties for thermoplastic elastomer characteristic (high tensile strength, moderate elongation at break and low tension set) due to co-continuous PVDF providing strength and co-continuous ENR-50 providing flexibility. From Figure 7.17, it can be seen that the most of mechanical properties abruptly decrease after adding ENR-50 in the range of 40 to 60 wt%, which can be considered as phase co-continuous region.

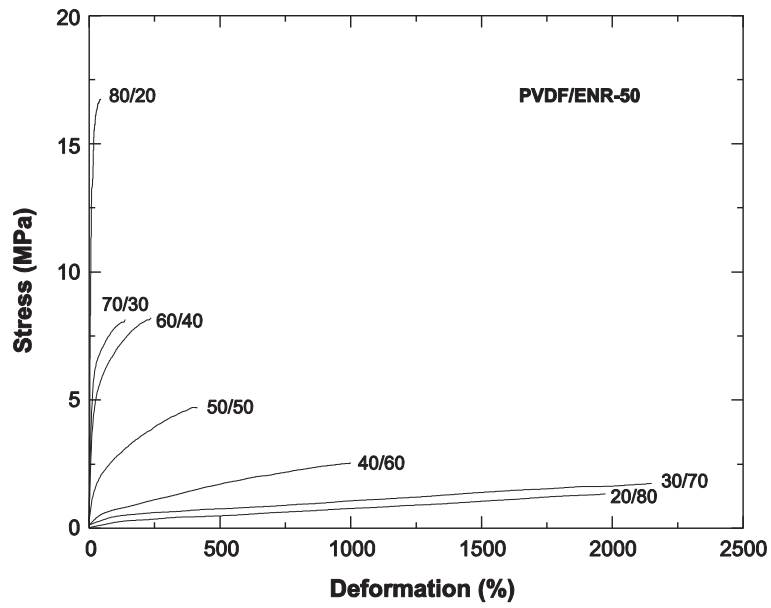


Figure 7.16 Stress-strain curves of PVDF/ENR-50 blend with different blend ratios

Table 7.7 Mechanical properties of PVDF/ENR-50 blends with different blend proportions

PVDF/ENR-50	Young's modulus (MPa)	Tensile strength (MPa)	Elongation at break (%)	Tension set (%)	Hardness (Shore A)
80/20	190.0 (±15.5)	17.2 (±1.64)	41 (±23)	-	94.0 (±1.1)
70/30	72.8 (±12.6)	8.2 (±1.80)	130 (±32)	-	93.0 (±1.1)
60/40	48.9 (±5.4)	8.2 (±0.77)	230 (±28)	63.5 (±1.5)	85.5 (±1.0)
50/50	19.0 (±2.6)	4.8 (±0.69)	440 (±58)	45.0 (±1.5)	58.5 (±1.2)
40/60	4.3 (±0.8)	2.6 (±0.21)	990 (±159)	34.8 (±1.1)	40.0 (±0.9)
30/70	2.9 (±1.0)	1.9 (±0.33)	2400 (±265)	24.9 (±0.9)	27.5 (±0.7)
20/80	2.3 (±0.9)	1.4 (±0.22)	1960 (±163)	25.2 (±2.7)	26.5 (±0.7)

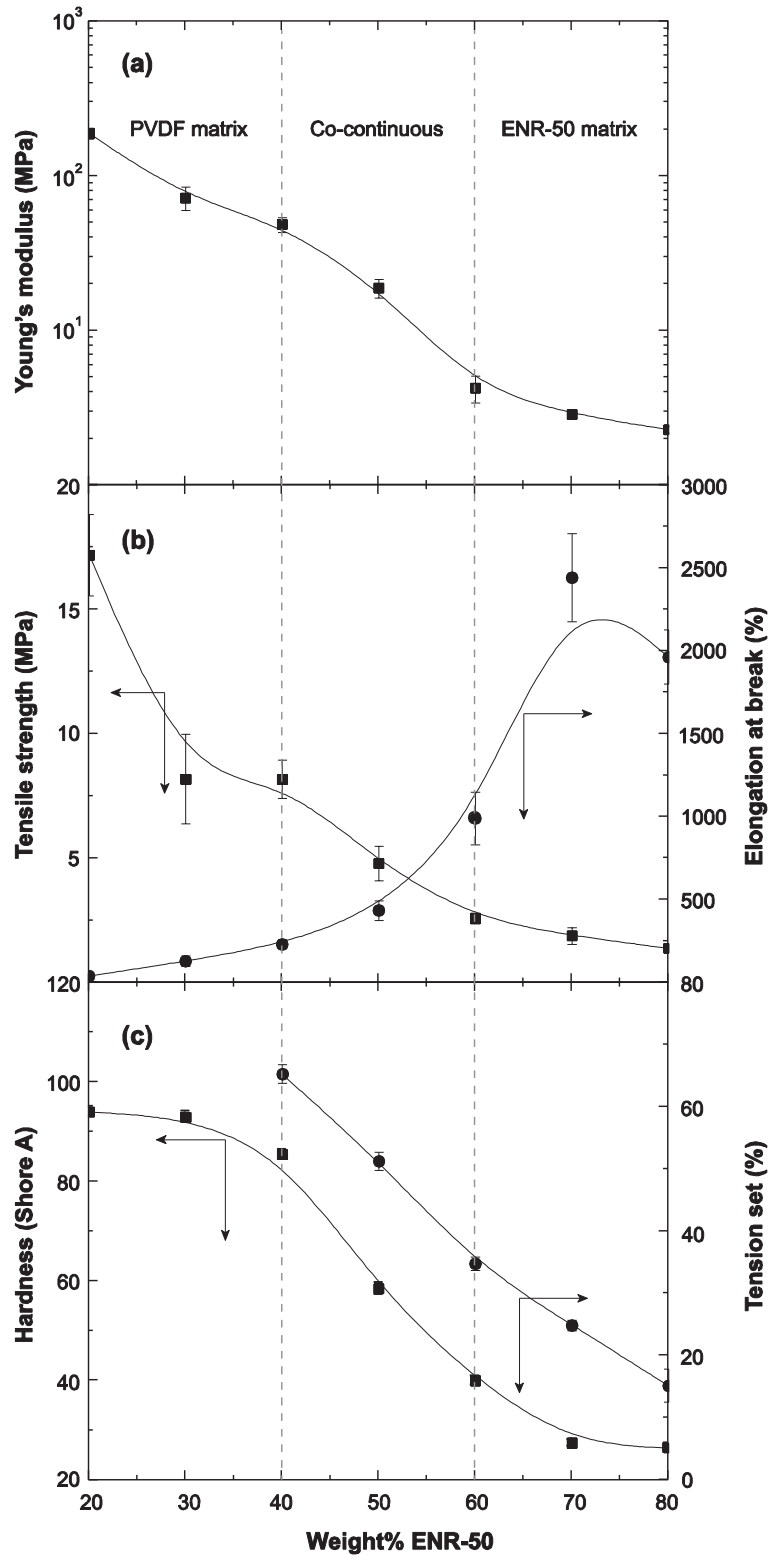


Figure 7.17 Mechanical properties as a function of ENR-50 content in PVDF/ENR-50 simple blends

7.3.3 Differential scanning calorimetry

DSC thermograms during heating and cooling of PVDF/ENR-50 blends with various blend proportions are shown in Figure 7.18. Also, the crystallization temperature (T_c), full width at half maximum (FWHM) of crystallization peak, melting temperature (T_m), melting enthalpy and degree of crystallinity are summarized in Table 7.8. It can be seen that the crystallization temperature (T_c) based on the cooling curves of the blend was shifted to higher temperature in the temperature ranges of 137.2 to 139.3°C compared with T_c of pure PVDF (i.e., $T_c = 135.8^\circ\text{C}$). On the other hand, the crystalline melting temperature (T_m) based on the heating curves of the blend was slightly decreased from 166.4 to 168.3°C compared with T_m of pure PVDF (i.e., $T_m = 168.4^\circ\text{C}$). Higher T_c s of the blends up to 50 wt% of ENR-50 indicates that higher crystallization and degree of crystallization of PVDF in the blends compared with the neat PVDF. In the DSC cooling curves, the crystallization peaks of the blends in the ENR-50 content of 20 to 30 wt% where the PVDF is the matrix to gather with blends with ENR-50 content of 40 to 50 wt% with the co-continuous structure, it is clear that the T_c s are shifted to higher temperature with similar values, as confirmed in Figure 7.19. However, the T_c s are shifted to lower temperature as further increasing the ENR-50 content in the blend higher than 50 wt%. This is attributed to large ENR-50 inclusion (ENR-50 is the matrix phase) which causes decreasing crystallization rate which is related to morphology of the blends (Figure 7.15 (e-g)) [39]. The Full width at half maximum of crystallization peak or FWHM of crystallization peak indicates the time distributions for the nucleation and growth of PVDF crystal. It can be seen that FWHM value decreased from 5.7 to 4.5°C by addition of 40 wt% ENR-50. This suggested for a narrower time for crystallization of PVDF crystal in the blends. Therefore, addition of ENR-50 up to 40 wt%, ENR-50 displayed as the nucleating agent for PVDF crystallization that causes increasing degree of crystallinity upon incorporation of ENR-50, as shown in Table 7.8. However, increasing content of ENR-50 to 50 wt%, transition from the co-continuous phase to dispersion of PVDF in the matrix is observed in Figure 7.15(e). Therefore, time for the nucleation and growth of PVDF crystalline is longer (FWHM = 5.24°C) and lower X_c is observed compared with the blend with fully co-continuous structure at the ENR content 30 and 40 wt%. Furthermore, the blend with ENR-50 content higher than 50 wt% (ENR is the matrix), ENR-50 retard the

growth of PVDF crystal. This caused the increase FWHM value and decrease degree of crystallinity [39, 56].

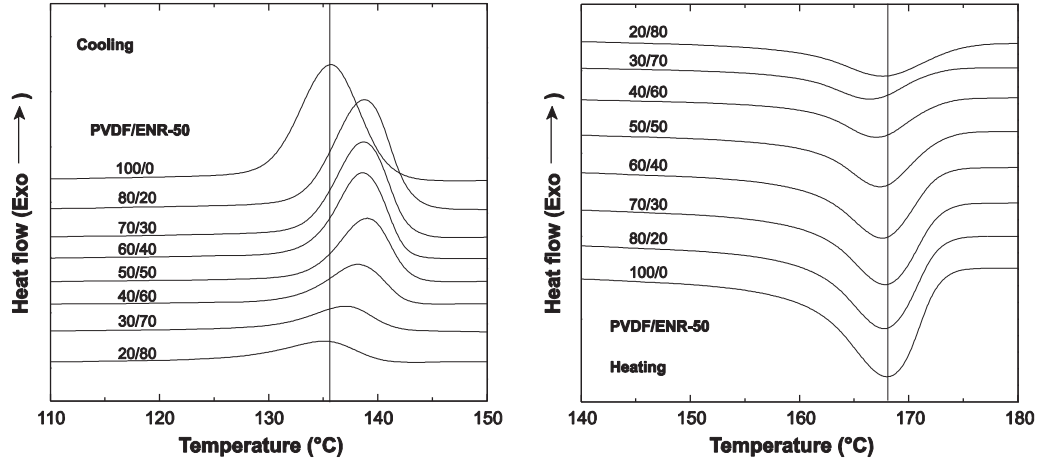


Figure 7.18 DSC (a) cooling and (b) heating sweeps for PVDF/ENR-50 blends

Table 7.8 Thermal characteristic of PVDF/ENR-50 blends with different compositions

PVDF/ENR-50	T_c (°C)	FWHM (°C)	T_m (°C)	ΔH_m (J/g)	X_c (%)
100/0	135.8	5.72	168.4	52.55	50.3
80/20	139.1	5.06	168.3	44.81	53.6
70/30	139.0	4.71	168.0	39.51	54.0
60/40	138.9	4.24	167.8	33.97	54.2
50/50	139.3	4.55	167.0	27.22	52.1
40/60	138.5	5.24	167.0	19.70	47.1
30/70	137.2	6.29	166.4	16.16	51.6
20/80	135.3	7.48	167.8	9.13	43.7

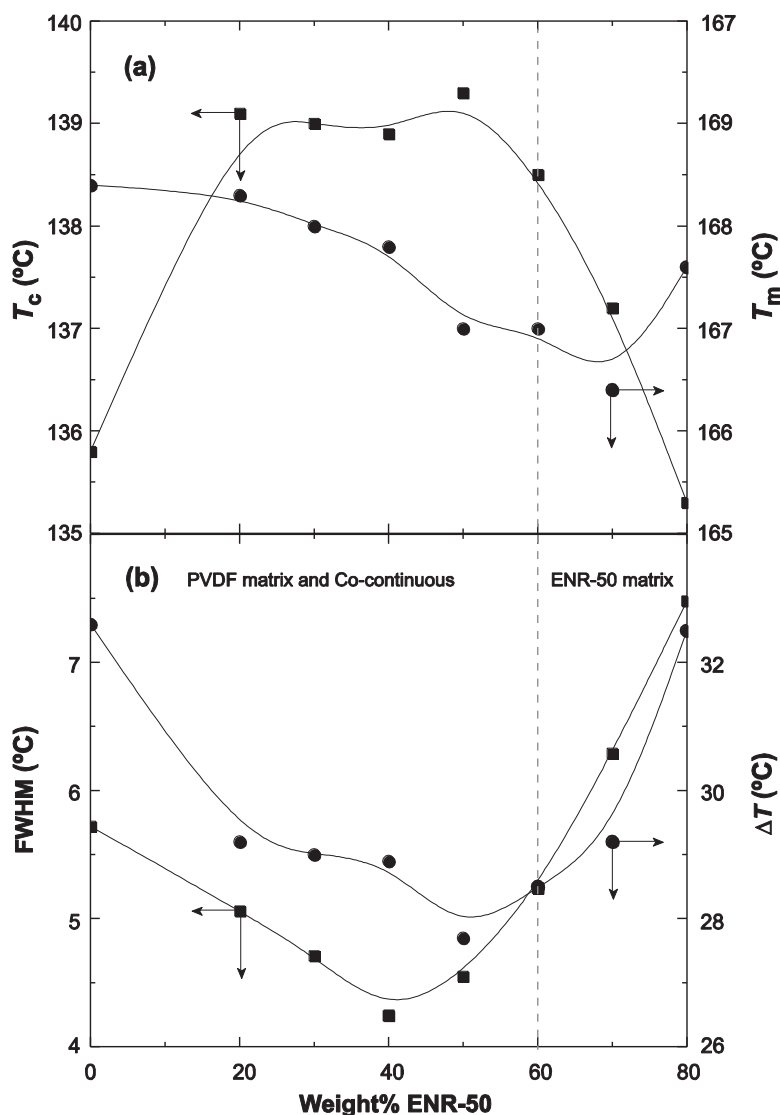


Figure 7.19 Thermal characteristics from DSC curves as a function of ENR-50 content

7.3.4 Dynamic mechanical analysis

Figure 7.20 shows the temperature dependence of storage modulus (E') and $\tan \delta$ of PVDF/ENR-50 blends with different blend compositions at a frequency 1 Hz. The dynamic mechanical properties of PVDF/ENR-50 blends with different blend ratios are summarized in Table 7.9. It is seen that in the transition zone, the E' showed a drastic drop with increasing ENR-50 content. Also, a sharp drop of E' was observed in the blends with higher content of ENR-50. This is due to the fact that increasing proportion of ENR-50 phase in the blends improves rubbery-like behavior. Consequently, decreasing trend of the E' in the rubbery region was observed.

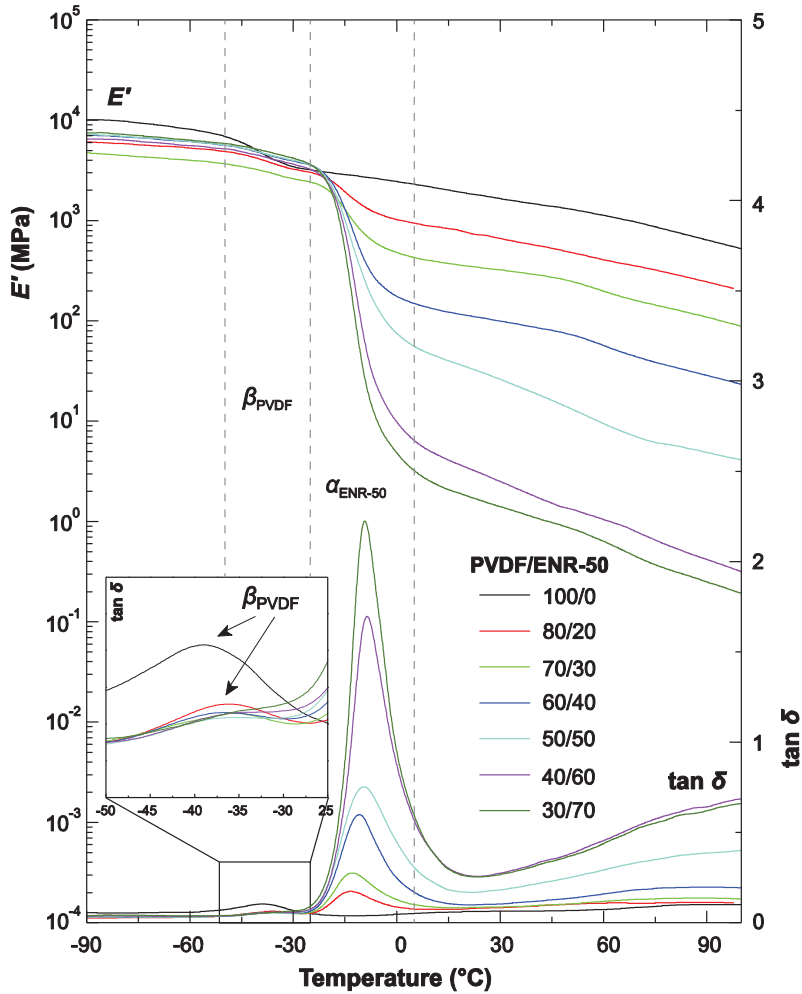


Figure 7.20 Temperature dependence of E' and $\tan \delta$ for PVDF/ENR-50 blend with different blend ratios

In the $\tan \delta$ plot, it is clear that the blends showed two transition regions and two relaxation peaks ($\tan \delta$) in the range of approximately -36.0 and -9.0°C , respectively. This again indicates phase separation in PVDF/ENR-50 blends. It is also noted that the $\tan \delta$ relaxation at the lower and higher temperature correspond to β and α relaxation of PVDF and ENR-50, respectively. They are associated to the glass transition temperature (T_g) of PVDF and ENR-50 phases, respectively. It is also seen that the β relaxation intensity of PVDF decreased while the α -relaxation of ENR-50 phase increased with increasing content of ENR-50. This is due to the dilution effect. Furthermore, it is clear that the β relaxation eventually disappeared in the blend with ENR-50 content of 70 wt%. The maximum peak of $\tan \delta$ is commonly used to indicate glass transition temperature,

as summarized in Figure 7.21. It can be seen that the T_g of PVDF and ENR-50 depended on blend composition. That is, the T_g of PVDF and ENR-50 in the blends was shifted to higher temperature with increasing ENR-50 content. Shifting of the glass transition temperature indicated partial miscibility between the two phases [14-16, 45, 56]. This can be explained by increasing chain entanglement in amorphous phase of each component as a result of strong intermolecular interaction. It is also noted that the ENR-50 might also acts as a nucleating agent to enhance the crystallization of PVDF in the blend, as described earlier. This leads to restriction of the molecular movement of the PVDF chains with the consequence to the increase in T_g of PVDF phase with increasing content of ENR-50 in the blends. The same phenomenon was observed in the PP/POE blends [56].

Table 7.9 Storage modulus (E') and loss tangent ($\tan \delta$) of PVDF/ENR-50 blends with various blend compositions

PVDF/ENR-50	Storage Modulus, E' (MPa)		Loss tangent ($\tan \delta$)			
	at -60°C	at 25°C	$\tan \delta_{\max}$		T_g (°C)	
			PVDF	ENR	PVDF	ENR
100/0	8100	1765	0.10	-	-39.8	-
80/20	5300	713.3	0.06	0.16	-35.6	-13.9
70/30	4000	336.8	0.06	0.28	-35.6	-13.7
60/40	6100	106.6	0.06	0.61	-36.1	-11.7
50/50	6200	30.4	0.05	0.77	-35.8	-9.7
40/60	5600	3.0	0.06	1.73	-33.5	-8.8
30/70	6340	1.7	0.06	2.33	-	-9.9
0/100	3800	1.9	-	2.70	-	-5.7

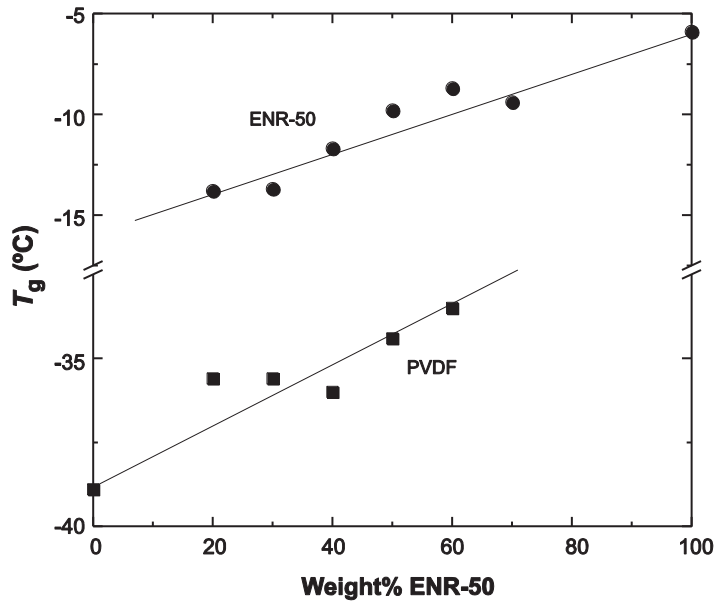


Figure 7.21 Glass transition temperature (T_g) of PVDF and ENR-50 phases as a function of ENR-50 content in PVDF/ENR-50 blend

Figure 7.22 shows the storage modulus, $\tan \delta$ at 25°C and $\tan \delta$ at -10°C as a function of ENR-50 content in PVDF/ENR-50 blends which are correlated to the blend morphology. It can be seen that these properties could be distinguished into three regions. In the first region is in the ranges of ENR-50 = 0 to 40 wt% where ENR-50 is dispersed in the PVDF matrix (as SEM micrographs indicated in Figure 7.15(a) and (b)). In this region, it is seen that the storage modulus was slightly decreased while the $\tan \delta$ was slightly increased until the phase inversion took place at the blend proportion prior to 40wt% of ENR-50. This is due to the fact that PVDF is the continuous or matrix phase and the properties of the blend are controlled by the matrix phase. Therefore, high E' but low $\tan \delta$ is observed in the blend with PVDF matrix. In the second region, when the content of ENR-50 in the blend is higher than 40 wt%, the co-continuous structure is observed until the ENR content of 60 wt%. This correlates to abrupt decreasing trend of the storage modulus but increasing trend of $\tan \delta$. The second phase inversion occurred when the addition of ENR-50 greater than 60 wt%. This forms the third region of the curves in the ranges of ENR-50 contents of 60 to 80 wt% where dispersion of PVDF in the ENR-50 matrix was observed. This causes slight plateau storage modulus with low magnitude due to the weak ENR-50 matrix. Slight plateau curves with high values of $\tan \delta$ is also observed due to the properties which are dominated by the ENR-50 matrix. This

result is in agreement with morphological (Figure 7.15), and mechanical properties (Figure 7.17) as well as crystallization and melting behavior (Figure 7.19).

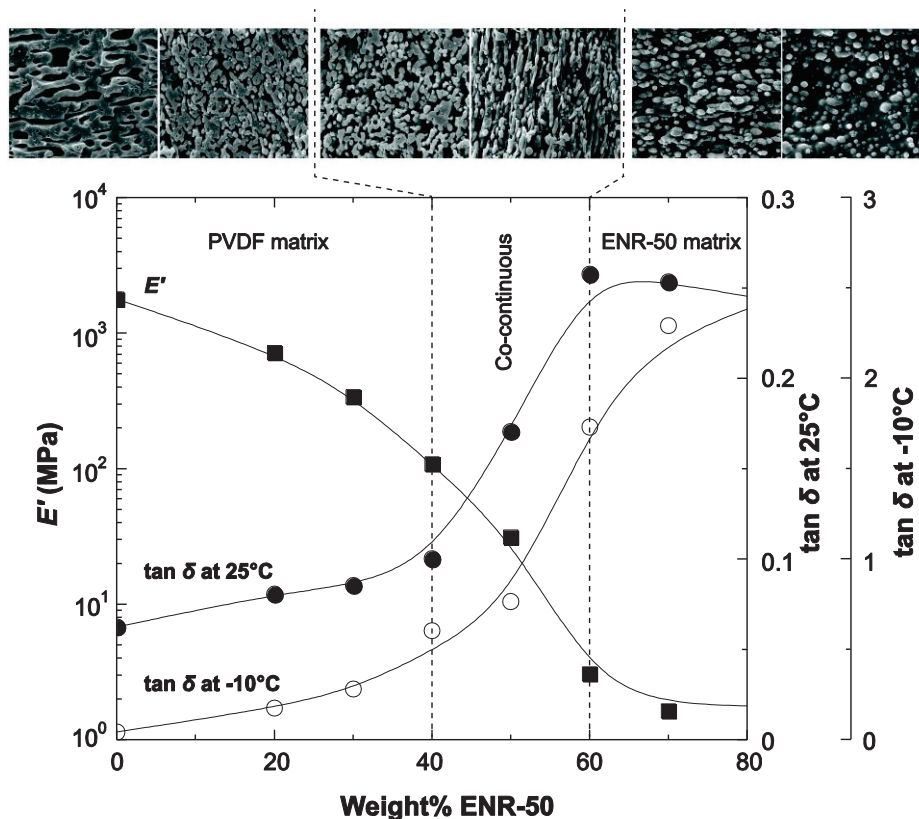


Figure 7.22 Storage modulus and $\tan \delta$ as a function of ENR-50 content in PVDF/ENR-50 blends

7.3.5 Dielectric analysis

The temperature dependence of permittivity (ϵ') and loss factor (ϵ'') of PVDF/ENR-50 blends with 20 and 70 wt% ENR-50 at several frequencies are shown in Figure 7.23 and 7.24, respectively. It is seen that all the blends showed low and frequency independent permittivity at glassy state. Then, the permittivity increased and strongly depend on frequency at temperature above glass transition temperature. It is also seen that the dielectric spectra of 80/20 PVDF/ENR-50 blend clearly shows two relaxations according to β and α -relaxation in PVDF phase and ENR-50 phase, respectively. This corresponds to phase separation between PVDF and ENR-50 as described in DMA result in Figure 7.20. However, the β -relaxation of PVDF totally disappeared in ENR-50-rich blends due to dilution effect.

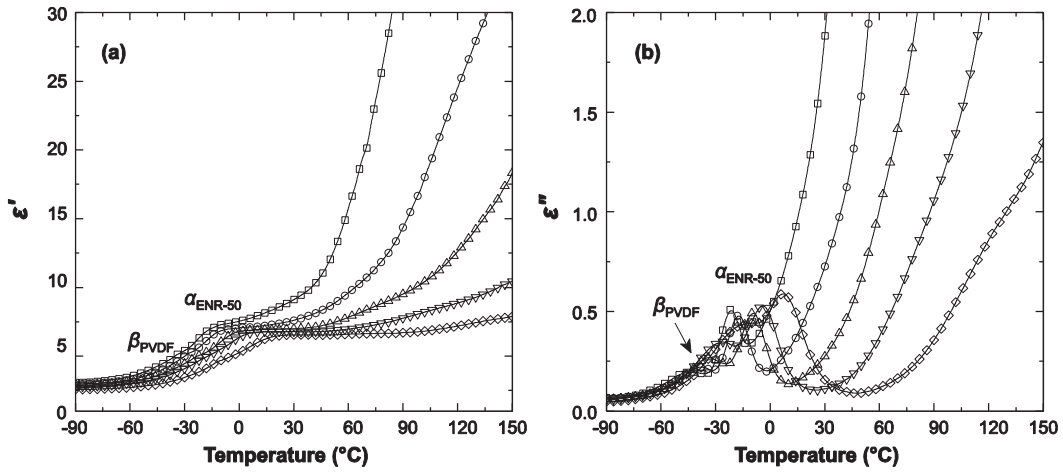


Figure 7.23 Temperature dependence of (a) ϵ' and (b) ϵ'' of 80/20 PVDF/ENR-50 blend at frequency (\square) 1, (\circ) 10, (\triangle) 100, (∇) 1k and (\diamond) 10k Hz

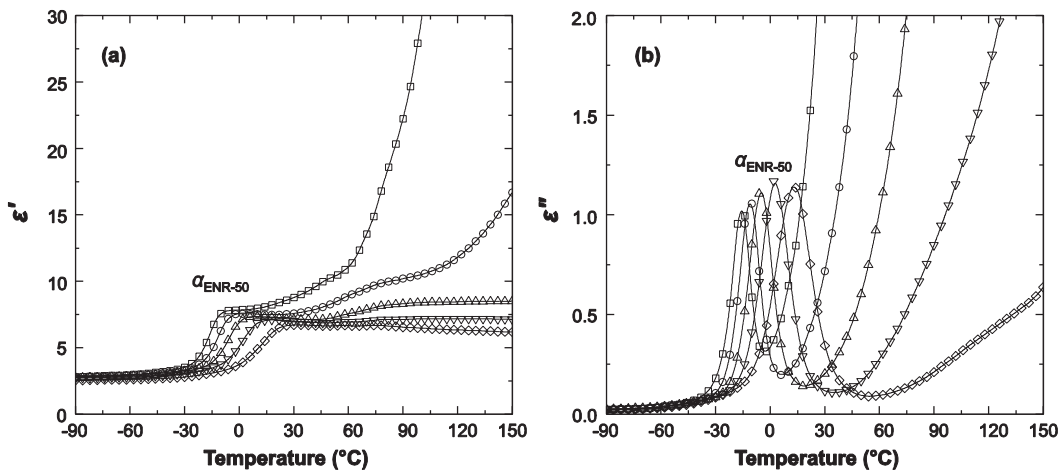


Figure 7.24 Temperature dependence of (a) ϵ' and (b) ϵ'' of 30/70 PVDF/ENR-50 blend at frequency (\square) 1, (\circ) 10, (\triangle) 100, (∇) 1k and (\diamond) 10k Hz

Figure 7.25 shows the temperature dependence of $\tan \delta$ based on DEA and DMA at frequency 1 Hz of PVDF/ENR-50 with different blend proportions. It is seen that the $\tan \delta$ peak of PVDF and ENR-50 phase tends to overlapped approach to each component. This is due to partial miscibility of PVDF/ENR-50 blends. This supported the DMA result that the relaxation curves of blend component shifted to each other (T_g of PVDF and ENR-50 move towards to higher and lower temperature, respectively). It is also seen that the β -relaxation of PVDF could not be clearly observed in the blends with addition of ENR-50 = 50 wt%. It appears as a shoulder of ENR-50 relaxation and totally

disappears when increasing the ENR-50 content up to 70 wt%. Furthermore, the α -relaxation of PVDF also disappeared in DEA due to the conductivity contribution with increasing of ε'' value that leads to masking the α -relaxation process of PVDF.

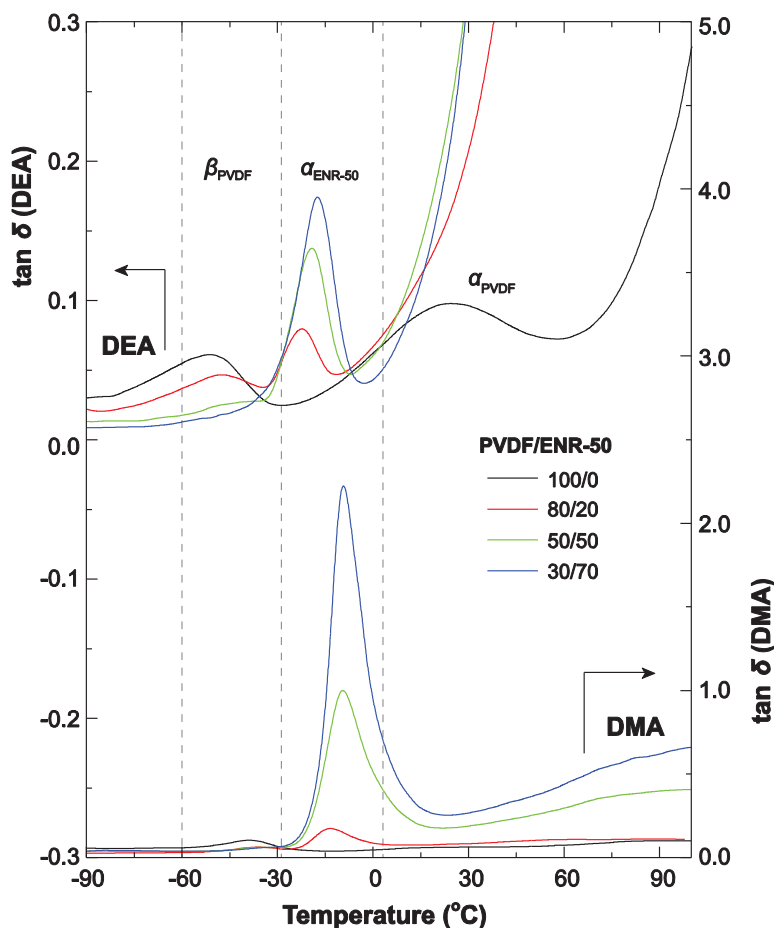


Figure 7.25 Temperature dependence of $\tan \delta$ obtained from DMA and DEA at 1 Hz for the blend with different blend compositions

The sharp increase of permittivity and loss factor observed at high temperature is due to conduction process as mentioned first in this chapter. This indicates the existence of space charge polarization and free charges motion within the blends. This process can be confirmed by using electric modulus formalism. The imaginary part of electric modulus (M'') of 80/20 and 30/70 PVDF/ENR-50 blends as a function of temperature for different frequencies are shown in Figure 7.26. It is seen that both blend compositions showed a new relaxation at high temperature which corresponds to conductivity current relaxation [20], as observed earlier (Figure 7.13). Furthermore, it can

be seen that 80/20 PVDF/ENR-50 blend shows four relaxation peaks corresponding to β -relaxation of PVDF followed by α -relaxation (glass transition) of ENR-50, α -relaxation of PVDF and conductivity current relaxation, respectively. Normally, the α -relaxation of PVDF in 80/20 PVDF/ENR-50 blends could not be observed in loss factor (ϵ'') spectra (Figures 7.23) but the electric modulus formalism (in Figure 7.26) reveals more evidence of the α -relaxation. This is the advantage of electric modulus formalism that is able to reveal the hidden relaxation in loss factor (ϵ'') curve, especially at high temperature and low frequency.

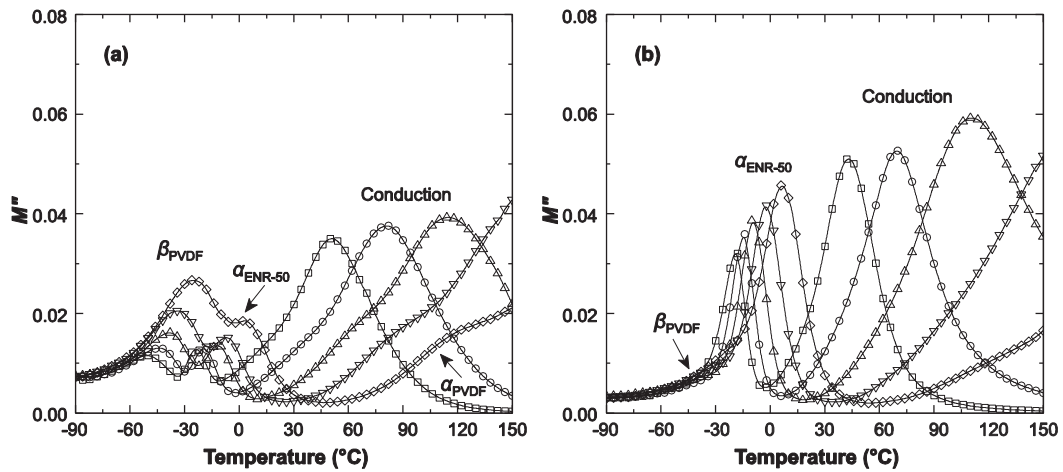


Figure 7.26 Temperature dependence of M'' of (a) 80/20 and (b) 30/70 PVDF/ENR-50 blends at several frequencies (\square) 1, (\circ) 10, (\triangle) 100, (∇) 1k and (\diamond) 10k Hz

As the plot of ϵ'' and M'' as a function of temperature for several frequencies, the relaxation peaks moved to higher temperature with increasing frequency. This can characterize the molecular motion which is observed in the temperature range. Figure 7.27 shows relaxation time (τ) as function of the reciprocal temperature for β -relaxation of PVDF, α -relaxation of ENR-50 phase and conductivity process. It is noted that the symbols in the Figure 7.27 are experimental data and lines are the best fitting of VFT equation. It can be seen that the curves of blends depend on blend composition: PVDF relaxation moved to higher temperature and ENR-50 relaxation moved to lower temperature. The curve of 80/20 PVDF/ENR-50 blend moved to higher temperature and greater than the one of 50/50 and 30/70 PVDF/ENR-50 blends, respectively. This can be assumed that some parts of two components are miscible in the blends. Such effect has been reported in some polymer blends [18, 20, 21]. The fitting parameters of glass-rubber

transition and conductivity obtained from the analysis are summarized in Table 7.10. It is seen that the T_0 of PVDF increased with decreasing PVDF content whereas T_0 of ENR-50 decreased with decreasing ENR-50 content in accordance with the shift of glass transition temperature which was observed in the DMA measurement. Conductivity current process of the blend has been described by Arrhenius equation. The activation energy of the blends was around 0.70–0.90 eV for the 80/20 and 50/50 PVDF/ENR-50 blends that is higher than that of the 30/70 PVDF/ENR-50 blend. This result can provide information of the charge transport mechanism within the materials [20]. The morphology changes in the blends is related to conductivity process in the blends. PVDF is under the form of continuous phase in 80/20 and 50/50 PVDF/ENR-50 blends while phase inversion occurs after ENR-50 content is higher than 60 wt% (Figures 7.15). It is interesting to note that conductivity or charge transport is easier when ENR-50 becomes the matrix phase.

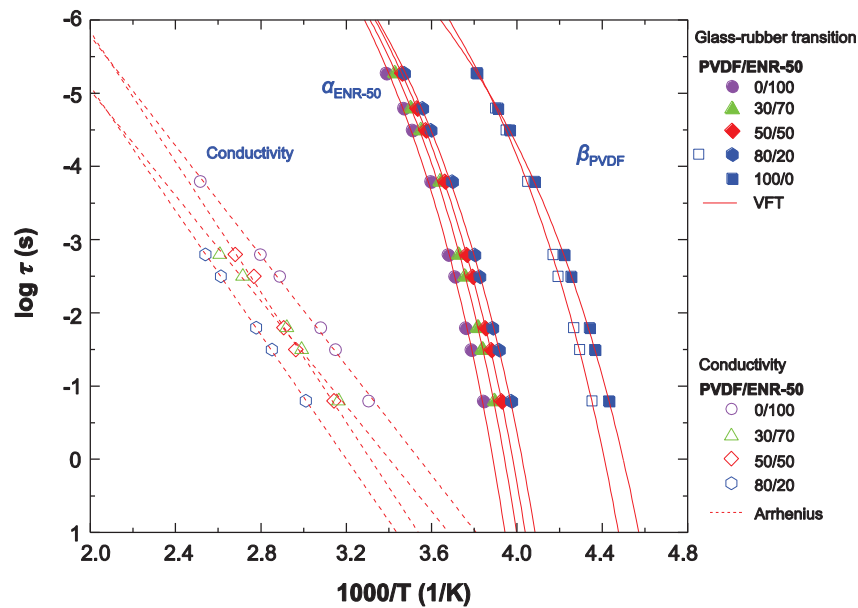


Figure 7.27 Relaxation time of glass rubber transitions and conductivity process as a function of reciprocal temperature for PVDF/ENR-50 blends with various blend ratios

Table 7.10 Fitting parameter for glass-rubber transition and conductivity peaks of PVDF/ENR-50 blends with various blend ratios

PVDF/ENR-50	Glass-rubber transition			Conductivity	
	$\log \tau_0$	B (K)	T_0 (K)	$\log \tau_0$	E_a (eV)
100/0	-10.85	1067	180		
80/20	-11.34	1224	203	-13.57	0.85
50/50	-11.47	1237	205	-14.73	0.89
30/70	-11.64	1229	208	-12.23	0.72
0/100	-12.04	1328	210	-13.28	0.75

7.4 Conclusions

The PVDF/ENR blends with different epoxidation levels of ENR and various blend proportions were prepared by simple blend technique. PVDF/ENRs blends are generally immiscible blends, however, the increase of epoxide group content in ENR showed significant role to enhance interfacial adhesion which leads to formation of small domains. The addition of ENR in PVDF decreases tensile strength but increases elongation at break, which is a usual characteristic of blended thermoplastic elastomer. The blend of PVDF/ENR-50 exhibited superior mechanical properties: high tensile strength, storage modulus and elongation at break due to good interfacial adhesion between the two phases. Thermal properties characterized by DSC revealed that ENR can accelerate crystallization and act as a nucleating agent in PVDF. The molecular dynamic of the blends has been characterized by DMA and DEA. Both technique revealed molecular relaxation of blend components. It was found that PVDF/ENR-25 showed a single relaxation due to some degree of overlapping of PVDF and ENR-25 relaxations, while PVDF/ENR-50 showed two relaxation peaks corresponding to glass transition temperatures of PVDF and ENR-50. The miscibility of PVDF/ENR-50 had been revealed by DMA and DEA measurement from shifting of the relaxations of blend components. The DEA plots showed a sharp increase in loss factor at high temperature and low frequency, which corresponded to contribution of conductivity.

The PVDF/ENR-50 blends with various blend ratios were prepared and their properties were investigated. The effect of blend compositions revealed phase

development of PVDF/ENR-50 blends. The blends consisting of ENR-50 dispersed in PVDF at low content of ENR-50 (<40 wt%) and fully co-continuous morphology can be observed when ENR-50 was added in the range of 40 to 50 wt%. The further increase of ENR-50 contents led to phase inversion to take place where ENR-50 became the matrix and PVDF became the dispersed phase. It was also found that increasing content of ENR-50 in the blends caused decreasing trends of the tensile strength, modulus (i.e., Young's modulus and storage modulus), tension set but showed increasing trends of elongation at break. The phase inversion of PVDF/ENR-50 blend had been confirmed by DMA measurement that storage modulus and $\tan \delta$ show a radically change at the formation of co-continuous structure in the blends. Furthermore, the addition of ENR-50 accelerated PVDF crystallization and ENR-50 acted as a nucleating agent in the blend. The molecular mobility of the blends was also investigated by dynamic mechanical analysis and dielectric analysis. The blends showed similar relaxation in the dynamic mechanical analysis and dielectric analysis. That is, all types of blend compositions showed two relaxations according to α -relaxation annotated to T_g of PVDF and ENR-50 due to phase separation. However, maxima positions of relaxations of PVDF and ENR-50 moved toward to higher and lower temperature, respectively. This generally occurred in the blends with partial compatibility. This is attributed to interaction and chain entanglement between PVDF and ENR-50 molecules. The temperature dependence of electric modulus revealed a new relaxation at high temperature which corresponded to conductivity process. The morphology of the blend seemed to influence the charge transfer in the blends. $\log \tau_0$ and E_a parameters calculated for 30/70 PVDF/ENR-50 blend seemed to indicate conductivity improvement when ENR is the matrix. This is in agreement with the flexibility of ENR compared to the one of PVDF.

7.5 References

- [1] Utracki, L.A. 2002. *Introduction to polymer blends*, in *Polymer Blends Handbook*, L.A. Utracki, ed. Springer, Dordrecht.
- [2] Nwabunma, D. 2007. *Overview of polyolefin blends*, in *Polyolefin Blends*, D. Nwabunma and T. Kyu, eds. John Wiley & Sons, New Jersey.
- [3] Jha, A., Dutta, B. and Bhowmick, A.K. 1999. *Effect of fillers and plasticizers on the performance of novel heat and oil-resistant thermoplastic elastomers from nylon-6 and acrylate rubber blends*. J. Appl. Polym. Sci. 74, 1490-1501.
- [4] Narathichat, M., Kummerlöwe, C., Vennemann, N., Sahakaro, K. and Nakason, C. 2012. *Influence of epoxide level and reactive blending on properties of epoxidized natural rubber and nylon-12 blends*. Adv. Polym. Tech. 31, 118-129.
- [5] Drobny, J.G. 2007. *Handbook of Thermoplastic Elastomers*. PDL(Plastics Design Library)/William Andrew Pub., New York.
- [6] Rooj, S., Thakur, V., Gohs, U., Wagenknecht, U., Bhowmick, A.K. and Heinrich, G. 2011. *In situ reactive compatibilization of polypropylene/epoxidized natural rubber blends by electron induced reactive processing: novel in-line mixing technology*. Polym. Adv. Technol. 22, 2257-2263.
- [7] Brown, S.B. 2002. *Reactive compatibilization of polymer blends*, in *Polymer Blends Handbook*, L.A. Utracki, ed. Springer, Dordrecht, The Netherlands.
- [8] Sailer, C. and Handge, U.A. 2007. *Melt viscosity, elasticity, and morphology of reactively compatibilized polyamide 6/styrene-acrylonitrile blends in shear and elongation*. Macromolecules. 40, 2019-2028.
- [9] Ma, H., Xiong, Z., Lv, F., Li, C. and Yang, Y. 2011. *Rheological behavior and morphologies of reactively compatibilized PVDF/TPU blends*. Macromol. Chem. Phys. 212, 252-258.
- [10] Elashmawi, I.S. and Hakeern, N.A. 2008. *Effect of PMMA addition on characterization and morphology of PVDF*. Polym. Eng. Sci. 48, 895-901.
- [11] Madbouly, S.A., Otaigbe, J.U. and Ougizawa, T. 2006. *Morphology and properties of novel blends prepared from simultaneous in situ polymerization and compatibilization of macrocyclic carbonates and maleated poly(propylene)*. Macromol. Chem. Phys. 207, 1233-1243.

- [12] Kim, K.J., Cho, H.W. and Yoon, K.J. 2003. *Effect of P(MMA-co-MAA) compatibilizer on the miscibility of nylon 6/PVDF blends*. Eur. Polym. J. 39, 1249-1265.
- [13] Mohanty, S., Nando, G.B., Vijayan, K. and Neelakanthan, N.R. 1996. *Mechanical and dynamic mechanical properties of miscible blends of epoxidized natural rubber and poly(ethylene-co-acrylic acid)*. Polymer. 37, 5387-5394.
- [14] Marin, N. and Favis, B.D. 2002. *Co-continuous morphology development in partially miscible PMMA/PC blends*. Polymer. 43, 4723-4731.
- [15] Bhadane, P.A., Champagne, M.F., Huneault, M.A., Tofan, F. and Favis, B.D. 2006. *Continuity development in polymer blends of very low interfacial tension*. Polymer. 47, 2760-2771.
- [16] Al-Malaika, S. and Kong, W. 2005. *Reactive processing of polymers: effect of in situ compatibilisation on characteristics of blends of polyethylene terephthalate and ethylene-propylene rubber*. Polymer. 46, 209-228.
- [17] Sy, J.W. and Mijovic, J. 2000. *Reorientational dynamics of poly(vinylidene fluoride)/poly(methyl methacrylate) blends by broadband dielectric relaxation spectroscopy*. Macromolecules. 33, 933-946.
- [18] Madbouly, S.A. and Otaigbe, J.U. 2007. *Broadband dielectric spectroscopy of nanostructured maleated polypropylene/polycarbonate blends prepared by in situ polymerization and compatibilization*. Polymer. 48, 4097-4107.
- [19] Linares, A., Nogales, A., Rueda, D.R. and Ezquerra, T.A. 2007. *Molecular dynamics in PVDF/PVA blends as revealed by dielectric loss spectroscopy*. J. Polym. Sci., Part B: Polym. Phys. 45, 1653-1661.
- [20] Kanapitsas, A., Pissis, P. and Garcia Estrella, A. 1999. *Molecular mobility in polyurethane/styrene-acrylonitrile blends studied by dielectric techniques*. Eur. Polym. J. 35, 923-937.
- [21] Carius, H.-E., Schönhals, A., Guigner, D., Sterzynski, T. and Brostow, W. 1996. *Dielectric and mechanical relaxation in the blends of a polymer liquid crystal with polycarbonate*. Macromolecules. 29, 5017-5025.
- [22] Li, R., Xiong, C., Kuang, D., Dong, L., Lei, Y., Yao, J., Jiang, M. and Li, L. 2008. *Polyamide 11/poly(vinylidene fluoride) blends as novel flexible materials for capacitors*. Macromol. Rapid Commun. 29, 1449-1454.

- [23] Drobny, J.G. 2000. *Technology of Fluoropolymers*. CRC Press. 190.
- [24] Nalwa, H.S. 1995. *Ferroelectric Polymers: Chemistry, Physics, and Applications*. Taylor & Francis. 904.
- [25] Li, Y., Oono, Y., Kadowaki, Y., Inoue, T., Nakayama, K. and Shimizu, H. 2006. A novel thermoplastic elastomer by reaction-induced phase decomposition from a miscible polymer blend. *Macromolecules*. 39, 4195-4201.
- [26] Keun Yoon, L. and Kyu Kim, B. 2000. *Compatibility of poly (vinylidene fluoride)(PVDF)/polyamide 12 (PA12) blends*. *J. Appl. Polym. Sci.* 78, 1374-1380.
- [27] Varughese, K.T., Nando, G.B., De, P.P. and De, S.K. 1988. *Miscible blends from rigid poly(vinyl chloride) and epoxidized natural rubber*. *J. Mater. Sci.* 23, 3894-3902.
- [28] Kalkornsurapranee, E., Nakason, C., Kummerlöwe, C. and Vennemann, N. 2013. *Development and preparation of high-performance thermoplastic vulcanizates based on blends of natural rubber and thermoplastic polyurethanes*. *J. Appl. Polym. Sci.* 128, 2358-2367.
- [29] Mathai, A.E. and Thomas, S. 2005. *Morphology, mechanical and viscoelastic properties of nitrile rubber/epoxidized natural rubber blends*. *J. Appl. Polym. Sci.* 97, 1561-1573.
- [30] Rocha, T.L.A.C., Rosca, C., Ziegler, J. and Schuster, R.H. 2005. *Influence of polymer polarity on phase morphology of NR blends*. *Kaut. Gummi Kunstst.* 58, 22-29.
- [31] Bottino, A., Capannelli, G., Munari, S. and Turturro, A. 1988. *Solubility parameters of poly(vinylidene fluoride)*. *J. Polym. Sci., Part B: Polym. Phys.* 26, 785-794.
- [32] Chee, K.K. 1995. *Solubility parameters of polymers from swelling measurements at 60°C*. *J. Appl. Polym. Sci.* 58, 2057-2062.
- [33] Na, B., Xu, W., Lv, R., Li, Z., Tian, N. and Zou, S. 2010. *Toughening of nylon-6 by semicrystalline poly(vinylidene fluoride): role of phase transformation and fibrillation of dispersed particles*. *Macromolecules*. 43, 3911-3915.
- [34] Pichaiyut, S., Nakason, C. and Vennemann, N. 2012. *Thermoplastic elastomers-based natural rubber and thermoplastic polyurethane blends*. *Iran Polym. J.* 21, 65-79.

- [35] Bourry, D. and Favis, B.D. 1998. *Cocontinuity and phase inversion in HDPE/PS blends: Influence of interfacial modification and elasticity*. J. Polym. Sci., Part B: Polym. Phys. 36, 1889-1899.
- [36] Tol, R.T., Groeninckx, G., Vinckier, I., Moldenaers, P. and Mewis, J. 2004. *Phase morphology and stability of co-continuous (PPE/PS)/PA6 and PS/PA6 blends: effect of rheology and reactive compatibilization*. Polymer. 45, 2587-2601.
- [37] Dmitriev, I., Bukosek, V., Lavrentyev, V. and Elyashevich, G. 2007. *Structure and deformational behavior of poly(vinylidene fluoride) hard elastic films*. Acta Chim. Slov. 54, 784-791.
- [38] Ramesh, P. and De, S.K. 1991. *Self-cross-linkable plastic-rubber blend system based on poly(vinyl chloride) and epoxidized natural rubber*. J. Mater. Sci. 26, 2846-2850.
- [39] Li, Y., Iwakura, Y., Zhao, L. and Shimizu, H. 2008. *Nanostructured poly(vinylidene fluoride) materials by melt blending with several percent of acrylic rubber*. Macromolecules. 41, 3120-3124.
- [40] Mano, J.F., Sencadas, V., Costa, A.M. and Lanceros-Méndez, S. 2004. *Dynamic mechanical analysis and creep behaviour of β -PVDF films*. Mat. Sci. Eng. A-Struct. 370, 336-340.
- [41] Sencadas, V., Lanceros-Méndez, S. and Mano, J.F. 2004. *Characterization of poled and non-poled β -PVDF films using thermal analysis techniques*. Thermochim. Acta. 424, 201-207.
- [42] Martins, J.N., Bassani, T.S. and Oliveira, R.V.B. 2012. *Morphological, viscoelastic and thermal properties of poly(vinylidene fluoride)/POSS nanocomposites*. Mat. Sci. Eng. C-Mater. 32, 146-151.
- [43] Linares, A. and Acosta, J.L. 1997. *Tensile and dynamic mechanical behaviour of polymer blends based on PVDF*. Eur. Polym. J. 33, 467-473.
- [44] Patro, T.U., Mhalgi, M.V., Khakhar, D.V. and Misra, A. 2008. *Studies on poly(vinylidene fluoride)-clay nanocomposites: effect of different clay modifiers*. Polymer. 49, 3486-3499.
- [45] Komalan, C., George, K.E., Kumar, P.A.S., Varughese, K.T. and Thomas, S. 2007. *Dynamic mechanical analysis of binary and ternary polymer blends based*

- on nylon copolymer/EPDM rubber and EPM grafted maleic anhydride compatibilizer. *Express Polym. Lett.* 1, 641-653.
- [46] Liao, W.B. 1999. *Dynamic mechanical relaxation of lightly cross-linked epoxidized natural rubber.* *Polymer.* 40, 599-605.
- [47] Nakason, C., Panklieng, Y. and Kaesaman, A. 2004. *Rheological and thermal properties of thermoplastic natural rubbers based on poly(methyl methacrylate)/epoxidized-natural-rubber blends.* *J. Appl. Polym. Sci.* 92, 3561-3572.
- [48] Chanachai, A., Meksup, K. and Jiraratananon, R. 2010. *Coating of hydrophobic hollow fiber PVDF membrane with chitosan for protection against wetting and flavor loss in osmotic distillation process.* *Sep. Purif. Technol.* 72, 217-224.
- [49] Nakhmanson, S.M., Korlacki, R., Johnston, J.T., Ducharme, S., Ge, Z. and Takacs, J.M. 2010. *Vibrational properties of ferroelectric β -vinylidene fluoride polymers and oligomers.* *Physical Review B.* 81, 174120.
- [50] Ray, S., Easteal, A.J., Cooney, R.P. and Edmonds, N.R. 2009. *Structure and properties of melt-processed PVDF/PMMA/polyaniline blends.* *Mater. Chem. Phys.* 113, 829-838.
- [51] Wang, P., Wang, Z., Wu, Z., Zhou, Q. and Yang, D. 2010. *Effect of hypochlorite cleaning on the physiochemical characteristics of polyvinylidene fluoride membranes.* *Chem. Eng. J.* 162, 1050-1056.
- [52] Hammami, H., Arous, M., Lagache, M. and Kallel, A. 2007. *Study of the interfacial MWS relaxation by dielectric spectroscopy in unidirectional PZT fibres/epoxy resin composites.* *J. Alloys Compd.* 430, 1-8.
- [53] Rekik, H., Ghallabi, Z., Royaud, I., Arous, M., Seytre, G., Boiteux, G. and Kallel, A. 2013. *Dielectric relaxation behaviour in semi-crystalline polyvinylidene fluoride (PVDF)/TiO₂ nanocomposites.* *Compos. Part B-Eng.* 45, 1199-1206.
- [54] Omonov, T.S., Harrats, C., Moldenaers, P. and Groeninckx, G. 2007. *Phase continuity detection and phase inversion phenomena in immiscible polypropylene/polystyrene blends with different viscosity ratios.* *Polymer.* 48, 5917-5927.

- [55] Willemse, R.C., Posthuma de Boer, A., Van Dam, J. and Gotsis, A.D. 1999. *Co-continuous morphologies in polymer blends: the influence of the interfacial tension*. Polymer. 40, 827-834.
- [56] Ying, J.R., Liu, S.P., Guo, F., Zhou, X.P. and Xie, X.L. 2008. *Non-isothermal crystallization and crystalline structure of PP/POE blends*. J. Therm. Anal. Calorim. 91, 723-731.

CHAPTER 8

SELECTIVE LOCALIZATION OF BARIUM TITANATE IN PVDF/ENR-50 BLENDS

8.1 Introduction

Recently, it has been reported that blending of polymeric materials with organic and inorganic filler is a useful method to produce novel materials known as polymer blend composites. Incorporation of organic and inorganic particles such as carbon black, silica, nanoclay, and carbon nanotube into immiscible polymer blends can develop the proper morphology of the blends with significantly affect various properties such as mechanical, barrier, thermal, flame retardancy and electrical properties. The presence of particles also caused the modification of miscibility/compatibility and morphology of the blends due to the compatibilization effect by adsorption of two polymers on solid surface, instead of using compatibilization agents [1, 2].

The immiscible blend composite is a combination of polymer blend and polymer composite, as many factors have the potential to impact their morphology and final properties. Thus, polymer blends containing micro and nano fillers have been the subject of intense investigation during the last decade. Selective localization of filler in polymer blend forces the microstructure. There are three possibilities for localization of the filler: a homogenous localization in the whole blend, a selective localization in one phase and selective localization at the interface between two phases. Generally, the migration of the filler in multiphase polymer blend tends to be in the phase which is more affine according to surface chemistry of filler and polymer, so-called thermodynamic effect. In addition, the preferential localization is also affected by kinetic effect and blending sequence [3, 4]. The addition of nanoparticles such as carbon black, silica, nanoclay, and carbon nanotube is now widely accepted that the presence of those particles causes decreasing of the size of dispersed phases in the blend.

Barium titanate (BT) is a filler which was widely incorporated into polymer to increase dielectric permittivity of polymer composite. Most of barium titanate-polymer composites have been prepared based on single polymer, as summarized in Table 2.2. However, the BT is rarely used in polymer blend. Therefore, the blendings poly(vinylidene fluoride) and epoxidized natural rubber have been studied in the chapter 7. It is seen that this type of blend exhibited thermoplastic elastomer (TPE) behavior with partial miscibility. It would thus be interesting to study the localization of BT in PVDF/ENR-50 blend with provide high permittivity thermoplastic/elastomer blend.

In this chapter, effect of barium titanate in simple blend and dynamically vulcanized blend of PVDF/ENR-50/BT composites was elucidated. Two different blend proportions (i.e., PVDF/ENR-50 = 80/20 and 50/50 wt%) and mixing procedures were used to investigate location of BT particles in the blend. Two mixing steps used in this investigation are the addition of BT particles before and after dynamic vulcanization. Moreover, the variation of BT loading in the simple and dynamically cured PVDF/ENR-50 blends was also studied. Morphological properties, mechanical properties, dynamic mechanical properties and dielectric properties of PVDF/ENR-50/BT composites were examined and discussed.

8.2 Effect of barium titanate in the simple and dynamically vulcanized PVDF/ENR-50 blends

The thermoplastic elastomer based on PVDF/ENR-50 blends filled with 5 vol% BT was prepared by simple blend and dynamic vulcanization techniques according to the methodology described earlier in section 3.2.5. The effect of barium titanate in simple and dynamically cured PVDF/ENR-50 blends on morphological, mechanical (characterized by tensile test and DMA) and dielectric properties were studied.

8.2.1 Morphological properties

SEM micrographs of simple blend of PVDF/ENR-50 = 80/20 and 50/50 without and with BT are shown in Figure 8.1. In the blend without BT, PVDF exhibited major phase in the blend with PVDF/ENR-50 = 80/20 while the co-continuous morphology is observed in the blend with PVDF/ENR-50 = 50/50. The addition 5 vol% of BT (5BT), the

morphology of PVDF-rich blend (i.e., PVDF/ENR-50 = 80/20) changed the shape of ENR-50 phase from elongated particles to more spherical domains dispersed in PVDF matrix.

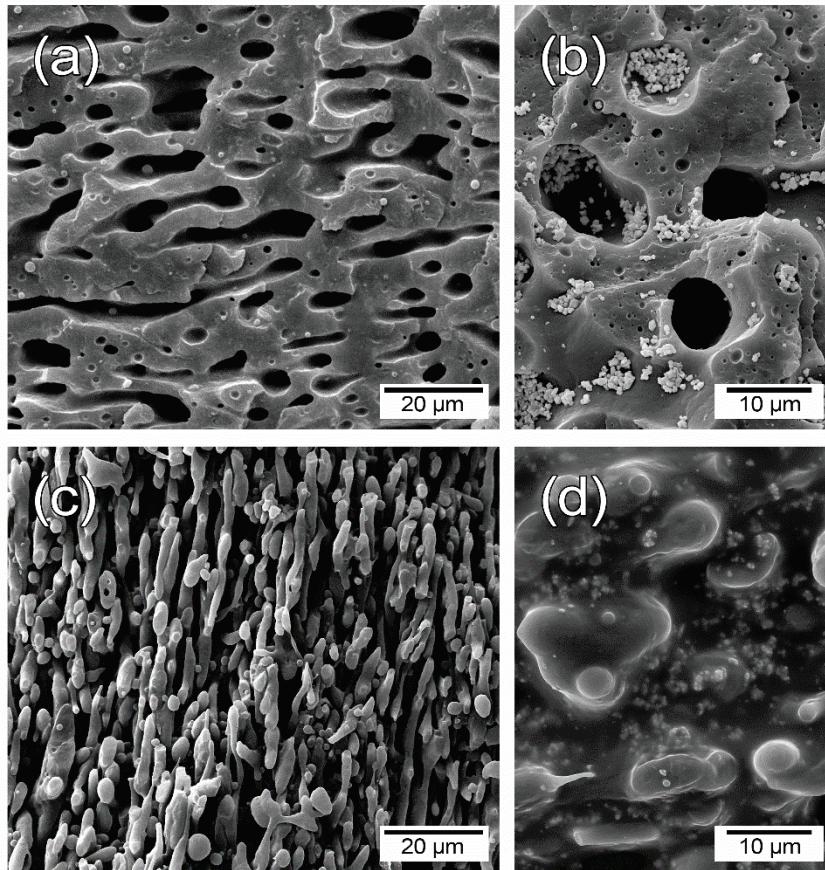


Figure 8.1 SEM micrographs of PVDF/ENR-50 simple blends (a) 80/20-0BT, (b) 80/20-5BT, (c) 50/50-0BT and (d) 50/50-5BT

The average domain size of ENR-50 in 80/20 PVDF/ENR-50 with 5 vol% BT (80/20-5BT) composites increased from approximately 5.6 μm to 8.4 μm , compared with the one of neat 80/20 PVDF/ENR-50 blend. Therefore, it is suggested that the filler localization in dispersed phase lead to the increase in dispersed domain size due to the change in viscosity of the dispersed phase. This was also led to decreasing droplet breakup against hydrodynamic force which is decreased by the consequent reduction in the deformability of the droplets [5, 6]. However, incorporation of BT particles in 50/50 PVDF/ENR-50 simple blend causes the morphology change from a co-continuous structure to a dispersed droplet-like structure (i.e., PVDF dispersed in ENR-50) and BT particles are mainly dispersed in ENR-50 phase, as shown in Figure 8.1(d). This indicates

that BT particles are preferentially localized in ENR-50 phase with phase inversion took place upon addition of BT in PVDF/ENR-50 = 50/50 blend. This might be attributed to a significant increase in the viscosity of ENR-50 phase as well as viscosity ratio between the ENR-50 to PVDF phases after addition of BT particle. This results in retardation of the break-up mechanism to form co-continuous phase morphology. Noticeably, the distribution of particles in the blend is governed by thermodynamic and kinetic effects through wetting parameter and viscosity of the polymer, respectively. The filler particles in the blend are typically migrated into more affinity (thermodynamic effect) and lower viscosity phases (kinetic effect) [4, 7-10]. Thus, the kinetic effect or viscosity of blend components has been concerned for prediction. In order to evaluate viscosity during blending, the mixing torque of pure PVDF and ENR-50 were measured at the same rotor speed and temperature, as shown in Figure 8.2.

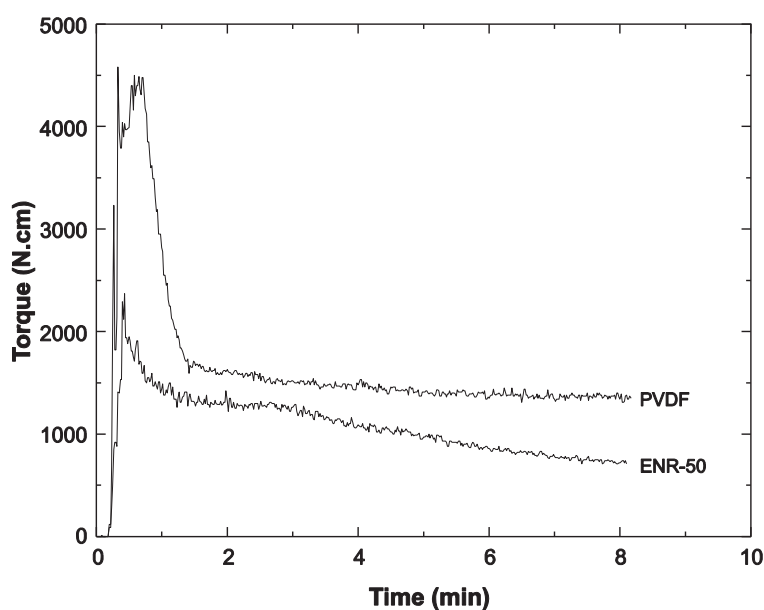


Figure 8.2 Mixing torque of pure PVDF and ENR-50 at a rotor speed 50 rpm and temperature 180°C

In Figure 8.2, it is seen that the mixing torque of ENR-50 was lower than PVDF to reveal lower viscosity of ENR-50 than that of PVDF during blending operation. Thus, the BT is preferentially located within lower viscosity ENR-50 phase. Selective localization of BT in ENR-50 phase of the blend caused an increasing in viscosity of this phase. Therefore, ENR-50 droplets were difficult to breakup during blending process,

resulting in bigger ENR-50 domains. This result complies with the morphological observation (Figure 8.1). As a consequence, the preferential distribution of BT in PVDF/ENR-50 simple blends at blend proportion of 80/20 and 50/50 wt% is schematically illustrated in Figure 8.3. The use of BT content of 5 vol% is equal to 20 wt% which is considered as relatively high amount of filler in the blend. This result is corresponded with the work of Lee *et al.* [11] that the co-continuous structure was transformed to a dispersed structure when high content of filler was introduced into the blend. This was speculated that changes in the dynamics of droplet breakup in the presence of the filler were responsible for the revolution of new morphologies.

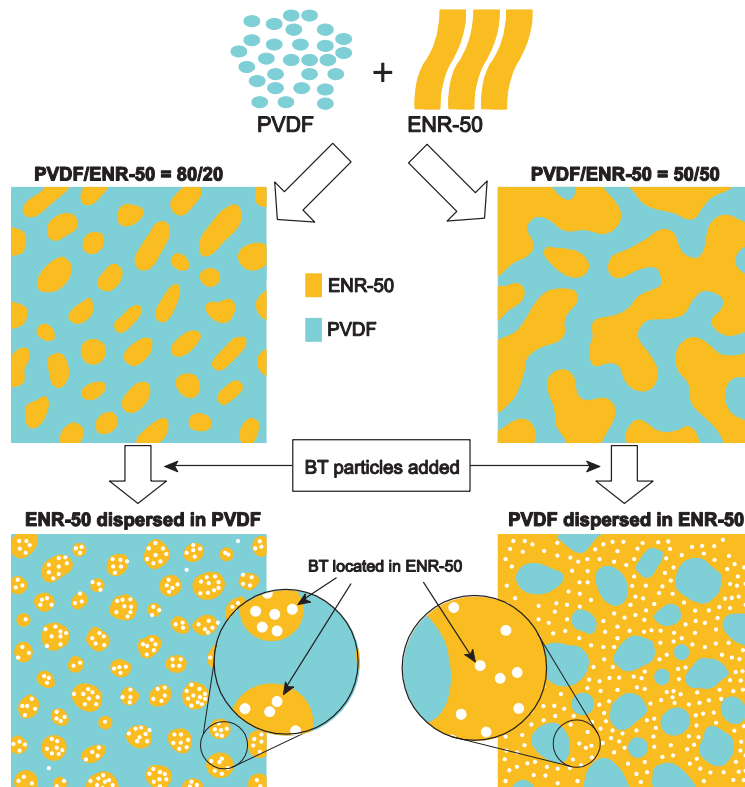


Figure 8.3 Schematic diagram illustration of selective localization of BT in PVDF/ENR-50 simple blends

Morphological properties of the dynamically cured PVDF/ENR-50 blends without BT was studied by SEM, as shown in Figure 8.4. The dynamically cured samples was examined without extraction. Therefore, the contrast between PVDF and ENR-50 phase in SEM is achieved with different microstructures of PVDF and ENR-50. This enables by the distinction between semi-crystalline or PVDF (rough) and amorphous or ENR-50

(smooth) regions. In Figure 8.4(a) and (b) shows a dispersion of the cross-linked ENR-50 particles in the PVDF matrix due to the dynamic vulcanization of the blend which leads to break-up of the co-continuous structure into droplet (cross-linked rubber)-matrix (thermoplastic) morphology. It can also be seen that size and shape of the ENR-50 phase are not uniform because the particle size distribution of the rubber phase depends on shear rate applied to the polymer melt during blending and particle shape depends on viscosity of matrix phase. At high rubber content, it is difficult to observe dispersion of ENR-50 in PVDF, nonetheless, ENR-50 particles remained surrounded shape by thermoplastic PVDF phase, which is a characteristic of TPV. This may be attributed to the connecting or overlapping and limiting break-up of dispersed phase at 50 wt% of rubber, giving the impression of partial co-continuity [12, 13]. Furthermore, SEM technique used in this investigation detected some secondary electron which emitted from the surface of a sample and thus SEM discarded some vital spatial information behind the surface. It is also seen that the ENR-50 appeared to be elongated and enlarged with increasing ENR-50 content (Figure 8.4(b)). This indicates that break-up of the rubber phase during dynamic vulcanization was not completed due to high rubber proportion.

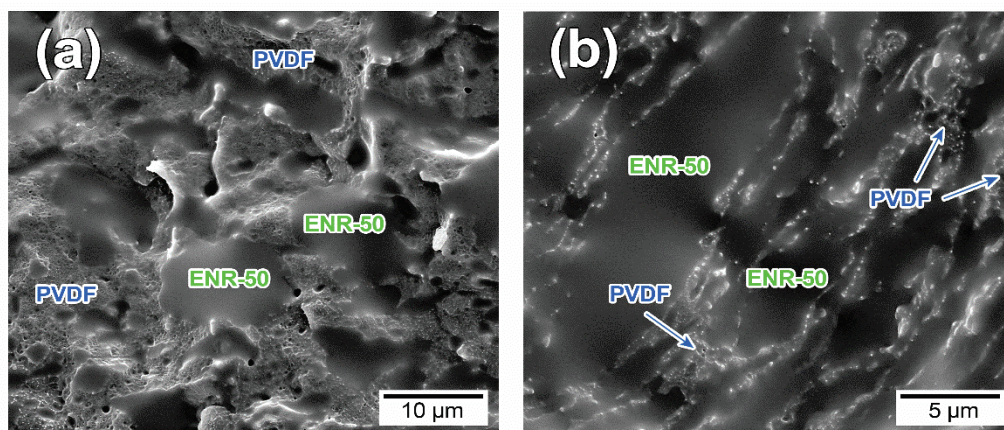


Figure 8.4 SEM micrographs of dynamically cured PVDF/ENR-50 blend at blend ratio (a) 80/20 and (b) 50/50

Figure 8.5 shows SEM micrographs of dynamically vulcanized PVDF/ENR-50 blends containing 5 vol% BT with different blend proportions. The dynamically cured blend filled with BT showed phase separation between PVDF and cross-linked ENR-50. That is, the PVDF domain presents a roughness surface, in opposite to smooth interfaces of ENR-50 domain. Addition of particles and blending sequence affect the blend morphology.

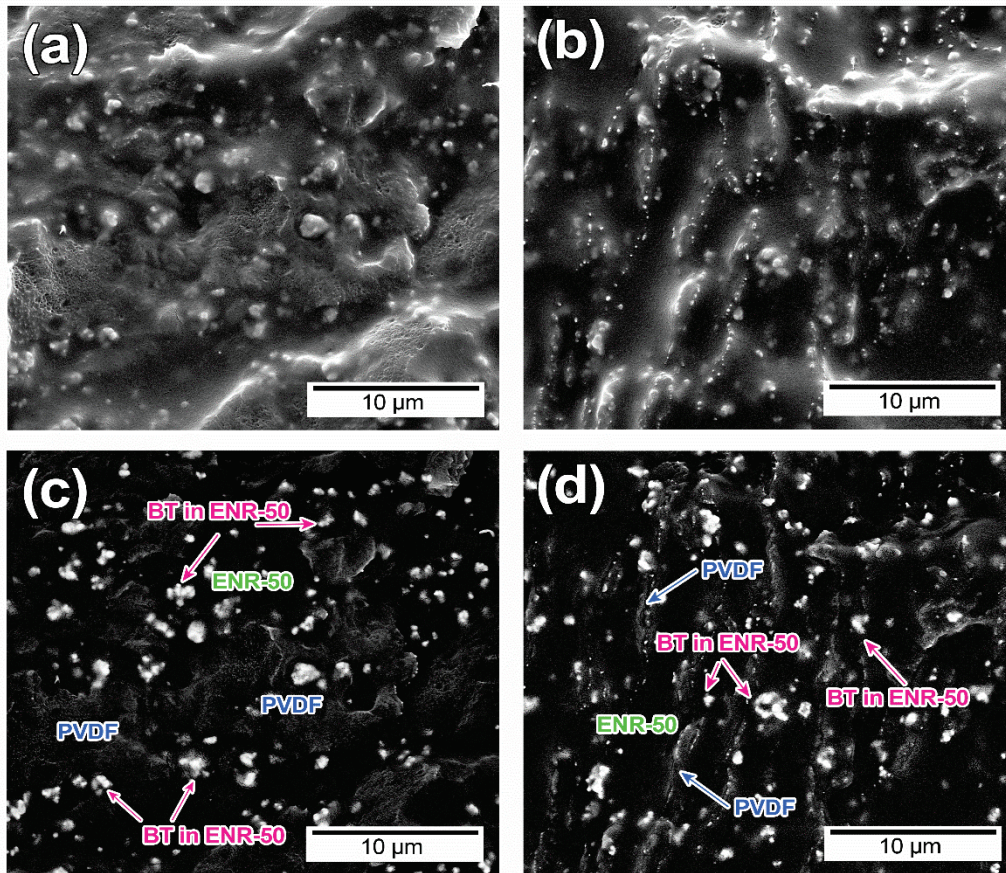


Figure 8.5 SEM micrographs of dynamically cured PVDF/ENR-50 blend containing 5 vol% BT prepared by BDV method with (a and c) PVDF/ENR-50 = 80/20 and (b and d) PVDF/ENR-50 = 50/50

As presented in Figure 8.5, it is clearly seen that BT particles located in ENR-50 phase in the TPV with addition of BT before dynamic vulcanization or BDV method. Meanwhile, the back-scattered electron (BSE) imaging (Figure 8.5(c) and (d)) revealed higher contrast between blend components, which corresponds to the atomic number of elements in the blend. Increasing brightness of the images can be interpreted as regions of different compositions with high average atomic number. In PVDF/ENR-50/BT composite, BT particles which consist of barium and titanium atoms appear to be bright spots in SEM. Meanwhile, the PVDF consist of fluorine atoms in each repeating unit. It is typically appeared to be brighter or whiter than the vulcanized ENR-50 phase. Therefore, SEM images based on BSE mode showed a selective localization of BT in vulcanized ENR-50 phase for the blend with incorporation of BT with BDV method. This is because

BT particles are preferentially migrated into ENR-50 phase prior to the introduction of vulcanizing agent (HRJ-10518) in the blend. Thus, BT still remained in the ENR-50 phase, where they have been located before addition of HRJ-10518 as observed in simple blend. The dynamic vulcanization in the blend resulted in formation of permanent crosslink of ENR-50 chains. Therefore, BT particles are trapped in ENR-50 phase by three-dimensional cross-linked network. For comparison between Figures 8.5 and 8.6, it appears that filler localization is different between the mixing sequence BDV and ADV methods. It is interesting to indicate that in ADV technique BT particles are selectively adhered at the interface and in PVDF phase, as shown in Figure 8.6. Moreover, this phenomenon could not be observed in the blend with BDV technique. Therefore, the dynamic vulcanization leads to formation of crosslink between ENR-50 chains which causes obstruction of migration of BT into ENR-50 phase by cross-linked network. Thus, BT located at interface and in PVDF phase. Therefore, the migration of BT particles are more difficult when the favorable phase is vulcanized before addition of BT. In addition, the mixing sequence overshadows the kinetic effect that BT particles attempt to localize in the preferential ENR-50 phase. From the SEM observation, it can be concluded that the difference in localization of BT in the blend with BDV and ADV methods are due to different mixing step, as schematically illustrated in Figure 8.7 and 8.8, respectively.

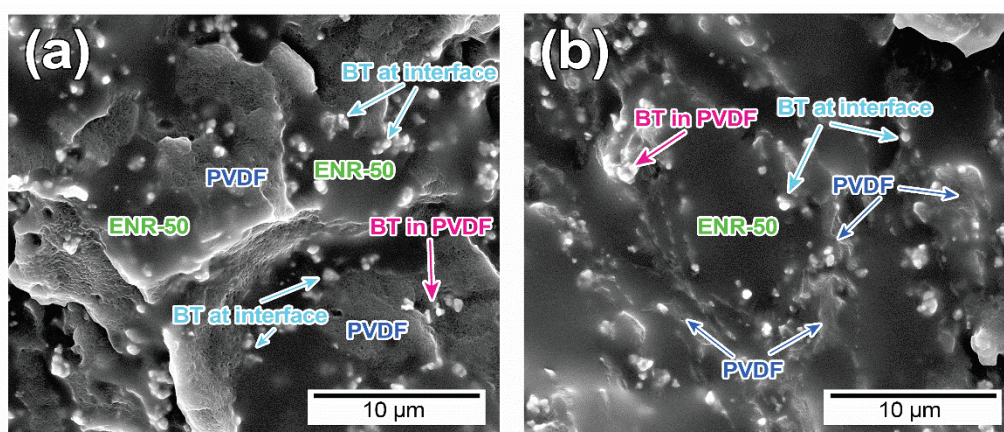


Figure 8.6 SEM micrographs of dynamically cured PVDF/ENR-50 blend containing 5 vol% BT prepared by ADV method for (a) PVDF/ENR-50 = 80/20 and (b) PVDF/ENR-50 = 50/50

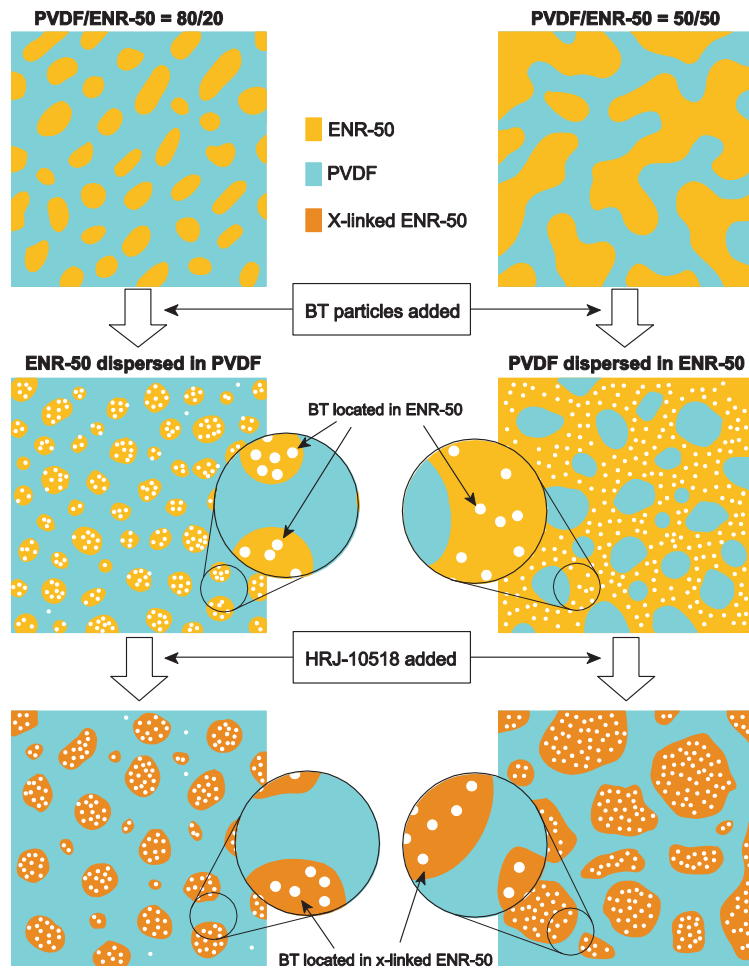


Figure 8.7 Schematic diagram for dynamically cured of BT/PVDF/ENR-50 blend prepared by BDV method

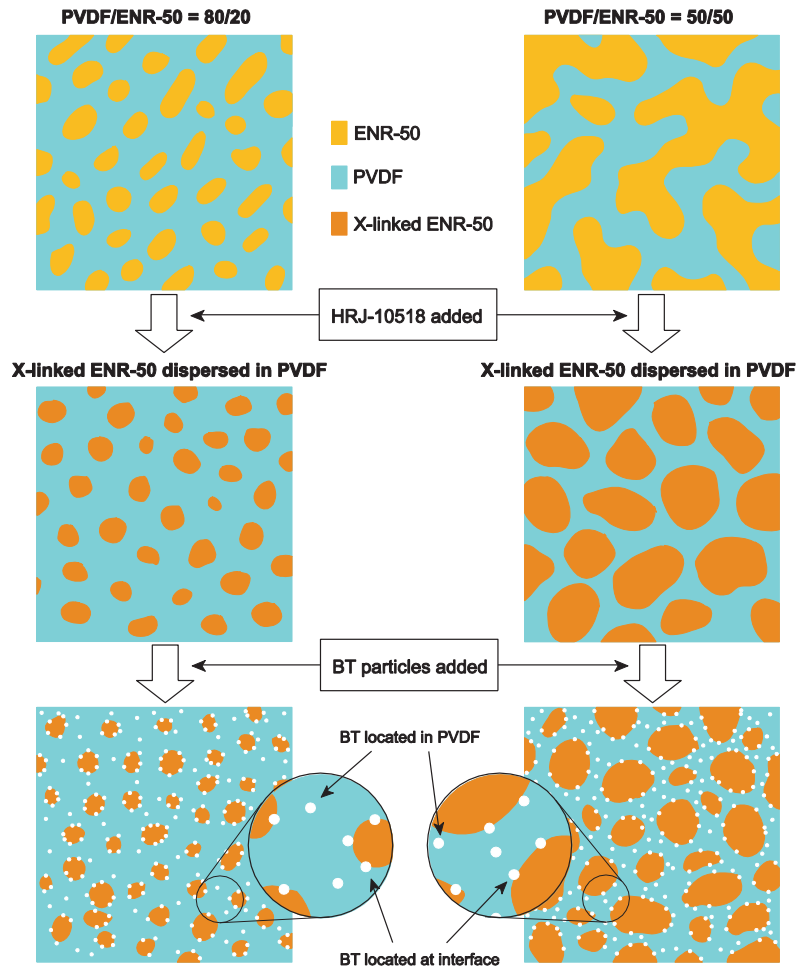


Figure 8.8 Schematic diagram for dynamically cured of BT/PVDF/ENR-50 blend prepared by ADV method

8.2.2 Mechanical properties

Figure 8.9 shows stress-strain curves of simple blend and dynamically cured PVDF/ENR-50 blends with and without BT and Table 8.1 summarizes their mechanical properties. It clearly shows that 80/20 simple and dynamically cured PVDF/ENR-50 blend showed very high Young's modulus, tensile strength but poor elongation at break which is characteristic of the brittle material. On the other hand, the 50/50 PVDF/ENR-50 simple blend and TPV showed uniform deformation behavior with low modulus and high elongation at break that indicates better elastomeric behavior. Therefore, the Young's modulus and tensile strength decreased, elongation at break increased with increasing ENR-50 content. This is due to soft ENR-50 phase in the blend provides lower modulus and stress at break but higher flexibility. However, dynamically cured PVDF/ENR-50 blend

with and without BT exhibited better physical properties compared with simple blend. This indicates that dynamic vulcanization improves physical properties of hard plastic/elastomer blend. The fully vulcanized rubber particles in thermoplastic matrix leads to an enhancement of the mechanical properties in term of Young's modulus, tensile strength, elongation at break, hardness and elastic recovery (lower tension set) [14]. However, the mechanical properties of 80/20 PVDF/ENR-50 simple blend are not affected by incorporation of BT, as shown in Figure 8.9 and Table 8.1. This suggests that ENR-50 phase still remains dispersed in PVDF matrix and tensile behavior is dominated by the matrix. In contrast, 50/50 PVDF/ENR-50 simple blend with BT showed decrease in tensile strength but increase in elongation at break. This implies the formation of phase inversion. SEM studies revealed that 50/50 PVDF/ENR-50 simple blend with BT consisted of PVDF dispersed in ENR-50 matrix phase and BT located in ENR-50 phase, as shown in Figure 8.1(d).

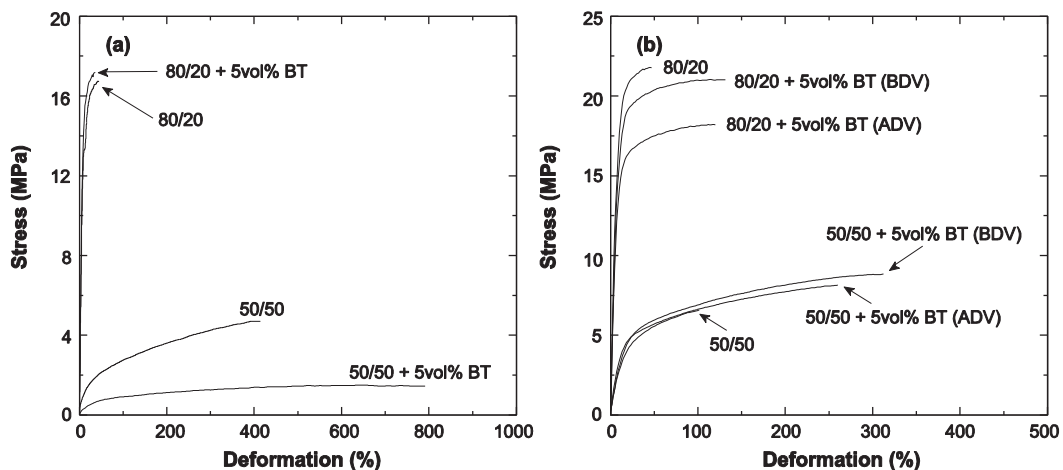


Figure 8.9 Stress-strain curves of (a) simple and (b) dynamically cured PVDF/ENR-50 blend with and without BT at 80/20 and 50/50 blend ratios

A significant enhancement in elongation at break is observed when the BT particles were introduced in TPV for PVDF-rich and ENR-50 rich blend, as shown in Figure 8.9. This demonstrates that the addition of filler improve elasticity of TPV. The incorporation of BT into dynamically cured 80/20 PVDF/ENR-50 blend showed a decrease in tensile strength for the blends with BDV and ADV techniques. It was also found that dynamically cured 50/50 PVDF/ENR-50 blend showed increasing tensile strength with the addition of BT. This denotes a positive effect on addition of BT on tensile strength of the

blend with high rubber content. Furthermore, higher Young's modulus of dynamically cured blend based on the ADV technique compared with the dynamically cured blend based on the BDV technique can be explained by the localization of BT at interface and PVDF phase. The initial deformation of dynamically cured blend is dominated by PVDF matrix. Thus, the presence of BT at the interface and PVDF matrix leads to restriction of PVDF molecular chain motion under stretch. Therefore, it can be deduced that the mechanical properties of PVDF/ENR-50 blend filled with BT is changed by localization of BT particles in the blend with different blend composition and mixing sequence. Addition of BT in the blends caused increasing hardness due to the presence of rigid particles.

Table 8.1 Mechanical properties of simple and dynamically cured PVDF/ENR-50 blends without and with 5 vol% BT

PVDF/ENR-50	Young's modulus (MPa)	Tensile strength (MPa)	Elongation at break (%)	Tension set (%)	Hardness (Shore A)	
Simple blend	80/20					
	0BT	190 (±15.5)	17.2 (±1.64)	41 (±23)	-	94.0 (±1.1)
	5BT	190 (±10.5)	17.3 (±1.06)	38 (±9)	-	95.0 (±0.7)
	50/50					
	0BT	19.0 (±2.6)	4.8 (±0.69)	440 (±58)	51.3 (±1.5)	58.5 (±1.2)
5BT	2.1 (±0.8)	1.6 (±0.19)	880 (±222)	38.5 (±1.6)	42.5 (±1.4)	
Dynamically cured blend	80/20					
	0BT	225 (±8.7)	21.8 (±1.53)	50 (±29)	-	94.5 (±0.6)
	5BT-BDV	200 (±10.7)	21.1 (±0.50)	125 (±21)	-	95.5 (±0.8)
	5BT-ADV	206 (±13.9)	18.3 (±1.05)	120 (±39)	-	95.5 (±0.6)
	50/50					
	0BT	33.9 (±3.3)	6.7 (±1.02)	95 (±54)	35.4 (±1.3)	88.5 (±0.7)
	5BT-BDV	31.0 (±2.1)	9.0 (±0.31)	300 (±36)	36.9 (±1.1)	90.5 (±0.8)
5BT-ADV	42.2 (±2.5)	8.2 (±0.43)	250 (±24)	35.9 (±0.7)	90.0 (±1.0)	

8.2.3 Dynamic mechanical analysis

Temperature dependence of storage modulus (E') and $\tan \delta$ of simple and dynamically cured 80/20 and 50/50 PVDF/ENR-50 blends with and without BT are shown in Figures 8.10 and 8.11, respectively. All blends show a high storage modulus in glassy state due to the restriction of molecular chains. Two transitions of storage modulus were observed for all blends which were assigned to molecular chain in amorphous region begins in Brownian-motion or glass-rubber transition (T_g), resulting in a significant reduction in storage modulus.

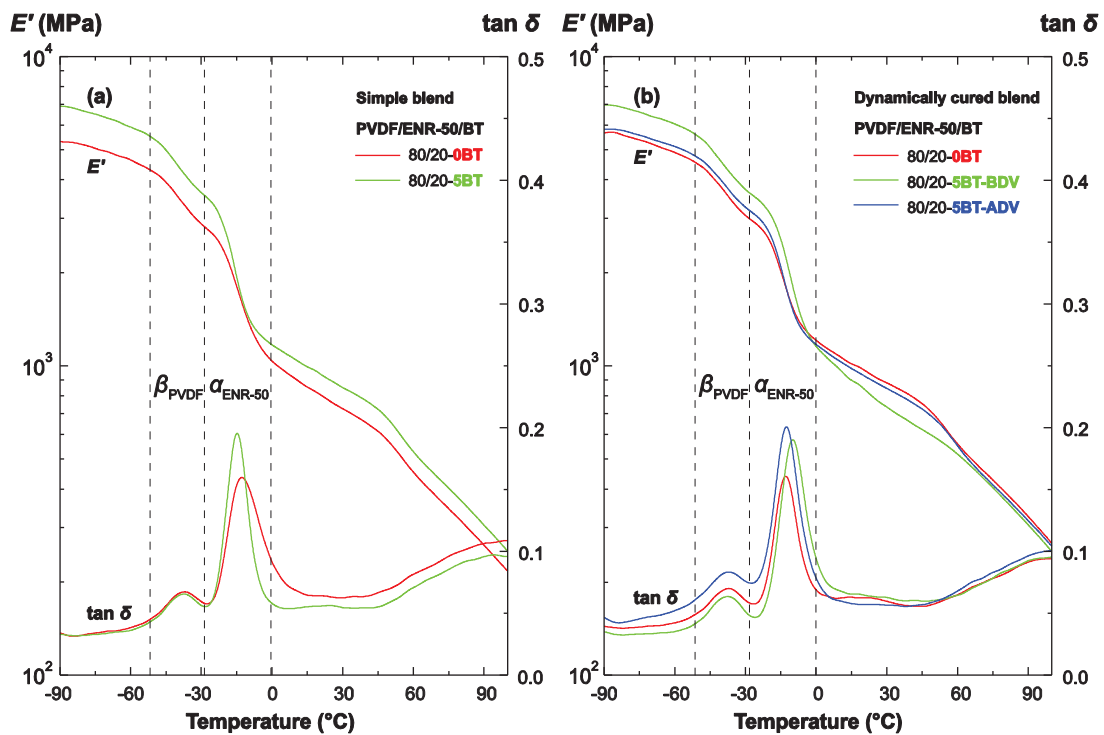


Figure 8.10 Temperature dependence of E' and $\tan \delta$ of 80/20 PVDF/ENR-50 (a) simple blend and (b) dynamically cured blend with and without BT

Data from DMA curve in terms of storage modulus (E') and $\tan \delta$ are listed in Table 8.2. It is clear that addition of 5 vol% of BT in 80/20 simple blend caused increasing storage modulus while the storage modulus of 50/50 simple blend is decreased with addition of BT. This can be explained by phase structure development of composite with immiscible blend. The addition of BT in 80/20 PVDF/ENR-50 simple blend changes the phase structure from elongated rubber phase to more spherical like rubber phase, leading to an increase in storage modulus of the blend. Furthermore, BTs are located at interface

of the two phases, resulting in an improvement of their compatibility due to adsorption of polymer segments of minor and major phases on filler with the reduction of interfacial tension between the two phases. In 50/50/5BT simple blend, the decreasing storage modulus is attributed to phase inversion after introducing BT particles in the blend, as shown in SEM (Figure 8.1(d)), that ENR-50 is responsible for deformation in dynamic mechanical properties. This was well correlated to the decreasing tensile strength of 50/50/5BT simple blend.

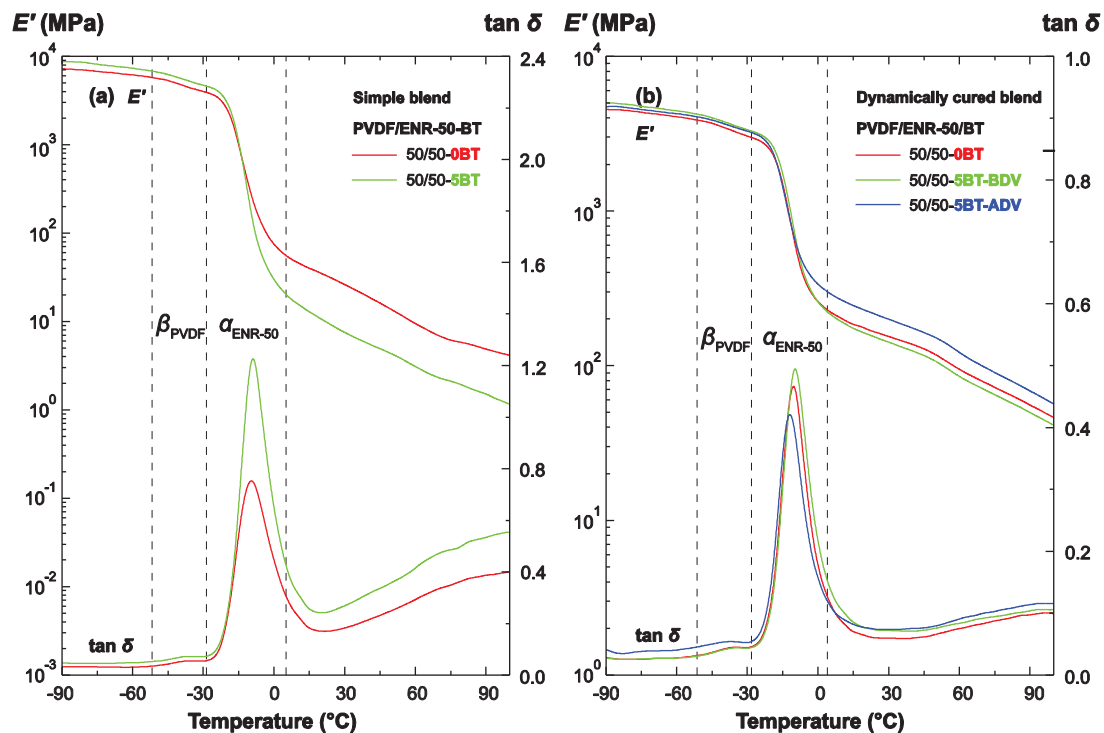


Figure 8.11 Temperature dependence of E' and $\tan \delta$ of 50/50 PVDF/ENR-50 (a) simple blend and (b) dynamically cured blend with and without BT

All dynamically cured blends (TPV) exhibited higher moduli in the rubbery plateau than those simple blend, indicating that the presence of cross-linked rubber particles in PVDF matrix improves physical properties of the TPVs. In the dynamically cured blends, a reduction of storage modulus is observed in the blend prepared by BDV-method for both compositions (i.e., 80/20 and 50/50). In contrast, the addition of BT after dynamic vulcanization or ADV method leads to increase of the storage modulus as compared with the blends without BT and the blend with BDV technique. This can be explained by the difference in selective localization of BT in the dynamically cured blend, which is reflected

in higher storage modulus. The composite with BDV technique consists of BT particles dispersed in ENR-50 phase, leading to no significant improvement of storage modulus. However, the improvement of storage modulus of the blend with ADV technique is attributed to localization of BT at interface and in PVDF phase. As may be expected, localization of the BT at interface evidently improves the interfacial adhesion of PVDF/ENR-50 blend, resulting in good transfer of stress between the two phases and restriction of molecular chain [15]. The dynamically cured blend with BT based on the ADV method shows the higher storage modulus in comparison with the neat and BDV blend. This is in agreement with Young's modulus result, as described in mechanical properties (Section 8.2.2).

In Figures 8.10 and 8.11 and Table 8.2, it can be seen that two distinct $\tan \delta$ peaks appeared around -35°C and -10°C . The relaxation at lower-temperature corresponds to β -relaxation or T_g of PVDF phase, whereas the higher-temperature relaxation corresponds to α -relaxation or T_g of ENR-50 phase, which are associated with segmental motion in amorphous region of PVDF and ENR-50, respectively. Summary of T_g data in the blend obtained from $\tan \delta$ peak in the simple blends and dynamically cured PVDF/ENR-50 blends with and without BT is summarized in Table 8.2. It is clearly showed that the variation in T_g of ENR-50 was affected by the incorporation of BT while T_g of PVDF was slightly affected in the simple and dynamically cured blends. The glass transition of ENR-50 is shifted to lower temperature for BT composite of PVDF-rich simple blend and the dynamically cured blend with ADV method. This can be explained by a selective localization of BT in the immiscible blend. The improvement of compatibility between PVDF and ENR-50 with BT at interface in TPV-ADV leads to thermodynamically stabilization of interface. This is typically the same as observed in the reactive blending or using blend compatibilizer, resulting in shifting of T_g towards each other as compared with the pure components [15, 16]. This is the reason for shifts in T_g of ENR-50 closer to the T_g of PVDF. In contrast, the T_g of ENR-50 is shifted to higher temperature for BT composite of 50/50 simple blend and dynamically cured blend with BDV method. This is because the BT is mainly dispersed in ENR-50 matrix, leading to restriction of motion of ENR-50 chains without compatibilization between the two phases and increased T_g of ENR-50 to higher temperature.

Table 8.2 Dynamic mechanical properties of simple and dynamically cured PVDF/ENR-50 blends without and with 5 vol% BT

PVDF/ENR-50	Storage Modulus, E' (MPa)		Loss tangent, $\tan \delta$				
	-60°C	25°C	$\tan \delta_{\max}$		T_g (°C)		
			PVDF	ENR	PVDF	ENR	
Simple blend	80/20						
	0BT	5300	713	0.06	0.16	-35.6	-13.9
	5BT	5900	896	0.07	0.20	-37.7	-15.0
	50/50						
	0BT	6200	30.4	0.05	0.77	-35.8	-9.7
	5BT	7300	8.9	0.07	1.2	-35.7	-8.1
Dynamically cured blend	80/20						
	0BT	4900	920	0.07	0.16	-37.6	-12.9
	5BT-BDV	6000	783	0.06	0.19	-37.6	-9.9
	5BT-ADV	5100	915	0.08	0.20	-37.7	-12.6
	50/50						
	0BT	4100	160	0.05	0.47	-34.7	-10.5
	5BT-BDV	4400	150	0.04	0.51	-34.6	-9.8
5BT-ADV	4300	210	0.05	0.43	-35.8	-12.0	

8.2.4 Dielectric properties

Dielectric permittivity and loss factor versus frequency for simple blend (SB) and dynamically cured PVDF/ENR-50 blend with and without BT are shown in Figure 8.12. Undoubtedly, the permittivity is found to slightly decrease with the increasing in frequency due to a decreasing in dipolar polarization and interfacial polarization in the composites with the fast change of applied electric field [17, 18]. The relaxation peak of loss factor can be observed with a rapidly decrease of permittivity when measured frequency is as high as 10^5 Hz. This relaxation peak corresponds to segmental motion of polymer chain. It is seen that the relaxation peak broadens upon increasing of PVDF content. This is attributed to the overlapping between relaxation peak of PVDF and ENR-50 because the segmental relaxation of ENR-50 and PVDF appears at 10^5 and 10^6 , respectively, as shown in Figure 8.13.

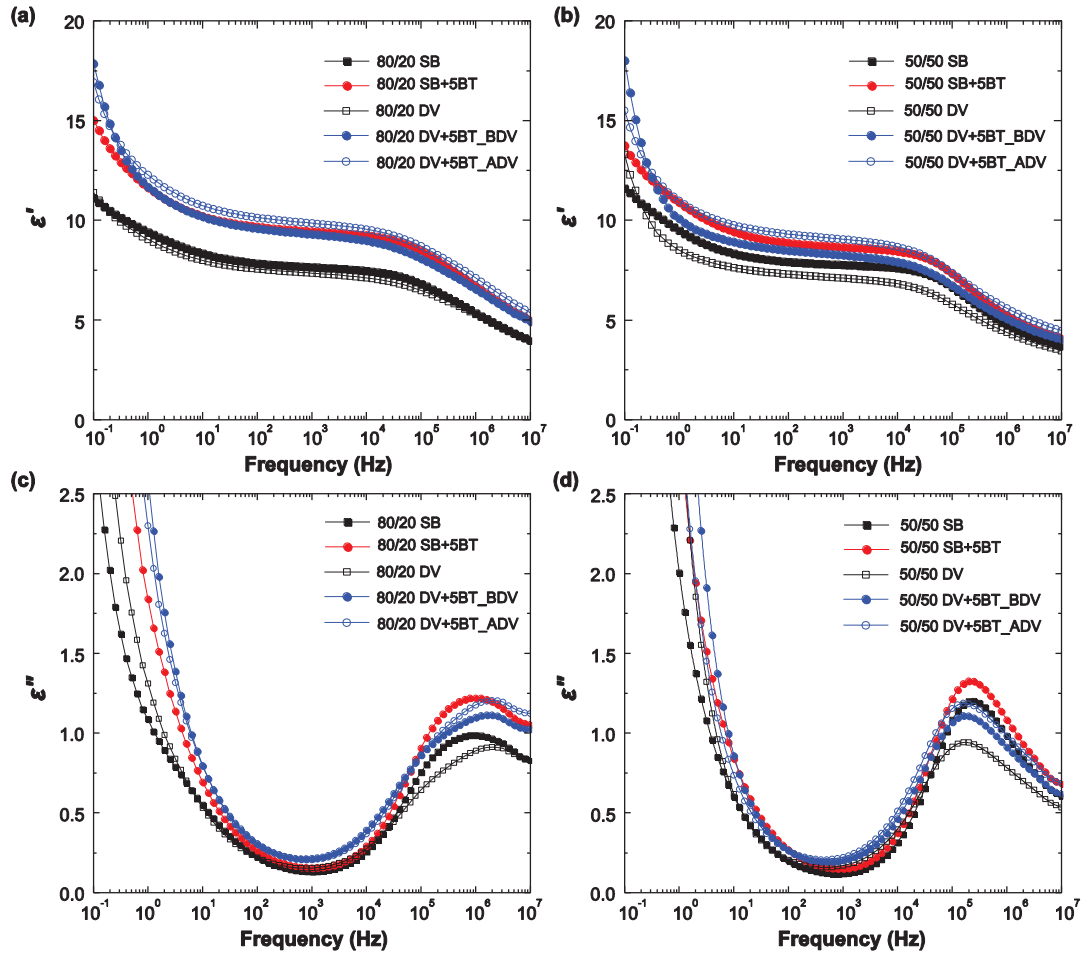


Figure 8.12 Frequency dependence of (a, b) ϵ' and (c, d) ϵ'' at room temperature of simple blends (SB) and dynamically cured PVDF/ENR-50 blends (DV) with the blend ratios of (a, c) 80/20 and (b, d) 50/50

Furthermore, two relaxations at low and high frequencies are clearly observed for PVDF, which correspond to relaxation in crystalline and amorphous region, respectively. These relaxations are denoted as α or α_c and β -relaxation, respectively. However, the β -relaxation of PVDF cannot be observed at low frequency ranges in all blends. It was hidden by the contribution of conduction process of ENR-50 phase. An increase in permittivity is observed in the simple and dynamically cured PVDF/ENR-50 blends with BT, as summarized in Table 8.3 and Figure 8.14. As may be expected, in the ϵ' of composites was improved because of the addition of ceramic filler with high ϵ' such as BT into relative low ϵ' as polymer. The presence of BT particles causes heterogeneous system with increasing of ϵ' of the composites. Besides, there is little effect of selective

localization of BT on ϵ' of composite. Additionally, higher permittivity is observed for the dynamically cure blends with ADV technique. The localization of BT at interface and in PVDF matrix of TPV with ADV technique would lead to better ϵ' , as shown in Figure 8.15. At very low frequencies, the contribution of charge migration and strong ionic conductivity process introduce an abrupt increase in dielectric loss. The results prove that the ADV method is a good method that could be used to prepare PVDF/ENR-50/BT TPV with good mechanical and dielectric properties.

Table 8.3 Permittivity (ϵ'), loss factor (ϵ'') and loss tangent ($\tan \delta$) at frequency 1 kHz of simple and dynamically cured PVDF/ENR-50 blends with and without BT

PVDF/ENR-50		ϵ'	ϵ''	$\tan \delta$
Simple blend	<i>80/20</i>			
	0BT	7.65	0.133	0.017
	5BT	9.46	0.158	0.017
	<i>50/50</i>			
	0BT	7.77	0.121	0.016
	5BT	8.67	0.152	0.018
Dynamically cured blend	<i>80/20</i>			
	0BT	7.35	0.154	0.021
	5BT-BDV	9.32	0.214	0.023
	5BT-ADV	9.86	0.208	0.021
	<i>50/50</i>			
	0BT	7.10	0.170	0.024
	5BT-BDV	8.27	0.205	0.025
	5BT-ADV	9.25	0.222	0.025

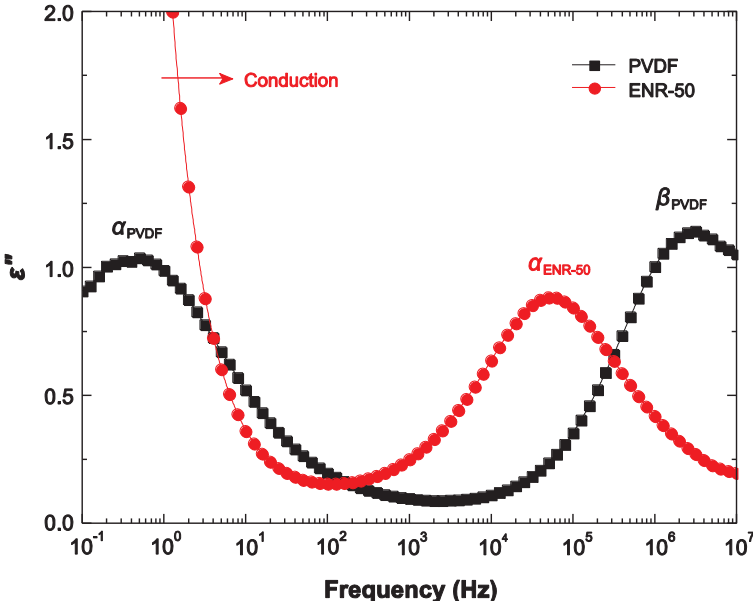


Figure 8.13 Loss factor (ϵ'') of PVDF and ENR-50 at room temperature

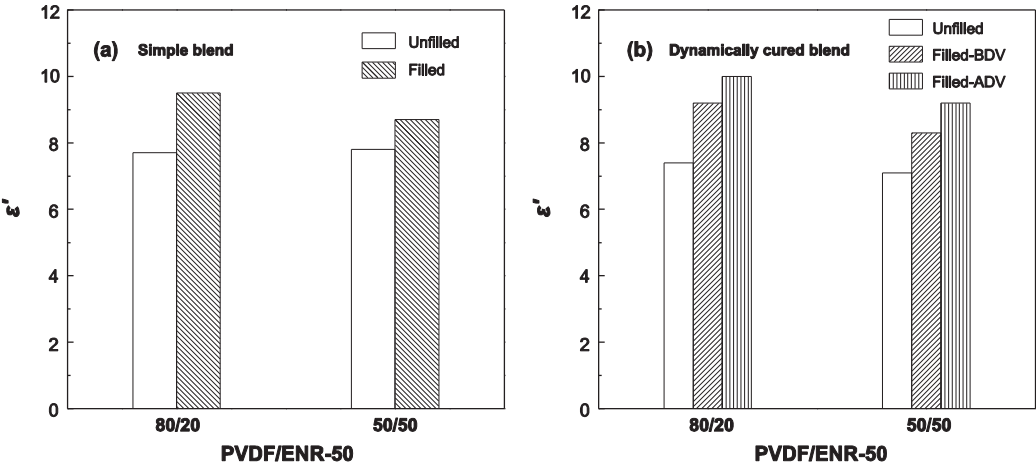


Figure 8.14 Permittivity (ϵ') at 1 kHz of PVDF/ENR-50 (a) simple blend and (b) dynamically cured blend with and without BT

8.3 Effect of barium titanate loading in dynamically vulcanized PVDF/ENR-50 blend

In this section, dynamically cured PVDF/ENR-50 blends with the blend ratios of 80/20 and 50/50 with various BT loading (i.e., 0, 5, 12, 25 and 35 vol%) were prepared by methodology described previously in section 3.2.5. Various important properties were studied as follows:

8.3.1 Morphological properties

The morphology of the PVDF/ENR-50 TPV filled with 0, 5, 12 and 25 vol% BT is shown in Figure 8.15. The smooth surface in the SEM images are ENR-50 phase and rough areas represent PVDF phases. In TPV without BT particles, SEM image clearly showed a dispersion of ENR-50 particles in the PVDF matrix with a large variation in particle size. The rubber connectivity and large size distribution without sharp interface are observed in the TPV with high rubber content, since the separate particles may appear connect or overlap. It can be also seen that the BT particles appear well disperse in the blend with both low and high proportion of PVDF. It has been reported that good dispersion along with homogeneous packing of ceramic filler is likely to exhibit high dielectric constant [19]. The BT particles are uniformly located in PVDF phase and at interface because of addition of BT after dynamic vulcanization. Thus inhibition of the particles in ENR-50 phase occurred, as mentioned earlier. There was no obvious aggregation in the nanocomposites with lower BT loading (5 and 12 vol%). Gradually increased loading, the average of interparticle distance decreased due to the formation of agglomerates. However, at higher BT content (25 vol%), the nanocomposites exhibited some BT agglomerates with discrete ceramic particles (Fig. 8.15(g) and (h)). Furthermore, there were many cavitations in the visual surface due to the composite materials became less compact. Therefore, it easily brought out slots and holes with decreasing concentration of BT. The agglomeration at high ceramic loading has also been reported elsewhere [20, 21]. As shown in Figure 8.15, the BT particles are almost spherical in shape and their sizes vary between 40 and 80 nm. The occurrence of small voids or pores in the nanocomposite with high content of BT could be ascribed to the agglomeration of BT nanoparticles.

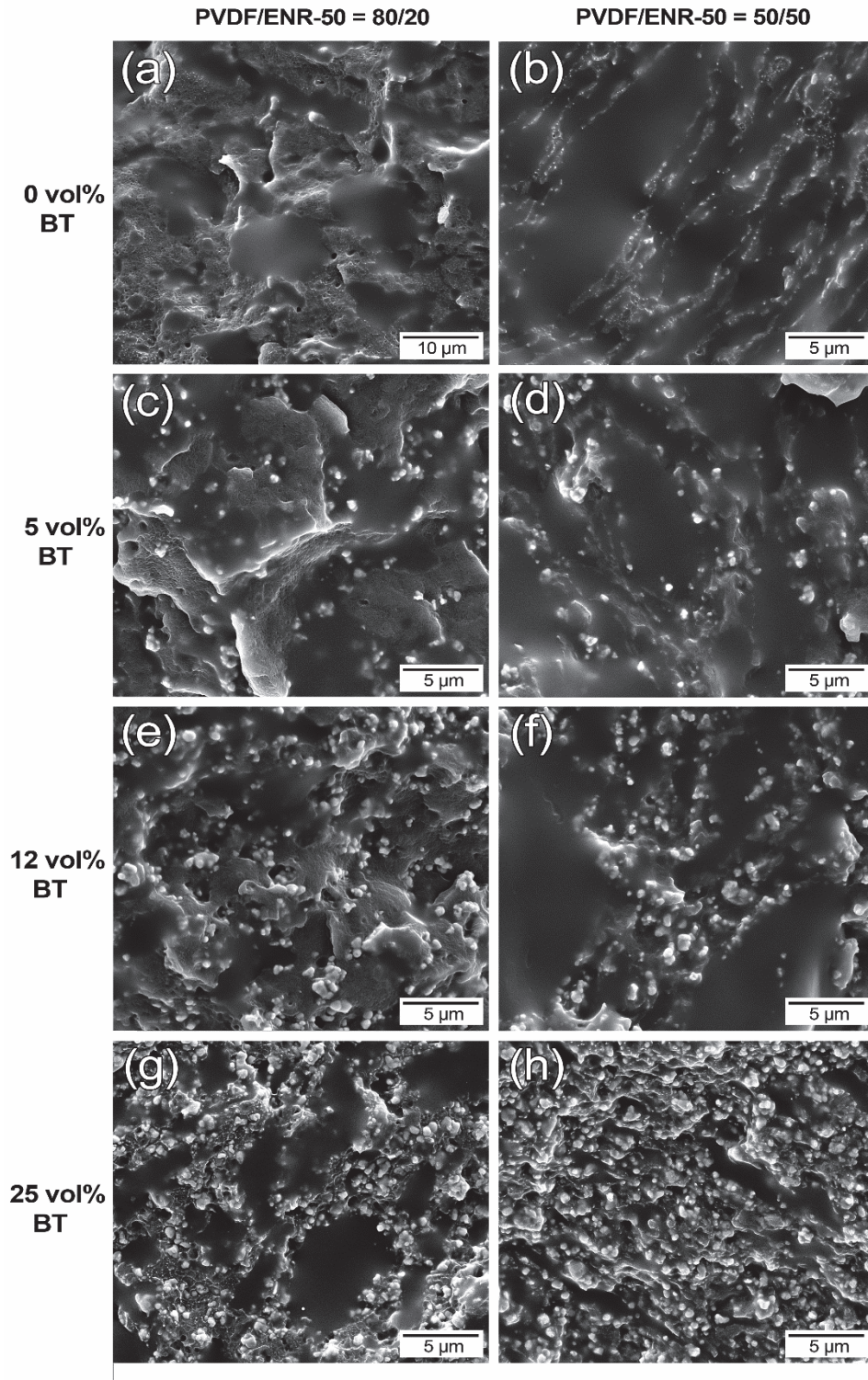


Figure 8.15 SEM micrographs of dynamically cured PVDF/ENR-50 blend containing various amounts of BT

8.3.2 Mechanical properties

Stress-strain behavior of dynamically vulcanized 80/20 and 50/50 PVDF/ENR-50 blend with different BT loadings is presented in Figure 8.16. Apparently, all blends exhibited high initial slope at beginning of the curves due to plastic deformation of the blend. Besides, the rubber-like deformation behavior was observed in 50/50 PVDF/ENR-50 blend. The mechanical properties based on the stress-strain behavior including hardness and tension set are summarized in Table 8.4. The dynamically cured PVDF/ENR-50 blend with various amounts of BT in this investigation was prepared by ADV method. This results in mainly localization of BT in PVDF matrix and at interface as observed in Figure 8.15. The inclusion of BT at interface and in PVDF matrix leads to a significant increase in the Young's modulus. Tensile strength of dynamically cured 50/50 PVDF/ENR-50 blend increased with addition of BT up to 12 vol% and decreasing trend was noticed above 12 vol%. However, the tensile strength of dynamically cured 80/20 PVDF/ENR-50 blend decreased with increasing of BT content, as shown in Figure 8.17. At low BT content (5-12 vol%), the PVDF/ENR-50 blend containing 20 and 50 wt% ENR-50 showed an increase in elongation at break compared with neat blends. However, the improvement of tensile strength is only observed in dynamically cured 50/50 PVDF/ENR-50 blend. As mentioned earlier, the BT is preferentially located at the interface and in PVDF phase which provides better adhesion between PVDF and ENR-50 phase. This results in an increase in the extensibility of the blends during stretching. Furthermore, the elongation at break was higher when filler was used, indicating an increase in toughness of the composites. The positive deviation of elongation at break in the immiscible blend with the presence of filler at interface was also reported by Yang *et al.* [2] and Calcagno *et al.* [22]. This was resulted from excessive amount of BT particles in the blend which leads to the restricted deformability of polymer chain. The necking behavior in stress-strain curve is observed in blend with high BT content at 25 and 35 vol% BT in 80/20, and at 35 vol% in 50/50 PVDF/ENR-50 blend, as shown in Figure 8.16. At a high filler content, the necking was also formed but it was not strong enough to support the drawing. Thus, the fracture occurred at low elongation at break. Additionally, the presence of BT agglomerates at high BT loading leads to lack of interfacial adhesion between polymer chain and filler. This caused cavitations which are in consequence with a decrease in mechanical property of the blend. The maximum value of mechanical properties at 12

vol% BT in the blend is affected by the highest stress transfer capability and improvement of compatibility between BT and blend components. Decreasing of tensile strength for 80/20 PVDF/ENR-50 blend with BT indicates the lack of interaction between BT and PVDF in PVDF-rich blend. It is not sufficiently strong to transfer the stress under large deformation. Despite, interaction is better with the high content of ENR-50. Furthermore, it is obvious that the hardness increased with increasing BT content in the TPV, as shown in Table 8.4. This is attributed to the presence of hard rigid particle in the TPV that leads to resisted deformation. However, no consistent trend was found for tension set with changing loading level of BT.

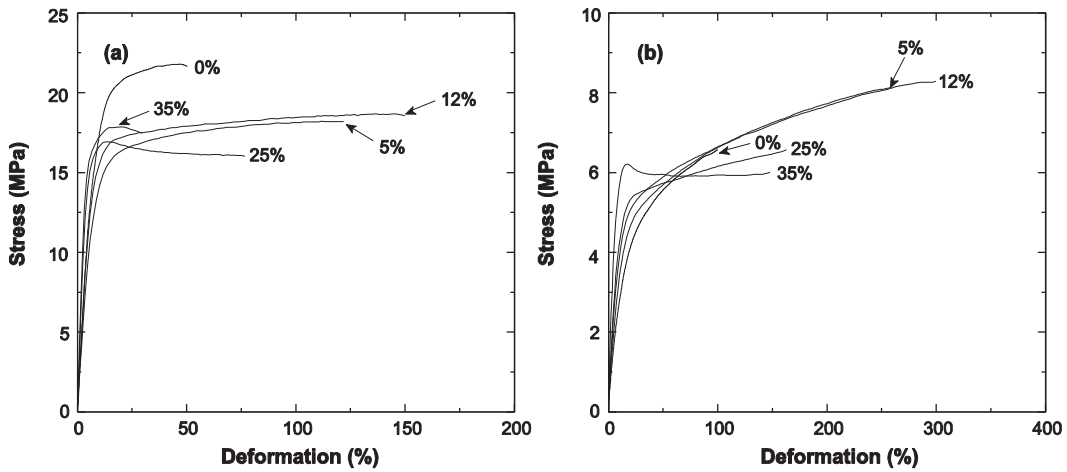


Figure 8.16 Stress-strain curves of dynamically cured PVDF/ENR-50 blend with blend ratios of (a) 80/20 and (b) 50/50 containing various BT loadings

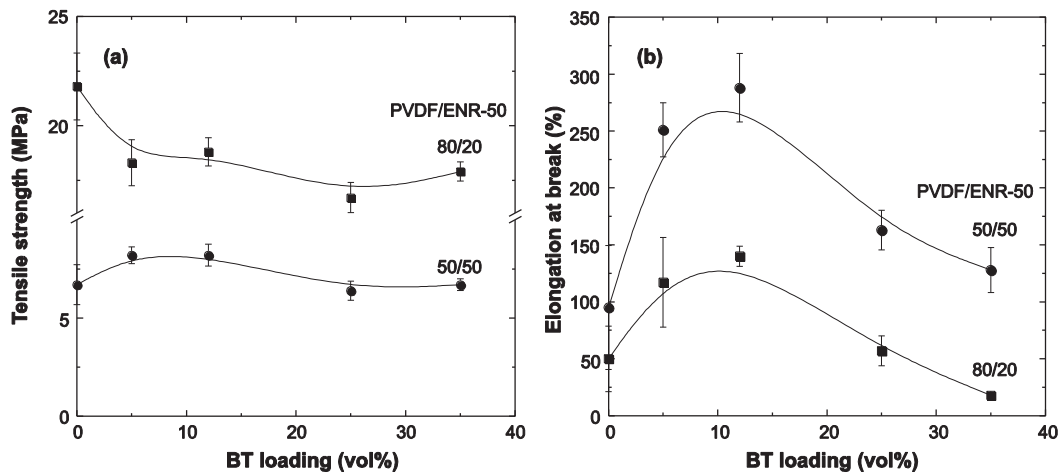


Figure 8.17 (a) Tensile strength and (b) elongation at break of dynamically cured 80/20 and 50/50 PVDF/ENR-50 blends containing various BT loadings

Table 8.4 Mechanical properties of dynamically cured PVDF/ENR-50 blend with various amounts of BT

PVDF/ENR-50	Young's modulus (MPa)	Tensile strength (MPa)	Elongation at break (%)	Tension set (%)	Hardness (Shore A)
80/20					
0BT	225 (±8.7)	21.8 (±1.53)	50 (±29)	-	94.5 (±0.6)
5BT	206 (±13.9)	18.3 (±1.05)	120 (±39)	-	95.5 (±0.6)
12BT	230 (±12.6)	18.8 (±0.64)	140 (±9)	-	95.5 (±1.0)
25BT	340 (±13.0)	16.7 (±0.69)	57 (±13)	-	96.0 (±0.7)
35BT	420 (±17.7)	17.9 (±0.43)	18 (±1)	-	95.0 (±0.8)
50/50					
0BT	34 (±3.3)	6.7 (±1.02)	95 (±54)	35.4 (±1.3)	88.5 (±0.7)
5BT	42 (±2.5)	8.2 (±0.43)	250 (±24)	38.5 (±1.6)	90.0 (±1.0)
12BT	50 (±7.3)	8.2 (±0.55)	290 (±30)	35.4 (±1.3)	91.5 (±0.4)
25BT	56 (±5.7)	6.4 (±0.49)	160 (±17)	36.9 (±1.1)	93.5 (±0.6)
35BT	85 (±1.9)	6.7 (±0.29)	130 (±20)	35.9 (±0.7)	93.5 (±0.7)

8.3.3 Dynamic mechanical analysis

Dynamic mechanical properties of the PVDF/ENR-50 blends as a function of BT content were analyzed using dynamic mechanical thermal analysis (DMA). The dependence of storage modulus (E') and $\tan \delta$ on temperatures of BT filled dynamically cured PVDF/ENR-50 blend which containing 20 and 50 wt% ENR-50 are presented in Figure 8.18(a) and (b), respectively. The storage modulus of the blends was decreased sharply around the glass transition regions of PVDF and ENR-50, respectively. The storage modulus of dynamically cured PVDF/ENR-50/BT composite increased with increasing of BT content in the tested temperature range. The results clearly showed that the addition of BT into dynamically cured blend resulted in a remarkable increase in the stiffness of material. The enhancement in modulus of PVDF/ENR-50/BT composite may originate from the presence of rigid BT particles in soft polymer matrix and restriction of polymer chain by filler-polymer interactions. Moreover, the presence of BT particles between PVDF and ENR-50 phases as observed in Figure 8.6 are possible to act as blend compatibilizer and improve stress transfer between two phases. This contributes to increase the storage modulus. At room temperature, the E' of PVDF/ENR-50 (80/20)

blend was improved by 143% higher and the E' of 50/50 PVDF/ENR-50 blend was improved by 270% higher with the addition of 35 vol% BT. At the same BT concentration, the higher increment of E' can be observed in 50/50 PVDF/ENR-50, as shown in Figure 8.19. This indicates that influence of the BT on E' becomes more pronounced with the blend containing the higher rubber fraction. Apparently, the rapid drop in storage modulus accompanied with the relaxation peak of $\tan \delta$. As stated earlier, the PVDF/ENR-50 blend showed two relaxations at low and high temperatures which corresponded to β -relaxation and α -relaxation of PVDF and ENR-50, respectively. These relaxations are assigned to glass-rubber transition (T_g) of PVDF and ENR-50, respectively. The influence of BT loading on glass transition temperature is summarized in Table 8.5. Clearly, it can be seen that the addition of BT has a significant influence on T_g of ENR-50 and PVDF. The T_g of ENR-50 in PVDF/ENR-50 (50/50) blend is shifted to lower temperature for small addition of BT. This indicates the localization of BT at interface act as compatibilizer for PVDF and ENR-50 blends which leads to shifting of relaxation peaks of blend components toward each other. However, T_g of ENR-50 in PVDF/ENR-50 (50/50) blend is shifted to higher temperature at high BT loading. This can be explained by strong interaction between BT and ENR-50 at the interface, which confines or immobilizes the polymer chains near the filler surface. This results in higher T_g of polymer [23]. Meanwhile, T_g of PVDF is shifted to lower temperature (close to T_g of pure PVDF -39) as BT content increased. This shift is explained by the fact that high content of filler prevents the packing of the polymer chain and consequently increases free volume for molecular mobility. Consequently, the cooperative motion of the polymer chains at lower temperature occurred [24]. The different T_g of PVDF and ENR-50 may occur because BT particles are mainly located in PVDF and interface. Thus, the preventing of polymer chain packing and increasing free volume with high BT loading become more pronounced in PVDF phase. This leads to decrease in T_g of PVDF to lower temperature. Moreover, restriction of ENR-50 chain movement occurred at interface.

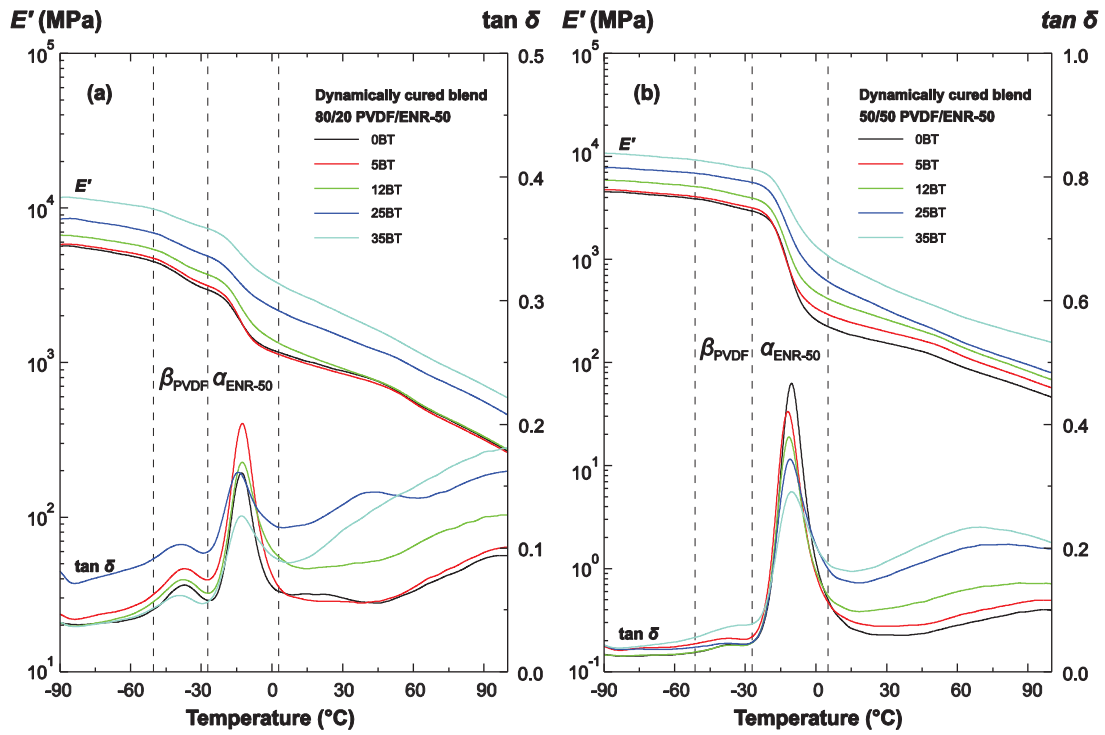


Figure 8.18 Temperature dependence of E' and $\tan \delta$ of dynamically cured (a) 80/20 and (b) 50/50 PVDF/ENR-50 blends with various BT loadings

Table 8.5 Dynamic mechanical properties of dynamically cured PVDF/ENR-50 blends with various amounts of BT

PVDF/ENR-50 TPV	Storage Modulus, E' (MPa)		Loss tangent, $\tan \delta$			
	-60°C	25°C	$\tan \delta_{\max}$		T_g (°C)	
			PVDF	ENR	PVDF	ENR
80/20						
0BT	4900	920	0.07	0.16	-37.6	-12.9
5BT	5100	915	0.08	0.20	-37.7	-12.6
12BT	5830	970	0.07	0.17	-37.6	-12.6
25BT	7440	1600	0.10	0.16	-38.6	-14.3
35BT	10470	2200	0.06	0.13	-39.9	-12.9
50/50						
0BT	4100	160	0.05	0.47	-34.7	-10.5
5BT	4300	210	0.05	0.43	-35.8	-12.0
12BT	5330	280	0.04	0.39	-35.7	-11.5
25BT	7120	370	0.05	0.35	-37.7	-11.1
35BT	9600	620	-	0.29	-	-10.4

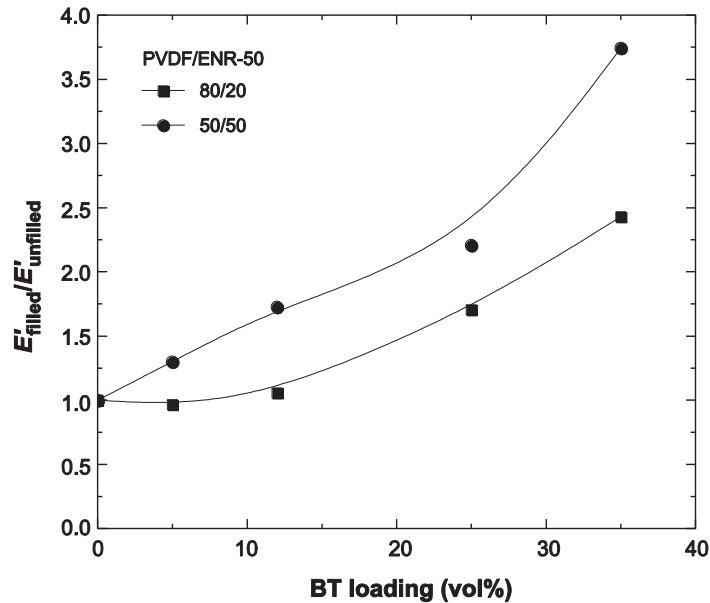


Figure 8.19 Relative storage modulus at 25°C as a function of BT loading

8.3.4 Dielectric properties

Effect of BT loading in PVDF/ENR-50 TPV on the permittivity and loss factor versus frequency of composites with 20 and 50 wt% ENR-50 is shown in Figure 8.20. The dielectric properties at frequency of 1 kHz of BT filled PVDF/ENR-50 composite is listed in Table 8.6. It is obviously seen that the permittivity of 80/20 and 50/50 PVDF/ENR-50 TPV is shifted to higher value as BT loading increased. The increasing permittivity of ceramic-polymer composite is generally caused by the fact that BT has higher permittivity than polymer matrix and is also due to interfacial polarization in the composite. In Figure 8.20, ϵ' of all composites decreased as frequency increased because dipolar groups are not able to create the variation of electric field at higher frequency. This contribution leads to the lack of polarization in the composites. The permittivity then rapidly decreased at high frequency range which corresponds to relaxation process of polymer molecules. This relaxation process correlated with apparent loss factor at higher frequency range. It should also be noticed that decreasing permittivity and appearance of loss factor peak become more pronounced in rich ENR-50 blend therefore it indicates that relaxation is influenced by ENR-50 phase. Moreover, the relaxation was broadened upon increasing PVDF content. This is attributed to the overlapping between relaxations of PVDF and ENR-50, as described in Figure 8.13. With increasing BT content, the intensity peak and value of

loss factor (ϵ'') increased in the specified frequency range, which originate from the contributions of dipole orientation, conduction loss and interfacial polarization in the composites [25, 26]. The extremely fast increasing dielectric loss with decreasing frequency was due to charge transfer. This behavior can be explained as the increased contribution of DC conductivity. Figure 8.21 shows permittivity, loss factor and $\tan \delta$ at frequency of 1 kHz as a function of BT loading in 80/20 and 50/50 PVDF/ENR-50 TPVs in comparison with BT/ENR-50 composite described in Chapter 5. It is obviously seen that the permittivity and loss factor significantly increased with increasing BT loading. The dielectric permittivity is increased from 7.3 to 36.7 (~400% higher) in the PVDF/ENR-50 (80/20) TPV composites and increased from 7.0 to 28.6 (~300% higher) in PVDF/ENR-50 (50/50) TPV composites with 35 vol% of BT. Besides, It is also seen that the composite of dynamically cured PVDF/ENR-50 blend with the blend ratio of 80/20 showed higher permittivity than those of the composite of 50/50 PVDF/ENR-50 TPV and ENR-50. This is due to strong dipole moment of the CF_2 in PVDF molecules which contribute to increase in permittivity of PVDF-rich blend. Furthermore, the PVDF/ENR-50 TPV filled with BT exhibits a lower loss tangent than that of the BT/ENR-50 composite, which is attributed to a higher loss factor of the ENR-50 than that of PVDF, as shown in Figure 8.13. This results in minimized loss factor and $\tan \delta$ in the blend. The TPV filled with BT showed very low $\tan \delta$ value which is lower than ENR-50 filled with BT. Also, the $\tan \delta$ value of TPV is nearly constant over the whole loading range of BT from 0 to 35 vol%. Since, the loss tangent ($\tan \delta$) is proportional to loss factor and permittivity. Hence, high permittivity and low $\tan \delta$ of samples are considered for selecting dielectric materials. Thus, the significant increase in permittivity and decrease in loss factor of the TPV with high PVDF content indicate that PVDF can improve dielectric properties of the composite. Therefore, the BT filled TPV composites prepared in this study are possible to be candidates for good dielectric material with most of loss tangents of the composites are lesser than 0.03.

Table 8.6 Permittivity (ϵ'), loss factor (ϵ'') and loss tangent ($\tan \delta$) at frequency 1 kHz of dynamically cured PVDF/ENR-50 blend with various BT loadings

BT loading (vol%)	PVDF/ENR-50 = 80/20			PVDF/ENR-50 = 50/50		
	ϵ'	ϵ''	$\tan \delta$	ϵ'	ϵ''	$\tan \delta$
0	7.35	0.154	0.021	7.10	0.170	0.024
5	9.86	0.208	0.021	9.25	0.222	0.025
12	13.13	0.293	0.022	11.71	0.296	0.025
25	13.31	0.548	0.023	20.62	0.530	0.026
35	36.74	0.886	0.024	28.56	0.782	0.027

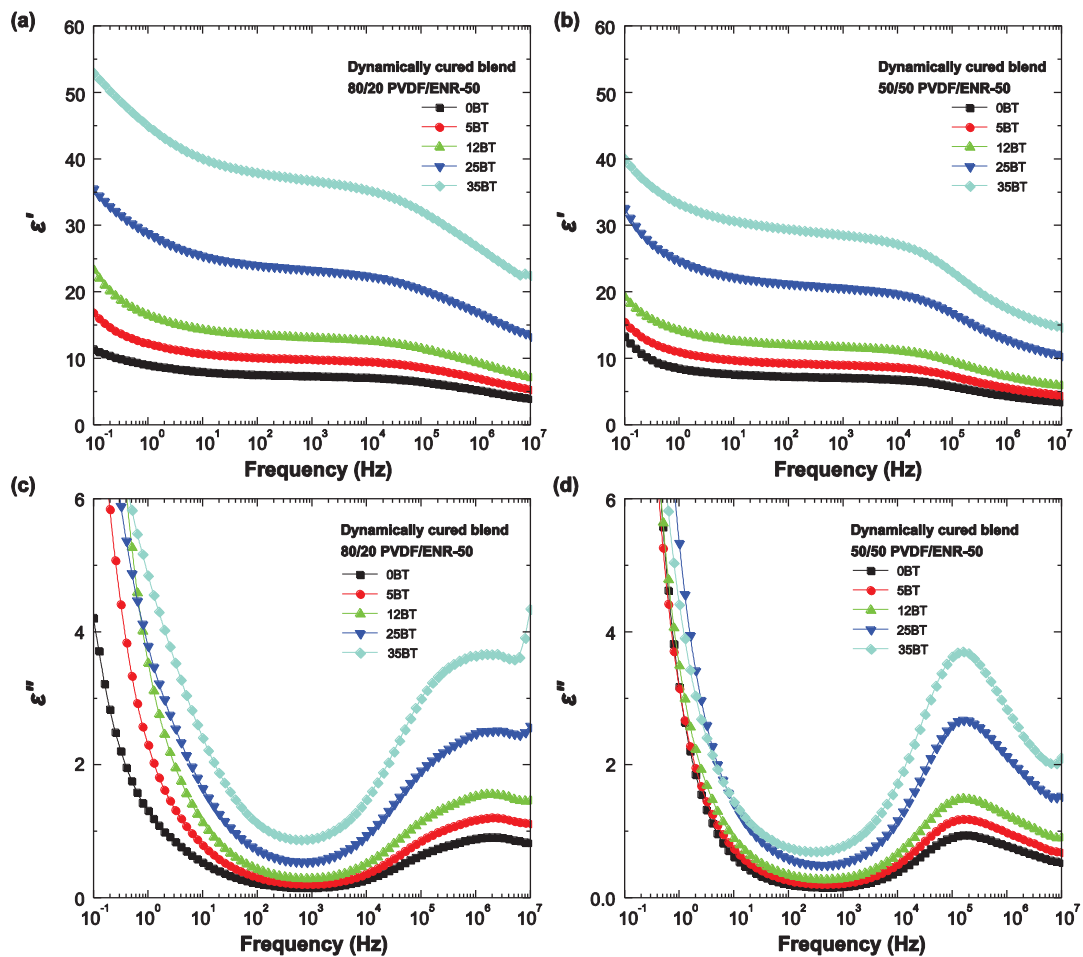


Figure 8.20 Frequency dependence of ϵ' and ϵ'' at room temperature of dynamically cured PVDF/ENR-50 blends with various BT loadings

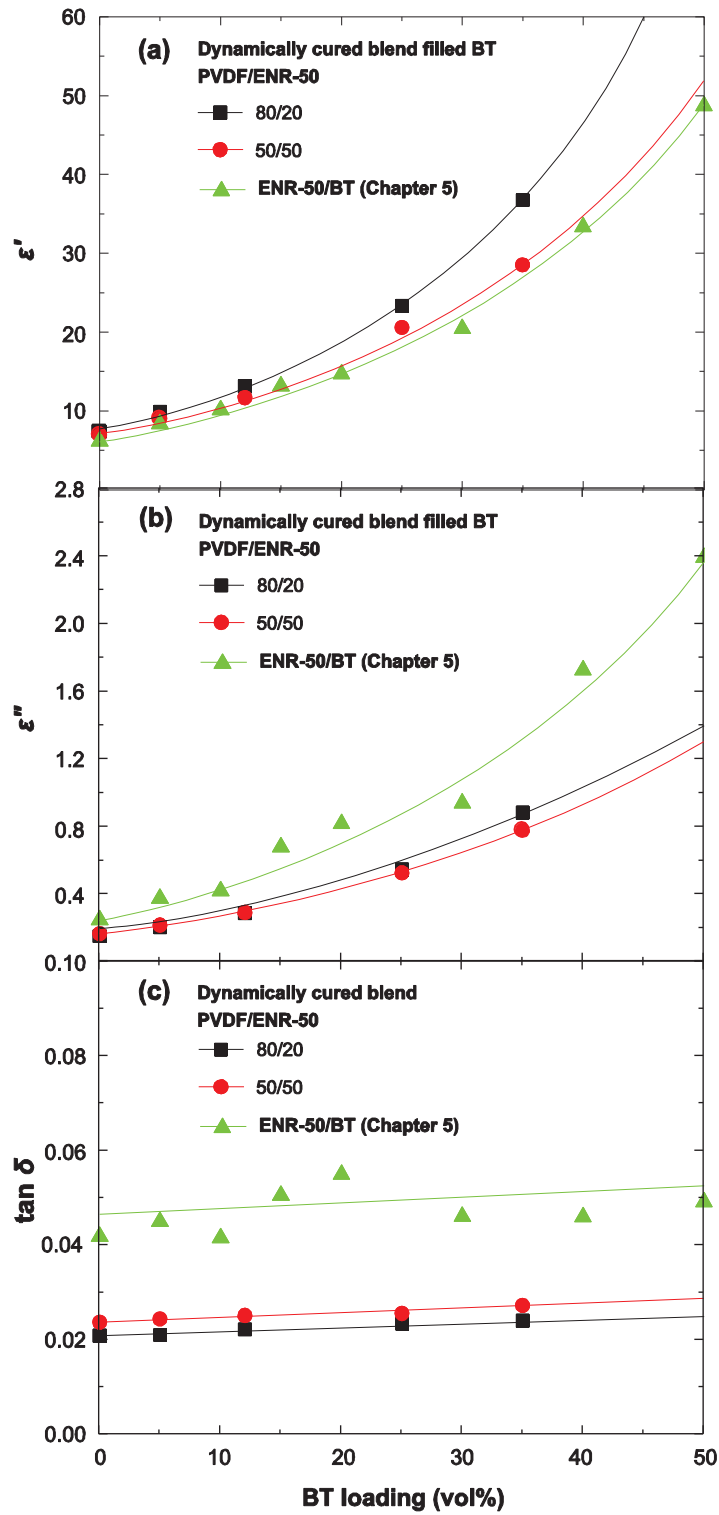


Figure 8.21 (a) Permittivity (b) loss factor and (c) loss tangent at frequency 1 kHz of dynamically cured PVDF/ENR-50 blends as a function of BT loading

8.4 Conclusions

Incorporation of barium titanate in the simple blend and dynamically cured PVDF/ENR-50 blends was performed. It was found that the BT particles preferential located in ENR-50 phase of simple blend and dynamically cured blend due to lower viscosity of ENR-50 component. The selective localization of 5vol% of BT in ENR-50 phase caused increasing in dispersed phase size of ENR-50 in the 80/20 PVDF/ENR-50 simple blend and changing of the morphology from co-continuous phase to dispersed-matrix phase in 50/50 PVDF/ENR-50 simple blend. Two different mixing sequences for addition of BT into dynamically cured blend were investigated. It revealed that incorporation of BT after dynamic vulcanization (ADV method) cause changes in of localization of BT in PVDF/ENR-50 TPV whereby the BT particles are mainly located at interface and in PVDF phase. This localization of BT caused increasing modulus (i.e., Young's modulus and storage modulus) of the blend. Furthermore, incorporation of BT into 80/20 PVDF/ENR-50 TPV caused decreasing tensile strength while 50/50 PVDF/ENR-50 TPV showed higher tensile strength. However, incorporation of BT increased elongation at break of 80/20 and 50/50 PVDF/ENR-50 TPVs. Also, interfacial localization of the BT evidently improved the interfacial adhesion of PVDF/ENR-50 blend. This results in good stress transfer between two phases and restriction of molecular chain.

The variation of BT loadings in dynamically cured PVDF/ENR-50 blend was also studied by adding BT after dynamic vulcanization (ADV method). It was found that the modulus (i.e., Young's modulus and storage modulus) increased with increasing BT content and the great increment of modulus was observed in the blend containing high rubber fraction. The tensile strength of 50/50 PVDF/ENR-50 TPV increased up to 12 vol% of BT, while decreasing trend was observed in the 80/20 PVDF/ENR-50 TPV in the composition range. Additionally, the elongation at break showed the maximum value at 12 vol% of BT in both types of TPVs. The dielectric permittivity and dielectric loss factor of PVDF/ENR-50 filled with BT increased with increasing BT content which is a typical trend for ceramic filled polymer composite. The TPV composites with higher PVDF proportion showed higher permittivity than the TPV composite with lower content of PVDF and ENR-50 composites at the same BT loading. Meanwhile, the TPV filled BT showed lower dielectric loss than BT/ENR-50, which is good characteristic of dielectric materials.

8.5 References

- [1] Entezam, M., Khonakdar, H.A., Yousefi, A.A., Jafari, S.H., Wagenknecht, U. and Heinrich, G. 2013. *On nanoclay localization in polypropylene/poly(ethylene terephthalate) blends: correlation with thermal and mechanical properties*. Mater. Design. 45, 110-117.
- [2] Yang, J.H., Feng, C.X., Dai, J., Zhang, N., Huang, T. and Wang, Y. 2013. *Compatibilization of immiscible nylon 6/poly(vinylidene fluoride) blends using graphene oxides*. Polym. Int. 62, 1085-1093.
- [3] Yun-yun, S., Jing-hui, Y., Ting, H., Nan, Z., Chen, C. and Yong, W. 2013. *Selective localization of carbon nanotubes at the interface of poly(L-lactide)/ethylene-co-vinyl acetate resulting in lowered electrical resistivity*. Compos. Part B: Eng. 55.
- [4] Jarnthong, M., Nakason, C., Lopattananon, N. and Peng, Z. 2012. *Influence of incorporation sequence of silica nanoparticles on morphology, crystallization behavior, mechanical properties, and thermal resistance of melt blended thermoplastic natural rubber*. Polym. Compos. 33, 1911-1920.
- [5] Hong, J.S., Namkung, H., Ahn, K.H., Lee, S.J. and Kim, C. 2006. *The role of organically modified layered silicate in the breakup and coalescence of droplets in PBT/PE blends*. Polymer. 47, 3967-3975.
- [6] Kontopoulou, M., Liu, Y.Q., Austin, J.R. and Parent, J.S. 2007. *The dynamics of montmorillonite clay dispersion and morphology development in immiscible ethylene-propylene rubber/polypropylene blends*. Polymer. 48, 4520-4528.
- [7] Bailly, M. and Kontopoulou, M. 2010. *Nanocomposite blends containing polyolefins*, in *Advances in Polyolefin Nanocomposites*, V. Mittal, ed. CRC Press, Boca Raton.
- [8] Wu, D.F., Lin, D.P., Zhang, J., Zhou, W.D., Zhang, M., Zhang, Y.S., Wang, D.M. and Lin, B.L. 2011. *Selective localization of nanofillers: effect on morphology and crystallization of PLA/PCL blends*. Macromol. Chem. Phys. 212, 613-626.
- [9] Shi, Y.Y., Yang, J.H., Huang, T., Zhang, N., Chen, C. and Wang, Y. 2013. *Selective localization of carbon nanotubes at the interface of poly(L-lactide)/Ethylene-co-vinyl acetate resulting in lowered electrical resistivity*. Compos. Part B: Eng. 55, 463-469.

- [10] Goldel, A., Marmur, A., Kasaliwal, G.R., Pötschke, P. and Heinrich, G. 2011. *Shape-dependent localization of carbon nanotubes and carbon Black in an immiscible polymer blend during melt mixing*. *Macromolecules*. 44, 6094-6102.
- [11] Lee, S.H., Kontopoulou, M. and Park, C.B. 2010. *Effect of nanosilica on the co-continuous morphology of polypropylene/polyolefin elastomer blends*. *Polymer*. 51, 1147-1155.
- [12] Sengupta, P. and Noordermeer, J.W.M. 2005. *Three-dimensional structure of olefinic thermoplastic elastomer blends using electron tomography*. *Macromol. Rapid Commun*. 26, 542-547.
- [13] Machado, A. and van Duin, M. 2005. *Dynamic vulcanisation of EPDM/PE-based thermoplastic vulcanisates studied along the extruder axis*. *Polymer*. 46, 6575-6586.
- [14] Drobny, J.G. 2007. *Handbook of Thermoplastic Elastomers*. PDL(Plastics Design Library)/William Andrew Pub., New York.
- [15] Wu, D.F., Zhang, Y.S., Zhang, M. and Yu, W. 2009. *Selective localization of multiwalled carbon nanotubes in poly(ϵ -caprolactone)/polylactide blend*. *Biomacromolecules*. 10, 417-424.
- [16] Das, A., Mahaling, R.N., Stockelhuber, K.W. and Heinrich, G. 2011. *Reinforcement and migration of nanoclay in polychloroprene/ethylene-propylene-diene-monomer rubber blends*. *Compos. Sci. Technol*. 71, 276-281.
- [17] Thomas, S., Deepu, V., Uma, S., Mohanan, P., Philip, J. and Sebastian, M.T. 2009. *Preparation, characterization and properties of $Sm_2Si_2O_7$ loaded polymer composites for microelectronic applications*. *Mater. Sci. Eng. B: Adv*. 163, 67-75.
- [18] Li, Y.C., Tjong, S.C. and Li, R.K.Y. 2011. *Dielectric properties of binary polyvinylidene fluoride/barium titanate nanocomposites and their nanographite doped hybrids*. *Express Polym. Lett*. 5, 526-534.
- [19] Windlass, H., Raj, P.M., Balaraman, D., Bhattacharya, S.K. and Tummala, R.R. 2003. *Colloidal processing of polymer ceramic nanocomposite integral capacitors*. *IEEE T. Electron. Pa. M*. 26, 100-105.
- [20] Choudhury, A. 2010. *Dielectric and piezoelectric properties of polyetherimide/ $BaTiO_3$ nanocomposites*. *Mater. Chem. Phys*. 121, 280-285.

- [21] Dang, Z.M., Zheng, Y. and Xu, H.P. 2008. *Effect of the ceramic particle size on the microstructure and dielectric properties of barium titanate/polystyrene composites*. J. Appl. Polym. Sci. 110, 3473-3479.
- [22] Calcagno, C.I.W., Mariani, C.M., Teixeira, S.R. and Mauler, R.S. 2008. *The role of the MMT on the morphology and mechanical properties of the PP/PET blends*. Compos. Sci. Technol. 68, 2193-2200.
- [23] Carretero-González, J., Retsos, H., Verdejo, R., Toki, S., Hsiao, B.S., Giannelis, E.P. and López-Manchado, M.A. 2008. *Effect of nanoclay on natural rubber microstructure*. Macromolecules. 41, 6763-6772.
- [24] Leu, C.M., Chang, Y.T. and Wei, K.H. 2003. *Polyimide-side-chain tethered polyhedral oligomeric silsesquioxane nanocomposites for low-dielectric film applications*. Chem. Mater. 15, 3721-3727.
- [25] Huang, X., Xie, L., Jiang, P., Wang, G. and Liu, F. 2009. *Electrical, thermophysical and micromechanical properties of ethylene-vinyl acetate elastomer composites with surface modified BaTiO₃ nanoparticles*. J. Phys. D: Appl. Phys. 42, 245407.
- [26] Logakis, E., Pandis, C., Peoglos, V., Pissis, P., Stergiou, C., Pionteck, J., Pötschke, P., Micusík, M. and Omastová, M. 2009. *Structure–property relationships in polyamide 6/multi-walled carbon nanotubes nanocomposites*. J. Polym. Sci. Pol. Phys. 47, 764-774.

CHAPTER 9

GENERAL CONCLUSIONS

The aim of this work was to understand the behavior of natural rubber composite and blend materials from the knowledge of their composition, microstructures and properties. Epoxidized natural rubber composite with barium titanate (BT) and carbon black have been prepared to improve permittivity and conductivity, respectively. The simple blend and dynamically cured blend of epoxidized natural rubber and poly(vinylidene fluoride) have also been prepared to study their miscibility and phase morphology. The results are summarized below.

Experimental results have initially focused on the characterization of natural rubber and epoxidized natural rubber (ENR). The cure characteristics of three types of natural rubber (i.e., NR, ENR-25 and ENR-50) were first investigated. It was found that the unmodified NR showed plateau curing curve and ENRs showed reversion phenomenon. Meanwhile, the presence of epoxide group in ENR caused an increase in modulus at high strain as compared to natural rubber without epoxide group (NR). However, elongation at break of ENRs was lower than that of the NR. Influence of epoxide group on molecular dynamics of NR and ENR were also observed by DMA and DEA experiments which showed that glass transition temperature (T_g) of rubber increased with increasing epoxidation level. This indicates the steric interference caused by the epoxide group which results in restriction of chain mobility. Furthermore, DEA experiment also revealed that polarity of epoxide group leads to enhance dielectric permittivity, loss factor and conductivity.

In order to prepare high permittivity polymer composite, addition of barium titanate (BT) was used to increase in permittivity of composite. Epoxidized natural rubber with 50 mole% of epoxide group (ENR-50) was used as polymer matrix for 0-3 composite. Ceramic-polymer 0-3 composites based on BT-ENR-50 containing BT 0 to 60 vol% were prepared in molten state. It was found that the composites showed a reduction in scorch

time and cure time, and increased in minimum and maximum torques with increase of the concentration of BT. As expected, the BT particles were dispersed uniformly in ENR-50, which established microstructure (0-3) connectivity of the composite. However, at high BT content, agglomerates formation of BT powders was easily observed. The mechanical and dielectric properties of nanocomposites were modified according to the volume fraction of BaTiO₃: the tensile strength and elongation at break are decreased as BT content increased. Besides, the real and imaginary part of the dielectric permittivity increased with increasing BT content. The evolution of ϵ' with the volume fraction was well described by the Jayasundere and Smith (J-S) and modified Lichtenecker's models in over range of BT loading. BT/ENR-50 composites at 50 vol% of BT nearly reached value of permittivity, loss factor and loss tangent of 48.7, 2.4 and 0.05, respectively at 1 kHz. Therefore, it is concluded that addition of BT into ENR-50 matrix was suitable ceramic-polymer pairs to obtain ceramic-polymer composites with high permittivity and flexibility.

The conductive elastomer composites have been also developed by using ENR-50 as the matrix phase. Two types of carbon black (CB) i.e., high abrasion furnace and extra conductive furnace were used to obtain conductive composite. It was found that the reinforcement of carbon black particle in rubber matrix played a role in the improvement of mechanical properties. The use of HAF and ECF showed maximum tensile strength at 20 and 10 phr, respectively. Furthermore, degree of reinforcement of ECF was higher than that of HAF, which has been estimated by Krause's relation. The electrical properties of the conductive composites were studied by employing dielectric spectroscopy. The dielectric permittivity and loss factor are increased with increasing CB content. It was found that the electrical conductivity increased gradually with increasing CB contents in the composites and then increased abruptly at the percolation threshold. The drastic rise in conductivity was due to the formation of continuous chains or network of carbon black that spanned throughout the insulating ENR-50 matrix. The electrical percolation threshold (p_c) in HAF and ECF composites was reached at 25.3 phr and 12.4 phr, respectively. The very low percolation threshold of ECF/ENR-50 composite is good candidate to prepare conductive elastomer composite because the production of conductive composite depends on conductive filler content, which must be as low as possible to avoid poor mechanical properties and high cost.

The miscibility and phase development of polymer blends based on poly(vinylidene fluoride) (PVDF) and epoxidized natural rubber (ENR) blends were also studied. The morphologies were observed by scanning electron microscopy (SEM) after minor phase etching. As expected, the morphology of PVDF/ENR blends became finer with increasing epoxide group content in ENR molecules due to small difference in solubility parameter and compatibilization between two phases. This results in an increase in tensile strength, elongation at break and storage modulus. The compatibilization reaction may occur between chemical interaction between PVDF and ENR-50 phases. The miscibility was also revealed by DMA and DEA techniques, which detected that the glass transition temperatures of PVDF and ENR-50 were shifted to each other.

Different morphologies of proportion PVDF/ENR-50 blends were observed as a function of the blend. That is, the ENR-50 dispersed in PVDF matrix at low ENR-50 content. The co-continuous interpenetrating phases were observed in the mixtures of 40/60 and 50/50 of PVDF/ENR-50 blends. The further increase of ENR-50 content led to inversion phenomenon which was confirmed by dynamic mechanical analysis. That is, a radically change of storage modulus and $\tan \delta$ was observed when formation of co-continuous structure occurring in the blends. Furthermore, the mechanical behavior of PVDF/ENR-50 blends, confirmed by tensile testing, revealed that the blends containing 20 wt% of ENR-50 exhibited very significant low deformation. The ENR-50 played a major role in increasing the elongation at break of the blend. However, the tensile strength is decreased with increasing ENR-50 content. The crystalline temperature (T_c) and melting temperature (T_m) of PVDF in the blend were also studied. The addition of ENR-50 into PVDF was found to increase T_c and crystallinity of PVDF in the blend while ENR-50 did not influence on the T_m . All blends showed two relaxation peaks which correspond to the glass transition temperature of PVDF and ENR-50. However, maximum positions of relaxation peaks of PVDF and ENR-50 moved toward higher and lower temperatures, respectively. This generally occurred in the blends with partial compatibility.

The localization of BT in PVDF/ENR-50 simple blend and dynamically cured blend was also studied by using the blends with the blend ratios of 80/20 and 50/50. In a simple blend, it was found that the BT particles tended to accumulate in ENR-50, which has lower viscosity. This selective localization of BT leads change of the viscosity ratio and morphology of the blends. In dynamically cured blend, the BT was also localized in ENR-

50 phase in the blend with addition of BT before dynamic vulcanization (BDV method). On the other hand, the BT particles were selectively localized at interface and in PVDF phase in the blend with addition of BT after dynamic vulcanization (ADV method). This causes an increase in Young's modulus and storage modulus of the blends. The variation of BT loadings in dynamically cured PVDF/ENR-50 blend has also been studied. It was found that increment of storage modulus was more pronounced in the 50/50 compared with 80/20 PVDF/ENR-50 TPV composites. Meanwhile, all blends showed maximum value of elongation at break at 12 vol% of BT. As may be expected, the dielectric permittivity and dielectric loss factor of PVDF/ENR-50 filled with BT increased with increasing BT content, which is a typical trend of the ceramic filled polymer composite. Furthermore, the blend with high PVDF proportion showed higher permittivity than the blend with low PVDF proportion and BT/ENR-50 composite at the same BT loading. Hence, dynamically cured blend filled with BT is good candidate for high permittivity composite which could be possible for apply in industries uses.

The natural rubber composites with high permittivity were successfully prepared using barium titanate as filler in dynamically cured PVDF/ENR-50 blends. This type of composites exhibit high permittivity and low dielectric loss, which may suitable for energy storage applications like a capacitor because it is obviously wish to maximize permittivity and minimize the dielectric loss.

APPENDIX

APPENDIX A

Published Article in Adv. Mat. Res. 626: 71–74 (2013)

Co-continuous Phase Structure and Properties of Poly(vinylidene fluoride)/Epoxidized Natural Rubber Blends

Subhan Salaeh^{1,2,a}, Charoen Nakason^{1,b}, Gisèle Boiteux^{2,c},
Philippe Cassagnau^{2,d}

¹Center of Excellence in Natural Rubber Technology (CoE-NR), Faculty of Science and Technology, Prince of Songkla University, Pattani Campus, 94000, Thailand

²University of Lyon, Université Claude Bernard Lyon1, Ingénierie des Matériaux Polymères (IMP), UMR CNRS 5223, 15 Boulevard Latarjet, 69622 Villeurbanne, France

e-mail : ^asnitwatee15@hotmail.com, ^bncharoen@bunga.pn.psu.ac.th,
^cgisele.boiteux@univ-lyon1.fr, ^dphilippe.cassagnau@univ-lyon1.fr

Keywords: Epoxidized natural rubber, poly(vinylidene fluoride), mechanical properties, Dielectric properties and morphological properties.

Abstract

Thermoplastic elastomer based on poly(vinylidene fluoride) (PVDF) and epoxidized natural rubber (ENR) blends at 50/50 by weight with different type of ENR (i.e., ENR with 25 and 50 mol% epoxide which are called as ENR-25 and ENR-50, respectively) has been prepared by melt blending method. Difference content of epoxide groups in ENR molecules on dynamic mechanical properties, dielectric properties and morphological properties of blends were investigated. The morphology reveals the co-continuous phase structure of PVDF and ENR phases. Furthermore, ENR-50/PVDF blend showed finer grain morphology and the glass transition (T_g) of the rubber phase was shifted to lower temperature. The structure of the blends correlated well with permittivity (ϵ') in dielectric properties with the permittivity of PVDF/ENR-50 higher than that of PVDF/ENR-25.

Introduction

Blending of polymer is an attractive way to develop new material which is combined the properties of the blend component. The blends of crystalline thermoplastic and elastomeric polymer with the co-continuous phase structure is defined as thermoplastic elastomer (TPE). This type of material exhibits rubber elasticity at ambient temperature and thermoplastic-like processability. The uncross-linked amorphous elastomer and semi-crystalline polymer blend which provides three-dimensional or co-continuous phase and TPE in nature. This is interesting material behavior with elastomeric properties with strength and flexibility. As most of blends are immiscible and form multi-phase structure with different morphology. The phase structure of the blends depends on several parameters, such as interfacial adhesion, blend ratio, viscosity and processing condition.[1]. Thus, enhancement of miscibility is one of importance development in polymer blends in order to archive high-performance blending materials. In compatibilized nylon-12/epoxidized natural rubber (ENR) blends, the interfacial adhesion increased with increasing epoxide groups in ENR molecules [2]. Acrylic rubber (ACM) is well known rubber which was typically used as a blend component for blending with polar thermoplastic, such as poly(ethylene terephthalate) [3] and polyacrylate [4] which led to increase in degree of compatibilization.

In this work, PVDF/ENRs blends with different types of ENR (i.e., ENR-25 and ENR-50) were prepared at a fixed blends ratio of 50/50 %wt. The dynamic mechanical properties, dielectric properties and morphological properties were investigated.

Experimental

Materials. The poly(vinylidene fluoride) (PVDF) and epoxidized natural rubber (ENRs) rubber used were commercially available Kynar 740 (Arkema, France) and Epoxyrene 25 and 50 (Muang Mai Guthrie Co., Ltd., Thailand), respectively.

Blends preparation. The blends were prepared by melt mixing at 180°C in an internal mixer (Haake Rheomix R600) with a mixing capacity of 50 cm³ at a rotor speed 50 rpm. PVDF was first melted for 3 minutes and then ENR was added and the mixing was continued for 5 minutes. The blends were fabricated to be a thin sheet with 1 mm thick by electrical compression molding at 180°C.

Testing and Characterizations. The dynamic mechanical properties of neat parent polymers and the ENR/PVDF blends were characterized using a TA instrument dynamic analyzer (DMA; model Q800) in a tension mode under the test temperature ranges of -90 to 100°C at a frequency of 1 Hz and heating rate 3°C/min under stream of liquid nitrogen. The dielectric properties were measured by Novocontrol broadband dielectric spectrometer system at room temperature in the ranges of frequency of 10⁻¹ to 10⁷ Hz. Morphological properties were determined by using a scanning electron microscope (SEM) FEI Quanta 400 instrument. The cryogenic-fractured surface was prepared in liquid nitrogen and ENR phase of the blends was then extracted using toluene. The extracted samples were dried in an air oven at 70°C for 48 hr to eliminate the solvent.

Result and discussion

Effect of type of ENR on storage modulus (E') and loss tangent ($\tan \delta$) of PVDF/ENR blends over the temperature ranges of -90 to 100 °C and a frequency 1 Hz are shown in Figure 1. It is seen that all types of blends exhibit high modulus in a glassy region. In the transition zone, the storage modulus of neat PVDF, ENR-25 and ENR-50 show drastic drop at temperature of approximately -42, -34 and -10°C, respectively. The substantial decreasing of storage modulus indicates transition from glassy to rubbery states. In the rubbery state, the PVDF/ENR-50 blend show higher storage modulus than that of the PVDF/ENR-25 blend. This might be due to ENR-50 contains higher level of epoxide groups than ENR-25 which caused higher interfacial adhesion between ENR-50 and PVDF. Furthermore, PVDF/ENR-25 exhibited one drastic drop in storage modulus while the PVDF/ENR-50 blends showed two regions for decreasing modulus. This behavior is confirmed by the appearance of loss tangent curves in Figure 1(b). The maximum peaks of loss modulus and loss tangent ($\tan \delta_{\max}$) which correspond to glass transition temperature (T_g) are summarized in Table 1. It can be seen that PVDF/ENR-25 blend shows a single peak of loss modulus and loss tangent due to overlap of transition of PVDF and ENR-25. However, the PVDF/ENR50 blend exhibit two separated peaks which indicating immiscibility blend of ENR-50 and PVDF. Furthermore, it is seen that the maximum peak of loss modulus and $\tan \delta$ of PVDF and ENR-50 phase shifted to higher and lower temperature, respectively. This shift indicates that partial miscibility blend of PVDF/ENR-50 blends.

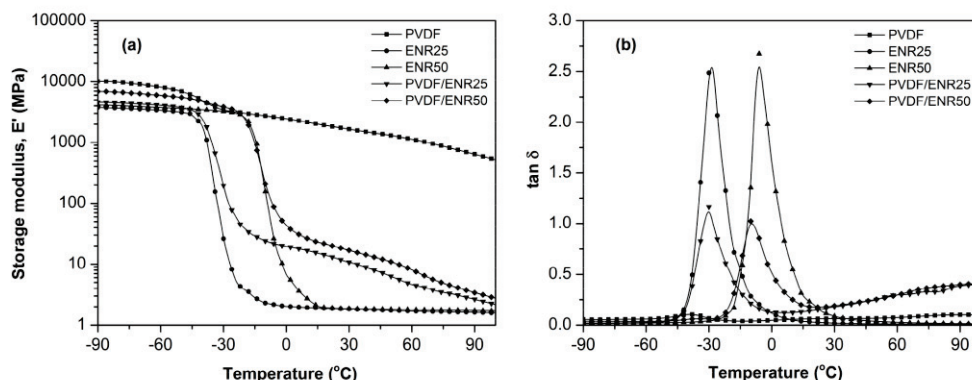


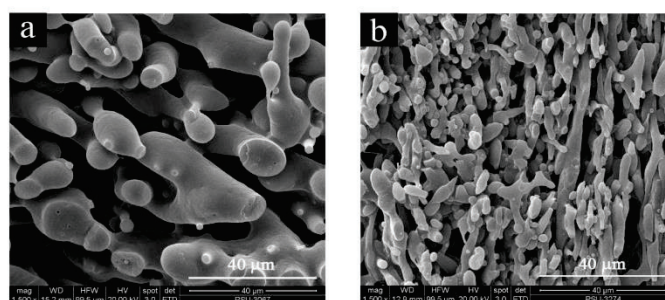
Figure 1. (a) Storage modulus (E') and (b) loss tangent ($\tan \delta$) of neat parent polymers and PVDF/ENRs blends as function of temperature

Table 1. The glass transition temperature of neat parent polymers and PVDF/ENR blends

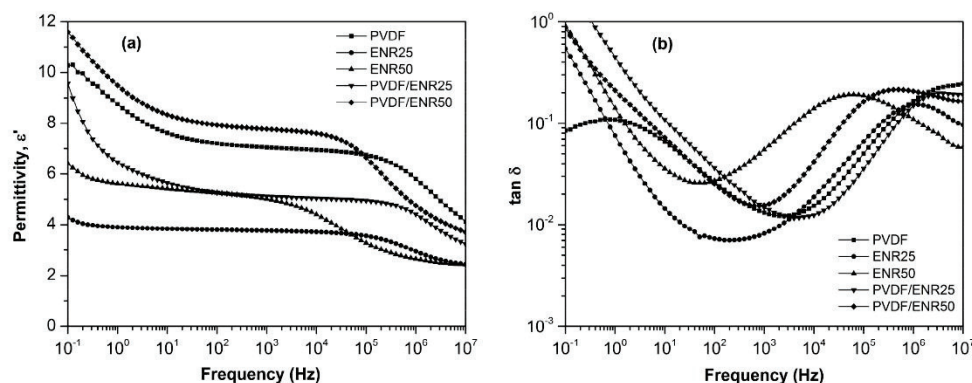
Samples	Glass transition temperature (T_g) (°C)			
	$\tan \delta_{\max}$ PVDF	$\tan \delta_{\max}$ ENR	E''_{\max} PVDF	E''_{\max} ENR
PVDF	-38.9	-	-41.8	-
ENR-25*	-	-28.7	-	-38.7
ENR-50*	-	-6.1	-	-15.2
PVDF/ENR-25	-30.2	-	-37.2	-
PVDF/ENR-50	-34.4	-9.8	-38.4	-17.1

*Cross-linked rubber

Morphological properties: SEM micrographs of the PVDF/ENR blends are shown in Figure 2. It can be seen that the blend exhibited co-continuous structure with ENR-50 blend exhibit finer grain of co-continuous structure compared with the PVDF/ENR-25 blend. This indicates that increasing epoxide groups in ENR molecules caused increasing interfacial adhesion and degree of compatibility between the two phases. This morphological properties correlate well with increasing trend of storage modulus and shifting of T_g in the PVDF/ENR50 blend.

**Figure 2.** SEM micrographs of (a) PVDF/ENR-25 and (b) PVDF/ENR-50

Dielectric properties: Permittivity and loss tangent as a function of frequency are shown in Figure 3. It is seen that the PVDF/ENR-50 blends show higher permittivity value than those of the two blend components, while the PVDF/ENR-25 blend shows permittivity value between the two blend

**Figure 3.** (a) Permittivity (ϵ') and loss tangent ($\tan \delta$) of neat parent polymers and PVDF/ENR blends as a function of frequency

components. This behavior can be explained in the term of Maxwell-Wagner-Sillars effect (MWS) that ENR-50/PVDF blend contains fine grain co-continuous phase structure which causes increasing of accumulating charges at the interfaces with difference permittivities and/or conductivities [5]. It is also seen that the $\tan \delta$ peak of ENR-50 in PVDF/ENR50 blend is shifted to higher frequency, as indicated in Figure 3(b). This might be due to partially miscibility between ENR-50 and PVDF blend.

Conclusion

The co-continuous structure of 50/50 PVDF/ENR blends with difference types of ENR were observed. It was also found that the storage modulus of the PVDF/ENR-50 blend shows higher value than that of the PVDF/ENR-25 blend. Furthermore, the T_g of ENR-50 and PVDF phases was shifted toward lower and higher temperature, respectively. This indicates partial miscibility blend of ENR-50 and PVDF. Furthermore, it was found that the PVDF/ENR-50 blend exhibited a finer grain co-continuous structure than that of the PVDF/ENR-25 blend. This structure caused higher permittivity of the PVDF/ENR-50 blend than that of the PVDF/ENR-25 blend which correlated well with the dynamic mechanical properties.

Acknowledgements

The authors gratefully acknowledge the Thailand Research Fund (TRF) through the Royal Golden Jubilee Ph.D. Program (Grant No. PHD/0245/2549) and French embassy in Thailand for financial support. This work was also supported by the Higher Education Research Promotion and National Research University Project of Thailand, Office of the Higher Education Commission.

References

- [1] J. G. Drobny, *Handbook of Thermoplastic Elastomers* (William Andrew Pub., USA, 2007).
- [2] M. Narathichat, C. Kummerlöwe, N. Vennemann, K. Sahakaro, and C. Nakason: *Adv. Polym. Tech* Vol. 31 (2012), p. 118
- [3] A. Jha and A. K. Bhowmick: *Polymer* Vol. 38, (1997), p. 4337
- [4] M. Kader, A. Bhowmick, T. Inoue, and T. Chiba: *J. Mat. Sci* Vol. 37 (2002), p. 1503
- [5] J. H. Daly, M. J. Guest, D. Hayward, and R. A. Pethrick: *J. Mat. Sci. Lett* Vol. 11 (1992), p. 1271

APPENDIX B

Accepted article in Int. J. Appl. Ceram. Technol. In press (2013)

International Journal of
**Applied
Ceramic
TECHNOLOGY**

Ceramic Product Development and Commercialization

Flexible 0–3 Ceramic-Polymer Composites of Barium Titanate and Epoxidized Natural Rubber

Subhan Salaeh

*Center of Excellence in Natural Rubber Technology (CoE-NR), Faculty of Science and Technology,
Prince of Songkla University, Pattani Campus 94000, Thailand*

*University of Lyon, Université Claude Bernard Lyon1, Ingénierie des Matériaux Polymères (IMP),
UMR CNRS 5223, 15 Boulevard Latarjet, 69622 Villeurbanne, France*

Gisèle Boiteux and Philippe Cassagnau

*University of Lyon, Université Claude Bernard Lyon1, Ingénierie des Matériaux Polymères (IMP),
UMR CNRS 5223, 15 Boulevard Latarjet, 69622 Villeurbanne, France*

Charoen Nakason

*Center of Excellence in Natural Rubber Technology (CoE-NR), Faculty of Science and Technology,
Prince of Songkla University, Pattani Campus 94000, Thailand*

Flexible composites with a high electrical permittivity are pursued in materials research, due to their potential applications in electrical devices. We synthesized such ceramic-polymer composites from BaTiO₃ and epoxidized natural rubber. The influence of BaTiO₃ concentration on cure characteristics, mechanical (static & dynamic), dielectric, and morphological properties of the composites was investigated. The tensile strength and elongation at break decreased with BaTiO₃ loading, while the storage modulus and permittivity of composites increased. As for dynamic electrical properties, the dielectric loss factor and $\tan \delta$ of the composites showed a maximum peak within the frequency range extending up to 10⁵ Hz, reflecting the relaxation process of the polymer matrix. All of the composites showed two peaks in the frequency dependence of electric modulus, due to conductivity and molecular relaxation. Scanning electron microscopy micrographs confirmed the 0–3 structure of composites, with isolated BaTiO₃ particles.

*charoen.na@psu.ac.th
© 2013 The American Ceramic Society

Introduction

Polymer composites incorporating reinforcing and nonreinforcing fillers have been consistently investigated to create useful property combinations. The typical modified characteristics include stiffness, stability, coloring, and antistatic properties. Ferroelectric ceramics are dielectric materials, with typically high dielectric constant and piezoelectric coefficient. On the other hand, polymers provide excellent flexibility and are easy to process, but generally have low dielectric constant. The synthesis of ferroelectric ceramic-polymer composites strives to combine some electrical properties of the ceramic with the viscoelastic properties of the polymer matrix. In prior studies, such 0–3 structured hybrid materials have provided stiffness and high permittivity from the ceramic and excellent flexibility and strength from the polymer. These types of composites are needed in various applications such as flexible capacitors, sensors, and piezoelectric and pyroelectric devices.^{1,2} Recently, ferroelectric polymers based on poly(vinylidene fluoride) and its copolymers have been reported; these materials have high permittivity and dielectric strength.^{3–5} Some other semicrystalline and amorphous polymers, such as polyimide,⁶ polyetherketone,⁷ and poly(methyl methacrylate) (PMMA)⁸ have also been used. The fabrication of ceramic-containing composites based on thermoset polymers, such as epoxy,^{9,10} cross-linked silicone rubber (PDMS),¹¹ and ethylene-vinyl acetate elastomer (EVA),¹² has reached relatively low degradation and high flexibility. Epoxidized natural rubber (ENR) is modified natural rubber containing epoxide groups in its molecular backbone. In our previous work, the presence of epoxide groups in isoprene units was found to enhance mechanical and dielectric properties, compared with unmodified natural rubber, due to the polarity of epoxy groups increasing the dielectric constant.¹³ The high mechanical strength, flexibility and high dielectric constant of ENR make it a prime candidate for the synthesis of ceramic-polymer composites with high dielectric constant.

In this work, composites of barium titanate (BaTiO_3) with ENR-50 were prepared by melt-mixing method. The effects of loading level of barium titanate on curing, static and dynamic mechanical, dielectric and morphological properties were investigated.

Experimental Procedure

Materials

The ENR with 50 mol% epoxide, epoxyrene 50 (ENR-50), was obtained from Muang Mai Guthrie Public (Surathani, Thailand). The zinc oxide (white seal) and stearic acid used as cure activators, in the sulfur vulcanization system, were manufactured by Metoxide Thailand (Pathumthani, Thailand) and Imperial Industry Chemical (Pathumthani, Thailand), respectively. Mercaptobenzothiazole (MBT) used as an accelerator was manufactured by Flexsys (Termoli, Italy). The sulfur used as curing agent was manufactured by Ajax Chemical (Samutprakarn, Thailand). Barium titanate (BT) was prepared in-house, as described in our previous work.¹³

Preparation of BaTiO_3 /ENR-50 Composites

BaTiO_3 /ENR-50 composites with BaTiO_3 loadings in the range 0–50 volume% were prepared in an internal mixer with 80 cm³ capacity (Brabender Plasticorder, model PLE331, Brabender OHG Duisburg, Germany), at 60°C with a rotor speed of 60 rpm. The compounding formulations used for the composites are shown in Table I. ENR-50 was first masticated for 5 min. Zinc oxide was added and mixed for 2 min and then mix with stearic acid for 1 min. Barium titanate powder was finally added into the mixing chamber. After dumping the mixes out, MBT was added and mixed in a two-roll mill for 1 min, then sulfur similarly with 2 min mixing. The rubber compound was then sheeted out and left at room temperature for 12 h before testing and vulcanizing.

Table I. Compounding formulation used to prepare BaTiO_3 /ENR-50 composites

Ingredients	Quantities (phr)
ENR-50	100.0
ZnO	6.0
Stearic acid	0.5
MBT	0.5
Sulfur	3.5
BaTiO_3	0–50 (vol%)

Cure Characterization

Curing characteristics of the composites were determined by Rotorless rheometer (rheoTECH MD+, Tech Pro, Cuyahoya Falls, OH) at 160°C for 60 min. The optimum cure time (t_{c90}), scorch time (t_{s1}), minimum torque (M_f), maximum torque (M_{FH}), and delta torque ($M_{FH} - M_f$) were determined from the curing curves. The compounds were then compression molded at 160°C according to the respective optimum cure time (t_{c90}) to obtain a thin sheet of approximately 1.0 mm thickness, used to test various properties of the final product.

Mechanical Properties

The stress-strain curves of composites were measured from the dumb-bell shaped specimens of ASTM die type C, with a universal tensile testing machine (Hounsfield Tensometer, model H 10KS, Hounsfield Test Equipment Surrey, U.K.). The grip separation speed was set to 500 mm/min and initial gauge length to 25 mm, following ASTM D412.

Dynamic Mechanical Analysis

Dynamic mechanical properties were determined with a Dynamic Mechanical Analyzer (TA Instrument Q800 DMA, New Castle, DE). The samples were rectangular, $35 \times 10 \times 1 \text{ mm}^3$. The storage modulus (E'), loss modulus (E''), and loss tangent ($\tan \delta$) were measured in tension mode, in the temperature range of -90 to 100°C , and the test frequency was fixed at 1 Hz.

Dielectric Analysis

Dielectric measurements with broadband dielectric spectroscopy (Novocontrol alpha analyser, Hundsagen, Germany) were carried out at room temperature, in the frequency range of 10^{-1} – 10^7 Hz. Both sides of a sample were coated with circular 30-mm-diameter aluminum electrodes by vacuum evaporation and deposition.

Morphological Analysis

Scanning electron microscopy (SEM) (Hitachi S800, Tokyo, Japan) was used to characterize microstructures of the composites. Cryogenic fracturing

generated surfaces that were coated with a thin layer of gold under vacuum, to enable observation.

Result and Discussion

Cure Properties

Curing characteristics of ENR-50 filled with various amounts of BaTiO_3 , in terms of torque versus time, are shown in Fig. 1. The torque increased with the amount of BaTiO_3 . Furthermore, a maximum torque is observed, with reversion, that is, a decreasing trend after the maximum. This is due to the low thermal stability of sulfidic bonds in the cross-link system, and the degradation of polysulfide linkage.¹⁴ The reversion behavior becomes more pronounced with BaTiO_3 content, due to the changes in cross-link structures of the vulcanizates after the maximum vulcanization.¹⁵ That is, after vulcanization reached to maximum, higher content of cross-link structure was thermally degraded due to better heat conductivity of the BaTiO_3 particles to nearby cross-linking networks. Therefore, increasing of filler content caused increasing of the heat conductivity of composites (i.e., rubber network and BaTiO_3 particles). This resulted in increasing of heat transfer in the composited system and degradation of the cross-link structure. Curing characteristics of the gum rubber and the $\text{BaTiO}_3/\text{ENR-50}$ compounds are summarized in Table II, in terms of minimum, maximum and delta torques, scorch time, and cure time. The minimum torque is proportioned to the viscosity of the uncured compound, while maximum torque is related to magnitude of cross-link

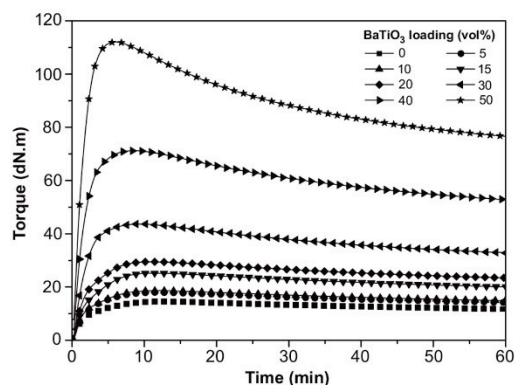


Fig. 1. Curing curves at 160°C of ENR-50 filled with various amounts of BaTiO_3 .

Table II. Cure characteristics of gum vulcanized and BaTiO₃/ENR-50 composites

Properties	BaTiO ₃ content (vol%)							
	0	5	10	15	20	30	40	50
Min. torque, M_L (dN.m)	0.99	0.78	0.84	0.92	1.10	1.59	3.72	7.55
Max. torque, M_H (dN.m)	14.53	17.97	18.66	25.22	29.50	43.68	71.23	112.08
Δ torque, $M_H - M_L$ (dN.m)	13.54	17.19	17.82	24.30	28.40	42.09	67.51	104.53
Scorch time, t_{s1} (min)	0.46	0.41	0.39	0.36	0.34	0.33	0.31	0.29
Cure time, t_{c90} (min)	6.49	6.23	6.22	6.19	5.73	3.99	3.70	3.05
Cure rate index, (CRI)	16.58	17.18	17.15	17.15	18.55	27.32	29.50	36.23

reaction and interaction in vulcanize rubber. As the BaTiO₃ loading increased, the maximum torque and torque difference also increased, due to filler–polymer and filler–filler interactions and also reduced mobility of the rubber chains. It is noted that filler–polymer (BaTiO₃–ENR-50) and filler–filler (BaTiO₃–BaTiO₃) interactions are physical and chemical interactions between BaTiO₃–BaTiO₃ and BaTiO₃–ENR-50. These interactions are parts of cross-linking system although filler–filler and filler–polymer network. It is also noted that the torque difference is measured as the difference between torque of uncured rubber and fully cross-linked rubber. Therefore, the torque difference is a primary examination of network density including physical and chemical interaction in the system. Thus, the torque difference between maximum and minimum torque, which is an indirect measurement of network density in the cross-link system, increases with the loading level of BaTiO₃. At scorch time, the torque is one unit above its minimum, and at cure time, we have 90% of maximum cure. In Table II, both scorch and cure times become shorter as BaTiO₃ content increases. This is due to an increase in the reaction rate of vulcanization; also, the cure rate index (CRI) increased with BaTiO₃ content, as shown in Table II.

Morphological Properties

Scanning electron microscopy micrographs of the fracture surfaces, of composites with various amounts of BaTiO₃, are shown in Fig. 2. The microstructure is a 0–3 structure, with unconnected particles in the continuous ENR-50 matrix. The thickness of the ENR-50 matrix layer, which surrounded BaTiO₃ particles, decreased when the BaTiO₃ concentration increased. At low particle loadings (5 and 15 vol%), the ceramic powder is well dispersed in the ENR-50 matrix without apparent agglomeration. However, at higher loading

levels, agglomeration of BaTiO₃ in composites was observed (encircled in Figs. 2c and d). At 50 vol% loading level of BaTiO₃ (arrows in Fig. 2d), the thin film becomes porous. This is due to poor adhesion between the polymer matrix and the ceramic particles.

Mechanical Properties

The stress–strain curves of gum and BaTiO₃-filled ENR-50 vulcanizates are shown in Fig. 3. It can be seen that the ENR-50 gum vulcanizate exhibits flexibility and high mechanical strength (i.e., high stress at break) due to the orientation of natural rubber molecules. The incorporation of filler particles in ENR-50 enhanced the stiffness (i.e., increasing initial slope of the curves) but reduced the flexibility due to poorer mobility of the molecular chains. Thus, the stiffness of composites is higher than that of the gum vulcanizate. The stiffness of composites can be estimated from Young's modulus or hardness, as shown in Figs. 4 and 5, respectively. It is clear that both Young's modulus and hardness increased with BaTiO₃ content (Fig. 5). This is attributed to the filler–polymer and filler–filler interactions that limit mobility of polymer molecules. This result agrees well with increasing delta torque (Table II). In Fig. 3, it is seen that the composites retain good flexibility even at a loading level of 40 vol%: the elongation at break is higher than 100%. However, at a loading level of 50 vol %, flexibility becomes low and the material is ductile. Mechanical properties in terms of tensile strength and elongation at break, based on the failure points of stress–strain curves in Fig. 3, are graphed in Fig. 6. An increasing volume fraction of BaTiO₃ is associated with decreasing tensile strength and elongation at break. In summary, BaTiO₃ particles in ENR-50 matrix enhanced Young's modulus but deteriorated tensile strength and elongation. At excessive filler, loading cavities were

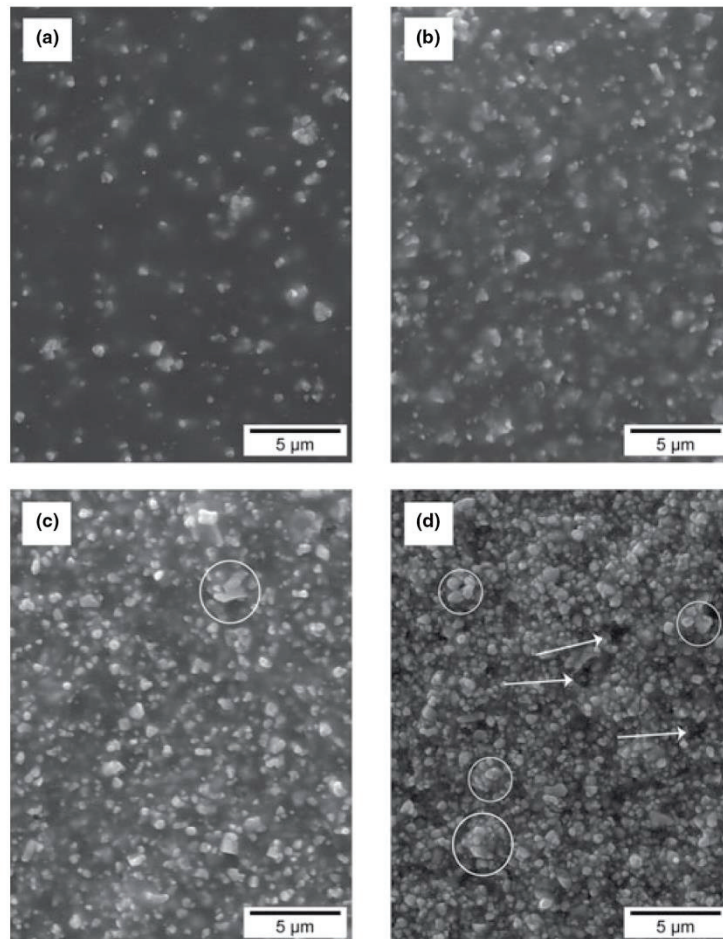


Fig. 2. Scanning electron microscopy micrographs of $\text{BaTiO}_3/\text{ENR-50}$ composites with BaTiO_3 loadings of (a) 5 vol%, (b) 15 vol%, (c) 30 vol% and (d) 50 vol%.

observed in the composites (as shown in Fig. 2d). This is due to lack of adhesion between matrix and filler, which also caused decreases of tensile strength and elongation at break.¹¹

Dynamic Mechanical Properties

The dependence of the storage modulus (E') and loss tangent ($\tan \delta$) on temperature, at different BaTiO_3 contents, is shown in Figure 7. The storage modulus drops drastically at a temperature around

-15°C , indicating apparent transition from glassy state to rubbery state. Loading with BaTiO_3 strongly enhances the storage modulus. The storage moduli increased in both glassy and rubbery states with BaTiO_3 concentration, as summarized in Table III, because of polymer–filler, filler–filler and filler–aggregate interactions. Figure 7 shows the loss tangent curves at 1 Hz, with relaxation peak maximum around -5°C . This relates to the glass transition temperature (T_g) of composites. Furthermore, in Fig. 7 and Table III, the characteristic of the full width at half maximum

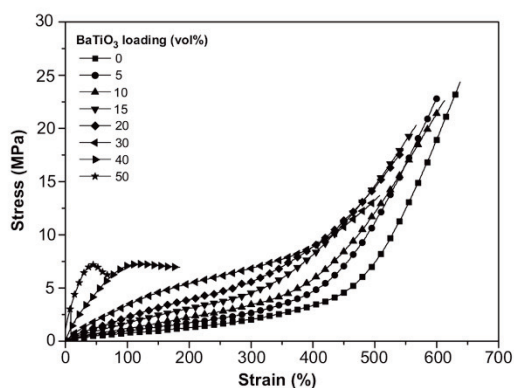


Fig. 3. Stress-strain curves of BaTiO_3 filled ENR-50 composites at room temperature.

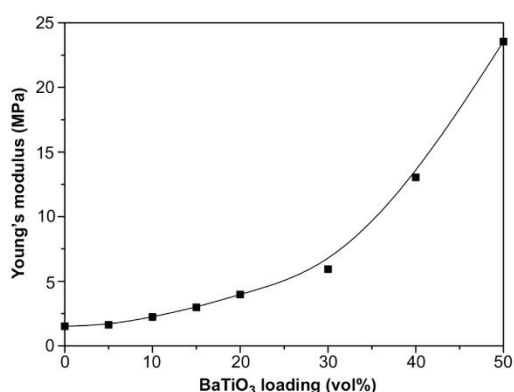


Fig. 4. Young's modulus as function of BaTiO_3 loading in $\text{BaTiO}_3/\text{ENR-50}$ composites.

(FWHM) and the amplitude of $\tan \delta$ are influenced by loading level of BaTiO_3 . That is, the FWHM of $\tan \delta$ peak is increased, but with a substantial decrease in the amplitude of $\tan \delta$. This is due to reduction in damping properties and heat build-up owing to increasing filler content, together with the filler-polymer interaction.¹⁶ The variation in T_g as function of BaTiO_3 content is shown in Fig. 8. The shift of T_g can be explained in terms of good dispersion at lower content of BaTiO_3 , which creates strong interactions between filler particles and polymer matrix: this reduces chain mobility.^{16,17} However, T_g decreases again at loadings over 15vol%, indicating formation of particle agglomerates, as shown

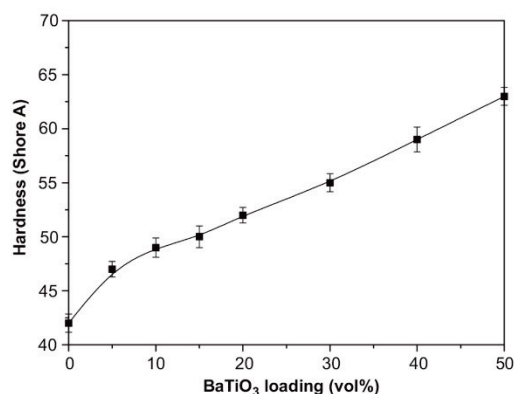


Fig. 5. Hardness as function of BaTiO_3 loading in $\text{BaTiO}_3/\text{ENR-50}$ composites.

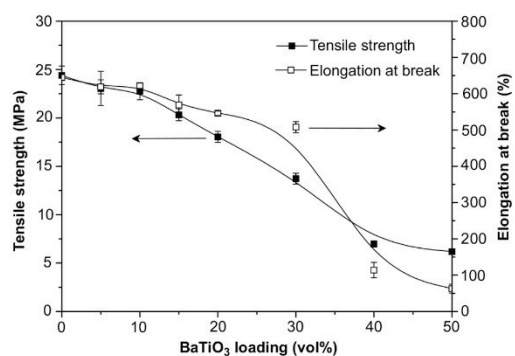


Fig. 6. Tensile strength and elongation at break as function of BaTiO_3 loading in $\text{BaTiO}_3/\text{ENR-50}$ composites.

in Fig. 2: this leads to an increase in the free volume, and consequently improves chain mobility.

Dielectric Properties

Permittivity (ϵ'), loss factor (ϵ''), and loss tangent ($\tan \delta$) of composites as function of frequency, at room temperature, are shown in Fig. 9. For each sample, the permittivity is nearly constant in the frequency range $1-10^4$ Hz, then decreases with the frequency, and drops drastically between 10^5 and 10^6 Hz. This is attributed to relaxation of ENR-50 matrix, which is also indicated by apparent relaxation peaks in the loss factor and loss tangent curves. Loading with BaTiO_3 increased permittivity, loss factor and amplitude of the

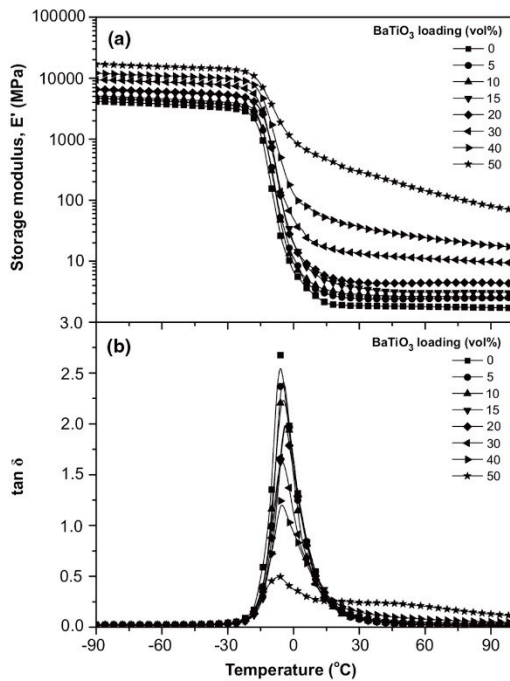


Fig. 7. (a) Storage modulus (E') and (b) loss tangent ($\tan \delta$) as functions of temperature for various $\text{BaTiO}_3/\text{ENR-50}$ composites.

loss factor, of the composites. The loss tangent, defined as the ratio of the imaginary and real parts of permittivity, is only little affected by the loading level of the composites.

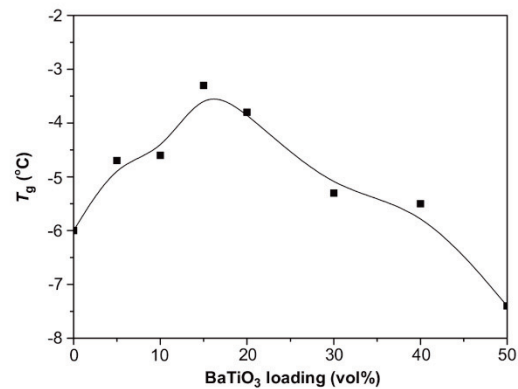


Fig. 8. Glass transition temperature (T_g) as function of BaTiO_3 volume fraction in $\text{BaTiO}_3/\text{ENR-50}$ composites.

Several models have been proposed to fit or predict the permittivity of composites. Key factors include the permittivity and volume fraction of each component, and the spatial arrangement in the mixture.⁶ The permittivity values of composites are intermediate between the pure components. We performed a comparison of the available models based on our experimental data, on the permittivity of composites.

The Lichtenecker logarithmic model is well known and predicts the permittivity of a two-component system^{6,9,18,19}:

$$\log \epsilon_{\text{eff}} = v_c \log \epsilon_c + (1 - v_c) \log \epsilon_p \quad (1)$$

Table III. Storage modulus and loss tangent obtained from Dynamic Mechanical Analysis of $\text{BaTiO}_3/\text{ENR-50}$ composites with different amount of BaTiO_3

BaTiO ₃ content (Volume %)	Storage Modulus (E')		Loss Tangent ($\tan \delta$)	
	Glassy state (-60°C) (MPa)	Rubbery state (30 °C) (MPa)	FWHM (°C)	$\tan \delta_{\text{max}}$
0	3769	1.9	11.9	2.7
5	4215	2.4	11.3	2.5
10	4610	2.9	12.1	2.3
15	5804	3.6	12.8	2.1
20	5992	4.5	12.8	2.1
30	8647	13.4	13.8	1.7
40	10,857	36.3	17.0	1.2
50	15,342	297.7	41.08	0.5

FWHM, full width at half maximum.

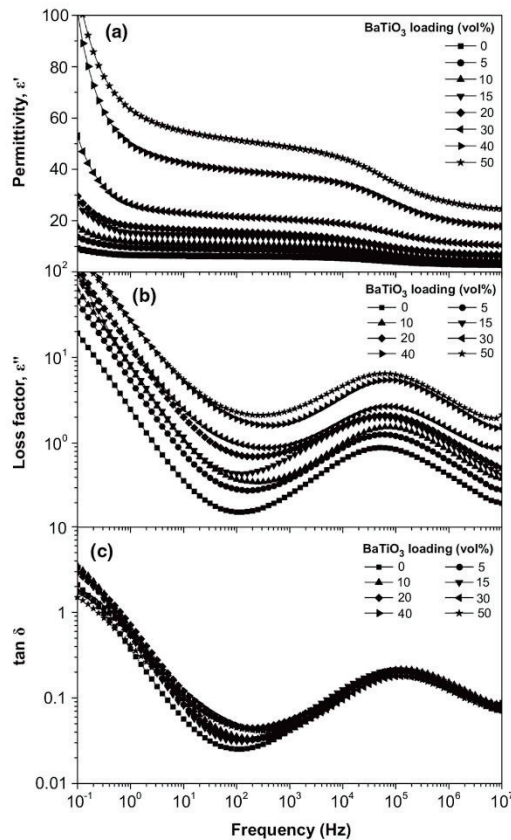


Fig. 9. (a) Permittivity, (b) loss factor, (c) loss tangent as function frequency of BaTiO₃/ENR-50 composites with various amount of BaTiO₃.

where ϵ_{eff} is the effective permittivity of a binary composite, ϵ_c is the permittivity of ceramic, ϵ_p is the permittivity of polymer, and v_c is the volume fraction of ceramic particles in the polymer matrix.

The effective medium theory (EMT) model has been used to calculate the permittivity of composites^{4,19–21}:

$$\epsilon_{\text{eff}} = \epsilon_p \left[1 + \frac{v_c(\epsilon_c - \epsilon_p)}{\epsilon_p + n(1 - v_c)(\epsilon_c - \epsilon_p)} \right] \quad (2)$$

where n is a shape factor of the ceramic particles. A small value of n corresponds to near-spherical shape, while a high value of n is used for elongated particle shapes.

Jayasundere and Smith (J–S) developed a model by modifying the well-known Kerner equations to include interactions between neighboring spheres, for calculating the permittivity of composites^{4,6,11,22}:

$$\epsilon_{\text{eff}} = \frac{\epsilon_p(1 - v_c) + \epsilon_c v_c(A)(B)}{(1 - v_c) + v_c(A)(B)} \quad (3)$$

where

$$A = \left[\frac{3\epsilon_p}{\epsilon_c + 2\epsilon_p} \right] \quad (4)$$

and

$$B = \left[1 + \left(\frac{3v_c[\epsilon_c - \epsilon_p]}{\epsilon_c + 2\epsilon_p} \right) \right] \quad (5)$$

The theoretical model of Bruggeman has the form^{5,10,11,23}:

$$\frac{\epsilon_c - \epsilon_{\text{eff}}}{(\epsilon_{\text{eff}})^{1/3}} = (1 - v_c) \frac{\epsilon_c - \epsilon_p}{(\epsilon_p)^{1/3}} \quad (6)$$

A comparison of the experimental values of permittivity, obtained from dielectric spectra at 1 kHz, and the above equations is shown in Fig. 10. The Logarithmic model matches well-experimental values up to 15 vol% of BaTiO₃, while the Jayasundere and Smith (J–S) model performs the best for higher particle loadings. This is due to the fact that J–S model includes field interactions between neighboring spheres, which gain importance when a high volume fraction of the ceramic phase is used. Poor dispersion of ceramic parti-

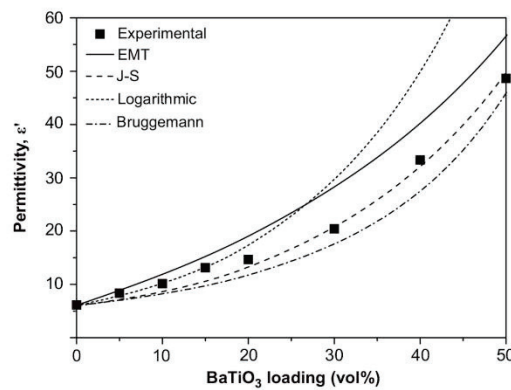


Fig. 10. Experimental values and different theoretical models of permittivity (at 1 kHz) of a bicomponent material, for BaTiO₃/ENR-50 composites.

cles and the presence of air (i.e., cavitation) in the composites, at high loadings, violate idealized assumptions that are typical on deriving models.

Our BaTiO₃/ENR-50 composites nearly reached permittivity value 50, at 50vol% of BaTiO₃, matching PVDF and its copolymer as matrix,^{24,25} and exceeding the permittivity of some polyimide/BaTiO₃ composites^{6,26} and epoxy/BaTiO₃⁹ at the same loading and same measurement frequency.

The electric modulus was used to analyze dielectric relaxation, as it is not disturbed by electrode effects. Electric modulus is defined as the inverse of complex permittivity^{12,27,28}:

$$M^* = \frac{1}{\epsilon^*} = \frac{1}{\epsilon' - j\epsilon''}$$

$$= \frac{\epsilon'}{(\epsilon')^2 + (\epsilon'')^2} + j \frac{\epsilon''}{(\epsilon')^2 + (\epsilon'')^2} = M' + jM'' \quad (7)$$

where ϵ' , M' are the real and ϵ'' , M'' are the imaginary parts of dielectric permittivity and electric modulus, respectively.

Figure 11 shows the frequency dependence of the imaginary part of electric modulus (M'') for the composites with various amounts of BaTiO₃ at room temperature. The electric modulus curves had two peaks, one at a low and another at a high frequency. The peak at low frequency might be due to conductivity and/or interfacial polarization within composites, as suggested by the plateau in the plot of AC conductivity (σ_{AC}) at matching frequencies, shown in Figure 12.

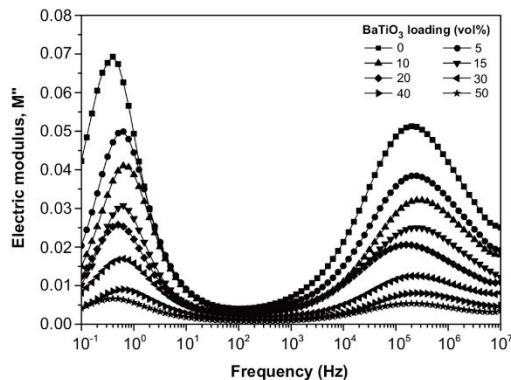


Fig. 11. Electric modulus (M'') as function of frequency for BaTiO₃/ENR-50 composites with various amounts of BaTiO₃.

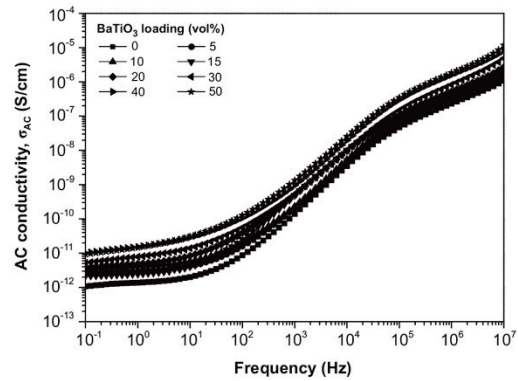


Fig. 12. AC conductivity (σ_{AC}) as function of frequency for BaTiO₃/ENR-50 composites with various amounts of BaTiO₃.

Constant AC conductivity at low frequencies stems from ionic or electronic conductivity, here attributed to the polar functional groups (epoxide ring) in ENR-50 or free charges in the ENR-50 matrix. A peak at low frequency is related to increase in permittivity and loss factor with decreasing frequency.^{27,28} The peak at high frequency here corresponds to α -relaxation of ENR-50.

Conclusions

Ceramic-polymer composites with 0–3 structure were fabricated from BaTiO₃ ceramic particles and ENR-50 as the polymer matrix. The composites showed with increasing concentration of BaTiO₃ a reduction in scorch time and cure time, and increased minimum and maximum torque. The tensile strength and elongation at break decreased while the moduli increased (i.e., Young’s modulus and storage modulus) with the loading level. Increasing torque difference, hardness, and modulus were observed with increasing content of BaTiO₃ due to interaction between BaTiO₃–ENR-50. Furthermore, cavities or voids were observed at high content of BaTiO₃ due to low level of adhesion between polymer and ceramic particles. This cavitation remained in the vulcanizate and showed weak point for the failure under high stress and deformation.

The permittivity increased with BaTiO₃ loading level, and the theoretical Jayasundere and Smith (J–S) model fit the experimental data the best of the model types tested. All of the samples tested showed relaxation around 0.1–1 Hz due to conductivity and/or interfacial

polarization, and around 10^5 – 10^6 Hz due to α -relaxation of ENR-50, in the dynamic electrical properties.

Acknowledgments

Financial support from the Thailand Research Fund through the Royal Golden Jubilee Ph.D. Program (Grant No. PHD/0245/2549) and French embassy in Thailand to Associate Professor Dr. Charoon Nakason (Mr. Subhan Salaeh, research assistance) is acknowledged. This work was also supported by the Higher Education Research Promotion and National Research University Project of Thailand, Office of the Higher Education Commission by Centre National de la Recherche Scientifique (CNRS) UMR 5223 “IMP@Lyon1”. We also thank to the Center of Electronic Microscopy of UCBL and Thierry Tamet for performing electronic microscopy analysis.

References

1. A. Patsidis and G. C. Psarras, “Dielectric Behaviour and Functionality of Polymer Matrix – Ceramic BaTiO₃ Composites,” *Express Polym. Lett.*, 2 [10] 718–726 (2008).
2. H. I. Hsiang, K. Y. Lin, F. S. Yen, and C. Y. Hwang, “Effects of Particle Size of BaTiO₃ Powder on The Dielectric Properties of BaTiO₃/Polyvinylidene Fluoride Composites,” *J. Mater. Sci.*, 36 [15] 3809–3815 (2001).
3. P. Kim, et al., “Phosphonic Acid-Modified Barium Titanate Polymer Nanocomposites With High Permittivity and Dielectric Strength,” *Adv. Mater.*, 19 [7] 1001–1005 (2007).
4. Z. Ahmad, A. Prasad, and K. Prasad, “A Comparative Approach to Predicting Effective Dielectric, Piezoelectric and Elastic Properties of PZT/PVDF Composites,” *Phys. B*, 404 [20] 3637–3644 (2009).
5. M. Wegener and K. Arlt, “PZT/P(VDF-HFP) 0–3 Composites as Solvent-Cast Thin Films: Preparation, Structure and Piezoelectric Properties,” *J. Phys. D Appl. Phys.*, 41 [16] 1–6 (2008).
6. A. Choudhury, “Dielectric and Piezoelectric Properties of Polyetherimide/BaTiO₃ Nanocomposites,” *Mater. Chem. Phys.*, 121 [1–2] 280–285 (2010).
7. D. Xu, et al., “Study on The Properties of A Nanocrystal and Polymer Composite PbTiO₃/PEK-c Film With Optical Anisotropy,” *J. Mater. Sci.*, 39 [21] 6577–6582 (2004).
8. H. Wang, F. Xiang, and K. C. Li, “Ceramic-Polymer Ba_{0.6}Sr_{0.4}TiO₃/Poly (Methyl Methacrylate) Composites With Different Type Composite Structures for Electronic Technology,” *Int. J. Appl. Ceram. Tec.*, 7 [4] 435–443 (2010).
9. S. D. Cho, S. Y. Lee, J. G. Hyun, and K. W. Paik, “Comparison of Theoretical Predictions and Experimental Values of the Dielectric Constant of Epoxy/BaTiO₃ Composite Embedded Capacitor Films,” *J. Mat. Sci-Mater. El.*, 16 [2] 77–84 (2005).
10. W. Peng, X. Huang, J. Yu, P. Jiang, and W. Liu, “Electrical and Thermophysical Properties of Epoxy/Aluminum Nitride Nanocomposites: Effects of Nanoparticle Surface Modification,” *Compos. Part A-Appl. S.*, 41 [9] 1201–1209 (2010).
11. G. Gallone, F. Carpi, D. De Rossi, G. Levita, and A. Marchetti, “Dielectric Constant Enhancement in a Silicone Elastomer Filled With Lead Magnesium Niobate-Lead Titanate,” *Mater. Sci. Eng., C*, 27 [1] 110–116 (2007).
12. X. Huang, L. Xie, P. Jiang, G. Wang, and F. Liu, “Electrical, Thermophysical and Micromechanical Properties of Ethylene-Vinyl Acetate Elastomer Composites With Surface Modified BaTiO₃ Nanoparticles,” *J. Phys. D Appl. Phys.*, 42 [24] 1–10 (2009).
13. S. Salaeh, N. Muensit, P. Bomlai, and C. Nakason, “Ceramic/Natural Rubber Composites: Influence Types of Rubber and Ceramic Materials on Curing, Mechanical, Morphological, and Dielectric Properties,” *J. Mater. Sci.*, 46 [6] 1723–1731 (2011).
14. L. Gonzáles, A. Rodríguez, J. L. Valentín, A. Marcos-Fernández, and P. Posadas, “Conventional and Efficient Crosslinking of Natural Rubber,” *Kaut. Gummi. Kunstst.*, 58 [12] 638–643 (2005).
15. J. Kruželák, C. Kyselá, and I. Hudec, “Elastomeric Magnetic Composites – Curing and Properties,” *Kaut. Gummi. Kunstst.*, 61 [9] 424–428 (2008).
16. R. Rajasekar, K. Pal, G. Heinrich, A. Das, and C. K. Das, “Development of Nitrile Butadiene Rubber-Nanoclay Composites With Epoxidized Natural Rubber as Compatibilizer,” *Mater. Design.*, 30 [9] 3839–3845 (2009).
17. J. Carretero-González, et al., “Effect of Nanoclay on Natural Rubber Microstructure,” *Macromolecules*, 41 [18] 6763–6772 (2008).
18. T. Hu, J. Juuti, and H. Jantunen, “RF Properties of BST-PPS Composites,” *J. Eur. Ceram. Soc.*, 27 [8-9] 2923–2926 (2007).
19. S. George and M. T. Sebastian, “Three-Phase Polymer-Ceramic-Metal Composite for Embedded Capacitor Applications,” *Compos. Sci. Technol.*, 69 [7–8] 1298–1302 (2009).
20. P. Thomas, K. T. Varughese, K. Dwarakanath, and K. B. R. Varma, “Dielectric Properties of Poly(Vinylidene Fluoride)/CaCu₃Ti₄O₁₂ Composites,” *Compos. Sci. Technol.*, 70 [3] 539–545 (2010).
21. P. S. Anjana, M. T. Sebastian, M. N. Suma, and P. Mohanan, “Low Dielectric Loss PTFE/CeO₂ Ceramic Composites for Microwave Substrate Applications,” *Int. J. Appl. Ceram. Tec.*, 5 [4] 325–333 (2008).
22. S. George, P. S. Anjana, M. T. Sebastian, J. Krupka, S. Uma, and J. Philip, “Dielectric, Mechanical, and Thermal Properties of Low-Permittivity Polymer-Ceramic Composites for Microelectronic Applications,” *Int. J. Appl. Ceram. Tec.*, 7 [4] 461–474 (2010).
23. X. X. Wang, K. H. Lam, X. G. Tang, and H. L. W. Chan, “Dielectric Characteristics and Polarization Response of Lead-Free Ferroelectric (Bi_{0.5}Na_{0.5})_{0.94}Ba_{0.06}TiO₃-P(VDF-TrFE) 0–3 Composites,” *Solid State Commun.*, 130 [10] 695–699 (2004).
24. Z. M. Dang, H. Y. Wang, Y. H. Zhang, and J. Q. Qi, “Morphology and Dielectric Property of Homogenous BaTiO₃/PVDF Nanocomposites Prepared via the Natural Adsorption Action of Nanosized BaTiO₃,” *Macromol. Rapid. Comm.*, 26 [14] 1185–1189 (2005).
25. P. Kim, et al., “High Energy Density Nanocomposites Based on Surface-Modified BaTiO₃ and a Ferroelectric Polymer,” *ACS Nano*, 3 [9] 2581–2592 (2009).
26. S. H. Xie, B. K. Zhu, X. Z. Wei, Z. K. Xu, and Y. Y. Xu, “Polyimide/BaTiO₃ Composites With Controllable Dielectric Properties,” *Compos. Part A-Appl. S.*, 36 [8] 1152–1157 (2005).
27. C. V. Chanmal, “Dielectric Relaxations in PVDF/BaTiO₃ Nanocomposites,” *Express Polym. Lett.*, 2 [4] 294–301 (2008).
28. H. Hammami, M. Arous, M. Lagache, and A. Kallel, “Study of the Interfacial MWS Relaxation by Dielectric Spectroscopy in Unidirectional PZT Fibres/Epoxy Resin Composites,” *J. Alloy. Compd.*, 430 [1–2] 1–8 (2007).

APPENDIX C

Published Article in Adv. Mat. Res. 844: 97-100 (2014)

Dynamic Mechanical and Dielectric properties of Poly(vinylidene fluoride) and Epoxidized Natural Rubber Blends

Subhan Salaeh^{1,2,a}, Gisèle Boiteux^{2,b}, Olivier Gain^{2,c}, Philippe Cassagnau^{2,d} and Charoen Nakason^{1,e}

¹Center of Excellence in Natural Rubber Technology (CoE-NR), Faculty of Science and Technology, Prince of Songkla University, Pattani Campus, 94000, Thailand

²University of Lyon, Université Claude Bernard Lyon1, Ingénierie des Matériaux Polymères (IMP), UMR CNRS 5223, 43 Boulevard du 11 Novembre 1918, 69622 Villeurbanne, France

e-mail ; ^asnitwatee15@hotmail.com, ^bgisele.boiteux@univ-lyon1.fr, ^colivier.gain@univ-lyon1.fr, ^dphilippe.cassagnau@univ-lyon1.fr, ^encharoen@bunga.pn.psu.ac.th

Keywords: Epoxidized natural rubber, poly(vinylidene fluoride), dynamic mechanical properties and Dielectric properties

Abstract

The blending of semi-crystalline polymer, poly(vinylidene fluoride), (PVDF) and uncross-linked elastomer epoxidized natural rubber with 50 mol% epoxide (ENR-50) blends were prepared in an internal mixer by melt mixing process. Dynamic mechanical analysis (DMA) and dielectric analysis (DEA) of PVDF/ENR-50 blends were investigated. It was found that the pure PVDF showed higher storage modulus than that of the pure ENR-50 and storage modulus of the PVDF/ENR blends decrease with increasing ENR-50 content. Furthermore, PVDF showed two relaxation peaks correspond to α_a -relaxation and α_c -relaxation, while ENR-50 showed only a single relaxation that is related to α -relaxation or glass transition temperature (T_g). Two relaxation peaks were observed in the PVDF/ENR-50 blends due to phase separation. However, the maximum peak of relaxation shifted toward to higher and lower temperature compared with the pure components which indicates the partial miscible blends. Moreover, at high temperature, the neat polymer and blends showed a sharp increase of loss factor (ϵ'') that correspond to conductivity and/or Maxwell-Wagner-Sillars (MWS) process.

1. Introduction

Blending of polymer is an attractive way to develop new material by combining two or more polymers, resulting in compromise of the properties based on the individual components. However, most of the blends are immiscible blends, hence phase structure of the blends is important to determine the physical properties [1]. The phase separation of polymer blends is decreased by blending polar polymer or using blend compatibilizer to stabilize or increase interfacial adhesion of multi-phases. The phase structure of the blends depends on several parameters, such as interfacial adhesion, blend ratio, viscosity and processing condition. Interfacial adhesion between two phases play importance role to control phase structure of the blends. Blending of PVDF has extensively been reported. It is well established that the PVDF is completely miscible with poly(methyl methacrylate) (PMMA) [2] and partial compatible with polyamide-12 (PA-12) [3]. Epoxidized natural rubber (ENR) is modified natural rubber consisting random epoxide group on rubber molecule. The presence of polar functional groups makes the ENR compatible with polar polymer and can be used as blend compatibilizer. In this work, PVDF/ENR-50 blends was prepared at blend ratio 80/20 and 50/50 PVDF/ENR-50 by using simple blend technique. Molecular mobility of the blends were examined by using dynamic mechanical analysis and dielectric technique. The miscibility of blends components was also investigated.

2. Experimental

Materials. The poly(vinylidene fluoride) (PVDF) and epoxidized natural rubber (ENRs) rubber used were commercially available Kynar 740 (Arkemar, France) and Epoxyprene 50 (Muang Mai Guthrie Co., Ltd., Thailand), respectively.

Blend preparation. PVDF/ENR-50 blends were prepared by melt mixing at 180 °C in an internal mixer (Haake Rheomix R600) with a mixing capacity of 50 cm³ at a rotor speed 50 rpm. Blending of PVDF and ENR-50 was performed using blend ratio of PVDF/ENR-50 = 80/20 and 50/50 wt%. The blends were then fabricated to be a thin sheet with 1 mm thick by compression molding at 180 °C.

Testing and characterization. Dynamic mechanical analysis of the neat parent polymers and blends was performed by using a TA instrument (DMA; model Q800). The storage modulus (E') and $\tan \delta$ were measured under the test temperature ranges of -90 to 100 °C at a frequency of 1 Hz. The temperature dependence of loss factor (ϵ'') of PVDF, ENR-50 and their blends were characterized by using dielectric analyzer (DEA) from TA instrument (model DEA 2970). The experiment was performed in the frequency range 1 to 3×10^4 Hz and in the temperature ranges of -90 to 150 °C.

3. Result and discussion.

Dynamic mechanical properties. The storage modulus and $\tan \delta$ as function of temperature are shown in Fig. 1. It can be seen that storage modulus decrease with increasing temperature due to increasing of mobility of molecular segment. In the rubbery plateau, storage modulus decreased as rubber content increased. It is also seen that the blends showed two relaxation peaks indicating to immiscible blend. The $\tan \delta$ peak at low temperature corresponds to β -relaxation or α_a -relaxation which related to glass transition temperature of PVDF [3]. The $\tan \delta$ peak at higher temperature corresponds to glass transition temperature of ENR-50. The maximum position of $\tan \delta$ peak of PVDF and ENR-50 phases shifted toward to higher and lower temperature, respectively. Shift in the T_g of two components can be described as a partial miscibility between two phases. Furthermore, It can be also seen the amplitude of $\tan \delta$ increase as rubber content increase. This is due to increasing of amorphous phase in the blends which is correlated well with the reduction of storage modulus in transition region.

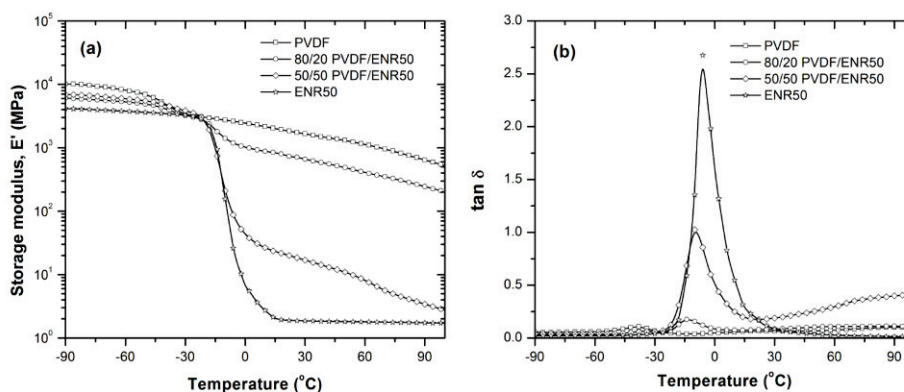


Figure 1. Temperature dependence of (a) storage modulus and (b) $\tan \delta$

Dielectric properties. Fig. 2 shows temperature dependence loss factor δ at difference frequency of PVDF and ENR-50. PVDF shows two relaxation peaks which are α and α_c -relaxation at low and high temperature, respectively. The α and α_c relaxation are associated to relaxation of segmental motion in amorphous and crystalline phase of PVDF, respectively [4]. In ENR-50, one main α -relaxation at low temperature was observed which is associated to segmental motion of

amorphous region. The α -process is generally attributed to the micro-Brownian segmental motion of polymer backbone that is associated with the glass transition temperature (T_g) of polymer materials.

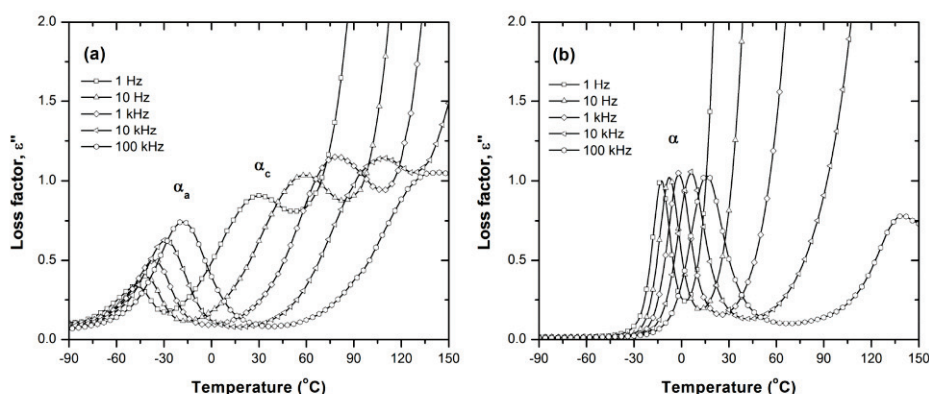


Figure 2. Temperature dependence of loss factor (a) PVDF and (b) ENR-50

The loss factor as function of temperature of PVDF/ENR-50 blends at blend ratio of PVDF/ENR-50 = 80/20 and 50/50 are shown in Fig. 3. It is seen that the 80/20 PVDF/ENR-50 blends showed two relaxation peaks according to α_a and α relaxation of PVDF and ENR-50 phases, respectively. This indicates that phase separation between PVDF and ENR-50 occurred. On the other hand, the 50/50 PVDF/ENR-50 blends showed only one main relaxation: the α -relaxation of ENR-50. It is clear that the α_a -relaxation relaxation peak decreases with increase amount of ENR-50 and could not be observed in the blends with high ENR-50 content due to dilution effect. Furthermore, the α_c -relaxation disappears among the blends due to higher dielectric loss of ENR-50 compared with the PVDF. This lead to overlap of α_c -process of PVDF.

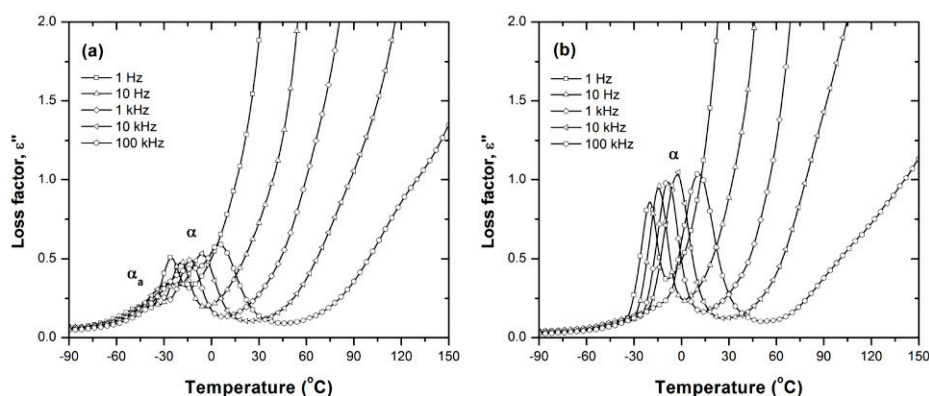


Figure 3. Temperature dependence of loss factor (a) 80/20 and (b) 50/50 PVDF/ENR-50

The pure polymers and their blends show a sharp increase in loss factor at high temperature. This is due to conductivity, associated with free charge at interface within the material which is called interfacial/Maxwell-Wagner-Sillar (MWS) polarization [5], as shown in Fig. 4.

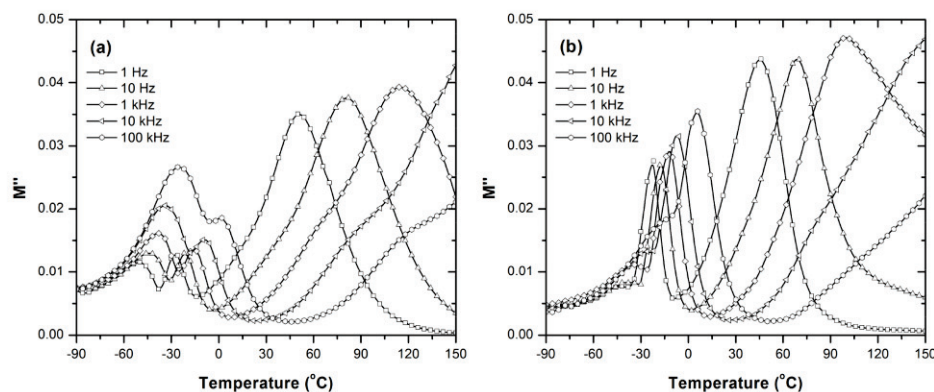


Figure 4. Temperature dependence of M'' (a) 80/20 and (b) 50/50 PVDF/ENR-50

The MWS process in the PVDF/ENR-50 initiates from two phases in polymer blend which have difference conductivity and permittivity. This lead to charge accumulation and polarization at boundaries between two phases. The maximum peak of loss factor of PVDF and ENR-50 also shifted toward to higher and lower temperature corresponded to the dynamic analysis results which indicates the partial miscible of PVDF/ENR-50 blends.

4. Conclusion

The PVDF/ENR-50 blends were successful prepared. It was found that the PVDF showed higher storage modulus than that of the ENR-50 and storage modulus of the blends are lined between the values of the two components. The PVDF/ENR-50 blends show two relaxation peaks or two T_g as is evident in dynamic mechanical and dielectric analysis. However, the relaxation peak was shifted between two relaxations of pure component which indicated the partial miscible blends. The pure polymer and blends show high loss factor at high temperature and low frequency which associated with free charge at interface within the material or interfacial/Maxwell-Wagner-Sillar (MWS) polarization within materials.

Acknowledgements

The authors gratefully acknowledge the Thailand Research Fund (TRF) through the Royal Golden Jubilee Ph.D. Program (Grant No. PHD/0245/2549) and French embassy in Thailand for financial support. This work was also supported by the Higher Education Research Promotion and National Research University Project of Thailand, Office of the Higher Education Commission.

References

- [1] A.Jha, B. Dutta, A.K. Bhowmick, *J. Appl. Polym. Sci.* 74 (1999) 1490-1501.
- [2] I.S. Elashmawi, N.A. Hakeem, (2008) *Polym. Eng. Sci.* 48 (2008) 895-901.
- [3] Y. L. Keun, K. B. Kyu, (2000) *J. Appl. Polym. Sci.* 78 (2000) 1374-1380.
- [4] H. Rekik, Z. Ghallabi, I. Royaud, M. Arous, G. Seytre, G. Boiteux, A. Kallel, *Nanocomposites. Composites Part B-Engineering* 45 (2013) 1199-1206.
- [5] G. Colomines, J. J. Robin, P. Notinger, B. Boutevin, *Euro. Polym. J.* 45 (2009) 2413-2427.

CURRICULUM VITAE



Name Mr. Subhan SALAEH

Student ID 5120330101

Educational attainment

Degree	Name of Institution	Year of Graduation
B.Sc (Rubber Technology) First Class Honors	Prince of Songkla University	2004-2008

Scholarship awards during enrolment

1. The Thailand Research Fund (TRF)-the Royal Golden Jubilee (RGJ) Ph.D. Program (Grant No. PHD/0245/2549)
2. French Government via the Embassy in Thailand.
3. The Graduate school, Prince of Songkla University, Pattani.

List of publications and communications

Publications:

1. Salaeh, S., Boiteux, G., Cassagnau, P., Nakason, C. Conductive Elastomer Composites with Low Percolation Threshold based on Carbon black/Epoxidized Natural Rubber Composites and Their Mechanical Properties. Carbon (submitted).
2. Salaeh, S., Boiteux, G., Cassagnau, P., Nakason, C. Phase Development and Electrical Properties of Poly(vinylidene fluoride)/Epoxidized Natural Rubber Blends. Polymer (submitted).
3. Salaeh, S., Boiteux, G., Gain, O., Cassagnau, P., Nakason, C. Dynamic Mechanical and Dielectric properties of Poly(vinylidene fluoride) and Epoxidized Natural Rubber Blends. Adv. Mat. Res. 844 (2014) 97.
4. Salaeh, S., Boiteux, G., Cassagnau, P., Nakason, C. Flexible 0-3 Ceramic-Polymer Composites of Barium Titanate and Epoxidized Natural Rubber. Int. J. Appl. Ceram. Technol. (2013) (In press).

CURRICULUM VITAE

5. Salaeh, S., Nakason, C., Boiteux, G., Cassagnau, P., Co-continuous Phase Structure and Properties of Poly(vinylidene fluoride)/Epoxidized Natural Rubber Blends. *Adv. Mat. Res.* 626 (2013) 71.
6. Salaeh, S., Nakason, C. Influence of Modified Natural Rubber and Structure of Carbon Black on Properties of Natural Rubber Compounds. *Polym. Composite.* 33 (2012) 489.
7. Salaeh, S., Muensit, N., Bomlai, P., Nakason, C. Ceramic/natural rubber composites: influence types of rubber and ceramic materials on curing, mechanical, morphological, and dielectric properties. *J. Mater. Sci.* 46 (2010) 1723.
8. Nakason, C., Worlee, A., Salaeh, S. Effect of vulcanization systems on properties and recyclability of dynamically cured epoxidized natural rubber/polypropylene blends. *Polym. Test.* 27 (2008) 858.

Communications:

1. Salaeh, S., Boiteux, G., Gain, O., Cassagnau, P., Nakason, C. Morphology and Molecular Mobility of a Novel Thermoplastic Elastomer based on Poly(vinylidene fluoride) and Epoxidized Natural Rubber Blends. The 2014 IUPAC World Polymer Congress (MACRO 2014), 6-11 July 2014, Chiang Mai International Convention & Exhibition Centre, Chiang Mai, Thailand. (Poster presentation)
2. Salaeh, S., Boiteux, G., Cassagnau, P., Nakason, C. Miscibility and Phase Development of Poly(vinylidene fluoride) and Epoxidized Natural Rubber Blends. RGJ-PhD Congress, 28-30 May 2014, Jomtien Palm Beach Resort, Pattaya, Thailand. (Poster presentation)
3. Salaeh, S., Boiteux, G., Gain, O., Cassagnau, P., Nakason, C. Dynamic Mechanical and Dielectric Properties of Poly(vinylidene fluoride) and Epoxidized Natural Rubber Blends. Oral presentation; The First Asia Pacific Rubber Conference (APRC2013), 5-6 September 2013, Surat Thani, Thailand. (Oral presentation)
4. Salaeh, S., Nakason, C., Boiteux, G., Tamet, T., Cassagnau, P. Development of phase structure in thermoplastic elastomer based on poly(vinylidene fluoride)/epoxidized natural rubber blends and their properties. The 28th Polymer

- Processing Society (PPS-28), 11-15 December 2012, Pattaya, Thailand. (Oral presentation)
5. Salaeh, S., Nakason, C., Boiteux, G., Cassagnau, P. Co-continuous Phase Structure and Properties of Poly(vinylidene fluoride)/Epoxidized Natural Rubber Blends. The International Conference on Advanced Material Engineering & Technology, 28-29 November 2012, Penang, Malaysia. (Oral presentation)
 6. Salaeh, S., Nakason, C., Boiteux, G., Cassagnau, P. Relaxation Behaviour of Poly(vinylidene fluoride) and Epoxidized Natural Rubber Blends. Broadband Dielectric Spectroscopy (BDS) and its Application. 3-7 September 2012, Leipzig, Germany. (Poster presentation)
 7. Salaeh, S., Nakason, C., Boiteux, G., Cassagnau, P. Structure-property relation of thermoplastic elastomer poly(vinylidene fluoride) (PVDF)/epoxidized natural rubber (ENR) blends. The 5th International Conference on Polymer Behavior (ICPB5) - Multiphysics Approaches for the Behavior of Polymers and Polymer-based Nanomaterials. 15-18 October 2012, Aveiro, Portugal. (Poster presentation).
 8. Salaeh, S., Nakason, C. Mechanical, Morphological and Electrical Properties of Ceramic/Natural Rubber Composites. The 12th International Seminar on Elastomers and 2nd Thailand-Japan Rubber Symposium. 8-11 March 2010, Cha-am, Thailand. (Oral presentation).